ABSTRACT

Title of dissertation: METHODS AND STANDARDS FOR THE ANALYSIS AND IMAGING OF LATENT FINGERPRINTS AND TRACE CONTRABAND USING AMBIENT IONIZATION MASS SPECTROMETRY AND SECONDARY ION MASS SPECTROMETRY

Edward Ryan Sisco, Doctor of Philosophy, 2014

Dissertation directed by: Professor Alice Mignerey
Department of Chemistry & Biochemistry

A recent report from the National Academy of Sciences (NAS), evaluating the state of forensic science, identified the need to more rapidly, accurately, and reproducibly provide scientifically validated forensic analyses of evidence to support the criminal justice system. The NAS report also highlighted the need for the forensic science community to collaborate with universities and national laboratories, as well as to forge relationships with the National Institute of Standards and Technology (NIST) to address method development, validation, and evaluation of new analytical techniques of relevance to forensic science.[1]

This thesis was completed as part of a unique collaboration between the University of Maryland (UM), the National Institutes of Standards and Technology (NIST) and the Defense Forensic Science Center (DFSC) to address several of the existing research needs in current forensic science practice while meeting the requirements for a Department of Defense (DOD) Science Mathematics and Research for Transformation (SMART) fellowship and supporting NIST efforts in trace contraband detection. Two distinct areas of research were pursued. First, studies were conducted on

method development and validation for the detection of explosives using four different ambient ionization mass spectrometry (AI-MS) techniques relevant to routine casework at DFSC and to other federal labs that screen for trace contraband. Additional method validation studies for the detection of adulterants in beverages and the analysis of bank dye are also presented. All methods were developed in accordance with the requirements specified by the International Organization of Standardization (ISO) 17025 guidelines, which is the accreditation standard for practicing forensic laboratories.

The second track of this thesis involved exploration of emerging analytical methods, and several novel applications, for mass spectrometry based chemical imaging of both endogenous and exogenous components in latent fingerprints. This work was driven by a recent National Science Foundation (NSF) report that identified mass spectral imaging (MSI) as a key goal for the future development of forensic science.[2] Both AI-MS and secondary ion mass spectrometry (SIMS) techniques were utilized and evaluated for their ability to chemically image fingerprints. To support these studies, a novel standard fingerprint test material was also developed during this research. As a result of this work there are now validated methods for the screening of trace explosives, as well as other types of forensic evidence such as adulterants and bank dye, that can be reliably employed into the casework scheme. Also, there are new applications and capabilities for MSI of fingerprints and an artificial fingerprint material that allows for the reproducible deposition of test fingerprints.

METHODS AND STANDARDS FOR THE ANALYSIS AND IMAGING OF LATENT FINGERPRINTS AND TRACE CONTRABAND USING AMBIENT IONIZATION MASS SPECTROMETRY AND SECONDARY ION MASS SPECTROMETRY

by

Edward Ryan Sisco

Dissertation submitted to the Faculty of the Graduate School of the
University of Maryland, College Park in partial fulfillment
of the requirements for the degree of
Doctor of Philosophy
2014

Advisory Committee:

Professor Alice C. Mignerey, Chair
Professor Catherine Fenselau
Dr. Greg Gillen
Professor Neil Blough
Professor John Fisher

Dedication

To my wife, Kimberly, for sticking next to me throughout this process and always telling me I could. And to my parents, Mark and Irene, for letting me follow my dreams and giving me their full support in everything I have tried to achieve.

Acknowledgements

Most importantly I have to thank my advisors, Dr. Alice Mignerey of the University of Maryland, Dr. Greg Gillen of the National Institute of Standards and Technology, and Dr. Candice Bridge of the Defense Forensic Science Center, for giving me this amazing opportunity to pursue a direction which was slightly untraditional, while providing the assistance and guidance to keep me on track. I must also thank the group at NIST which welcomed me with open arms and who, without them, I would not have been able to achieve what I have. Specifically, I would like to thank Marcela Najarro, Dr. Thomas Forbes, Dr. Christopher Szakal, Dr. Shin Muramoto, and Dr. Timothy Brewer, for always listening to my seemingly outlandish questions, absurd ideas, and teaching through my mistakes. I must also thank the group of people at the DFSC who helped me make my time in Atlanta as productive as possible. Specifically, Jeffrey Dake, for being an excellent mentor, the Trace Evidence Branch, for providing your expertise on all things trace and otherwise, Henry Maynard, for always being up for trying eccentric ideas, Henry Swofford, for your fingerprint expertise, and Dr. Jeff Salyards, for without his approval I would not have been given this opportunity. I must also thank the SMART scholarship program, for providing financial support throughout my endeavor. Finally, I must thank my friends for their constant support, their expertise, and their willingness to stick by my side throughout this process.

Table of Contents

List of Tables

List of Figures

List of Abbreviations

1,3-DNB: 1,3-Dinitrobenzene

1,3,5-TNB: 1,3,5-Trinitrobenzene

2,4-DNT: 2,4-Dinitrotoluene

2,6-DNT: 2,6-Dinitrotoluene

2-A-4,6-DNT: 2-Amino-4,6-dinitrotoluene

2-NT: 2-Nitrotoluene

3-NT: 3-Nitrotoluene

4-A-2,6-DNT: 4-Amino-2,6-dinitrotoluene

4-NT: 4-Nitrotoluene

AI-MS: Ambient Ionization Mass Spectrometry

AP: Ammonium Picrate

APGDI: Atmospheric Pressure Glow Discharge Ionization

ATR: Attenuated Total Reflectance

CI-GC-MS: Chemical Ionization Gas Chromatography Mass Spectrometry

DAPNe: Direct Analyte-Probed Nanoextraction

DART / DART-MS: Direct Analysis in Real Time Mass Spectrometry

DEFFI / DEFFI-MS: Desorption Electro-Flow Focusing Mass Spectrometry

DEGDN: Diethylene Glycol Dinitrate

DESI / DESI-MS: Desorption Electrospray Ionization Mass Spectrometry

DFMS: Double Focusing Magnetic Sector

DFSC: Defense Forensic Science Center

DOD: Department of Defense

DOJ: Department of Justice

EGDN: Ethylene Glycol Dinitrate

EI-GC-MS: Electron Impact Gas Chromatography Mass Spectrometry

EIC: Extracted Ion Chromatograph

ETN: Erythritol Tetranitrate

FBI: Federal Bureau of Investigation

FTIR: Fourier Transform Infrared Spectroscopy

GC-MS: Gas Chromatography Mass Spectrometry

HMDD: Hexamethylene Diperoxide Diamine

HMTD: Hexamethylene Triperoxide Diamine

HMX: Cyclotetramethylenetetranitramine

HPLC-MS: High Performance Liquid Chromatography Mass Spectrometry

HS-GC-MS: Headspace Gas Chromatography Mass Spectrometry

IAFIS: Integrated Automated Fingerprint Identification System

IMS: Ion Mobility Spectrometer

ISO: International Organization for Standardization

LTP / LTP-MS: Low Temperature Plasma Mass Spectrometry

MAAQ: 1-Methylaminoanthraquinone

MALDI / MALDI-MS: Matrix Assisted Laser Desorption Ionization Mass Spectrometry

MSI: Mass Spectral Imaging

NAS: National Academy of Sciences

NB: Nitrobenzene

NCFS: National Committee on Forensic Science

NG: Nitroglycerin

NIST: National Institute of Standards and Technology

NSF: National Science Foundation

NSI-MS: Nanospray Ionization Mass Spectrometry

PA: Picric Acid

PEG : Polyethylene Glycol

PETN: Pentaerythritol Tetranitrate

PYX: 2,6-Bis(picrylamino)-3,5-dinitropyridine

QA/QC: Quality Assurance Quality Control

RDX: Cyclotrimethylenetrinitramine

SIMS: Secondary Ion Mass Spectrometry

SMART: Science Mathematics and Research for Transformation

TATP: Triacetone Triperoxide

TDI: Thermal Desorption Ionization

TFA: Trifluoroacetic Acid

TNT: Trinitrotoluene

TOF: Time-of-Flight Mass Spectrometer

TOF-SIMS: Time-of-Flight Secondary Ion Mass Spectrometry

UM: University of Maryland

XRD: X-Ray Diffractometry

Chapter 1: Introduction

Section 1.1: Overview

This work was the product of a unique collaboration between the University of Maryland (UM), the Department of Defense (DOD) Defense Forensic Science Center (DFSC), and the National Institute of Standards and Technology (NIST), that focused on supporting the mission of the DFSC as well as complimenting current homeland security related projects at NIST. Within this thesis, two distinct areas of research were completed. First, in order to support the development of state-of-the-art analytical techniques, studies were conducted on method development and validation for the detection of explosives using ambient ionization mass spectrometry (AI-MS) techniques. The second area of research explores the next generation of forensic analyses, focusing on evaluation and method development for the chemical analysis and mass spectral imaging (MSI) of latent fingerprints using both AI-MS and secondary ion mass spectrometry (SIMS) techniques.

This first chapter provides a brief introduction on the history of forensic science with a focus on latent fingerprint analysis and trace contraband screening. In addition, this chapter provides an overview of the analytical techniques that were used in this work. Subsequent chapters of the thesis follow two distinct tracks, the first of which focuses on the development of analytical protocols for the analysis of forensic related samples. This work is highlighted in Chapter 2, which is a summary of two papers on the method development for analysis of trace explosives by direct analysis in real time mass spectrometry (DART-MS), and in Chapter 3, where other AI-MS sources are evaluated and compared for potential application as trace screening techniques. Appendix 2 and

Appendix 3 provide additional examples on the method development and validation work completed for the analysis of adulterants in solutions and the analysis of bank dye from various surfaces by DART-MS.

The second area of focus for this thesis is development and optimization of techniques for chemical analysis and imaging of latent fingerprints. This work is presented in Chapters 4 through 7. Chapter 4 discusses the need for and development of an artificial fingerprint material and artificial fingerprints to help to provide a standard material for the cross comparison of analytical and visualization techniques. Chapters 5 through 7 discuss the benefits, weaknesses, and novel applications of three mass spectrometry-based techniques for the analysis of latent fingerprints. Chapter 5 summarizes a paper which discusses the capabilities of desorption electro-flow focusing mass spectrometry (DEFFI-MS) for the chemical analysis and imaging of fingerprints. Chapter 6 summarizes a paper that outlines the strengths and weaknesses of C_{60}^{+} double focusing magnetic sector (DFMS) secondary ion mass spectrometry (SIMS) for the analysis of fingerprints, highlighting chemical imaging and the unique capability of depth profiling a fingerprint. Chapter 7 provides discussion on the ability to obtain high spatial resolution chemical imaging using time-of-flight secondary ion mass spectrometry (TOF-SIMS), and how this type of analysis has the potential open the door for better understanding the changes in fingerprint chemistry as a function of time and environmental exposure. The common theme through both tracks is the evaluation of several techniques, namely AI-MS and SIMS, and their applicability and relevance for providing useful forensic information. Finally, Chapter 8 provides a brief discussion on the conclusions and the future directions of this work.

Section 1.2: Forensic Science and the Inspiration for this Work

Forensic science can be defined as "the science of associating people, places, and things in criminal activities".[3] Historical evidence of the beginnings of forensic science can be found as far back as the fifth century, though the first written documentation of the use of forensic techniques for criminal prosecution was in 1248 in China, where a scientist used the presence of flies to aid in the identification of the murder weapon and elucidation of the killer.[4] In the 17th and 18th centuries, the study of evidence-based techniques for criminal prosecution became more commonplace, especially in Europe. It was here that many techniques were introduced and would eventually be used in what is now commonly referred to as "forensic science". As the 18th and 19th centuries progressed, research became more focused on personal identification, such as the work by Alphonse Bertillion, who developed a way to measure specific physical features of individuals as a method for identification.[3] Soon after that, aided by the invention of photography, fingerprint analysis became widely used. During this time, chemical analysis techniques also became increasingly popular in all branches of forensic science. Throughout the twentieth century there were two major developments in forensic science, fingerprint identification and DNA typing, which was first used in the field in 1984.[3] Currently, modern day forensic science involves a vast range of scientific disciplines, from DNA and fingerprints to trace evidence, forensic odontology, and forensic entomology. Forensic scientists are now working in a large network of strictly regulated laboratories, the majority of which are state or federally run and International Organization for Standardization (ISO) 17025 certified as testing laboratories. However,

even with the tight regulation, and the great deal of research being done, many areas for improvement in the system still exist, as articulated in several recent reports.[1,2]

The focus of this thesis was inspired by two recent reports on forensic science that outlined areas in need of improvement for practicing forensic labs, as well as opportunities for new research. The first report, commissioned by Congress, and issued in 2009 by the National Academy of Sciences (NAS), titled "Strengthening Forensic Science in the United States: A Path Forward" provided an in-depth critique of the major disciplines of the science.[1] The report identified the strengths and pitfalls of each branch as well as the science as a whole, highlighting that "there is a dearth of peer-reviewed, published studies establishing the scientific bases and reliabilities of many forensic methods".[1] It also pointed out the need for standards and protocols for a number of different branches, including latent fingerprints, trace evidence, and firearms.[1] From this report a number of committees, scientific working groups, and federal grants have been established. Most recently, a group of examiners, professors, and other professionals has been organized, by the Department of Justice (DOJ), establishing the National Commission on Forensic Science (NCFS).[5] The task of the NCFS will be to advise the Attorney General and create requirements that examiners and examinations must adhere to. A reorganizing of the scientific working groups related to forensic science is also currently being completed as a joint agreement by DOJ and NIST, to help encourage uniform practices and languages across the many disciplines. The first part of this thesis focuses on addressing some of the recommendations proposed by the report, specifically, the need to "address issues of accuracy, reliability, and validity" and to "establish protocols for forensic examinations, methods and practices" by providing cross

comparison and method validity for the analysis of trace explosives and other types of forensic evidence.

The second report, which was the result of a National Science Foundation (NSF) workshop organized by Professor R.G. Cooks from Purdue University, titled "Science on Location: Forensic Science on the Move", discussed future directions of forensic science in regards to both education and analytical techniques.[2] Specifically, the report highlighted several key areas of instrumental development that will play major roles in the advancement of forensic science. These included on-site chemical analysis, development of statistics and databases, and mass spectral imaging (MSI). Findings within this report helped to motivate the directions for this thesis. One of the major findings of this work stated, "multimodal imaging including imaging without prior sample preparation should be strongly encouraged for the detailed new information it will provide when used with appropriate imaging processing".[2] Detailed findings under this umbrella include identifying SIMS as, "a powerful tool for MS imaging which shows great potential in forensic applications" and AI-MS as, "a useful experiment that might be particularly appropriate to crime scene analysis".[2] Other findings also support the increased acceptance of AI-MS techniques in forensic science, such as "ambient ionization used in combination with a handheld MS system has the potential as a method of performing forensic analysis on-site".[2] This report, along with the NAS report, highlights the increased need for traditional method validation of current state-of-the-art techniques, as well as the development and evaluation of the next generation of chemical analysis techniques, with regards to forensic samples.

Section 1.3: Trace Contraband Screening

One of the major focus areas of this thesis is the optimization and method development for the screening of trace explosives with AI-MS techniques, which are discussed in the detail in Section 1.6. The basis of trace contraband screening is the observation that the handling, construction, or concealment of explosives devices will invariably contaminate the individuals involved, their belongings, and the environment around them with micrometer sized trace particles of explosives or their precursors. The goal of screening technologies is to be able to detect the chemical signatures from these traces. A number of agencies including the Department of Homeland Security – Transportation Security Agency, DOD, Customs and Border Patrol, the Secret Service, the United States Postal Service, and many others utilize trace screening technologies at security checkpoints. In a forensic laboratory setting, evidence from a blast site, from a device itself, or from an area thought to be used in the construction of such a device will be collected and screened for the presence of explosives using several different screening techniques.

The main difference between explosive screening at a checkpoint and in a forensic laboratory is the requirement for the forensic laboratory to use a confirmatory test. The gold standard for confirmatory explosives characterization in the forensic laboratory is chromatographic separation followed by mass spectrometry. These techniques, typically high performance liquid chromatography mass spectrometry (HPLC-MS) or gas chromatography mass spectrometry (GC-MS), are highly specific and sensitive to a wide range of explosives. The major drawback of these techniques is lengthy sample preparation, long analysis times, on the order of one half of an hour, and

the requirement for well-trained analysts.[6] Due to these limitations there has been interest in utilization of rapid screening techniques in forensic laboratories to help probe the evidentiary value of a sample prior to analysis by a confirmatory technique. By screening first, the number of samples that are required to be run by the confirmatory technique can be reduced, thus improving throughput and also reducing the overall case backlog.

Homeland security checkpoints utilize a number of trace contraband analysis techniques that could be adopted for use into the forensic science setting. One of the most widely implemented classes of screening instruments are ion mobility spectrometers (IMS), which are commonplace in airports and border crossings across the country. Some of the major benefits of IMS include low cost, a small footprint, the ability to complete analysis under ambient conditions, and high sensitivity, all of which make this technique appealing for screening checkpoints.[7] Furthermore, certain models allow for the simultaneous detection of peroxide based explosives and nitro based explosives.[8] Sensitivities for detection of explosives by this technique range from picograms to nanograms.[9] Some of the pitfalls of IMS include interferences from complex matrices, co-elution, poor peak resolution, and the use of radioactive ion sources.[7] Chemiluminescence techniques, such as the EGIS® III system, utilize the luminescence of the excited state NO_2 molecules, and have been coupled with gas chromatography as a trace explosives detection instrument. However, these type of commercial systems can only detect a limited number of nitro-containing explosives, making the technique less versatile then IMS or AI-MS instruments.[7] Chemiluminescence techniques such as this are also incapable of detecting peroxide based explosives.

Detection of explosives using canines is also widely implemented at checkpoints but is impractical for use in the forensic laboratory. In addition to the impracticality of using canines in the laboratory, analytical instruments allow for uninterrupted, around-the-clock analysis and the ability for the technique to provide the user with a differentiation of possible threats and unambiguous results.[10] An instrument will also typically provide a longer lifetime than a canine, at a lower total cost.

Optical spectroscopy techniques, which include infrared and Raman, represent another approach to trace explosives detection. Unlike IMS and mass spectrometry techniques that detect molecules based upon structure, size, mass, and characteristic fragmentation pattern of ions, spectroscopy techniques measure absorption and scattering of electromagnetic waves based upon characteristic functional groups of the molecule. Infrared spectroscopy of explosives has been well studied, however its major pitfall is the possibility for interference from the matrix.[11] Furthermore, analysis of trace samples often requires direct contact with the sample for analysis, though minimal sample is typically required.[7] Raman spectroscopy offers a little more flexibility over infrared spectroscopy, and has been shown to be used as a standoff detection technique.[12–14] However, fluorescing backgrounds provide increased difficulties in analysis by Raman. Powders that are dark can be difficult, and even dangerous, to analyze as well.[12] Lastly, chemical identification colorimetric kits provide the ultimate in portability. However, they are often one-time-use, have poorer sensitivities than other techniques, and are not specific to individual compounds, leading to potential user interpretation errors.[15]

While spectroscopy techniques like Raman microscopy are gaining traction in the forensic community as a screening techniques, another potential candidate for trace

screening applications is AI-MS, utilizing instrumentation such as DART, desorption electrospray ionization (DESI), low temperature plasma (LTP), and matrix assisted laser desorption ionization (MALDI).[16–18] These techniques provide rapid analysis times, on the order of seconds, with minimal sample preparation and a high degree of specificity. These techniques have previously been explored for the analysis of trace explosives, with reported sensitivities, of nanograms to picograms, that are comparable to those reported herein.[17–25]

This work examines the development of AI-MS techniques for the analysis of trace explosive residues. These AI-MS techniques have been shown to potentially minimize many of the limitations of the other techniques. With AI-MS, sensitivity and specificity are equal to or surpass those of other analytical techniques. The footprint of these systems allows them to be deployed both to forensic laboratories as well as screening checkpoints. Analysis of samples is extremely rapid, and can be completed from any number of surfaces with minimal substrate interference. These techniques are capable of detecting a many of the different classes of explosives including nitro-based, peroxide, and inorganic. The current limitations of the techniques in a forensic laboratory setting are very few, the most obvious being lack of reproducibility. General acceptance in the court systems is also lacking in many stated. In a screening setting, current lack of portability and the need for gas cylinders and solvents also could hinder widespread deployment, though miniature, field-able mass spectrometers are currently being developed to mitigate these issues.[26,27]

Section 1.4: Traditional and Chemical Analysis of Fingerprints

The use of fingerprints for identification and forensic analyses is a relatively recent development. Though ancient government documents have been found containing fingerprints – where it has been theorized they were used as a way to sign contracts – the first documented scientific observation of fingerprints in the modern world was completed by Marcello Malpighi in 1686.[28] Malpighi, a university professor, had no understanding of the importance of fingerprints but did note that fingerprints are composed of ridges that form a number of spirals and loops. Following Malpighi, it was not for another century until another document regarding fingerprints was written, this time by Jan Evangelista Purkinje. In this paper, Purkinje discussed his findings that fingerprints could be grouped into one of nine specific patterns.[28] Though this work was ground breaking, it, like Malpighi's, made no mention of individuality or evidentiary value of these deposits.

The first use of fingerprints for identification purposes was completed, inadvertently, by Sir William Herschel. Herschel, the chief magistrate for a district court in India, required locals to leave their hand print, or at least several of their fingerprints, on contracts that they signed. As he completed contracts throughout the years, Herschel noticed that no two prints were the same.[28] In addition to understanding individuality, Herschel also studied persistency of fingerprints by analyzing his fingerprints that were present on all of the contracts he signed in his many years as a magistrate. He found that his fingerprint pattern was consistent throughout all contracts; establishing the persistence of one's fingerprint. Herschel's idea of using fingerprints as a contract signature was

brought to the United States by Gilbert Thompson, a geologist who also used his fingerprint to prevent forgery of his documents.[29]

In between Herschel and Thompson, there were two important advancements in the utilization of fingerprints for forensic applications. The first advancement was the development of an iodine fuming method to allow for the visualization of fingerprints on paper. This was the first mention of the development of fingerprints and was discovered by Paul-Jean Coulier, a French professor. Coulier was also one of the first scientists to note that fingerprints could be analyzed using a magnifying glass.[29] The second advancement was due to Henry Faulds, a British surgeon, who was the first to comprehend the evidentiary value of fingerprints. From his research, Faulds was able to determine both the uniqueness of fingerprints, as well as the ability to use printing ink to records one's fingerprint.[28] Also, because of his research, Faulds developed a new classification system, based on the fingerprint ridge structure, that was published in *Nature* in 1880.[30] This method of classification was adopted by the British police force as a means of identification, in addition to the Bertillion system, that used measurements of various physical features, not fingerprints.[28]

It was not until 1892 that fingerprints were first utilized in a criminal investigation. Known as the Rojas murder, the case involved the murder of two children in Argentina. A search of the room in which the children were found led to the discovery of a thumb print, in blood, on the door post. Comparison of the fingerprint to suspects revealed that the print matched the mother of the children, Francis Rojas. When Francis was told this, she confessed to killing her children in order to begin a relationship with her love interest.[29]

In 1900 the fingerprint classification system proposed by Faulds was replaced by that of Sir Edward Henry, which was published in his book "The Classification and Use of Fingerprints".[31] Shortly after the incorporation of the Henry classification system, Scotland Yard established the first fingerprint section of a police force.[29] Just two years later, in 1903, the first use of fingerprints in a criminal justice setting in the United States began as the New York State Prison System utilized fingerprints to keep track of prisoners.[28] In 1905, the United States DOJ formed the Bureau of Criminal Identification to act as a central location for the collection and analysis of fingerprints cards.[28] This division was later replaced by the Identification Division of the Federal Bureau of Investigation (FBI). In 1946, the FBI processed its 100 millionth fingerprint card. In 1999, the Integrated Automated Fingerprint Identification System (IAFIS) was established by the FBI, becoming the first integrated, computerized, fingerprint identification system. At the present time, the IAFIS has 60 million fingerprints from the FBI and over 120 million from the Department of Homeland Security.

In the 1980's researchers began to explore the feasibility of measuring the chemical composition of fingerprints. Initial research focused on utilization of commonplace analytical approaches, including optical microscopy, Fourier transform infrared spectroscopy (FTIR) and GC-MS. More recently, the chemical composition of fingerprints is now being investigated using more sophisticated techniques such as MALDI-MS, SIMS, X-ray diffractometry (XRD), and AI-MS.[32–35] Techniques such as these allow for chemical imaging of entire latent fingerprints, as well as methods to simultaneously probe both the organic and inorganic components in a latent fingerprint. The use of these more sophisticated techniques, combined with chemical imaging and

multivariate statistics can and will continue to allow for novel types of examinations. These examinations may allow for the determination of age, gender, or race of individual, as well as providing information as to the age of a fingerprint deposit. Chemical imaging may also be advantageous for biometric studies where fingerprints are overlapped and/or are difficult to visualize using traditional fingerprint development techniques. These types of analyses may fundamentally change the state of current fingerprint examinations.

Evaluating new techniques for the ability to chemically image fingerprints is one of the areas of emphasis of this work. The techniques that were evaluated have been shown to potentially allow for the biometric readability of the fingerprint post-analysis, provide adequate spatial and mass resolution, are capable of detecting both exogenous and endogenous compounds in addition to differentiating fingerprint ridges versus valleys. Another major area of fingerprint research presented in this thesis focuses on the development and validation of a chemically relevant artificial fingerprint, and artificial fingerprint material, the benefits of which are discussed in Chapter 4.

Section 1.5: Mass Spectrometry

Mass spectrometry has become commonplace in the field of forensic analysis due to its ability to be used as both a screening and confirmatory instrument capable of analyzing a wide range of compounds of forensic interest.[1] The work presented herein focuses on two classes of mass spectrometry, SIMS and AI-MS. The remainder of this chapter outlines each of these techniques and provides background on instrumental construction, ionization mechanisms, potential benefits and limitations, and general

considerations that must be taken in account in regards to both the analysis and sample type.

Section 1.6: A Background on Ambient Ionization Sources

Ambient ionization mass spectrometry (AI-MS) represents a class of newer mass spectrometry techniques that consist of a variety of different possible ionization sources.[36,37] AI-MS techniques allow for the desorption and ionization of samples under ambient conditions, using a probe. Once analyte molecules are successfully desorbed and ionized, they are transferred to the mass spectrometer, and analyzed. Probes that can be used in the desorption and ionization of the analyte include liquid droplets, gas streams or plasmas, thermal methods, lasers or other light sources, and acoustics. Ionization of the sample typically occurs after dissolution, if a liquid droplet probe is being used, or conversion in the gas phase. Once ionized, the analyte ions are transferred to the mass spectrometer and are typically aided by a potential difference in the sampling area which attracts positively or negatively charged ions towards the mass spectrometer inlet. Over traditional mass spectrometry based techniques such as GC-MS or HPLC-MS, benefits of AI-MS techniques include little to no sample preparation, rapid analysis times. Over other techniques like SIMS, AI-MS offers the capability of analyzing vacuum incompatible samples with minimal to no restrictions on sample size. The benefits of AI-MS for fingerprint and explosives analysis are that the sample can be rapidly interrogated with little to no sample preparation. There are now a large number of AI-MS sources.[37,38] In this work two liquid droplet based sources, desorption electrospray ionization (DESI) and desorption electro-flow focusing ionization (DEFFI), in addition to

two plasma based techniques, direct analysis in real time (DART) and low temperature plasma (LTP) are used. In this research, the DEFFI, DESI and LTP sources were all interfaced to an AB Sciex (Framingham, MA, USA) 4000 QTRAP hybrid triple quadrupole / linear ion trap mass spectrometer, whereas the DART was interfaced to a JEOL (Toyko, Japan) AccuTOF™ time of flight mass analyzer. Discussion of the mass analyzers is not presented here, but can be found elsewhere.[39–42] A table outlining the different ionization sources used in this work as well as their common applications is presented in Table 1.1.

Table 1.1 Cross comparison of the various AI-MS techniques used in this work.

	DART	**DESI**	**DEFFI**	**LTP**
Desorption Mechanism	Thermal / Gas Phase	Solution	Solution	Gas Phase
Orientation relative to interface	On-axis	Off-axis	Off-axis	Off-axis
Year of development	2005	2004	2013	2008
Analysis of explosives	Well established	Well established	Demonstrated	Demonstrated
Analysis of narcotics	Well established	Well established	Demonstrated	Demonstrated
Imaging capabilities	No	Yes	Yes	Yes
Current deployment in forensic laboratories	Yes	No	No	No
Other sample types analyzed	Biomolecules, chemical warfare agents, pesticides, polymers, food	Biomolecules, chemical warfare agents, pesticides, textiles, proteins, metabolites	Biomolecules	Food safety, pharmaceuticals, biomedical

Subsection 1.6.1: Direct Analysis in Real Time

DART is combination thermal desorption gas phase ionization technique that was developed and published by Cody *et al* in 2005.[43] The source itself is composed of three separate chambers, as shown in the schematic in Figure 1.1. In the first chamber, a gas is fed, at approximately 2 L/min, through a needle electrode that has an applied voltage of 2 kV to 4 kV. The applied voltage on the needle causes the formation of a corona-to-glow discharge plasma, creating both gas phase ions and excited state gas atoms.[44,45] Typically, helium is used as the carrier gas, though nitrogen and argon can also be employed. The second chamber is separated from previous and subsequent chambers by perforated disk electrodes, the first of which is grounded and the second of which has several hundred volts applied.[45] The perforated disc electrode at the leading edge of the second chamber, with the applied voltage, is used to remove gas phase ions. The gas then enters the third chamber where it can be variably heated, up to 500 °C. Before exiting the source, the gas stream passes through a third grid electrode that removes remaining gas phase ions and electrons. By doing this, the only gas atoms that are exiting the source are neutral or metastable atoms. The grid electrode has additional functions, that include acting as an ion repeller to remove any ions that formed because of ion-ion recombination and to produce electrons if desired.[45]

Ionization via the DART source is believed to follow differing pathways depending on the polarity of the ion and is believed to occur after the sample (*M*) is thermal desorbed into the gas phase (eq. 1.1). The formation of positively charged ions is believed to begin when a metastable helium atom interacts with a water molecule, producing a radical water molecule that reacts with other water molecules creating a

charged water cluster (eq. 1.2).[45] The charged water cluster then interacts with an analyte molecule and completes charge transfer in the gas phase, as shown below (eq. 1.3).[46]

$$M_{(s)} \xrightarrow{heat} M_{(g)} \qquad \textit{(eq. 1.1)}$$

$$He^*_{(g)} + nH_2O_{(g)} \rightarrow He_{(g)} + (H_2O)_{n-1}H^+_{(g)} + OH^-_{(g)} \quad \textit{(eq. 1.2)}$$

$$(H_2O)_mH^+_{(g)} + M_{(g)} \rightarrow M(H_2O)_{m-1}H^+_{(g)} + H_2O_{(g)} \xrightarrow{-(m-1)H_2O} MH^+_{(g)} \quad \textit{(eq. 1.3)}$$

The formation of negative ions occurs by the interaction of the metastable helium atoms with the grid electrode. Bombardment of the metastable atoms releases electrons from the grid electrode that are slowed in the gas stream and react with oxygen in the atmosphere (eq 1.5 and 1.6).[47] The oxygen ions then react with analyte molecules via charge transfer to create analyte ions (eq 1.7). Deprotonation from dissociation can also occur (eq. 1.8).[45] Like other ionization sources, dopant ions (*X*) can be incorporated into the gas stream to encourage adduct formation, which can greatly enhance the signal of the specific analyte molecules (eq 1.9).[45] One example is the incorporation of methylene chloride into the gas stream to create chloride adducts of common explosives, such as RDX and HMX.

$$He^*_{(g)} + surface \rightarrow He_{(g)} + surface + e^- \qquad \textit{(eq. 1.5)}$$

$$e^- + O_{2(g)} \rightarrow O_2^-{}_{(g)} \qquad \textit{(eq. 1.6)}$$

$$M_{(g)} + O_2^-{}_{(g)} \rightarrow [M + O_2]^{-\bullet}_{(g)} \rightarrow M^{-\bullet}_{(g)} + O_{2(g)} \quad \textit{(eq 1.7)}$$

$$MH_{(g)} \rightarrow [M\text{-}H]^-_{(g)} + H^+_{(g)} \qquad \textit{(eq 1.8)}$$

$$M_{(g)} + X^-_{(g)} \rightarrow [M+X]^-_{(g)} \qquad \textit{(eq 1.9)}$$

The major difference in the setup of the DART source compared to the other ionization sources used in this work is that DART is operated in transmission mode instead of off-axis mode. Transmission mode allows for the gas stream to be aligned on-axis with the mass spectrometer inlet as the sample is introduced, typically on glass microcapillary or other sampling device, by placing it near the outer edge of the gas stream. While an off-axis mode of DART is commercially available, in which the gas stream is oriented at approximately 45 ° from normal and the stream bounces off of a sampling surface and then into the mass spectrometer inlet, it has not been shown to have the sensitivity of transmission mode DART and was not available for this work. Optimization of methods for analysis by DART requires a number of different parameters to be altered. These include: gas flow rate, needle voltage, gas stream temperature, and the incorporation of a dopant ion. The effects of these parameters are discussed in subsequent chapters.

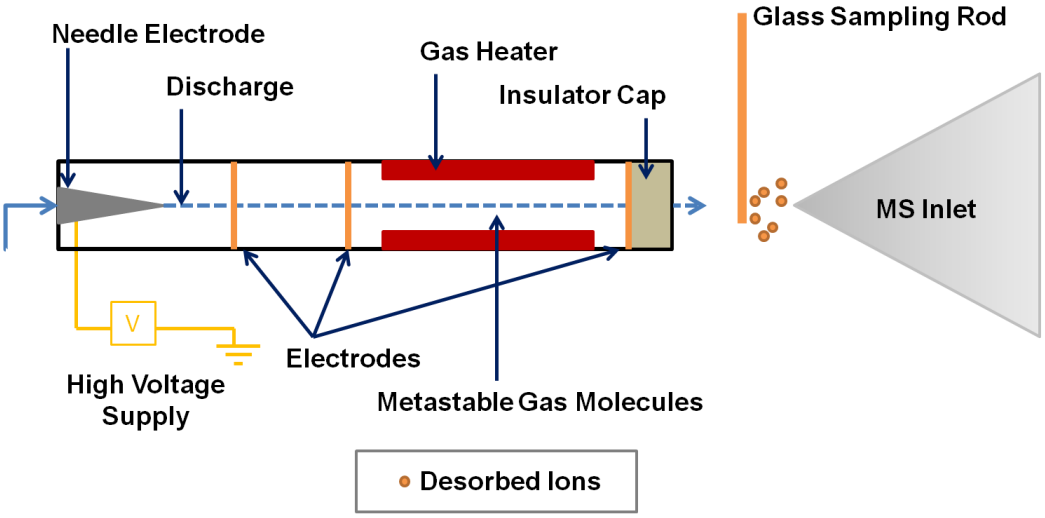

Figure 1.1 A schematic of a typical DART ionization source.

Subsection 1.6.2: Desorption Electrospray Ionization

DESI is an ionization source that was first developed by R. G. Cooks and is based on a variant of electrospray ionization, where a pneumatically assisted electrospray impinges on a surface to be analyzed.[37] The DESI source is comprised of a high voltage line, a source gas line, a solvent microcapillary, and a spray emitter tip. The emitter tip, located in the source, is where the solvent spray is pushed through and is also where the high voltage, typically 1 kV to 5 kV, is applied, causing charged droplets to be created. [48] These charged droplets are propelled towards the sample by the source spray gas, typically at 400 kPa to 800 kPa, that flows around the emitter tip, producing a spray of charged micro droplets. A schematic of a typical DESI source is shown in Figure 1.2. Ionization of the sample occurs in several steps. The first step involves the dissolution of the analyte (*M*) by solvent (*S*) molecules as the DESI spray interacts with the surface (eq. 1.10).[24] Upon dissolution, it is possible for ions to be formed via charge transfer from the spray microdroplets (eq. 1.11).[49] Once dissolved and ionized, repeated bombardment by the solvent spray forces ejection of secondary charged liquid drops of solvent containing analyte that decrease in size as they evaporate while being pulled into the inlet of the mass spectrometer. This desolvation the results in removal of solvent molecules from the analyte ions by the time the secondary droplet reaches the mass spectrometer (eq. 1.12)[50]. Transmission into the mass spectrometer is aided by the mass spectrometer inlet plate and ion transfer tube being held at a potential, typically ± 500 V.

$$M_{(s)} + nS_{(l)} \rightarrow [M+nS]_{(l)} \qquad \textit{(eq. 1.10)}$$

$$[M+nS]_{(l)} + S^{\pm}_{(l)} \rightarrow [M+nS]^{\pm}_{(l)} + S_{(l)} \qquad \textit{(eq. 1.11)}$$

$$[M+nS]^{\pm}_{(l)} \xrightarrow{-nS} M^{\pm}_{(g)} \qquad (eq.\ 1.12)$$

Ionization in DESI is believed, in general, to follow one of two ionization mechanisms. For low molecular weight compounds, such as narcotics and explosives, ionization is believed to be caused by the charge transfer of an electron or proton.[49] The charge transfer can occur between a solvent ion and an analyte on the surface of a droplet, between a gas phase ion and an analyte on the surface, or between a gas phase ion and a gas phase analyte molecule.[51] The first case, charge transfer between a solvent ion and analyte on the surface, occurs most frequently. For larger molecular weight compounds, such as proteins, multiply charged ions are often observed, which is consistent with multiple charge transfers from solvent ions to the analyte post-desorption.[48] Detection of analyte molecules can be aided with the addition of a small amount of pre-formed ions into the DESI solvent spray. Inorganic salts, or strong acids, have been shown to greatly increase the signal of difficult to detect analytes by providing species in the solvent spray to react or adduct with.[17]

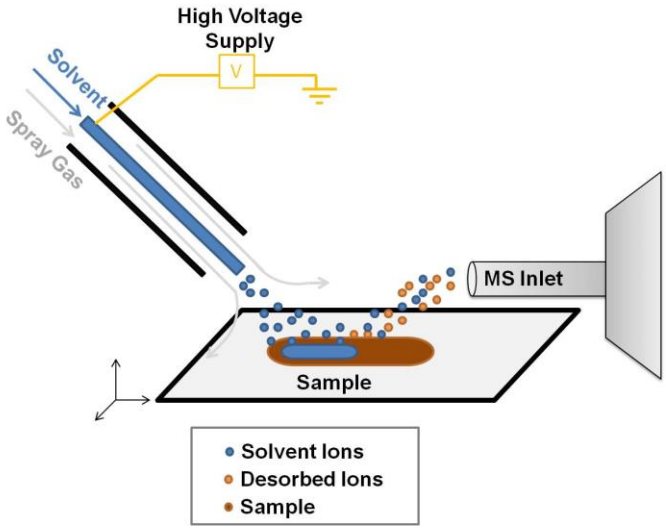

Figure 1.2 A schematic of a DESI ionization source.

With the DESI setup, there are many parameters that can be modified to achieve the greatest signal to noise ratio. Some of these parameters include: solvent composition, solvent flow rate, incidence angle, gas flow rate, and distance between the source and the sample.[24,37,48] These parameters each play crucial roles in obtaining optimal signal, and are dependent upon both one another, as well as the analyte of interest. Further discussion of the effects of these parameters is presented in Chapter 3.

One of the potential benefits to DESI is the fact that it does have imaging capabilities. Spatial resolution for imaging DESI has been reported as low as 35 μm.[37,52] There are some limitations to imaging with DESI and they include the dispersion of the spray when it interacts with the sample, and obtaining a small enough spot size to produce spatially resolved details within an image. As a comparison, SIMS has a spatial resolution of as low as 100 nm depending on configuration and sample type. Ionization efficiency may also be an issue with imaging, depending on the compound(s) of interest.[37] Nevertheless, studies have been completed that highlight that imaging a fingerprint using this technique is possible.[34,53] DESI has also been shown to image other samples, including medical tissue, pharmaceuticals, and illicit drugs.[37]

Subsection 1.6.3: Desorption Electro-Flow Focusing Ionization

Desorption electro-flow focusing ionization (DEFFI) is an ionization technique first interfaced to a mass spectrometer by Dr. Thomas Forbes at NIST and based off of the work of Dr. Alfonso Ganan-Calvo of the University of Seville, who created and commercialized electro-flow focusing.[54–57] DEFFI can be seen as a variant of DESI, with the major differences between the DESI and the DEFFI source being that the spray of the

DEFFI is focused using a small orifice at the tip of the source and that the electric field in the DEFFI setup is contained within the source. Within the DEFFI source there is a recessed solvent capillary to which a voltage is applied, as well as a gas inlet, a schematic of which is shown in Figure 1.3. The concentric gas stream and the solvent spray interact within the source, allowing the solvent spray to be focused prior to exiting the source. This is unlike DESI, where there is no focusing of the solvent spray. Another difference between DESI and DEFFI is that the DEFFI source contains a grounded orifice that confines the electric field. Confining the electric field inside the source allows for the production of a corona discharge to occur within the area between the charged solvent and grounded orifice electrode at applied potentials as low as several hundred volts.[55] The corona discharge allows for the production of dissolved nitrate ions in the solvent gas stream that can aid in the detection of certain analytes that will readily bind with anions. Solvents used in DEFFI, like DESI, typically consist of a combination of water, methanol, and/or acetonitrile.

Carrier gas pressures used in the DEFFI are typically around 130 kPa, which is significantly lower than that of DESI. The low voltage and low gas pressure is also accompanied by a low solvent flow rate (typically 1 µL/min – 10 µL/min). DEFFI has been shown to be able to detect a number of explosives and narcotics, at levels comparable to that of other AI-MS sources.[54]

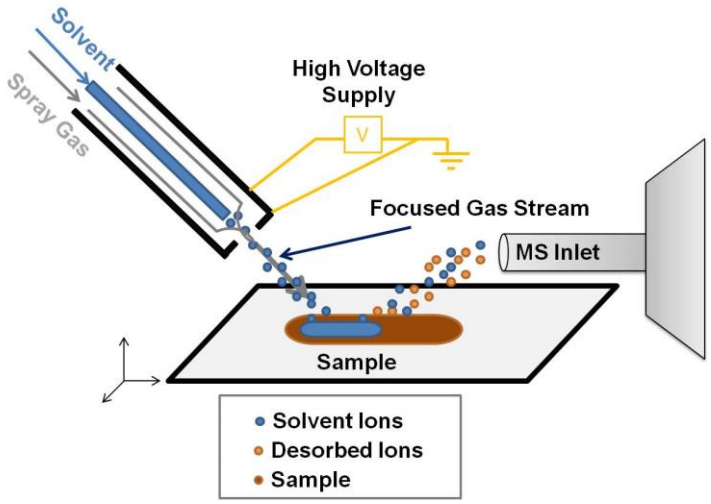

Figure 1.3 A schematic of a typical DEFFI ionization source.

Ionization via DEFFI has not yet been rigorously studied but is believed to be carried out in a method similar to that of DESI. The analyte molecules are likely dissolved and ionized by the solvent spray and then ejected via subsequent bombardment by spray droplets. Also the parameters that affect the analyte ion signal are similar to those of DESI. Spray gas backpressure, solvent flow rate, applied potential, incidence angle, and distances all play crucial roles in obtaining optimal signal.

There are a number of advantages and disadvantages for the use of the DEFFI source over the DESI source, the biggest being the ability to operate DEFFI at gas pressures and applied voltages significantly lower than those of DESI. If the source is being used on a field deployable instrument, this would allow for less consumption of electricity and require less source gas. Alternatively, if the source was being used in a large scale screening operation, this would lead to lower operating costs, when compared to DESI. Additional benefits of the DEFFI source include nitrate ion formation, to help produce adducts with certain molecules without having to incorporate a dopant into the

solvent stream, a wide stable operating range of applied voltages, and the ability to ionize via electrospray-like droplet charging as well as corona discharge chemical ionization from the same source. The main disadvantages to the DEFFI source, when compared to the DESI source, include trouble maintaining spray stability with low surface tension solvents such as pure methanol or acetonitrile and the difficulty in repairing the source if it becomes damaged or clogged.

Subsection 1.6.4: Low Temperature Plasma

Another category of AI-MS techniques involves the use of purely gas phase ions and a gas stream for ionization and desorption, instead of charged liquid droplets. This class of AI-MS techniques includes sources such as LTP. The LTP source utilizes an AC electric field, several thousand volts at several thousand Hertz, to produce a dielectric barrier discharge in a flowing gas stream, typically He or N_2 at several hundred millimeters per minute.[67] The unheated plasma is then allowed to interact directly with the sample.[64] The setup is such that the gas stream is pushed through a tapered glass capillary that has an inner electrode, and an outer electrode. The outer electrode is typically copper tape applied directly to the glass capillary. The glass acts as the dielectric barrier, and when the AC voltage is applied, the discharge is created which is extracted using the carrier gas. A pictorial representation of an LTP source is shown in Figure 1.4. Benefits of LTP sources include rapid production of both positive and negative ions in the afterglow and little damage to the surface. The technique is non-destructive enough that it can be used for analysis directly off of human skin.[67] The benefit to using an LTP source for analysis with fingerprints is that the lack of solvent or

heat diminishes the ability of dissolving the ridges of a fingerprint, potentially increasing the maintenance of the biometric information of the fingerprint. Many applications of LTP have been found and include explosives, detection of fatty acids, food science, and electronics.[64] To date, LTP analysis of fingerprints has not been completed.

Ionization of analyte molecules via the LTP source has been proposed to occur through the formation of He_2^+ dimers and reactions of those dimers with other species.[58] While He_2^+ is the dominant species within the plasma, it is believed that the dimer will react with atmospheric nitrogen in the afterglow region on the plasma producing N_2^+ ions.[58] This process can occur through both charge transfer and Penning ionization. The N_2^+ ion may further react with other atmospheric constituents and form additional ions, such as water clusters, similar to those formed through reaction with the helium metastable atoms in the DART gas stream.[59] These ions, present in the plasma afterglow, then transfer charge to the analyte molecule, that is desorbed by the high gas flow and carried into the mass spectrometer. This process is believed to occur for the production of positive ions. Penning ionization, in which the ionization of helium produces free electrons, is believed to be one potential mechanism for negative mode ionization, and is again similar to the DART ionization mechansim.[60] Some of the major parameters that must be optimized in this technique include: applied voltage, applied frequency, gas flow rate, incidence angle, and whether or not the sample is heated. The effects of some of these parameters are discussed in a Chapter 3.

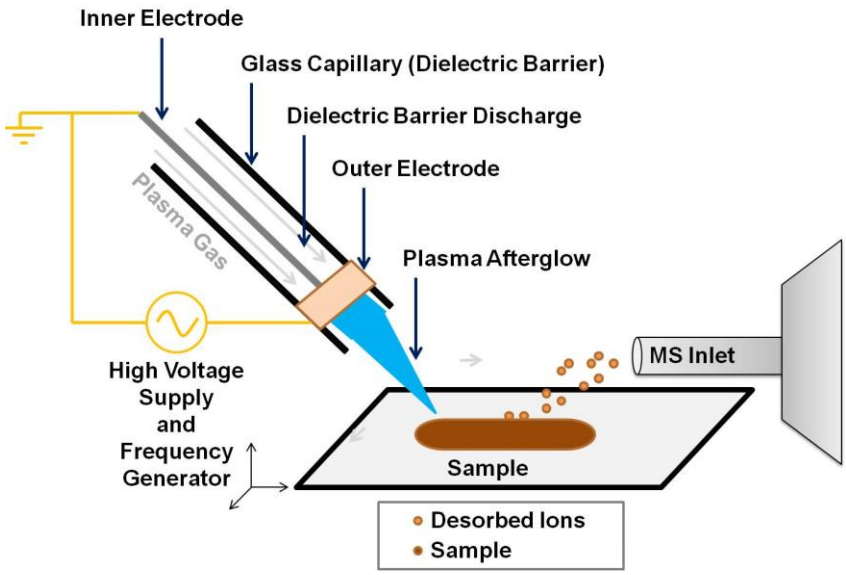

Figure 1.4 A schematic of a typical LTP ionization source.

Section 1.7: A Background on Secondary Ion Mass Spectrometry

SIMS is an ultra-high vacuum mass spectrometry technique known for its surface sensitivity. SIMS is based on the use of an energetic primary ion beam that is accelerated towards a sample. The impact of the ion results in the formation of a collision cascade. If this collision cascade intersects the target surface and if a surface atom or molecule is given sufficient energy it can be desorbed or "sputtered" from the sample surface. A small fraction of the desorbed species will be ionized and it is these secondary ions that are then collected and analyzed via a mass spectrometer, as shown in Figure 1.5. The primary ion beam can be composed of a variety of different species. Traditionally, SIMS ion sources include liquid metal (Ga^+, In^+, Bi_n^+), cold cathode duoplasmatrons (Ar^+, O_2^+), and field ionization sources (Cs^+). More recent research has focused on the implementation of cluster sources such as fullerene C_{60}^+ or large gaseous argon clusters (Ar_n^+ where *n* is several thousand). These new cluster sources have several benefits over

monatomic sources, the most crucial of which is lower penetration into the sample due to a partitioning of energy per primary atom after collision with the surface. The deposition of energy closer to the surface results in a higher sputtered volume, providing the capability for molecular depth profiling or sustained (high ion dose) desorption from organic surfaces with minimal sample degradation. Furthermore, higher deposition of energy near the surface results in the desorption of larger molecular species that contain higher mass chemical information.

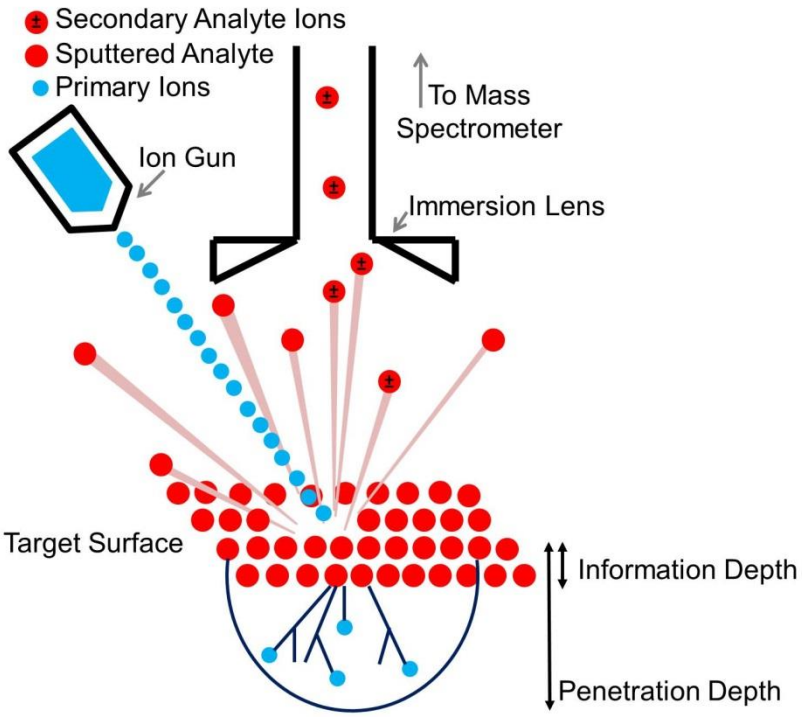

Figure 1.5 A pictorial representation of how sputtering and ionization occurs in a SIMS instrument.

Once ionization of the primary species is completed, typically via electron impact of gaseous primary molecules, ions are accelerated through a primary ion column. The primary column is composed of a series of deflector plates, lenses, and apertures that are

used to focus the primary ion beam into a spot with a diameter ranging from sub-micrometer to several hundred micrometers depending on the primary ion source and the capabilities of the optics. The primary ion column is oriented such that it is anywhere from normal to sixty degrees from normal with respect to the sample surface. A detector can also be located on the primary ion column so that the primary ion current can be measured. Once the primary ions exit the primary column, they bombard the sample to produce secondary ions. These secondary ions are ejected from the sample, which is commonly held at high potential, and guided through the extraction lens, the first of which is held at ground. If the sample is insulating, charging may occur, in which case an auxiliary electron gun may be used to help neutralize the charge. The secondary ions, once extracted, can then be sent through a series of focusing lenses before being accelerated through the mass spectrometer.

In a SIMS analysis there are two types of analysis modes, static and dynamic. In static SIMS, the goal of the analysis is to minimize damage to the sample surface by preventing the majority of the sample from being impacted more than one time. In order to do so, a low primary ion dose must be utilized, typically below 10^{12} ions/cm^2 or 10^{13} ions/cm^2. By keeping the ion dose low, it is possible to obtain information about the sample surface, as well as to prevent fragmentation of large organic molecules. In contrast, dynamic SIMS is used to obtain bulk analysis of a sample by maximizing ion dose which will increase the secondary ion yield. Maximizing the primary ion dose will allow for rapid erosion of the sample, and can increase sensitivity for bulk impurities under the right operating conditions.

In addition to operating in two different analytical modes, SIMS techniques can also be equipped with two different analysis beam setups, single beam and dual beam. With a single beam instrument, the primary analysis beam is operated in direct current mode and is used for both sample interrogation and erosion. The benefit to using a single beam, which is typically found on magnetic sector instruments and some time-of-flight (TOF) instruments, is that it allows for continuous sputtering and ionization of the sample and is well suited for depth profiling. Depth profiling allows a sample to be interrogated and eroded monolayer by monolayer to obtain a profile of composition versus depth of penetration with nanometer depth resolution. In contrast, a dual beam instrument contains a primary ion analysis beam and a separate sputtering beam that operate in tandem. This type of technique utilizes alternate pulsing of the primary ion beam and the sputtering beam to allow for analysis of several monolayers at a time with the sample being "cleaned" by the sputter beam in between analysis layers. This allows for removal of damage caused by the primary analysis beam. The pulsed nature of dual beam analysis makes it well suited for coupling with a TOF mass spectrometer.

Two types of SIMS instruments were used in this work, a Cameca IMS 4f (Cameca, Instruments, Genneviller Cedex, France), which is a magnetic sector dynamic SIMS instrument, and an IonTof IV (IonTof, Munster, Germany), which is a dual beam SIMS instrument but with the relevant samples was analyzed in the static regime. The Cameca IMS 4f was equipped with an IonOptika (IonOptika Ltd, Hampshire, England) C_{60}^{+} ion source.[61,62] The Cameca is unique in that it can be used either as a microprobe or as an ion microscope, as the spatial location of ejected secondary ions is maintained throughout the mass filtering process analysis. The mass spectrometer is a double

focusing magnetic sector (DFMS) mass spectrometer, with a mass range of 0 *m/z* – 1200 *m/z*. Spectra are collected via the electron multiplier or faraday cup, depending upon signal strength. Imaging can be completed using the electron multiplier, the micro channel imaging plate, or the resistive anode encoder.

The second SIMS instrument used in this work was an IONTOF IV (ION-TOF GmbH, Munster, Germany) dual beam SIMS instrument equipped with a bismuth primary ion source, a sulfur hexafluoride sputter source, and a TOF mass spectrometer. The focusing of the bismuth is much tighter than the C_{60} beam in the 4f, and, therefore, a much higher image resolution can be obtained. The rapid scan rate of the TOF, coupled with automated stage motions, make this technique ideal for rapid mass spectral imaging.

The reason SIMS was chosen as one of the techniques was because of its surface sensitivity, low detection limits, ability to analyze both elemental and molecular species, relatively high spatial resolution, and potential for molecular depth profiling. By combining SIMS and the C_{60}^{+} source, the depth of penetration of the primary ion beam can be less than 100 Å, imparting minimal damage to the sample.[62] SIMS is also used as a chemical imaging microscope, allowing for the imaging of different fingerprint components with a lateral resolution of approximately 1 µm, which is significantly better than the lateral resolution achieved using other imaging mass spectrometers.[63]

Chapter 2: Method Optimization and Validation for the Analysis of Explosives and Extraction of Single Crystals from Fingerprints using Direct Analysis in Real Time Mass Spectrometry

Adapted From:

(1) Sisco, E.; Dake, J.; Bridge, C. *Forensic Sci. Int.* **2013**, *232*, 160–168.

(2) Clemons, K.; Dake, J.; Sisco, E.; Verbeck, G. *Forensic Sci. Int.* **2013**, *231*, 98–101.

Direct analysis in real time (DART) is the only ambient ionization source which has begun to gain widespread popularity amongst forensic labs across the country as it is seen as the next generation for rapid screening of casework, especially narcotics and explosives.[64–67] The popularity which DART has seen is likely due to a combination of its commercial availability, robustness, and acceptance into the justice system of several states. This chapter explores potential applications of direct analysis in real time mass spectrometry (DART-MS) for analysis of forensic trace residues by first presenting a validation of the technique for analysis of explosives in both negative and positive ionization modes in Sections 1 through 7, followed by a proof of concept for detection of explosives in post-blast residue in Section 8, and finally a proof-of-concept demonstration for the analysis of single crystals in a fingerprint using Direct Analyte-Probed Nanoextraction (DAPNe) coupled to DART-MS in Sections 9 and 10.

The focus of this chapter is the development of screening method for the analysis of trace explosives to be incorporated into a traditional analysis scheme at the Defense

Forensic Science Center (DFSC). In order for a method to be accepted into routine casework, it must meet the demands set forth by the International Organization for Standardization (ISO) 17205 guidelines, which are the accreditation that forensic laboratories in the United States seek. Considerations that must be investigated and discussed in the course of method development include uncertainty measurements, limits of detections, selectivity, reproducibility, and robustness against an external influence.[68] Furthermore, method development should also address any sampling requirements, a positive check to ensure the method is working properly, and a statement of validity. The ISO 17025 guidelines also outline that calibration, comparison of the results with other validated laboratory methods, and a systematic assessment of parameters affecting the result, should be completed when possible.[68] Methods that were developed in this chapter follow this format. The only point that was not explored in this study was measurement uncertainty, since quantification was not pursued.

Section 2.1: Introduction

Screening techniques for the analysis of trace explosives are utilized in a wide range of situations including both laboratory and field based applications. While the necessary characteristics of a screening technique will vary based upon the specific situation, there are a number of benchmarks these techniques will have to be able to accomplish in all cases. A useful screening technique must be able to rapidly detect a number of possible compounds of interest with minimal or no sample preparation. The sensitivity of the screening technique should be equal to or exceed that of the confirmatory technique. Other qualities of a good screening technique include a high

level of accuracy and reproducibility, the ability to detect threats even in complex matrices, and the minimization of false alarms. One such technique that has exhibited all of these characteristics is DART-MS.

Even though DART-MS is a relatively new technique, it has already been applied to a number of different forensic specimens, including bank dye, inks, and illicit drugs.[64–66,69] DART-MS has also been applied to the detection of counterfeit pharmaceuticals, identifying adulterants in food, and chemical warfare agents.[70–72] The application of this technique for the detection of explosives has been discussed;[16,67,73] however, prior to this work, little had been done in establishing a comprehensive method optimization that measures the sensitivity in the detection of explosives, as well as studies how it compares against currently employed techniques. Nilles *et al*[67] has shown that detection of a number of different explosives is possible using DART-MS. Furthermore, it was shown that detection of these compounds off of a number of surfaces, as well as detection in a number of different liquid samples can be accomplished.[67,73] Detection of trace explosives within latent fingerprints using DART-MS has also been discussed.[74] Some limits of detection have been reported, however they have included only a limited number of compounds.[43,74,75]

This chapter outlines the capabilities and limitations of DART-MS as a useful screening tool for the analysis of trace explosives. Topics that are discussed for both nitro and peroxide based explosives include method optimization, method reproducibility, limits of detection, construction of a search library, analysis of mixtures, and blind sampling. Additional work is shown to prove the capability to analyze "real world" post-blast samples in the negative ionization mode. In all, twenty-four explosives

were analyzed, two peroxide-based explosives and twenty-two nitro based explosives. Also discussed in this chapter is the development and implementation of calibration compounds, outside of the traditional polyethylene glycol (PEG) generally employed in DART analysis.

Another technique explored in this chapter is DAPNe. DAPNe allows for the extraction of single crystals out of a complex matrix, such as a fingerprint. The benefit of DAPNe is that it manages to alleviate the primary issues that arise with other sampling methods, namely matrix effects and sample destruction.[76–78] Traditionally coupled to nanoelectrospray ionization mass spectrometry (NSI-MS), this technique has displayed its value in trace analysis with extraction of illicit drugs from fibers[76], electro-static lifts[78], and within fingerprints.[77] Developed by Verbeck *et al*, the DAPNe setup consists of a nanomanipulator mounted to the stage of a bright-field microscope. The nanomanipulator contains a capillary tip with a conductive coating which can be directed to a particle of interest sub-micron translational resolution. Additionally, this method is minimally invasive and leaves latent fingerprints virtually unchanged, allowing the ridge detail to be preserved for identification purposes. Further discussion of this technique is presented in Section 9.

Section 2.2: Materials and Methods

Subsection 2.2.1: Solvents, Standards, and Sampling Materials

All of the explosives used were purchased as analytical standards from AccuStandard (New Haven, CT, USA) at initial concentrations of either 100 µg/mL or

1000 µg/mL in methanol, acetonitrile, or a solution of both. A list of the explosives that were analyzed and the abbreviations used to represent them throughout this chapter is presented in Table 2.1. Two commercially available mixtures were also used in this study – a 14 component high performance liquid chromatography (HPLC) mixture purchased from AccuStandard as well as a 6 component mixture that was purchased from ThermoScientific (Waltham, MA, USA). Serial dilutions of the individual explosives and the 14 component mixture were completed using methanol, purchased from Sigma-Aldrich (St. Louis, MO, USA).

Several different mass calibrants and independent quality assurance quality control (QA/QC) compounds were also required for this study. For the detection of nitro based explosives, the mass calibrants used were PEG 600 (Acros Organics, Geel, Belgium) and a series of saturated fatty acids (Supelco, Bellefonte, PA, USA). A mixture of glycol ethers was used as the mass calibrant for the peroxide explosives, with individual glycol ethers being purchased from AccuStandard. The independent QA/QC compounds that were used included oleic acid, purchased from Acros, and methyl decanoate, purchased from AccuStandard.

Glass microcapillaries were used to introduce the samples into the DART gas stream. The 90 mm closed capillaries were purchased from Corning Incorporated (Corning, NY, USA). Before analysis, the capillaries were introduced into the gas stream to burn off any contaminants that may be present on the rods. This was especially necessary for the positive ionization mode, where a signal due to dioctyl adipate from the plastic container the rods were stored in was readily detectable on any uncleaned rods.

Table 2.1 Explosives, and their abbreviations, used in the optimization studies.

Explosive	Abbreviation
Nitroaromatics	
Trinitrotoluene	TNT
2,4-Dinitrotoluene	2,4-DNT
2,6-Dinitrotoluene	2,6-DNT
Tetryl	Tetryl
2,6-Bis(picrylamino)-3,5-Dinitropyridine	PYX
Ammonium Picrate	AP
Picric Acid	PA
Nitrobenzene	NB
1,3-Dinitrobenzene	1,3-DNB
1,3,5-Dinitrobenzene	1,3,5-TNB
2-Nitrotoluene	2-NT
3-Nitrotoluene	3-NT
4-Nitrotoluene	4-NT
2-Amino-4,6-Dinitrotoluene	2-A-4,6-DNT
4-Amino-2,6-Dinitrotoluene	4-A-2,6-DNT
Nitramines	
Cyclotrimethylenetrinitramine	RDX
Cyclotetramethylenetetranitramine	HMX
Nitrate Esters	
Nitroglycerin	NG
Ethylene Glycol Dinitrate	EGDN
Diethylene Glycol Dinitrate	DEGDN
Pentaerythritol Tetranitrate	PETN
Erythritol Tetranitrate	ETN
Peroxides	
Triacetone Triperoxide	TATP
Hexamethylene Triperoxide Diamine	HMTD

Subsection 2.2.2: Development of Mass Calibration Mixtures

During the validation study it was found that the traditional mass calibration compound, PEG 600, responded poorly in the sub 150 *m/z* mass region, as well as at the lower temperatures and voltages required to analyze peroxide explosives. Therefore, it

was necessary to develop new mass calibration mixtures. To aid in the calibration of the low mass range for negative mode, a fatty acid mixture was used. The fatty acid mixture contained approximately 100 µg each of hexanoic acid, octanoic acid, decanoic, acid, dodecanoic acid, tetradecanoic acid, hexadecanoic acid, octadecanoic acid, eicosanoic acid, docosanoic acid, and tetracosanoic acid, dissolved in 2 mL of hexane, to give a solution concentration of approximately 50 µg fatty acid per mL. A tunable mass range of 100 *m/z* – 600 *m/z* was obtained by monitoring the $[M-H]^-$, $[M+O_2-H]^-$, and $[2M-H]^-$ ions of each fatty acid.

For the peroxide explosives it was necessary to have a calibration material that responded well in the positive ionization mode, at a low mass range, low temperature, and low orifice voltage. It was determined that a mixture of glycol ethers provided the desired characteristics. The mixture was developed to calibrate a mass range, of 75 *m/z* – 380 *m/z*, which encompassed all of the peaks identified for the peroxide explosives. Nine glycol ethers were chosen and included: 2-methoxyethanol, di(ethyleneglycol)methyl ether, 2-ethoxyethanol, 2-hexoxyethanol, 2-(2-n-hexoxy)-ethanol, 2(2-butoxyethoxy)ethanol, and 2(phenoxyethanol). The mixture was made by diluting 50 µL of each of the nine neat glycol ethers in 1,650 µL of methanol, giving a final solution concentration of approximately 30 µg glycol ether per mL. Using this mixture, the calibration points included protonated ions $[M+H]^+$ as well as the protonated dimers $[2M+H]^+$ for each glycol ether. Both of these mass calibration mixtures provided more than the necessary number of peaks for calibration, as well as producing calibration correlation coefficients lower than 1×10^{-12}. Both mixtures were also cross compared to

PEG 600 under conditions in which both calibrants had sufficient signal to verify mass accuracy to ensure calibration was identical regardless of which mass calibrant was used.

Subsection 2.2.3: Parameters for the AccuTOF™-DART

Two individual methods were developed for the detection of different explosives. One method was developed in negative ion detection mode for explosives containing nitro groups while the second method was developed for positive ion detection of peroxide explosives. The instrument that was used in the study was a JEOL (Toyko, Japan) AccuTOF™ mass spectrometer (JMS-T100LC) coupled with an IonSense (Saugus, MA, USA) DART source. Within each method, three different parameters were varied in order to optimize the technique, the first of which was the orifice 1 voltage. The orifice 1 voltage provides a mechanism to control the amount of fragmentation that a molecule undergoes, with high orifice 1 voltages typically increasing fragmentation as gas molecules are provided more kinetic energy. A range of orifice 1 voltages from -10 V to -70 V was evaluated for the negative mode. Due to the fragility of the peroxide explosives, a range orifice 1 voltages from +5 V to +20 V was chosen for the positive mode. The second parameter that was altered was the gas stream temperature. Increasing the gas temperature increases desorption, although thermal decomposition may occur if the temperature is increased too far. In this study the gas temperature for negative mode was varied from 150 °C to 300 °C, while the temperature was altered from 100 °C to 200 °C for positive mode. The final parameter that can be altered is the addition of a dopant species to the gas stream. A dopant can work by providing a free ion for the formation of adduct ions via incorporation of dopant ions with the sample molecules or

by providing a mechanism to aid in ionization through other pathways.[45,47] Four dopants were tested in negative mode and included chloroform, methylene chloride, trifluoroacetic acid, and acetone. One dopant, ammonium hydroxide, was evaluated in positive mode.

To analyze the effects of these parameters in an orderly fashion, a matrix of different orifice 1 voltages and gas temperatures was first completed. Once an optimal voltage and temperature were chosen, the effects of dopant addition were studied. Optimization was based off of the response from TNT, RDX, and PETN for negative mode and TATP and HMTD for positive mode. In order to remove the greatest amount of background signal possible without losing necessary response peaks a mass range of 100 *m/z* – 600 *m/z* was monitored for negative mode, and a mass range of 60 *m/z* – 400 *m/z* was monitored for positive mode. All mass spectra were calibrated, background subtracted, and the peaks were centroided prior to evaluation.

A number of parameters relating to both the DART source and the AccuTOF™ mass analyzer were unchanged throughout the study. These parameters, which are highlighted in Table 2.2, include the use of ultra-pure helium was used as the ionizing gas with a flow rate of 1.75 L/min. For analysis in negative mode, the needle voltage was -3,000 V, the electrode 2 voltage was +200 V, and the grid electrode voltage was -225 V. Parameters of the mass spectrometer inlet included a varied orifice 1 voltage and an orifice 2 voltage of -5 V. The ring lens voltage was -3 V, and the detector voltage was set to +2,500 V. A peaks voltage of 600 V was also used. For analysis in the positive mode, needle, electrode 2, and grid electrode voltages were -3,000 V, +200 V, and +225 V respectively. The orifice 2 voltage was +5 V with a ring voltage of +10 V. A

peaks voltage of 500 V was used with a detector voltage of -2,500 V. In both instances the orifice 1 and gas stream temperature were varied. Figure 2.1 represents a schematic of the locations of the various voltages and parameters utilized in the DART source and mass spectrometer inlet.

Table 2.2 Operating parameters of the DART source and the TOF mass analyzer for negative ionization mode and positive ionization mode.

Source Parameters			Analyzer Parameters		
Parameter	**Negative Mode**	**Positive Mode**	**Parameter**	**Negative Mode**	**Positive Mode**
He Gas Flow	1.75 L/min	1.75 L/min	Orifice 1 Voltage	Varied -10 V → -70 V	Varied +5 V → +20 V
Needle Voltage	-3,000 V	+-,000 V	Ring Lens Voltage	-3 V	+10 V
Electrode 1	Grounded	Grounded	Orifice 2 Voltage	-5 V	+5 V
Electrode 2	+200 V	+200 V	Peaks Voltage	600 V	500 V
Grid Electrode	-200 V	+225 V	Detector Voltage	+2,500 V	-2,500 V
Gas Stream Temperature	Varied 150 °C → 300 °C	Varied 100 °C → 200 °C	Orifice 1 Temperature	100 °C	100 °C

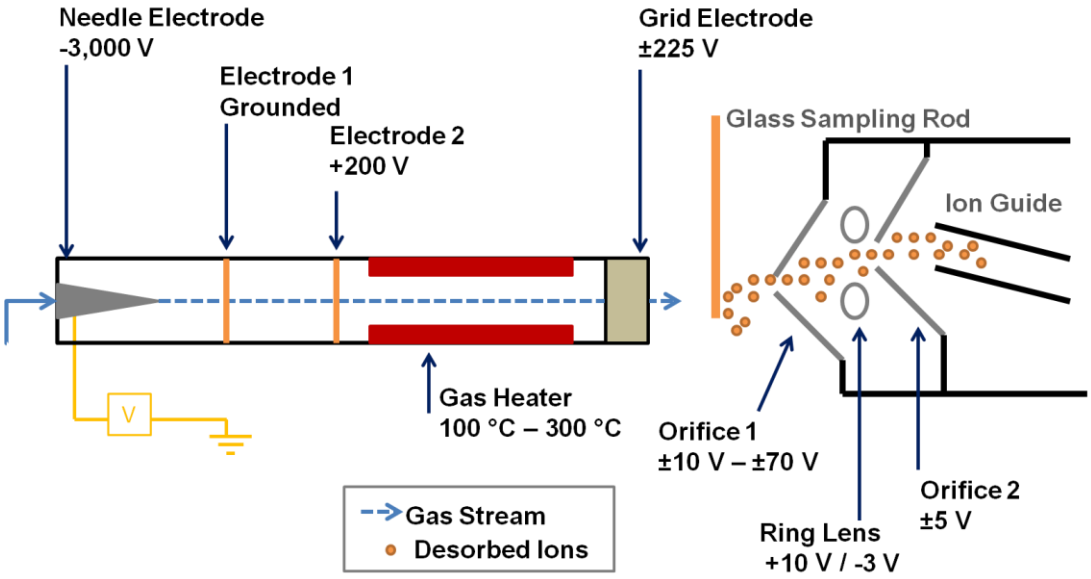

Figure 2.1 Schematic of DART source and mass spectrometer inlet parameters used for positive ionization and negative ionization mode respectively.

Subsection 2.2.4: GC-MS Methods

In order to compare the limits of detection for the DART-MS to current confirmatory techniques, explosives were also analyzed by gas chromatography mass spectrometry (GC-MS). The nitro explosives were analyzed in negative ionization mode by chemical ionization gas chromatography mass spectrometry (CI-GC-MS), using an Agilent 6890N gas chromatograph with a 5973 mass spectrometer (Santa Clara, CA, USA), while the peroxides were analyzed in positive ionization mode by electron impact gas chromatography mass spectrometry (EI-GC-MS), using an Agilent 7890A gas chromatograph with a 5975C mass spectrometer.

The CI-GC-MS method utilized a 15-m J&W Scientific 123-5012 DBS column (Agilent Technologies) with an outer diameter of 320 µm and a film thickness of 0.25 µm. Helium carrier gas was used at a flow rate of 3.0 L/min, with methane employed as the ionization gas. The inlet temperature was 175 ^{0}C with a 1 µL splitless injection. The oven was ramped from an initial temperature of 50 ^{0}C, which was held for 1 minute, to 220 ^{0}C at a rate of 20 ^{0}C/min. The oven was then held at 220 ^{0}C for 4 minutes. A mass range of 42 *m/z* – 350 *m/z* was scanned.

The EI-GC-MS method utilized a 30 m HP-5MS 5% Phenyl Methyl Siloxane column (Agilent Technologies) with a 250 µm outer diameter and a 0.25 µm film thickness. Hydrogen carrier gas was used at a flow rate of 0.045 L/min. A 1 µL splitless injection was introduced into the front inlet at 150 ^{0}C. The oven was ramped from an initial temperature of 50 ^{0}C to 200 ^{0}C at a rate of 10 ^{0}C/min, and then held at 200 ^{0}C for 20 minutes. A mass range of 15 *m/z* – 550 *m/z* was scanned.

Section 2.3 Effect of Altering DART Parameters

Subsection 2.3.1 Negative Mode Ionization

In order to evaluate the effects of different DART-MS parameters, three explosives, one representative of each class of nitro based explosive, were chosen. TNT was chosen as a representative nitroaromatic, RDX as a representative nitramine, and PETN as a representative nitrate ester. The first parameter that was analyzed was orifice 1 voltage. Of the orifice 1 voltages that were analyzed, -10 V, -30 V, and -50 V, did not show any differences in fragmentation patterns, however as the orifice voltage was increased in this range, up to a two-fold decrease in signal was observed in this range, as seen in Figure 2.2. When the orifice voltage was raised to -70 V increased fragmentation was seen; however, overall signal intensities were greatly diminished. Analysis was further complicated at -70 V as tuning was difficult because the mass calibration compounds were also heavily fragmented at this voltage. Voltage switching, in which alternating mass spectra are collected at different orifice voltages, between -10 V and -70 V was also attempted, however signal intensity dropped significantly compared to runs in which the voltage was not switched, likely due to increased dead time as the mass spectrometer must cycle the orifice voltages. Since the purpose of the study was to evaluate DART as a screening technique, the voltage that provided the greatest sensitivity, -10 V, was chosen.

The second parameter that was altered was the gas stream temperature. It was found that as the gas stream temperature was increased from 150 °C to 225 °C, the intensity of all three explosives increased. When the gas temperature was raised above

225 °C, the intensity of the peaks began to decrease, possibly due to thermal decomposition or because of an analyte desorption rate that was to rapid for the mass spectrometer to handle. The 75 ^{0}C increase in temperature, from 150 ^{0}C to 225 ^{0}C, provided up to a factor of five increase in the signal of the base peak. Figure 2.2 depicts the average signal of TNT obtained by altering gas stream temperature.

After evaluating the initial three explosives and expanding to the rest of the samples, it was found that two of the explosives tested, DEGDN and EGDN, responded poorly at 225 °C, but were more readily ionized at 125 °C. Up to a sixteen-fold increase in signal was observed for the detection of DEGDN by lowering the temperature, as shown in Figure 2.3. This is likely due to the small size and fragility of these two molecules, with thermal decomposition accelerated at the elevated temperatures. All other explosives showed maximum intensity at, or near, 225 °C.

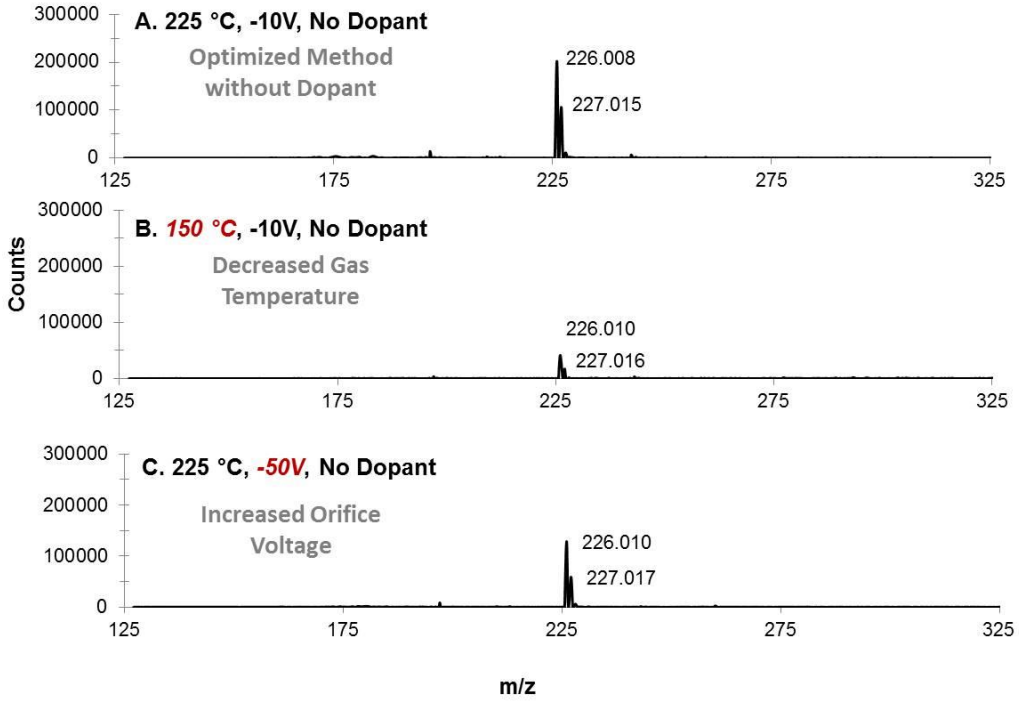

Figure 2.2 Effect of lowering the DART gas stream temperature (A. → B.) and increasing the orifice 1 voltage (A. → C.) on the response of TNT.

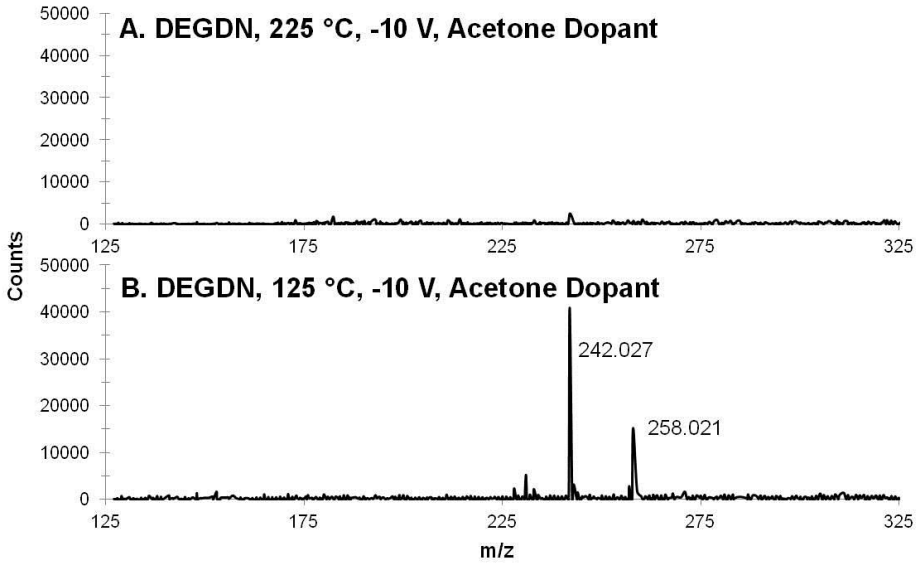

Figure 2.3 Response of DEGDN at a gas stream temperature of 225 °C (A.) and 125 °C (B.).

The final parameter that was analyzed was the addition of a dopant species into the gas stream. This was accomplished by using a capped GC-MS vial with a shortened melting point capillary tube pierced through the rubber septum, in order to steadily introduce only a small amount of the dopant species at a time. Additional methods of dopant introduction were attempted, however this method was found to produce the most consistent results, in addition to being one of the easiest methods to implement. The effects of four dopants were studied: acetone, chloroform, methylene chloride, and trifluoroacetic acid (TFA). The TFA dimer produced a strong background ion at 226.977 *m/z*, which fell in between two prominent TNT peaks (at 226 *m/z* and 227 *m/z* nominal mass), and was shown to hinder the detection of both peaks. Also, due to the proximity in mass between TFA and TNT, it could be possible that a poorly calibrated run using TFA as a dopant could incorrectly be mistaken for TNT. An example of the TFA background peak is shown in Figure 2.4. The chloride ion producing dopants, methylene chloride and chloroform, were shown to enhance the signal for both RDX and PETN, through adduct formation, however it decreased the signal of TNT and several other nitroaromatic explosives. No adduct ions for TNT and PETN were produced in the presence of either dopant. Acetone was shown to increase the signal intensity of nearly all explosives, even though it did not produce adduct ions.

Two separate operating parameters where developed to screen for nitro based explosives. A "high temperature" method was developed using a 225 °C gas stream temperature, a -10 V orifice 1 voltage, and an acetone dopant. This method allowed for detection of all but one of the nitro-containing explosives analyzed, EGDN. In order to screen for that explosive as well as to increase the sensitivity for DEGDN, a "low

temperature" method was also developed that was identical to the "high temperature" method, with the exception that the gas stream temperature was lowered to 125 °C.

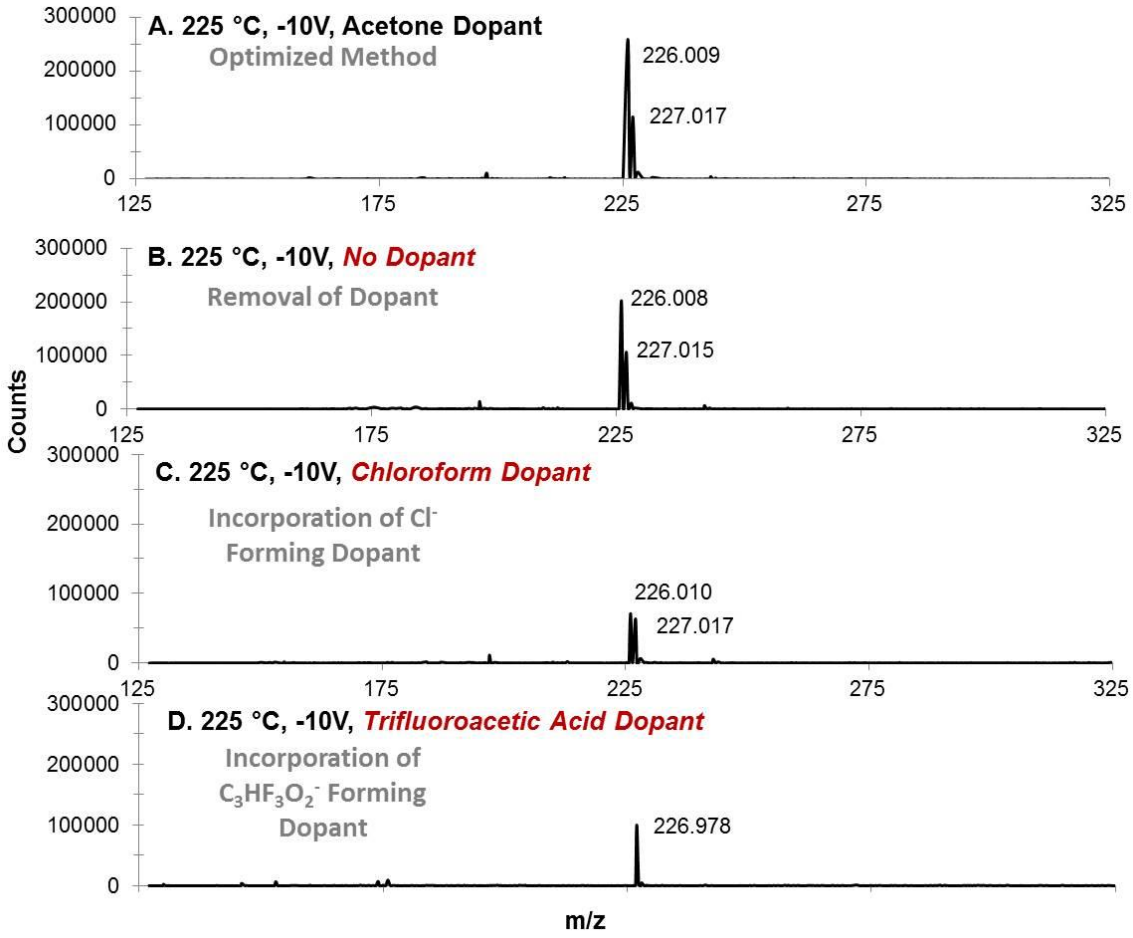

Figure 2.4 Response of TNT in the presence of several dopants. Dopants shown include acetone (A.), chloroform (C.), and trifluoroacetic acid (D.). The response of TNT in the absence of a dopant (B.) is also shown.

Subsection 2.4.1 Positive Mode Ionization

Since the peroxide based explosives readily produce positive ions, a positive ion detection method was also developed. The two peroxide explosives that were analyzed were TATP and HMTD. A glycol ether mixture was used as a mass calibrant, and

methyl decanoate was the independent QA/QC compound. When the method was optimized, it was found that maximum signal was achieved with a gas temperature of 125 °C, an orifice 1 voltage of +5 V, and no dopant was necessary. Increasing the gas stream temperature from 125 °C up to 200 °C provided a marginal decrease in the signal and increased variability in signal for both TATP and HMTD as thermal degradation likely increased. The largest decrease in signal occurred when ammonium hydroxide was introduced as a dopant. The signal for TATP was decreased by approximately a factor of four, while the signal of HMTD was decreased by approximately half. No additional fragmentation or adduct production was noted with the introduction of ammonium hydroxide. Figure 2.5 shows the average signal intensities of the base peak of TATP and HMTD under a number of different conditions.

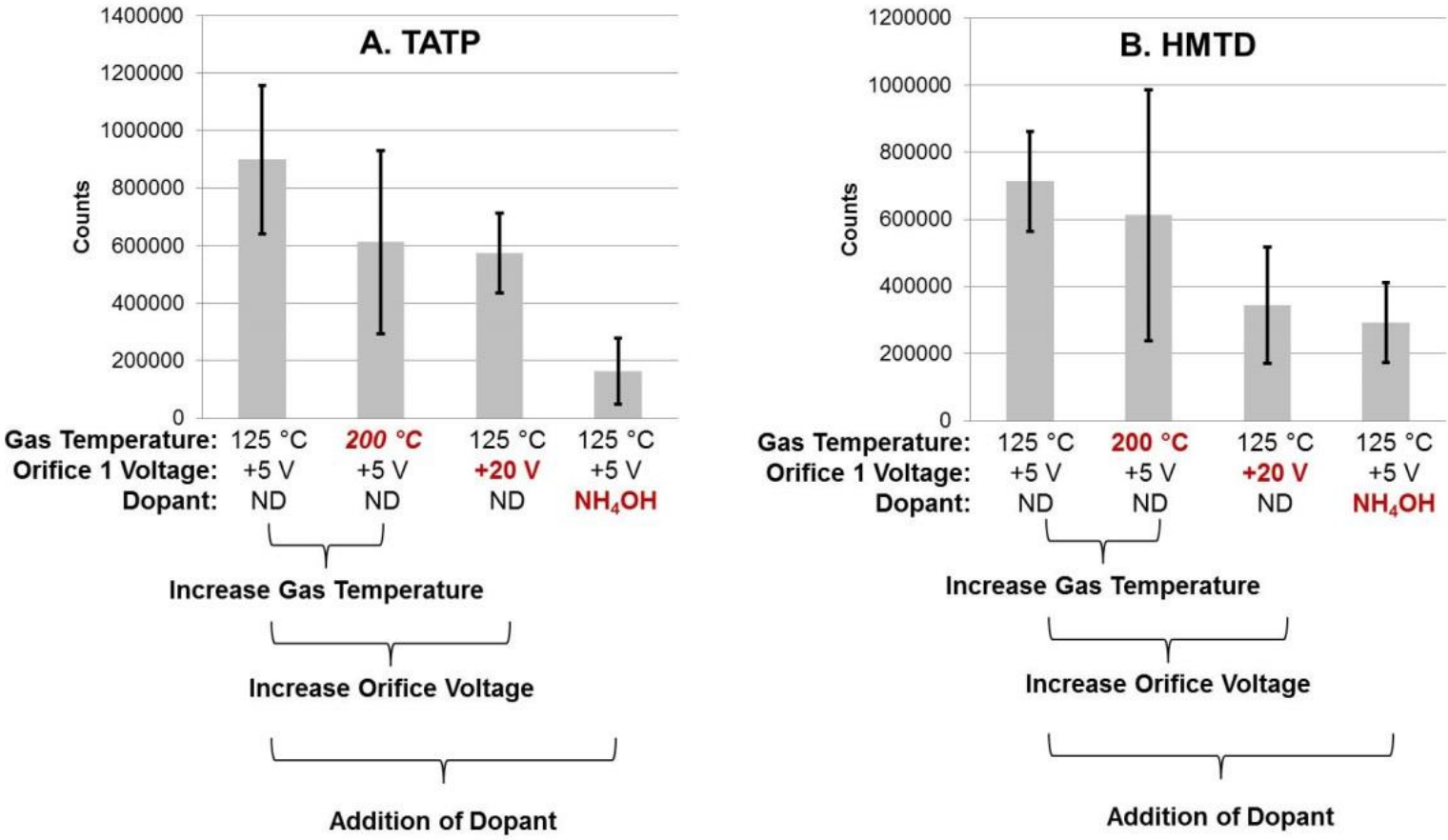

Figure 2.5 Spectral responses of TATP (A.) and HMTD (B.) under several different operating parameters. "ND" indicates that no dopant was used in that sample run. The parameter that is highlighted in red is the parameter altered from the optimized method (leftmost bar).

Section 2.4 Method Reproducibility

Subsection 2.4.1 Negative Mode Ionization

A study on the reproducibility of the method for the analysis of a number of explosives was also undertaken. Six different explosives, TNT, 2,6-DNT, PETN, DEGDN, RDX, and HMX, were analyzed to determine how reproducibly the system detected the peaks related to these explosives. To do so, the three most abundant peaks from each explosive were monitored to determine if the detected masses fell within ±0.005 Da of the theoretical masses. The ±0.005 Da tolerance was chosen based on mass analyzer manufacturer specifications for peak accuracy tolerance. Forty-eight replicates were completed, with eight runs being completed on six different sampling days. In addition to monitoring the three masses from each explosive, six masses from the calibration compound, and the mass of the independent QA/QC compound were also monitored. It was found that for the six explosives analyzed, there are 11 of 864 measured masses that do not fall within the ±0.005 Da tolerance from the theoretical mass. Of those eleven masses, 5 are associated with DEGDN, three are associated with HMX, two with PETN, and one is associated with 2,6-DNT, giving an overall explosives reproducibility of 98.7%. Oleic acid, the QA/QC compound, had an accurate mass in 100% of the measurements. The fatty acid mass calibrant mixture, in which six masses were monitored, contained 2 out of 96 missed masses. Overall, a percent accuracy of 98.8% is achieved.

Upon further analysis of the failed masses, it was found that there were two situations that caused the masses of the peaks to fall out of the tolerance range. The first situation occurred when a shoulder was present on the peak of interest. The presence of

the shoulder caused the center of the mass peak to shift when the spectrum was centroided. If the shoulder caused a large enough shift, the centroided peak was shown to fall outside of the acceptable mass range. The other situation that caused a peak to fall outside of the tolerable range occurred when the peak had both low intensity and poor resolution. It was found that the peaks without a shoulder that failed had an intensity of less than 1,000 counts and a mass resolution of less than 4,000. These two situations explained all but one of the masses which fell outside of the range.

Subsection 2.4.2 Positive Mode Ionization

A reproducibility study identical to that carried out for the negative mode was completed in the positive mode. The three most abundant peaks for both TATP and HMTD were monitored in addition to six peaks for the glycol ether mixture and one peak for methyl decanoate. With a ±0.005 Da tolerance, it was determined that all masses measured fell within the threshold limit, providing 100 % mass accuracy for the positive mode. The reason 100 % mass accuracy may have been achieved is due to the lower number masses analyzed (392 in positive mode versus 976 in negative mode), as well as overall higher abundance of the three most abundant peaks in TATP and HMTD, as compared to explosives like DEGDN and HMX, which repeatedly had low intensity responses.

Section 2.5 Limits of Detection

Subsection 2.5.1: Limit of Detection Determinations

Limit of detection determinations were completed by creating serial dilutions from the stock solutions of explosives. Each dilution was run in triplicate on the DART-MS, with 1 µL of sample being deposited onto a clean glass microcapillary via a microsyringe. A new microcapillary was used for every replicate to prevent concentration buildup on the rod with repeated analyses. The limit of detection was defined as the lowest amount of deposited explosive at which the signal was at least three times greater than the background levels for all three replicates. The peak that was required to be above background was one that was unique to that particular explosive. The nitrate peak was not monitored for limit of detection determinations as its signal does not provide useful discriminating information about the identity of the explosive, even though lower limits of detection could be accomplished through monitoring an increase in the nitrate signal. Furthermore, the presence of a nitro group does not provide sufficient information to consider it a presumptive test for an explosive, as many nitro containing compounds are not explosives.

Subsection 2.5.2 Negative Mode Ionization

The limit of detection was determined for the nitro explosives on DART-MS and compared to their limit of detection on CI-GC-MS. Table 2.3 represents the comparison of limits of detection between the two techniques. For thirteen of the twenty one explosives analyzed (PA was not included in the limit of detection measurements because of the lack of an analytical standard) the limit of detection was better on DART-MS than

on CI-GC-MS. Seven of the explosives, including 2,4-DNT and 2,6-DNT, had limits of detection on that were equal on both DART-MS and on CI-GC-MS. Additionally, using the "high temperature method" two explosives had limits of detection that were more sensitive on CI-GC-MS than on DART-MS – DEGDN and EGDN. DEGDN and EGDN have low boiling points and high vapor pressures, making detection via DART-MS difficult. Furthermore, the predominant fragment of both explosives is nitrate, which was not monitored in this instance. The limit of detection of both DEGDN and EDGN were determined using the "low temperature" method as well. The "low temperature" method allowed for a lower limit of detection for these two explosives, giving DART-MS increased sensitivity over CI-GC-MS for the detection of DEGDN. In the case of EGDN, DART-MS was not as sensitive as CI-GC-MS even at the lower temperature run.

Subsection 2.5.3 Positive Mode Ionization

The limits of detection for both TATP and HMTD were determined using the optimized method discussed in Section 2.5.1 and were compared to the limits of detection observed on the EI-GC-MS. For both TATP and HMTD, the limit of detection of the DART-MS method was determined to be 10 ng. An identical limit of detection was found for TATP on EI-GC-MS, while the HMTD was undetectable using this technique. These results, as well as those presented for the negative mode, illustrate the ability of DART to be an extremely useful screening technique for a number of explosives.

Table 2.3 Limits of detection via DART-MS and CI-GC-MS for characteristic explosives. An asterisk (*) indicates that the limit of detection was obtained using the "low temperature" DART-MS method. The number in red indicates the lower limit of detection between the two techniques.

Explosive	DART-MS LOD	CI-GC-MS LOD
TNT	**0.25 ng**	1.0 ng
2,4-DNT	0.50 ng	0.50 ng
2,6-DNT	0.50 ng	0.50 ng
1,3,5-TNB	0.50 ng	0.50 ng
2-A-4,6-DNT	**1.0 ng**	5.0 ng
4-A-2,6-DNT	**1.0 ng**	5.0 ng
2-NT	0.50 ng	0.50 ng
3-NT	0.50 ng	0.50 ng
4-NT	0.50 ng	0.50 ng
NB	0.50 ng	0.50 ng
1,3-DNB	**0.50 ng**	2.5 ng
PYX	**10 ng**	>100 ng
Tetryl	**1.0 ng**	5.0 ng
AP	**50 ng**	>100 ng
RDX	**0.50 ng**	25 ng
HMX	**10 ng**	>1000 ng
NG	**5.0 ng**	50 ng
EGDN	100 ng*	**10 ng**
DEGDN	**10 ng***	25 ng
PETN	**5.0 ng**	50 ng
ETN	**1.0 ng**	50 ng

Section 2.6 Search List Development and Analysis of Mixtures

Subsection 2.6.1 Negative Mode Ionization Search List Development

In order to appropriately analyze mixtures and complete the blind sampling study, a search list for the explosives that were analyzed was developed. A copy of the search list, and representative mass spectra for each explosive, can be found in Appendix 1. In the development of the search list, it was determined that there are three types of peaks that exist for the explosive compounds – unique peaks, shared ion peaks, and mass overlap peaks. These types of peaks can be used to explain a number of different phenomena that were observed in the analysis of mixtures and unknowns. Unique peaks are defined as a peak that could be assigned to only one explosive. These peaks are extremely useful in characterizing explosives – though not all explosives were shown to produce unique peaks. In the case of NB and 1,3-DNB, no unique peaks were found. Furthermore, isomeric explosives such as 2,4-DNT and 2,6-DNT have nearly all peaks in common with one another – the major difference being the relative intensity of the peaks to one another. Similar trends are also seen in 2-A-4,6-DNT and 4-A-2,6-DNT.

In many instances a particular peak can be assigned to multiple different explosives, and is therefore labeled a shared ion peak. In shared ion peaks, the fragments from each of the individual explosive have identical molecular formulas, and therefore the molecular masses are also identical. An example of a shared ion peak is presented in Figure 2.6. A number of shared ion peaks have been identified and occur between explosives of the same class (i.e. two or more nitroaromatics share the same peak). It was determined that in a mixture or "real world" sample, when a search list is being used, it may be difficult to assign an individual peak to one particular explosive, and therefore all possible explosives are listed as potential matches for these peaks. By identifying

other peaks present in the spectra, it is possible to rule out one or more of the explosives listed for a shared ion peak.

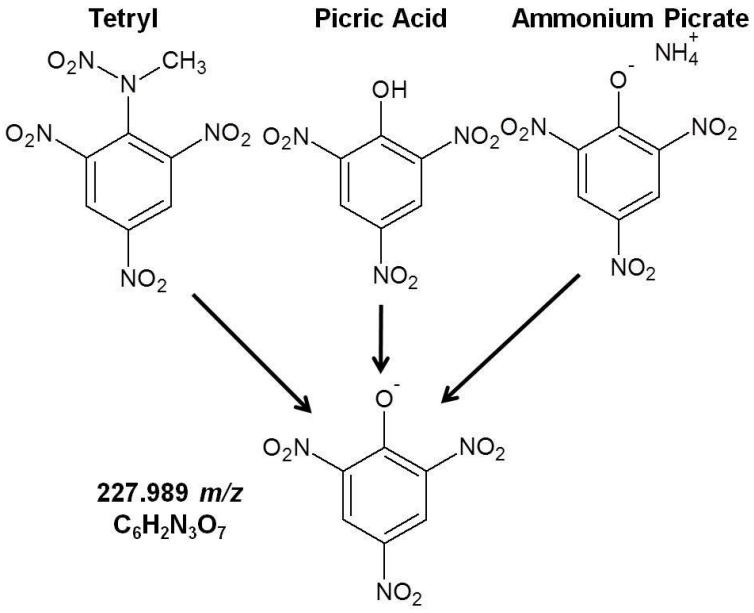

Figure 2.6 An example of a shared ion peak, in which Tetryl, picric acid, and ammonium picrate fragment into the same ion.

The other types of peaks identified are mass overlap peaks, which can be difficult to interpret. Mass overlap peaks are defined as peaks from two or more ions, from different explosives, which have theoretical masses less than 0.005 Da apart from one another. Each of the peaks has a different molecular formula, and, therefore, a slightly different molecular mass. An example of a mass overlap instance is shown in Figure 2.7. A list of mass overlap occurrences is presented in Table 2.4. Since a number of mass overlap peaks involve Tetryl and DEGDN, identification of peaks pertaining to these explosives can be difficult, as peaks can be incorrectly assigned or dually assigned depending on the calibration of that particular run. Furthermore, an isotopic peak from a nominal mass one Dalton less than a mass overlap peak will also fall within the 0.005 Da

tolerance of the mass overlap peaks, which adds a third possible peak that can be detected, depending on the explosive(s) present.

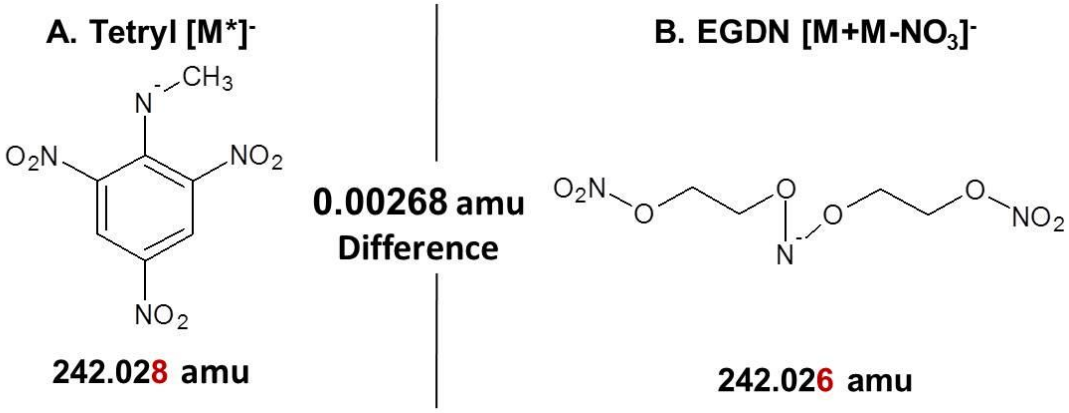

Figure 2.7 An example of a mass overlap occurrence. The M* ion of Tetryl (A) and a dimer of EGDN (B) have masses which lie within 5 mDa of one another.

Table 2.4 Examples of mass overlap occurrences that were found during this study.

Nominal Mass	Theoretical Mass	Assignment	Formula	Mass Difference
228	228.020452	TNT ^{13}C isotope	$C_7H_5N_3O_6$	2.53 mDa
	228.022983	DEGDN	$C_4H_8N_2O_9$	
	228.025662	TNT -or- 2-A-4,6-DNT	$C_7H_6N_3O_6$	2.68 mDa
242	242.023305	Tetryl ^{13}C isotope	$C_7H_5N_4O_6$	2.75 mDa
	242.026057	EGDN -or- DEGDN	$C_4H_8N_3O_9$	
	242.028736	Tetryl	$C_7H_6N_4O_6$	2.68 mDa
258	258.018227	Tetryl ^{13}C isotope	$C_7H_5N_4O_7$	2.75 mDa
	258.020972	EGDN -or- DEGDN	$C_4H_8N_3O_{10}$	
	258.023651	Tetryl	$C_7H_6N_4O_7$	2.68 mDa
259	259.026057	Tetryl ^{13}C isotope	$C_7H_6N_4O_7$	2.75 mDa
	259.028797	DEGDN	$C_4H_9N_3O_{10}$	
	259.031476	4-A-2,6-DNT	$C_7H_7N_4O_7$	2.68 mDa

Examining the mass overlap occurrences it is noted that the mass overlap occurrences exhibit nearly identical characteristics. In all instances one of the mass overlap peaks is a nitrate ester (DEGDN and/or EGDN) while the other is a nitroaromatic (typically Tetryl). Furthermore, in every instance, the difference in mass between the two peaks that are not isotopes is always 2.68 mDa. The differences in chemical formulas are also identical in every occurrence. This could be attributed to similar fragmentation and recombination patterns amongst explosives as well as the similarities in the molecular formula ratios amongst the two classes. Using these phenomena, all anomalies that were encountered in the analyses of mixtures and blind samples could be explained.

Subsection 2.6.2 Negative Mode Ionization Mixture Analysis

To evaluate the ability of the technique to detect multiple explosives simultaneously, three mixtures were analyzed. The first mixture was a commercially available 6 component mixture containing TNT, 2,6-DNT, PETN, RDX, NG, and EGDN with individual explosive concentrations ranging between 20 µg/mL and 40 µg/mL. Since the mixture contained EGDN, it was analyzed using both the "high temperature" and "low temperature" methods. A representative mass spectrum of a "high temperature" run is shown in Figure 2.8. In the fifteen replicates that were completed using the "high temperature" method, all explosives except EGDN were identified in every replicate by searching against the in house created search list described above and presented in Appendix 1.

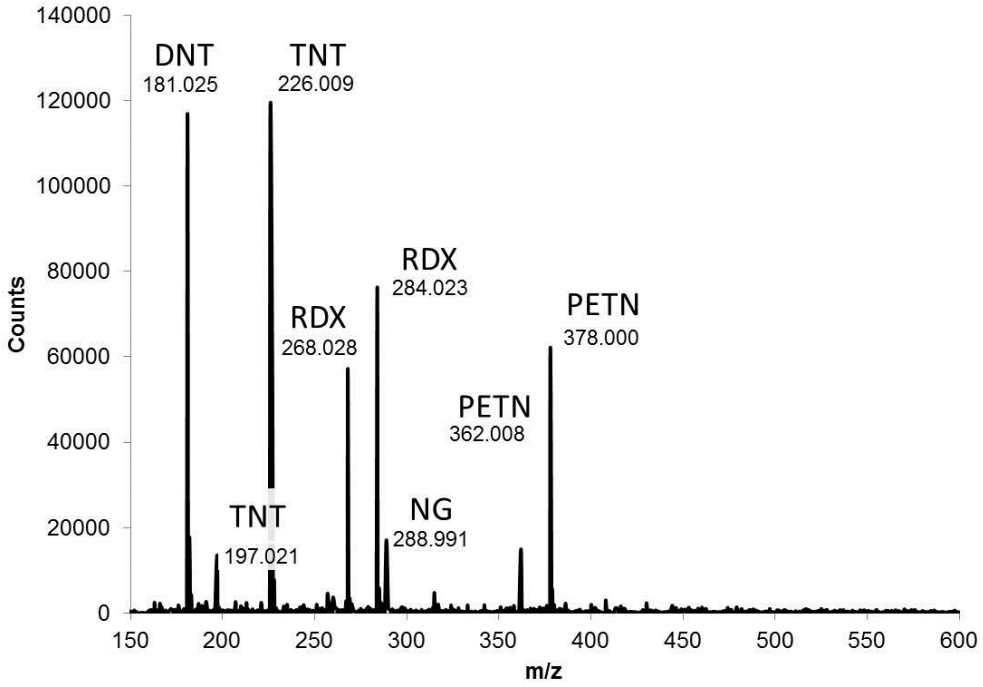

Figure 2.8 A representative mass spectrum of the six-component mixture.

In order for a peak to be identified by the search list it needs to be present at greater than 1% of the normalized intensity and within ±0.005 Da of the theoretical mass. In this mixture, peaks that are unique to TNT, PETN, RDX, and NG were detected in all replicates, and peaks that are shared between 2,6-DNT and 2,4-DNT were detected in all replicates. Only one replicate produced a hit for EGDN. Difficulties in detecting EGDN are expected since it responds poorly at the higher temperature. However, analysis of the mixture using the "low temperature" method also only produced one hit for EGDN out of the nine individual runs, indicating that competitive ionization may be occurring which is hindering the detection of EGDN in a mixture.

The second mixture was a commercially available 14 component mixture containing TNT, 2,4-DNT, 2,6-DNT, Tetryl, NB, 1,3-DNB, 1,3,5-TNB, 2-NT, 3-NT, 4-NT, 2-A-4,6-DNT, 4-A-2,6-DNT, RDX, and HMX. This mixture was far more complex than the previous mixture; however, similar results were obtained. A representative spectrum of this mixture is shown in Figure 2.9. In all replicates, peaks for every explosive were identified after being searched against the library. Unique peaks were identified in all replicates for TNT, Tetryl, RDX, HMX, 4-A-2,6-DNT, and 1,3,5-TNB. Detection of unique peaks for 2,4-DNT, 2-A-4,6-DNT and 2,6-DNT as well as the 2-NT, 3-NT, 4-NT, NB, and 1,3-DNB were not achieved, due to ion sharing that occurs between like explosives. Even though all explosives were detected, an anomaly was observed as some searches produced hits for DEGDN, due to mass overlap with a nitroaromatic explosive. As Tetryl and DEGDN share a number of the same nominal masses, hits for DEGDN were produced in each replicate. However, it was possible to rule out the presence of DEGDN by searching for the presence of isotopes and through the absence of additional DEGDN peaks.

The third mixture that was analyzed was an in-house made mixture which contained 8 components, TNT, 2,4-DNT, PYX, RDX, HMX, NG, PETN, and EGDN at a concentration of 100 μg/mL for all explosives. The purpose of this mixture was to evaluate not only whether or not the components could be detected, but to also understand the relative signal to neat for each explosive. Relative signal to neat is a ratio of the peak height of the base peak of an explosive in a mixture to the peak height of the same peak from the explosive at the same concentration in a neat solution. Using this metric it is possible to determine which explosive classes, or particular explosives, are

more negatively affected by being in a mixture. Figure 2.10 shows a representative mass spectrum as well as the relative signal to neat for the 8 component mixture. As expected EGDN was undetectable in the mixture, however PYX was also undetectable. This is likely due to the high boiling point and very low vapor pressure of PYX, making it difficult to be desorbed off of the sampling rod. Relative signal to neat of the remaining explosives showed that the signal of particular explosive which were detected was diminished by a factor of 0.2 to 5.0. Nitroaromatics were shown to have the highest relative signal to neat, which may be due to the abundance of free charge in the gas stream. The other explosive classes, nitramines and nitrate esters, form nitrite and nitrate adducts and thus are likely competing for free ions, lowering their relative signal to neat.

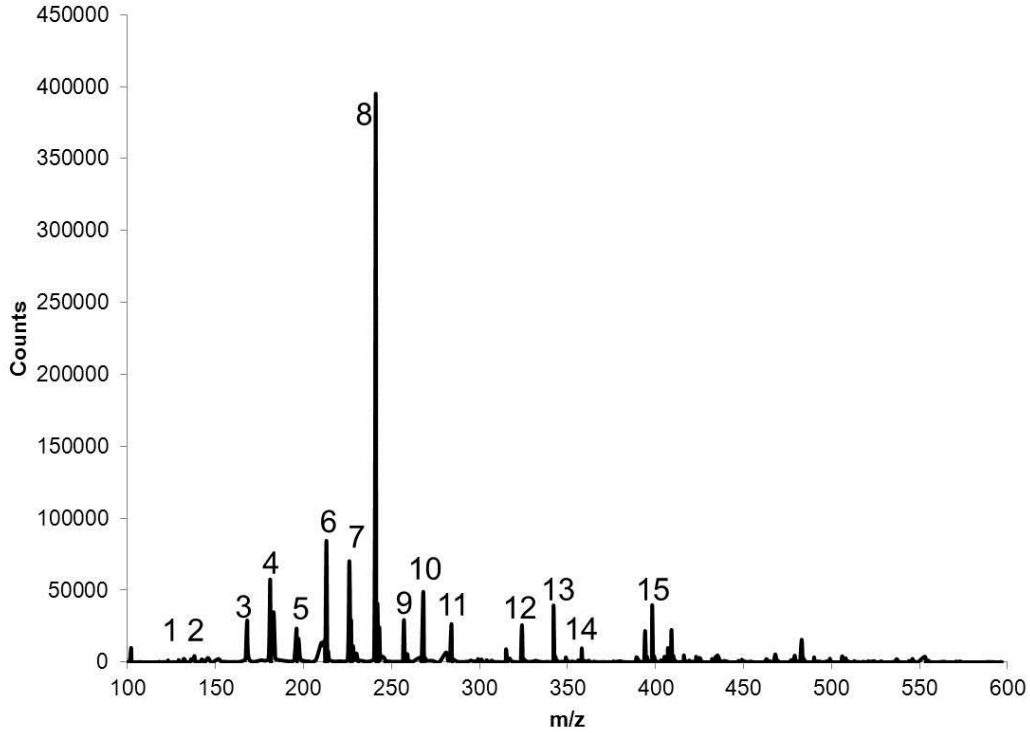

Peak	Explosive	Mass	Peak	Explosive	Mass	Peak	Explosive	Mass
1	NB	123.0320	6	Tetryl, TNT	210.0151	11	RDX	284.0227
2	2-NT, 3-NT, 4-NT	136.0399	7	TNT	226.0100	12	RDX	324.0652
3	1,3-DNB	168.0171	8	Tetryl	241.0209	13	HMX	342.0396
4	2,4-DNT, 2,6-DNT	181.0249	9	Tetryl	257.0153	14	HMX	358.0332
5	2-A-4,6-DNT, 4-A-2,6-DNT	196.0358	10	RDX	268.0278	15	HMX	398.0769

Figure 2.9 A representative mass spectrum of the fourteen-component mixture. Select peaks are highlighted to indicate which explosives were detected.

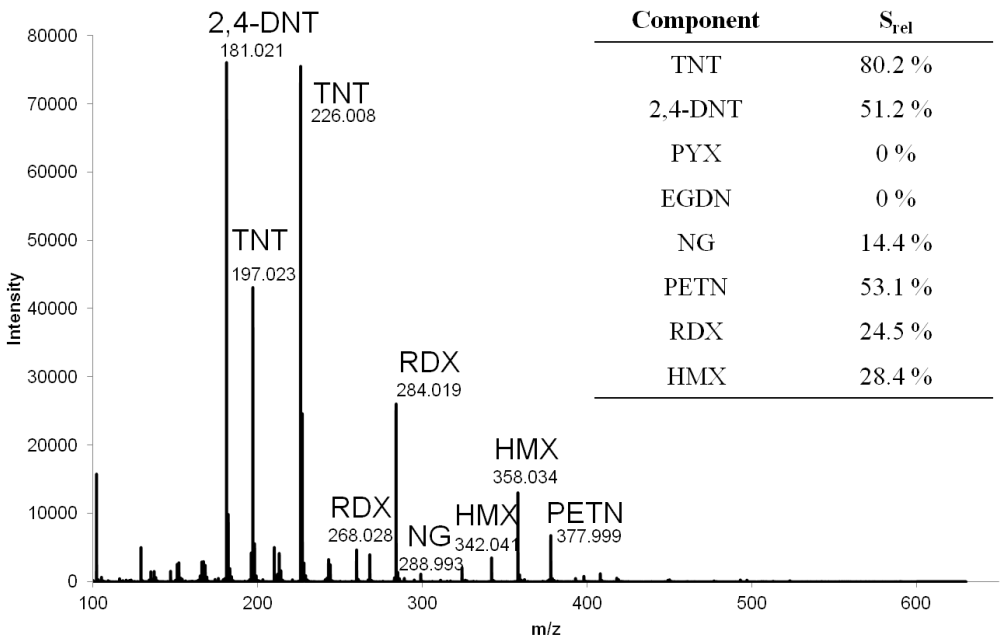

Component	S_{rel}
TNT	80.2 %
2,4-DNT	51.2 %
PYX	0 %
EGDN	0 %
NG	14.4 %
PETN	53.1 %
RDX	24.5 %
HMX	28.4 %

Figure 2.10 A representative mass spectrum and calculated relative signal to neat for the eight component mixture.

Subsection 2.6.3 Positive Mode Ionization Analysis of Mixtures

A 1:1 mixture of TATP and HMTD was prepared and analyzed to evaluate the ability for the DART-MS to detect both explosives simultaneously. A search list was also created for the peroxide explosives (located in Appendix 1), and it was found that two peaks are shared ion peaks between TATP and HMTD. TATP has one additional peak that is unique to that explosive, while HMTD has four additional unique peaks. When the mixture was analyzed using the positive method, all replicates produced results with at least one unique peak for HMTD detected. In 75% of the replicates two or more peaks unique to HMTD were detected. Furthermore, both of the peaks shared by TATP and HMTD were detected in all replicates. Roughly 25% of the replicates produced the sole unique TATP peak, with intensities under 6% relative to the base peak in all cases. From these results it is unclear whether the lack of detection of the unique TATP peak in

many of the sample runs is due to competitive ionization with HMTD or if it is due to the intensity for the unique TATP peak being below the 1% relative intensity threshold utilized in the searches. Lowering the detection threshold to 0.5% relative intensity did lead to 95 % detection of the unique TATP peak, indicating that it is likely a low abundance of the peak which was leading to the lack of detection.

Section 2.7 Blind Sampling

A blind sampling study was also completed to evaluate the ability of the technique to identify unknowns and determine if there was bias due to the method or the examiners. In this study, twelve mock-case samples were prepared by an examiner at the DFSC who was not involved with the study. The samples then were run, in triplicate, by examiners involved in the study using the "high temperature" method in addition to the "low temperature" method – which was used solely to screen for DEGDN and EGDN. The results of the study are shown in Table 2.5. In every sample, peaks unique to the explosive present were identified, with two or more unique peaks being present in all but two samples. Furthermore, the blank sample produced no search list hits, indicating that the search list was not falsely identifying peaks that were due to background contaminants. The blind sampling results demonstrate that there was no bias present in either the method or the examiners, and that the use of a search list to detect the presence of an explosive was reliable.

Table 2.5 Results of the blind sampling study. The column titled "# of Unique Peaks" identifies how many peaks were detected that can only be attributed to that explosive. An asterisk indicates the explosive shares all peaks with another explosive (also indicated with an asterisk) and therefore the number of peaks unique to that pair of explosives that were detected is listed. The last two columns indicate the identities of hits that were produced and are shared between explosives either due to shared ions or mass overlap.

Sample	Contents	# of Unique Peaks	Additional Explosives Hits	
			Shared Ion	Mass Overlap
1	AP	4*	*PA, Tetryl	None
2	Blank	0	None	None
3	PETN	2	ETN	None
4	HMX	4	RDX	None
5	RDX	3	HMX	None
6	DEGDN	2	EGDN	Tetryl, TNT, & 2-A-4,6DNT
7	ETN	3	None	None
8	2,6-DNT	3*	*2,4-DNT, TNT	None
9	2-A-4,6-DNT	3*	*4-A-2,6-DNT	DEGDN
10	Blank	0	None	None
11	NG	1	None	None
12	Tetryl	4	AP/PA & TNT	DEGDN & EGDN

Section 2.8 Analysis of Real World Post-Blast Samples

To evaluate the applicability of this technique for the analysis of "real-world" samples, an assortment of different materials were obtained from an explosive ordinance training site and analyzed via the optimized method for the presence of explosives. The samples which were recovered had been exposed to a blast containing a mixture of TNT and PETN. Samples were collected from various locations around the blast site and stored in separate, sealed, plastic bags. The samples were then analyzed directly in the gas stream of the DART source without any preparation. Blanks were sampled in between runs to assure no sample to sample contamination or sample carry over was occurring.

The post-blast materials that were obtained included a piece of exploded detonation cord, a plastic water bottle, a piece of plywood, dirt, grass, leaves, and tree bark from near the detonation site, water from a puddle near the detonation site, a piece of electrical tape, and a piece of PVC pipe. Of the ten samples that were analyzed, six produced hits for explosives when directly analyzed by DART-MS. The samples that produced hits were the PVC pipe, detonation cord, plastic water bottle, plywood, tree bark, and dirt. All six of the samples produced hits for TNT and four of the six (tree bark, plywood, dirt, and detonation cord) produced hits for PETN as well. Figure 2.11 shows the mass spectra of the various samples that produced hits for TNT and/or PETN. After analysis by DART-MS, all samples were extracted and analyzed via CI-GC-MS using the validated method discussed in Subsection 2.2.4, and in all cases the sample results between DART and CI-GC-MS matched. This study proved that "real world" samples could be analyzed and explosives could be detected using this method.

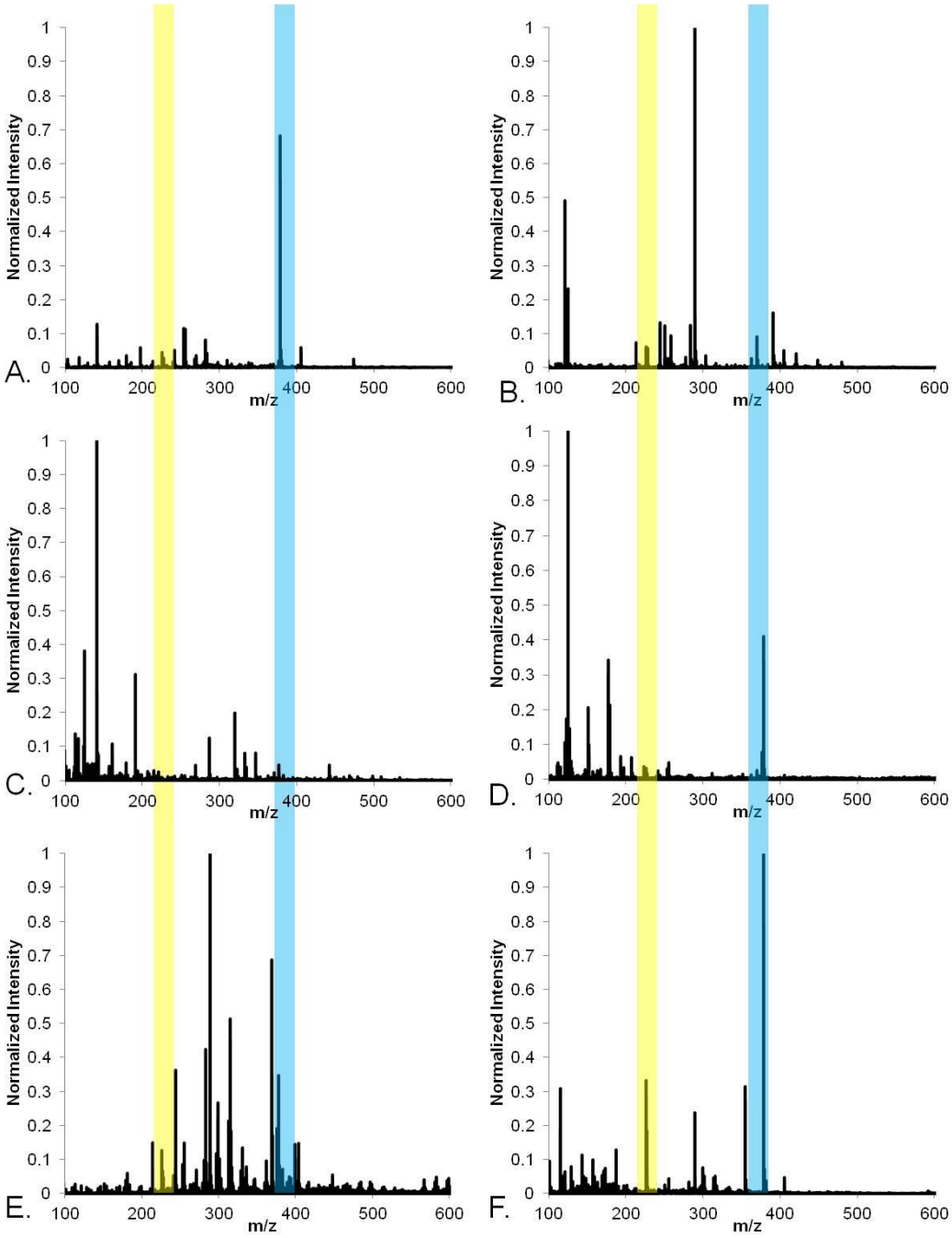

Figure 2.11 Mass spectra of the post-blast samples that produced hits for explosives. The samples analyzed include exploded detonation cord (A.), PVC pipe (B.), a plastic water bottle (C.), dirt (D.), tree bark (E.), and plywood (F.). The yellow bar indicates the position on the mass spectra for the TNT base peak at nominal mass 226 *m/z*. The blue bar indicates the location for the PETN base peak at nominal mass 378 *m/z*.

Section 2.9: DAPNe Set-up and Procedures

Another type of real world sample which is likely to be recovered from a crime scene and contain explosives is latent fingerprints. With fingerprints, however, it is desirable to obtain information on the presence of explosives while not destroying the biometric information of the print itself. To combat this issue, since the DART stream is sufficiently hot to destroy fingerprints, the DAPNe set-up was evaluated. DAPNe allowed for the direct analysis of crystals within a fingerprint while maintaining the visual quality of the fingerprint. Extractions of crystals from within doped fingerprints were performed with a 2-positioner nano-manipulator (DCG Labs, Richardson, TX) mounted on the stage of an Olympus BX40 bright field microscope (Olympus, Center Valley, PA). A joystick controller was employed to maneuver the positioners. Extractions were performed using 4 µm inner diameter uncoated capillary tips (New Objective, Woburn, MA). Aspiration of dissolved analytes into the capillary tip was facilitated by a PE2000b 4-channel pressure injector (MicroData Instruments Inc., S. Plainfield, NJ). A depiction of this setup can be seen in Figure 2.12.

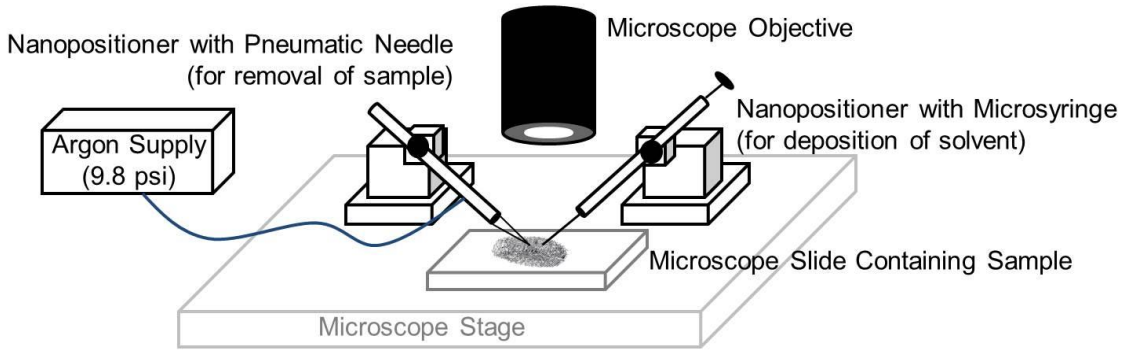

Figure 2.12 Schematic of the DAPNe set-up.

After examining the sample surface under the microscope and identifying the location of particle of interest, the extraction solvent (1.5 µL methanol) was ejected via the microsyringe. The capillary tip was then positioned within 1 mm of the dissolved particle and the solvent aspirated back into the capillary using the pressure injector and 9.8 psi of argon. The sample was then introduced into the DART gas stream by holding the capillary tip near the mass spectrometer inlet. Solvent was emitted from the tip via capillary action.

Section 2.10 Using DAPNe for Direct Analysis of Particles

To test this method, fingerprints were doped with 5 µg of TNT or RDX and deposited onto a clean glass slide. Particles were then located using the attached microscope and extracted and analyzed directly in the DART stream. The extraction of a particle 20 µm in diameter of TNT from metal and glass surfaces resulted in $[M–H]^-$ and $[M]^-$ ions at nominal masses 226 *m/z* and 227 *m/z* respectively, as shown in Figure 2.13. The extraction of an RDX particle of 15 µm in diameter from a glass slide resulted in the $[M+NO_2]^-$ ion at 268 *m/z* as the major peak, as shown in Figure 2.14. Both TNT and RDX were successfully detected from a sample particle of 20 µm diameter or less with minimal matrix interference. Furthermore, the peaks that were detected correlated with the peaks produced by the standards, enabling direct comparison. The other major benefits of this technique are that the fingerprint remains essentially unaltered, and one is not limited to the 30 mm inlet distance for sample introduction in the DART, though this can be mitigated by remote sampling DART as well. By completing a nanoextraction outside of the DART source, any size piece of material can be interrogated. Samples of fingerprints containing explosives that were run directly in the DART gas stream to

illustrate the increase in background present with direct analysis and are presented in Appendix 1.

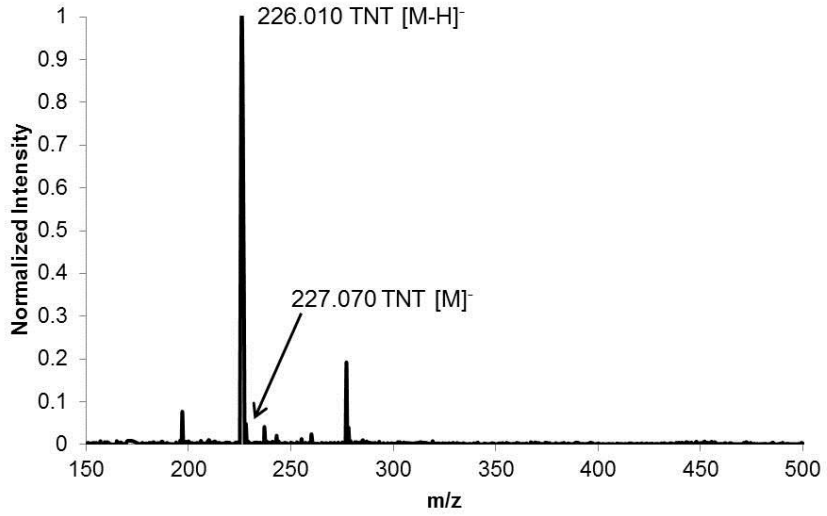

Figure 2.13 Mass spectra of a single crystal of TNT extracted out of a fingerprint using DAPNe and then analyzed by DART-MS.

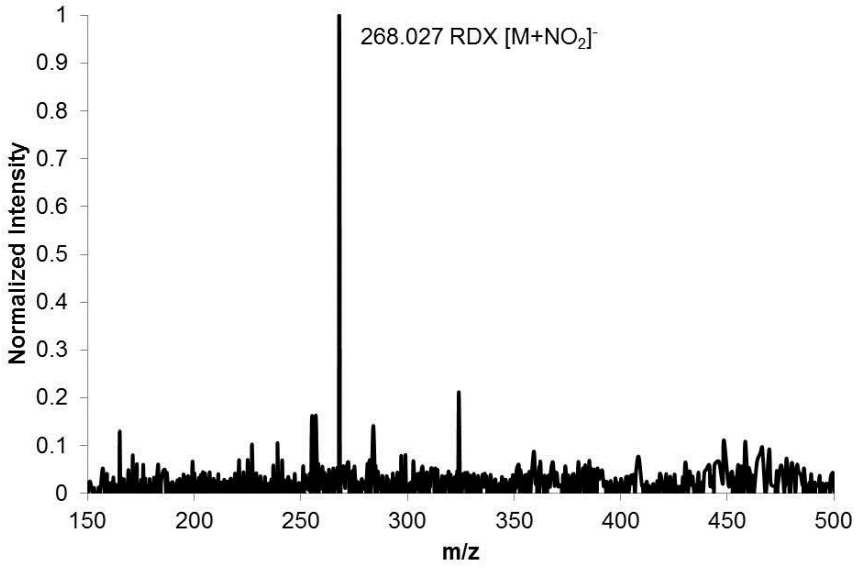

Figure 2.14 Mass spectra of a single crystal of RDX extracted out of a fingerprint using DAPNe and then analyzed by DART-MS.

Section 2.11 Conclusions

The DART-MS technique provides an extremely powerful screening tool for the analysis of trace explosives. It has been shown to accurately and reproducibly detect a wide range of explosives, with sensitivities equal to or exceeding that of current analytical techniques. However, due to the lack of a pre-separation, such as by a chromatographic method, confirmatory identification of specific explosives can be difficult due to similar fragmentation patterns of explosives in the same class. Detecting multiple explosives simultaneously is easily achieved with the technique, and the use of a search list to analyze unknowns has been demonstrated to be highly effective. While false positives can be encountered in analysis, they are easily accounted for by shared ions and mass overlap. Furthermore, the use of new mass calibration compounds expands the possibilities of potential calibrants outside of the standard PEG 600. "Real world" samples were also successfully analyzed with no sample preparation. DAPNe–DART-MS effectively eliminates many of the matrix interferences typically shown in DART spectra. It can efficiently extract single particles without significant interference from matrix effects from either surfaces or latent print constituents. Moreover, latent fingerprints may be preserved once extractions have been performed due to the small extraction area and solvent selection. This provides a minimally invasive, highly informative technique for trace analysis of explosives. As a screening tool, the DART-MS shows promise as a leading technique in the detection of trace explosives. See Appendices 2 and 3 for examples of other methods developed for the analysis of forensic samples by DART-MS.

The overarching goal of the work presented in this chapter was to provide a validated screening technique for the analysis of trace explosives in routine casework. The methods described in this chapter have been combined into a single analytical scheme for the analysis of unknowns, a pictorial representation of which is shown in Figure 2.15. Using this analytical process, it possible to screen ten or more pieces of evidence in less time than is required for a single GC-MS confirmatory run. Sample consumption is minimal, with only 10 µL of a liquid sample or 3 cm^2 of a solid sample being consumed. When there are a significant number of samples to analyze, as is the case in a large crime scene, screening via DART-MS will greatly decrease the time spent by the analysts.

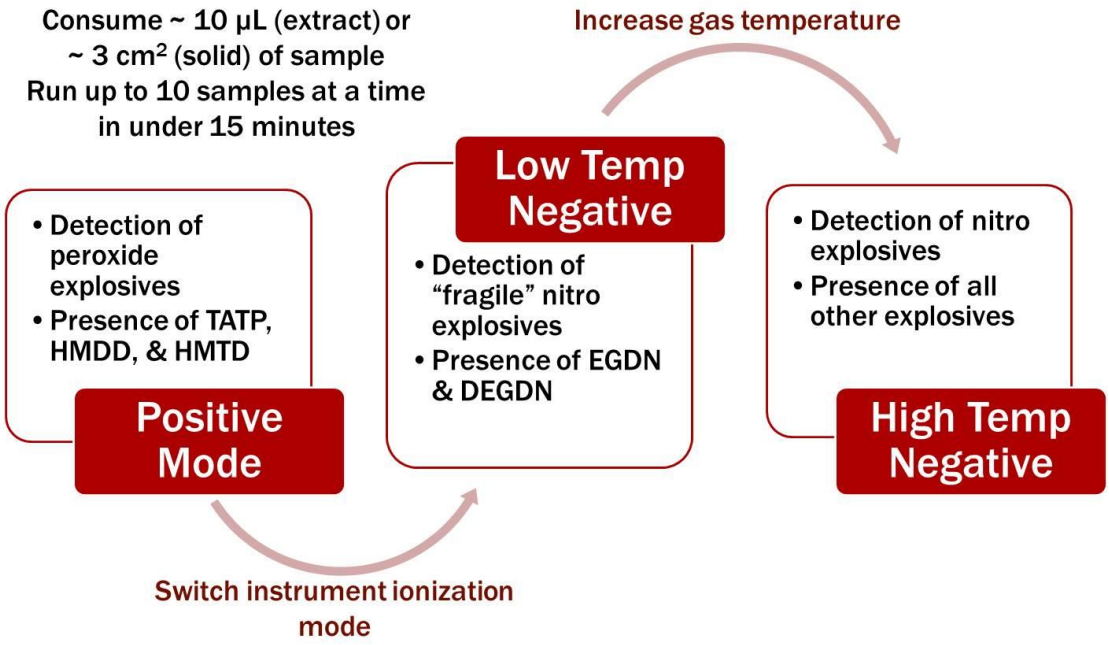

Figure 2.15 Proposed analytical scheme for the screening of an unknown believed to contain explosives.

Chapter 3: Evaluation of Additional Ambient Ionization Sources for Trace Explosives Analysis

Section 3.1 Introduction

While significant focus in the forensic science field has been placed on direct analysis in real time mass spectrometry (DART-MS), there are a number of other possible ambient ionization sources that could be used in a similar fashion. Therefore, it is important to evaluate which source would be most appropriate for the analysis of different forensic samples. Amongst these other sources are desorption electrospray ionization (DESI), desorption electro-flow focusing ionization (DEFFI), and low temperature plasma (LTP). Some sources, like DESI, have already been extensively researched and shown to have performance characteristics, in terms of sensitivity and specificity, similar to that of DART-MS.[17] Initial studies of DEFFI and LTP have shown it is likely that similar results to DART could be obtained[18,54,79] although significant validation studies have not yet been undertaken. This chapter evaluates three ambient ionization mass spectrometry (AI-MS) sources, in addition to comparing them to the results obtained by DART-MS. The benefit to this cross comparison is that all of the sources discussed in this chapter are able to be interfaced to the same mass spectrometer, which allows for variations due to the mass spectrometer to be accounted for. The aspects of the validation plan that were looked at in this study include: method optimization, limits of detection, reproducibility, ability to analyze mixtures, and useful yields. From these results it was found that all sources perform at similar levels when compared to one another. However, each has different strengths and weakness as to which substances it is most well suited to analyzing. It is important to mention that, like

Chapter 2, the focus of this study was to develop optimal screening methods for as many compounds as possible, and not to develop confirmatory, or explosive-specific methods.

Section 3.2 Materials and Methods

Subsection 3.2.1 Instrumentation

All three of the ionization sources were coupled to an ABSciex 4000 QTrap mass spectrometer. The mass spectrometer was run in Q1 scan mode, where only the first quadrupole was used to scan a desired mass range of 50 *m/z* – 600 *m/z* in both negative mode and positive mode. Each scan was completed over 30 seconds, aside from the useful yield scans, and summed at 1 second intervals per scan. The useful yield scans were run for the total length of time required to have the analyte ion signal reach background. The resolution of the mass spectrometer was set to 0.1 Da, the best resolution possible on this instrument. Other mass spectrometer settings that were kept constant throughout the experiment include: a curtain gas pressure of 12 psi (~85 kPa), an ion source 1 gas pressure of 7 psi (50 kPa), no ion source 2 gas, a declustering potential of ±75 V, an entrance potential of ±10 V, and an interface heater temperature of 150 °C. Also, the interface used in these experiments was a 36 mm extension tube which had a 15° angled tip.

The DESI source used in these experiments was a Prosolia (Indianapolis, IN) 1-D source, which was used without any modification. The only parameter that was kept constant throughout the study was the use of nitrogen as the source carrier gas. Parameters that were altered to optimize the methods include: solvent composition and flow rate, spray voltage, source gas back pressure, distance from source to sample,

distance from sample to inlet, and angle of incidence. All samples were deposited onto Prosolia Omni-Slides, as described in Subsection 3.2.2.

The DEFFI source used in these experiments was an electro-flow focusing nebulizer from Ingeniatrics Technologias (Seville, Spain), which was outfitted to fit the ABSciex mass spectrometer. The same interface and extension tube used for the DESI source was employed with this source. Additional details about the DEFFI source itself are presented elsewhere.[54] As with the DESI source, the only parameter of the DEFFI source that was kept constant was the use of nitrogen as the source gas. The gas pressure was also fixed at the backpressure necessary to maintain a constant solvent spray. This backpressure varied with solvent composition and flow rate but was in the range of 17 psi to 23 psi (115 kPa to 160 kPa). Parameters that were optimized for these experiments include: solvent composition and flow rate, spray voltage, incidence angle, and distances between sample and source as well as sample and inlet. Like DESI, all samples were prepared on Prosolia Omni-Slides.

The LTP source used in these experiments was produced in house and consisted of a gas flow controller that provided a steady stream of ultra-pure helium gas to the glass capillary. Two pieces of copper were wrapped around opposing ends (approximately 3 cm apart) of a glass capillary and were attached to electrodes. The dielectric barrier discharge was initiated by applying a voltage and frequency to the electrodes. The tip of the glass capillary was narrowed to 300 μm to allow for a focused plasma beam. Optimizing parameters for the LTP include: gas flow rate, plasma voltage and frequency, incidence angle, and sample to source and sample to inlet distances. Samples for analysis were deposited onto Prosolia Omni-Slides.

Subsection 3.2.2 Materials and Sample Deposition

The explosives used in this study were identical to those used in the Chapter 2 study, and were purchased from AccuStandard. Three mixtures were also used in this section, a six component and eight component mixture identical to those in Chapter 2 as well as a ten component commercially available mixture purchased from AccuStandard. Serial dilutions of all the explosives were completed in acetonitrile (Sigma-Aldrich). Solvents that were used for the sprays in both DESI and DEFFI sources were made up of varying concentrations of methanol, water, and acetonitrile, all at HPLC grade or higher (Sigma-Aldrich).

Unlike the DART source, which allowed for analysis of samples in a transmission setting, the DESI, DEFFI, and LTP sources were all operated off-axis relative to the mass spectrometer inlet. Because of this, a different method of sample deposition was required, instead of analysis using a glass capillary. For these experiments, all samples were deposited, in 1 µL aliquots, onto Teflon spots of a Prosolia HTC Omni-Slide 66 spot microscope slide. Each spot was used for only one analysis, and blank spots were run intermittently between samples to ensure no cross-over of samples, or contamination of the mass spectrometer.

Subsection 3.2.3 Useful Yield Calculations

Subsection 3.3.8 of this chapter compares the useful yields of some exemplary compounds across these different sources. Useful yield is one metric for inter-comparison of the performance of different techniques. Typically used as a performance metric in secondary ion mass spectrometry (SIMS), the useful yield measures the ratio of

the number of characteristic molecular ions detected to the total number of neutral analyte molecules available to be sampled. The useful yield can provide a framework for evaluation of signal loses throughout the entire analysis process as the value incorporates loss in a number of different areas such as ionization and desorption efficiencies, ion transfer efficiencies, and detector efficiency. In order to calculate the useful yield, a precise amount of starting material must be known, and the sample must be entirely consumed during the analysis. Therefore, for the useful yield measurements discussed, 1 µL of a 1 ng/µL solution of TNT, PETN, or RDX was deposited onto each of ten Teflon spots. Using the optimized methods, each of the ten spots was interrogated until the signal of the base peak reached background levels for at last thirty seconds, indicating the entire sample was consumed. The extracted ion chromatographs (EICs) of the base peaks were then integrated to obtain the total number of counts in each of the runs. This was divided by the total number of molecules, as determined by mass, in the starting sample to obtain the useful yield.

Section 3.3 Results & Discussion

Subsection 3.3.1 Optimization of Methods for Explosives Analysis

Optimization of all of the sources was completed for two methods, one negative ionization mode which was used to detect the nitroaromatic, nitramine, and nitrate ester explosives, and one positive ionization mode which was used to detect peroxide explosives. A matrix of possible combinations of parameters was completed to determine the optimal parameters for the detection of three characteristic explosives, TNT, RDX, and PETN, in negative mode, and the two peroxides, TATP and HMTD, in

positive mode. Once an optimal method was completed that was able to detect the entire suite of target explosives, the remaining explosives were run to ensure sufficient detection and signal. An overview table of the parameters optimized for each of the three sources is presented in Table 3.1.

Table 3.1 Overview of parameters which were optimized, and the ranges interrogated, for each of the three sources of interest.

Parameter	DESI	DEFFI	LTP
Incidence Angle	30 ° - 60 °	30 ° - 60 °	40 ° - 55 °
Applied Voltage	2000 V – 4500 V	500 V – 1250 V	3000 V – 4000 V
Gas Flow / Pressure	550 kPa – 825 kPa	Dependent on Solvent Flow Rate	300 mL/min – 500 mL/min
Plasma Frequency	-----	-----	2000 Hz – 3000 Hz
Tip-to-Surface Distance	0.5 mm – 5.0 mm	0.5 mm – 5.0 mm	0.5 mm – 5.0 mm
Surface-to-Inlet Distance	0.5 mm – 5.0 mm	0.5 mm – 5.0 mm	0.5 mm – 5.0 mm
Solvent Flow Rate	1 µL/min – 10 µL/min	1 µL/min – 10 µL/min	----
Solvent Spray Composition	5 Compositions	5 Compositions	----

Subsection 3.3.2 The DESI Source

The parameters that were used to optimize the DESI source were: solvent composition and flow rate, source gas backpressure, spray voltage, incidence angle, and distances between source sample and inlet. Solvent composition plays an important role in detection as it is possible to alter the solution chemistry that is occurring at the interface of the sample and the spray by changing the composition of the spray. In this instance, five different solvents were explored, a 50:50 methanol–water mixture, a 70:30

methanol–water mixture, a 50:50 methanol–water mixture containing 2 μg/mL $AgNO_3$, a 50:50 methanol-water mixture containing 2 μg/mL NaCl, and pure acetonitrile. The differing compositions of methanol–water mixtures were chosen as prior work has shown the potential for a significant increase in signal by increasing the methanol concentration, as well as decreased puddling of the spray into the sample.[80] The addition of sodium chloride or silver nitrate into the spray solvent was completed to provide pre-formed ions to allow for adduct formation and potential enhancement in signal. Prior work has shown an affinity for explosives such as RDX to adduct easily with chloride ions to form $[M+Cl]^-$ ions when analyze by DESI.[24] Explosives will also commonly adduct with free nitrate ions to form nitrate adducts. Acetonitrile was chosen to study the effect of a purely organic spray solvent. Formation of these adducts could help to increase overall sensitivity of classes of explosives.

Figure 3.1 shows a parametric plot for the signal of the base peak ion for the three characteristic negative ion explosives with respect to the different spray solvents which were analyzed. Characteristic mass spectra for these and other explosives for the three sources discussed in this chapter can be found in Appendix 4. In the case of the negative mode explosives, optimal signal was achieved for most explosives when a 50:50 methanol–water spray solvent with 2 μg/mL $AgNO_3$. Both RDX and PETN formed nitrate adducts with the incorporation of the nitrate salt into the solvent spray, thus increasing the signal of their respective base peaks. Nitroaromatics appeared to respond best in pure acetonitrile as the spray solvent. However, the decrease in signal with use of the $AgNO_3$ spray solvent was less substantial than the increase it delivered to the other explosives, even though it did not adduct with the nitrate ion. RDX, as expected,

produced chloride adducts with the NaCl solution, however it was shown to decrease the obtainable signal for TNT and PETN. For positive mode, the detection of TATP and HMTD were most successful with the sodium chloride solution, as the two explosives readily formed sodiated molecular ions.

Spray voltage was also optimized in the range of ±2000 V to ±4500 V. As the spray voltage is increased the available charge per solvent droplet is increased. Increased charge can lead to increased ionization efficiencies of analyte molecule. Increased charge can also lead to increased fragmentation as charged solvent droplets are more rapidly accelerated in the electric field. If increased fragmentation occurs, detection of particular compounds may become more convoluted and detection at low levels becomes more difficult. This was the case, especially in the detection of peroxide explosives, which are particularly fragile. A marked decrease in signal intensity was noted with spray voltages exceeding +2500 V for these compounds, as fragmentation was greatly increased above this voltage. For the negative mode explosives, maximum signal was achieved at -4500 V for all explosives except for DEGDN and EGDN, where maximum signal occurred at -3000 V, again due to the fragility of these molecules. Figure 3.2 shows the response of the three negative ion mode exemplary explosives as a function of voltage.

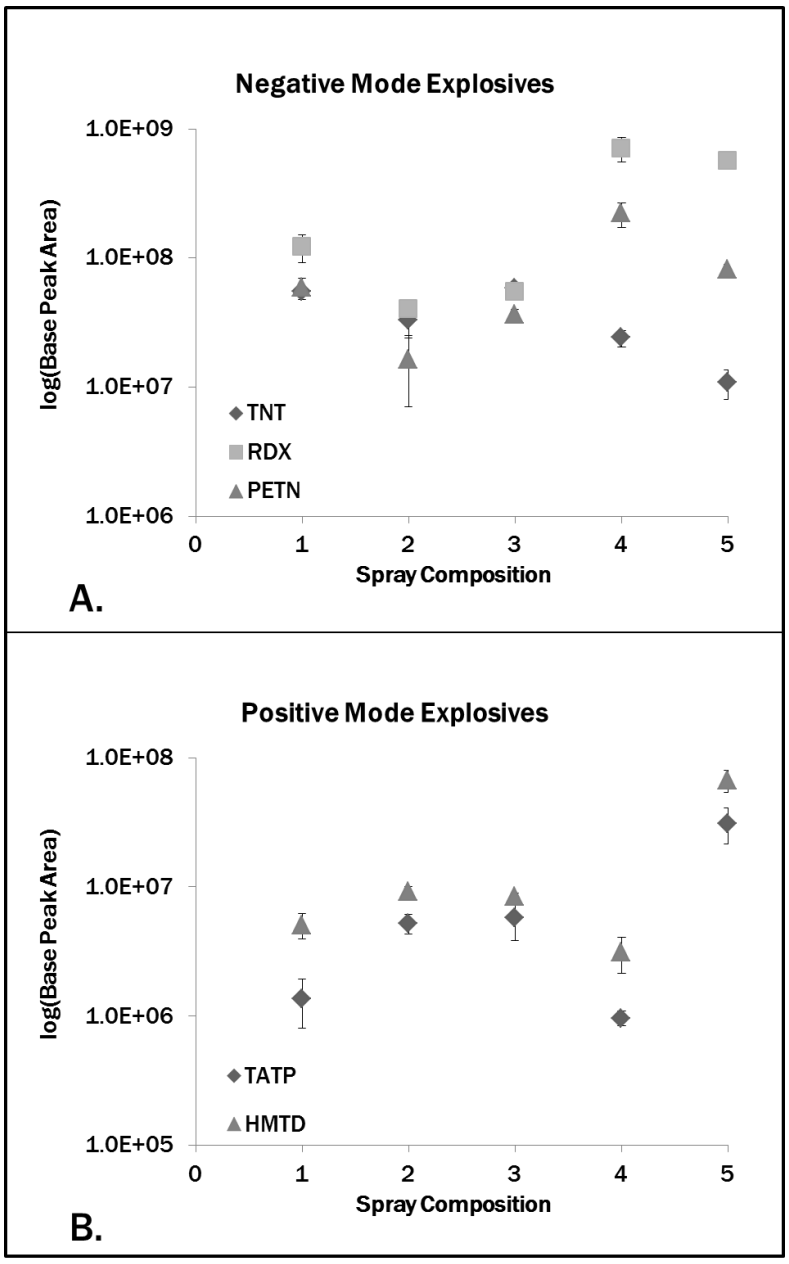

Figure 3.1 Effect of solvent composition on the response of characteristic negative ion explosives (A.) and positive ion (B.) explosives when analyzed by DESI-MS. Spray compositions are pure acetonitrile (1), 50:50 methanol-water (2), 70:30 methanol-water (3), 50:50 methanol-water with 2 μg/mL $AgNO_3$ (4), and 50:50 methanol-water with 2 μg/mL NaCl (5).

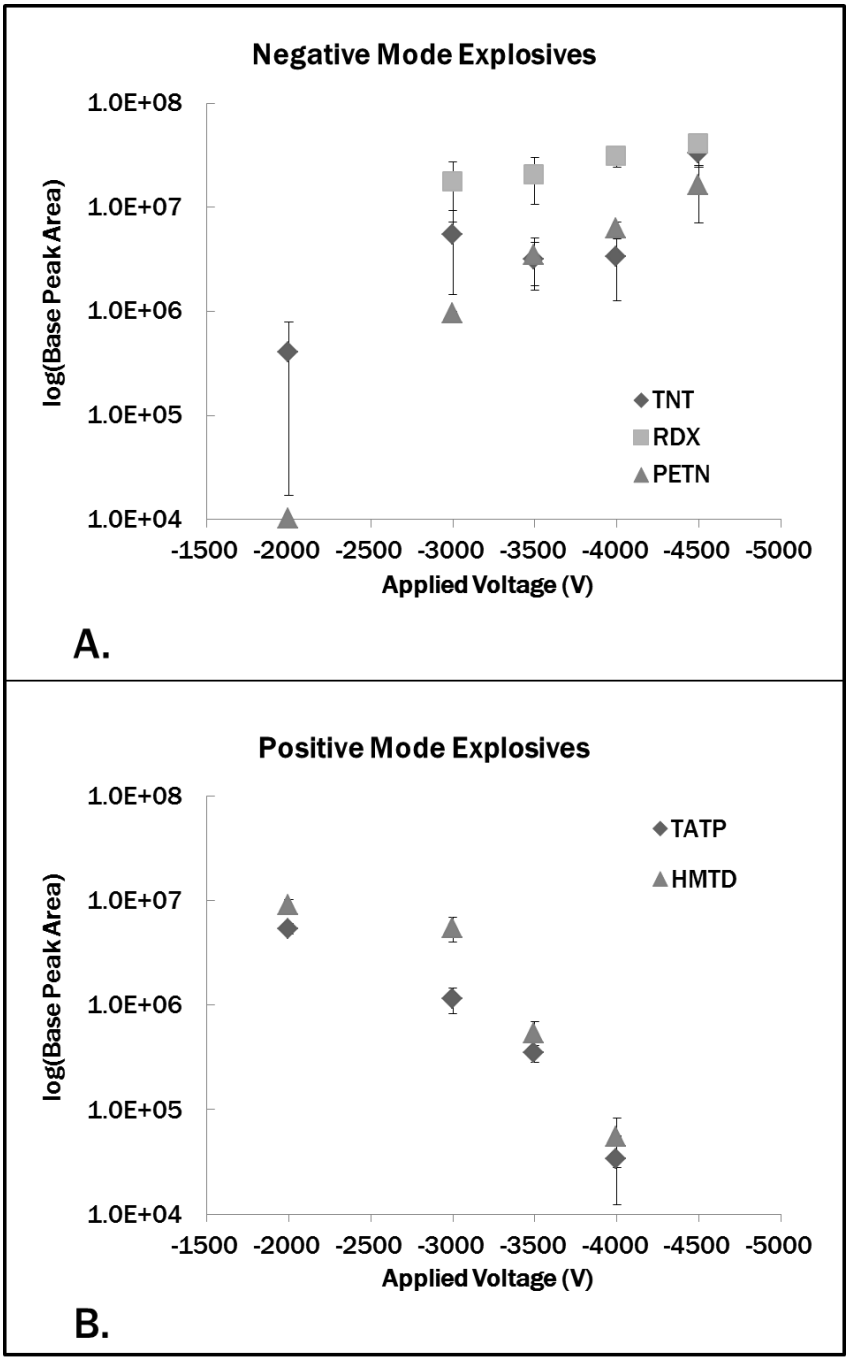

Figure 3.2 Effect of spray voltage on the response of characteristic negative ion explosives (A.) and positive ion explosives (B.) when analyzed by DESI-MS.

Source gas backpressure and incidence angle were the other two parameters which were optimized for the DESI source. The source gas backpressure will affect how rapidly solvent molecules interact with the sample, as well as affect the rate of evaporation of the solvent droplets. As backpressure is increased, so is the rate of desolvation of analyte molecules and the rate of evaporation of the solvent molecules. For this study the backpressure was altered from 80 psi (550 kPa) to 120 psi (825 kPa). It was found that 100 psi (~675 kPa) provided the highest signal intensity in both positive and negative modes. The incidence angles that were analyzed ranged from 30° to 60°. Optimal incidence angles have been shown to vary amongst samples and substrates, though small molecules typically prefer lower incidence angles, while larger molecules prefer higher incidence angles.[51,81] In the case of the test explosives, the optimal incidence angle was found to be at 40 ° with respect to the normal. Figure 3.3 shows the parametric table for the detection of the five explosives. In all cases, the greatest average signal intensity is observed in the range of 35 ° to 45 °, and a significant decrease is signal is seen past 50 °.

Distances were also optimized between 0.5 mm and 5 mm from source to sample and sample to inlet. The highest signal intensities were shown to be when there was a source to sample distance of approximately 1 mm and a sample to mass spectrometer distance of 0.5 mm. The optimized method that was used for the analysis of explosives in negative mode was a 50:50 methanol–water solvent composition with 2 µg/mL $AgNO_3$, an applied spray voltage of -4500 V, a gas backpressure of 100 psi and a source incidence angle of 40 ° with respect to the sample. For positive mode, a 50:50 methanol–water solution containing 2 µg/mL NaCl was used with a spray voltage of

+2000 V; source gas backpressure and incidence angle were identical to that in negative mode.

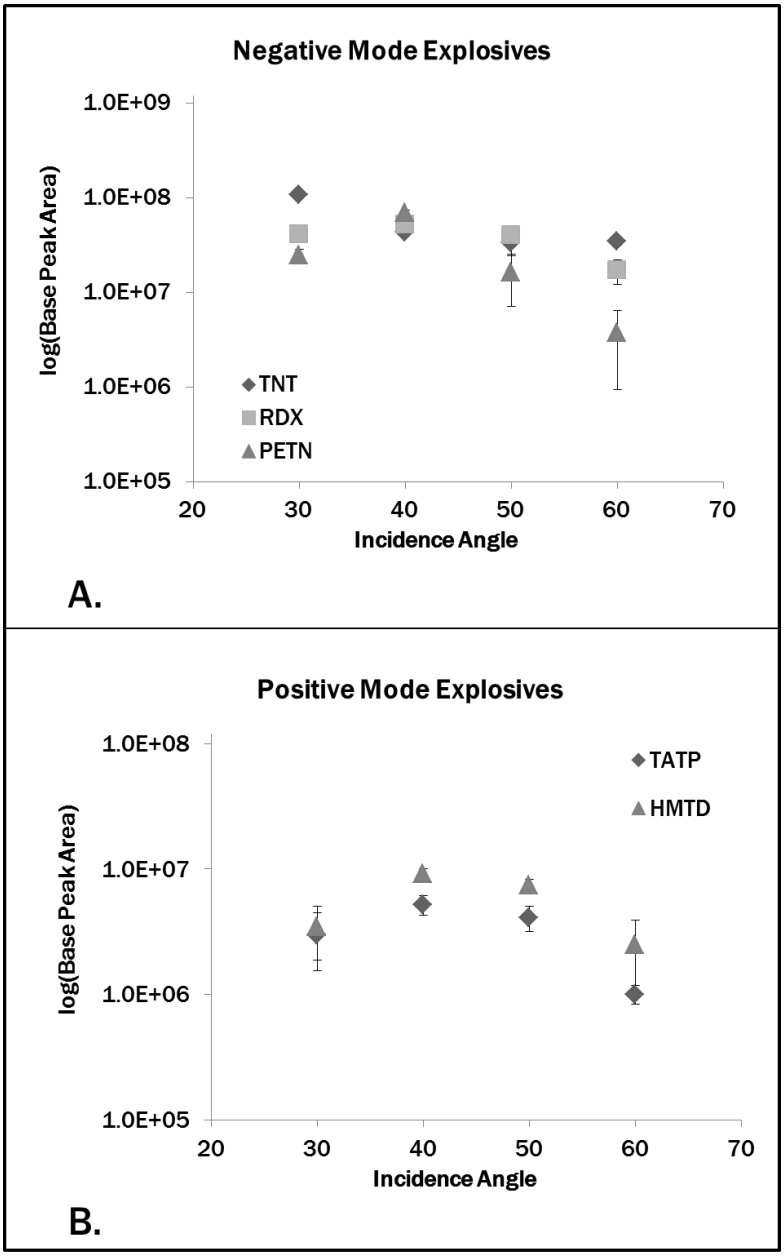

Figure 3.3 Effect of incidence angle on the response of characteristic negative ion explosives (A.) and positive ion explosives (B.) when analyzed by DESI-MS.

Subsection 3.3.3 The DEFFI Source

Since the DEFFI and DESI sources work on similar principles, similar parameters were optimized. The spray solvents that were tested were identical for DESI and DEFFI as the solution chemistry between the two sources is assumed to be similar. One difference between the two, that is relevant to this work, is that because of the corona discharge that occurs inside the DEFFI source, there is an abundance of nitrate ions in the solvent spray, at voltages greater than approximately ±300 V regardless of solvent composition. Figure 3.4 depicts the signal response from the varying solvents used. Optimal signal intensity, in both modes, was obtained with the pure acetonitrile spray. With this spray solvent, the negative mode explosives that were not aromatic, all produced nitrate adducts. Addition of the sodium chloride to the spray solvent formed chlorinated molecular ions in addition to nitrate adducts, which split the signal between two peaks, further convoluting the spectra and lowering overall peaks intensities and peak areas. In the case of the peroxide explosives, addition of the sodium or silver ions to the spray solvent did not enhance signal intensity.

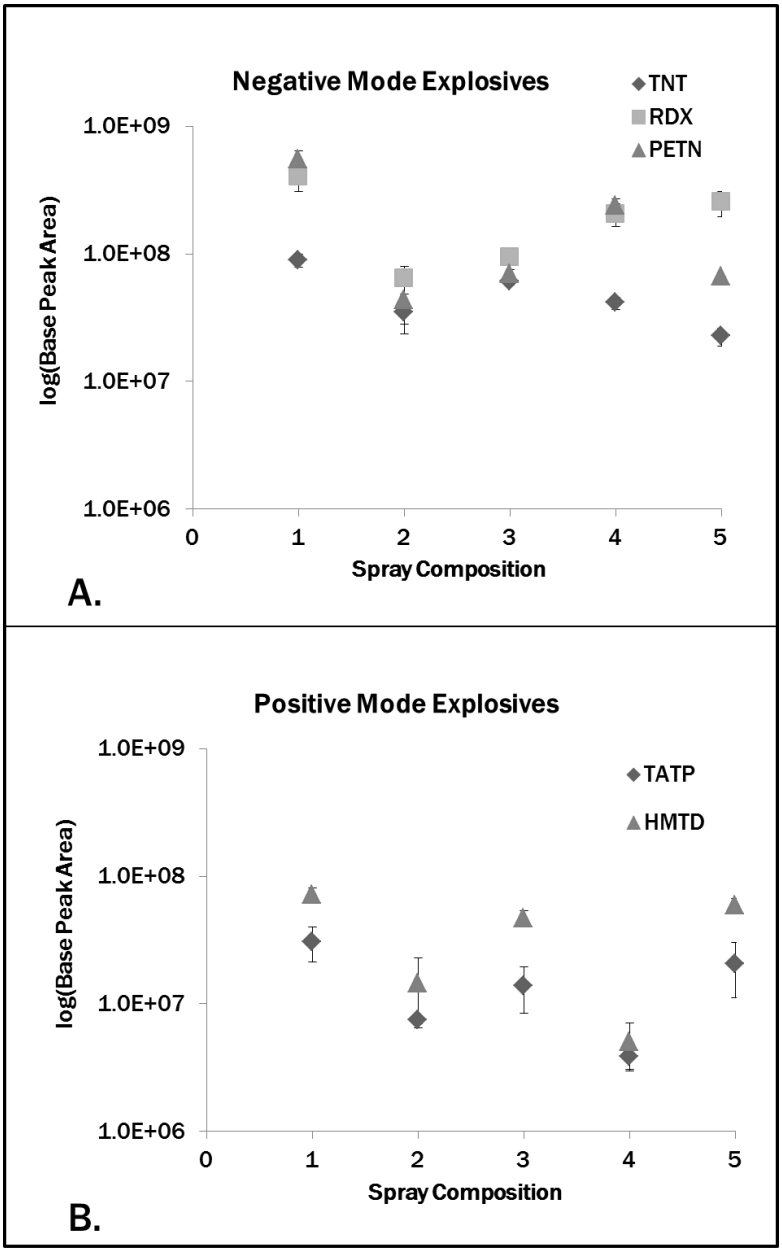

Figure 3.4 Effect of solvent composition on the response of characteristic negative ion explosives (A.) and positive ion (B.) explosives when analyzed by DEFFI-MS. Spray compositions are pure acetonitrile (1), 50:50 methanol-water (2), 70:30 methanol-water (3), 50:50 methanol-water with 2 μg/mL $AgNO_3$ (4), and 50:50 methanol-water with 2 μg/mL NaCl (5).

The other spray parameter that was optimized was the spray voltage. For DEFFI, common spray voltages range from ±500 V to ±2000 V. As the voltage is increased there is an increased corona discharge, which can aid in increased detection of negative mode ions via nitrate addition. At voltages near ±2000 V however, the spray can become unstable and in some cases cease, as equilibrium inside the source is no longer maintained. Since the voltages used in DEFFI are much lower than those used in DESI, fragmentation and molecular breakdown are lesser concerns, with the bigger concern being the ability to maintain consistent spray characteristics. For the explosives analyzed, the optimal voltage was found to -1000 V for negative mode, as shown in Figure 3.5, and +500 V for positive mode. Like the DESI results, DEFFI was shown to break down peroxide explosives at high spray voltages in the positive mode. In negative mode, there was no substantial increase in signal for voltages above -1000 V, and fragmentation of fragile compounds, like EGDN and DEGDN was noted. Furthermore, there was increased variability in high voltages due to increased instability in the spray.

Distances tested for the DEFFI source, in regards to source, sample, and inlet were identical to those tested with the DESI source. It was found that optimal signal was obtained with a source to sample distance of approximately 1 mm and a sample to inlet distance of approximately 1 mm to 2 mm. Unlike DESI, it was found that the optimal incidence angle was 50° which was slightly higher than that required for DESI. Figure 3.6 shows the response of the varying explosives over a range of different incidence angles. The optimal settings for the analysis of explosives in negative mode was shown to be a solvent spray of acetonitrile, at a voltage of -1000 V, and an incidence

angle of 50°. For the analysis of explosives in positive mode, the same spray solvent and incidence angle were shown to be optimal; however a spray voltage of +500 was used.

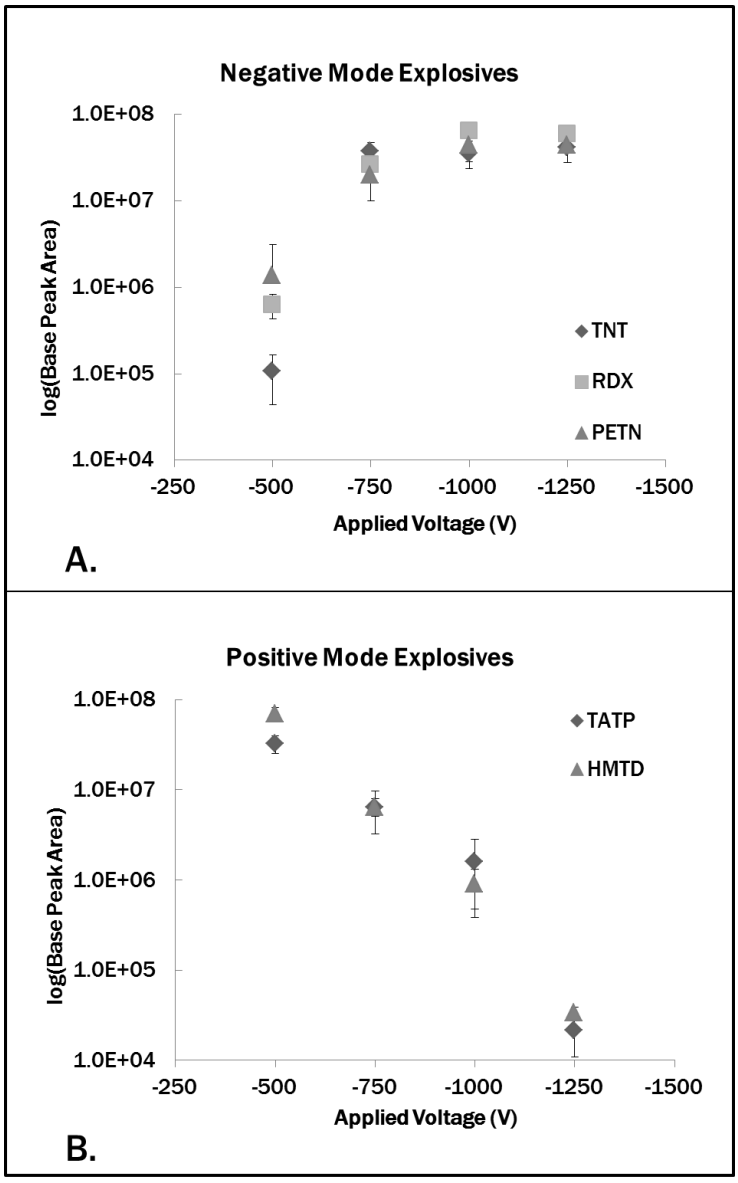

Figure 3.5 Effect of spray voltage on the response of characteristic negative ion explosives (A.) and positive ion explosives (B.) when analyzed by DEFFI-MS.

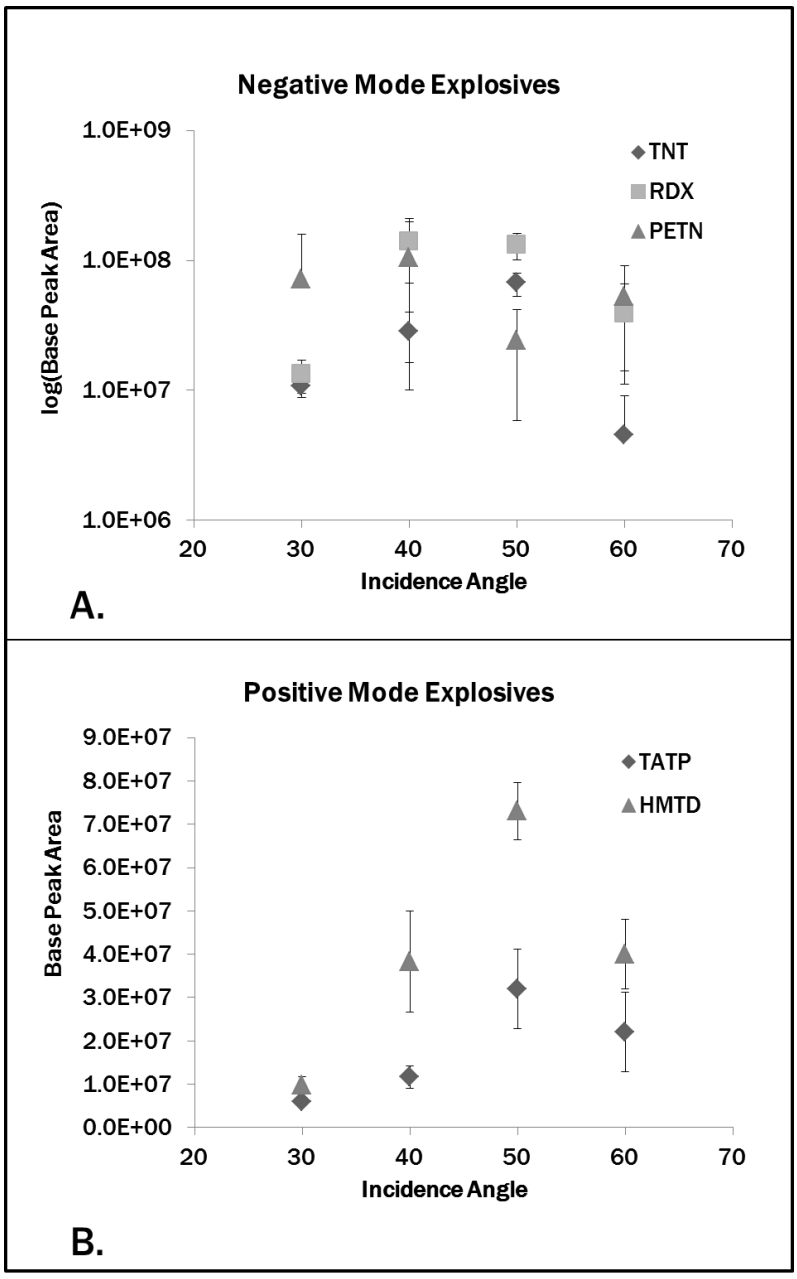

Figure 3.6 Effect of incidence angle on the response of characteristic negative ion explosives (A.) and positive ion explosives (B.) when analyzed by DEFFI-MS.

Subsection 3.3.4 The LTP Source

The LTP source required a different set of source parameters to be optimized because ionization was based on plasma formation rather than dissolving of the analyte by a charged liquid droplet. Three of the parameters that were optimized – gas flow

rates, applied voltage, and applied frequency – were specific to the source. An optimal incidence angle and sampling distances were also investigated. The gas flow rate, which was optimized from 300 mL/min to 500 mL/min, affects the plasma size and the efficacy of desorption. Figure 3.7 shows the parametric response for the samples with respect to gas flow rate. At low flow rates, insufficient desorption occurs as there is minimal force for the desorption of ions. At gas flow rates near 500 mL/min, it was found that the gas stream was strong enough for desorption to occur without pushing or blowing the sample away. The optimal flow rate for both positive and negative mode was found to be approximately 500 mL/min.

The applied voltage and frequency were also optimized. The voltage and frequency of the alternating voltage produce the dielectric barrier discharge and therefore, increased the ionizing strength of the plasma. Voltages attempted ranged from ±3000 V to ±4000 V with frequencies ranging from 2000 Hz to 3000 Hz. It was determined that for both positive and negative modes, a frequency of 3000 Hz and a voltage of ±4000 V provided optimal signal.

The incidence angle and sampling distances were also optimized for the LTP source. The response of characteristic explosives when analyzed at varying incidence angles is presented in Figure 3.8. The optimal sampling distances were shown to be similar to those for DESI and DEFFI. The optimal incidence angle was found to be approximately 50 °; with response steadily decreasing with deviation from this angle for all explosives. The optimal method, for both positive mode and negative was a gas flow rate of 500 mL/min, a plasma frequency of 3000 Hz, a plasma voltage of ±4000 V, and an incidence angle of 50 °. Representative spectra of explosives by the three sources can

be found in Appendix 4. A table outlining the optimal parameters for the three sources is presented in Table 3.2.

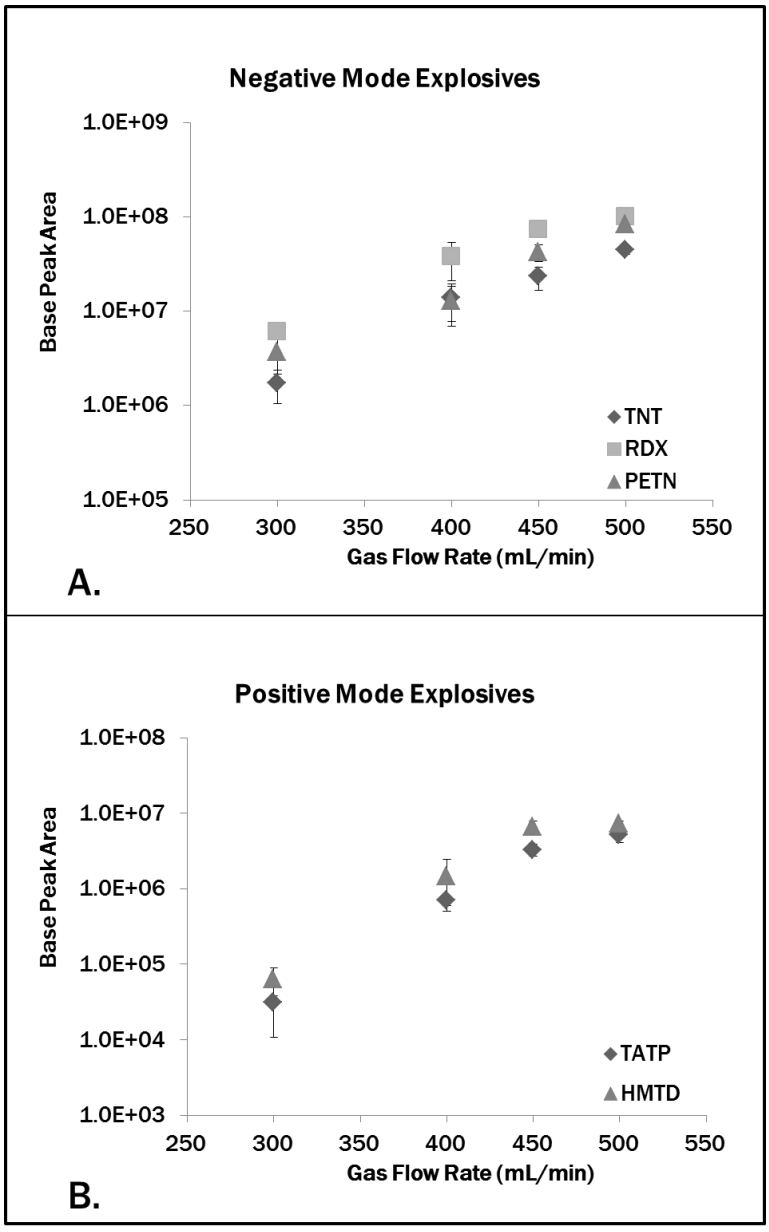

Figure 3.7 Effect of gas flow rate on the response of characteristic negative ion explosives (A.) and positive ion explosives (B.) when analyzed by LTP-MS.

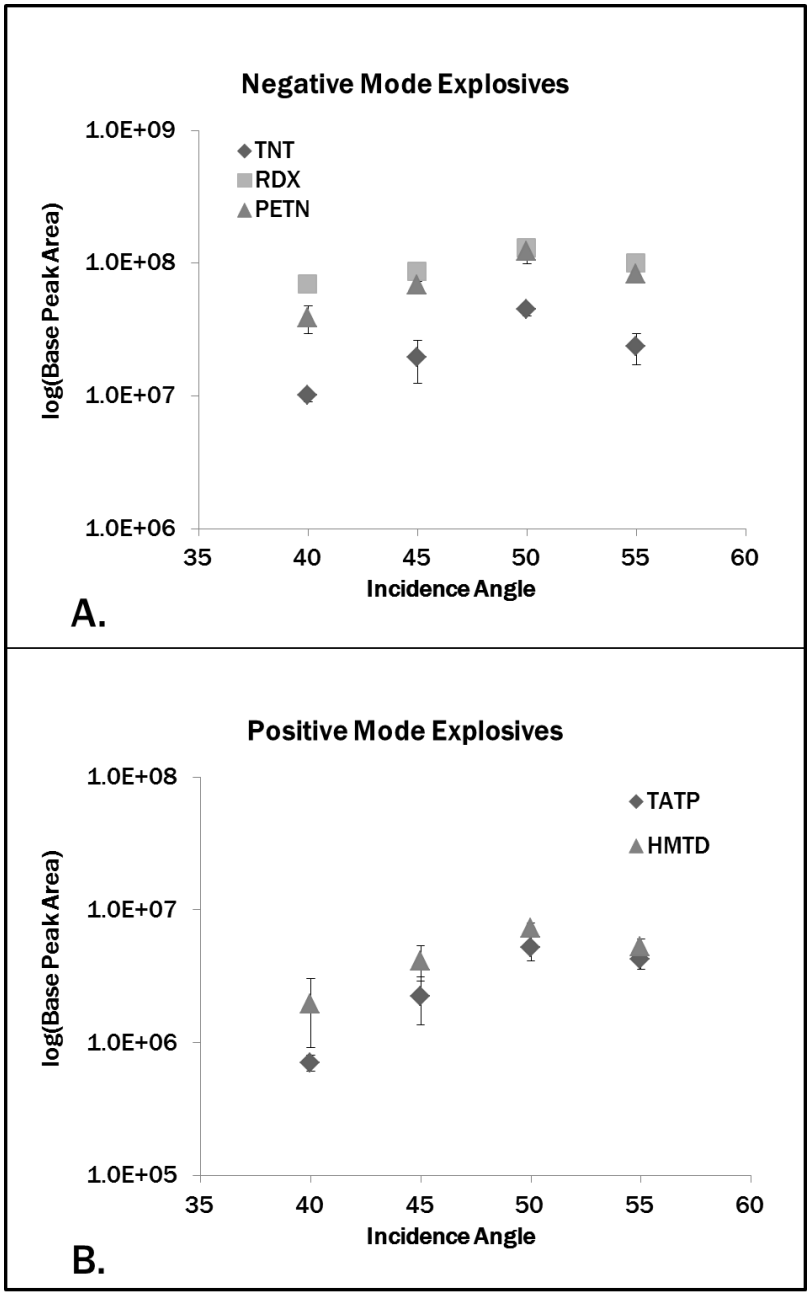

Figure 3.8 Effect of incidence angle on the response of characteristic negative ion explosives (A.) and positive ion explosives (B.) when analyzed by LTP-MS.

Table 3.2 Optimized method parameters for the detection of explosives in negative and positive mode by DESI, DEFFI, and LTP.

Parameter	DESI		DEFFI		LTP	
Ionization Mode	Negative	Positive	Negative	Positive	Negative	Positive
Incidence Angle	40 °	40 °	50 °	50 °	50 °	50 °
Applied Voltage	-4500 V	+2000 V	-1000 V	+500 V	-4000 V	+4000 V
Gas Flow / Pressure	675 kPa	675 kPa	Varied	Varied	500 mL/min	500 mL/min
Plasma Frequency	----	----	----	----	3000 Hz	3000 Hz
Tip-to-Surface Distance	1.0 mm	1.0 mm	1.0 mm	1.0 mm	2.0 mm	2.0 mm
Surface-to-Inlet Distance	0.5 mm	0.5 mm	~1.5 mm	~1.5 mm	2.0 mm	2.0 mm
Solvent Flow Rate	5 µL/min	5 µL/min	5 µL/min	5 µL/min	----	----
Solvent Spray Composition	50:50 MeOH:H_2O with 2 µg/mL $AgNO_3$	50:50 MeOH:H_2O with 2 µg/mL NaCl	Acetonitrile	Acetonitrile	----	----

Subsection 3.3.5 Limits of Detection

The limits of detection were determined, using the optimized methods, for each of the explosives analyzed. For all analyses the limit of detection was determined by finding the lowest level at which three replicates produced at least 3:1 signal-to-noise ratio for the base peak (excluding 62 *m/z*) on three separate days. Analysis was completed on three separate days to ensure repeatability from day to day. Table 3.3 depicts the limits of detection for the compounds analyzed using the three techniques. It was determined that in all instances the limits of detection across the different techniques are within an order of magnitude of one another. However, it was noticed that DEFFI is the most sensitive for the detection of nitramine explosives, such as RDX and HMX, likely due to its production of nitrate ions. LTP is generally better at detecting low levels of

nitrate esters like NG and ETN. All sources had difficulty detecting low levels of DEGDN and EGDN as well as the peroxides TATP and HMTD, as they are all fragile molecules which are easily fragmented.

Table 3.3 Obtained limits of detection for select explosives when analyzed by DESI-MS, DEFFI-MS, and LTP-MS.

Explosive	DESI (ng)	DEFFI (ng)	LTP (ng)
TNT	0.50	0.50	1.0
Tetryl	1.0	0.50	1.0
NG	1.0	1.0	0.50
DEGDN	10.0	10.0	10.0
PETN	0.50	0.50	0.50
RDX	0.10	0.050	1.0
TATP	100	100	100
HMTD	100	100	100

Subsection 3.3.6 Reproducibility

In order to establish the reproducibility of these techniques both inter-day and intra-day, three characteristic negative mode explosives, TNT, RDX, and PETN, and two peroxide explosives, TATP and HMTD were analyzed three times per day for a total of five different days by depositing 100 ng of each onto individual Teflon spots and monitoring the presence and mass accuracy of the three most abundance peaks in each of the spectra. The peaks were determined to be present if they were at a level of 1% or greater when the spectra were normalized and within ±0.5 Da of their theoretical mass. Table 3.4 depicts the reproducibility, as measure by percent of positive identification, for the three sources. In all cases, reproducibility of the techniques exceeded 98 % overall,

indicating that they would be sufficient for screening of trace compounds. The instances where reproducibility was lower than 100%, for TNT analysis by DESI and LTP, were caused by shouldering of the base peak due to the presence of an additional peak 1 Da apart.

Table 3.4 Reproducibility measurements for select explosives when analyzed by DESI-MS, DEFFI-MS, and LTP-MS.

Explosive	DESI	DEFFI	LTP
TNT	98.6 %	98.0 %	97.0 %
PETN	100 %	99.0 %	100 %
RDX	100 %	100 %	100 %
TATP	100 %	100 %	100 %
HMTD	100 %	100 %	100 %
Overall	**99.0 %**	**99.4 %**	**98.5 %**

Subsection 3.3.7 Ability to Analyze Mixtures

Another important aspect of an ideal screening technique that was investigated was the ability to analyze complex mixtures. To evaluate this capability, two mixtures were run five times, on two different days and searched against in-house search lists for the presence of the explosives. Detection was defined as the base peak being present at greater than 1% normalized intensity and within ±0.5 Da of their theoretical mass in an individual run. The first mixture contained ten components (2-A-4,6-DNT, 4-A-2,6-DNT, 1,3-DNB, 2,4-DNT, 2,6-DNT, 1,3,5-TNB, TNT, RDX, HMX, and Tetryl) all at a concentration of 100 µg/mL. Detection of each individual compound is presented in Table 3.5. Detection of the compounds is 90% or greater for all components. The

instances in which detection is lower than 100% are not due to the absence of peaks but rather the peaks being present below the 5% threshold. The second mixture contained six explosives (TNT, PETN, RDX, NG, 2,4-DNT, and EGDN) present at concentrations ranging from 20 µg/mL to 40 µg/mL. Detection of the fragile compound EGDN was shown to be extremely difficult in a mixture, as is shown in Table 3.6. For all sources, detection of EGDN was shown to be either not possible or extremely difficult. It is expected that other compounds like DEGDN and NG would behave similarly when present in a mixture. Representative spectra of each of the mixtures can be found in Appendix 4.

Table 3.5 Percent detection of the components in the ten-component explosive mixture when analyzed by DESI-MS, DEFFI-MS, and LTP-MS. A checked box indicates 100 % detection of that particular compound.

Explosive	DESI	DEFFI	LTP
2-A-4,6-DNT	☑	☑	☑
4-A-2,6-DNT	☑	☑	☑
1,3-DNB	90%	90 %	☑
2,4-DNT	☑	90 %	☑
2,6-DNT	☑	90 %	☑
1,3,5-TNB	90%	☑	☑
TNT	☑	☑	☑
RDX	☑	☑	☑
HMX	☑	☑	90%
Tetryl	☑	☑	☑

Table 3.6 Percent detection of the components in the six-component explosive mixture when analyzed by DESI-MS, DEFFI-MS, and LTP-MS. A checked box indicates 100 % detection of that particular compound.

Explosive	DESI	DEFFI	LTP
TNT	☑	☑	☑
PETN	☑	☑	☑
RDX	☑	☑	☑
NG	☑	☑	☑
2,4-DNT	☑	90 %	☑
EGDN	0%	0 %	0%

The third mixture which was analyzed was the eight component mixture that was used, similarly in Chapter 2, to measure not only the percent detection of the explosive classes but also to determine relative signal to neat for the various classes. Table 3.7 depicts the calculated relative signal to neat for DESI and DEFFI in addition to comparing those values to the values obtained with the DART source. The nitrate production in the DEFFI source is believed to help maintain the signal of nitrate adducting explosives such as RDX, HMX, and PETN. Poor retention of the nitroaromatic signal in DESI can likely be attributed to charge competition with the mixture. While the goal of this work was prove that detection of explosives in a mixture was possible, future work is going to focus on better understanding the processes which are occurring in mixtures such as this, as well as develop potential ways to combat the lower relative signals to neat or complete lack of detection in a mixture.

Table 3.7 Calculated relative signal to neat for the components within an eight-component mixture when analyzed by DART, DESI, and DEFFI.

Component	DART		DESI		DEFFI	
	S_{rel}	% RSD	S_{rel}	% RSD	S_{rel}	% RSD
TNT	80%	± 21.7%	18%	± 51.0%	74%	± 30.2%
2,4-DNT	51%	± 17.5%	17%	± 30.0%	47%	± 19.8%
PYX	0%	n/a	13%	± 36.6%	10%	± 34.3%
EGDN	0%	n/a	0%	n/a	0%	n/a
NG	14%	± 15.2%	0%	n/a	17%	± 36.8%
PETN	53%	± 21.4%	27%	± 48.4%	146%	± 32.9%
RDX	24%	± 17.3%	65%	± 68.5%	98%	± 38.1%
HMX	28%	± 16.8%	13%	± 56.7%	68%	± 39.3%

Subsection 3.3.8 Useful Yields

The final portion of the cross comparison study was to analyze the useful yields of characteristic explosives across the various sources. Three explosives, TNT, RDX, and PETN, were chosen as they represent the main explosive in each of the three classes, nitroaromatics, nitramines, and nitrate esters. Table 3.8 depicts the useful yield measurements for each of these explosives when analyzed using each of the sources. The table also shows the same calculations completed for other techniques discussed in this thesis, for comparison purposes. When comparing the three ionization sources, it is evident that the yields are relatively close to one another, indicating similar performance across the various sources. DESI provided the highest yields, at 10^{-5}, which can likely be attributed to the more robust and consuming nature of the source. For perspective, a useful yield of 1×10^{-6} indicates that roughly one in every one million neutral molecules is successfully desorbed, ionized, transported into and through the mass spectrometer,

and is detected. Since the source gas pressure of the DESI is much higher than that of DEFFI, it would be expected that DESI gives higher yields since desorption of the analyte off of the surface may be greater. Similarly, since LTP is relying solely on a gas stream for desorption and transfer of the analyte into the mass spectrometer, its yield is significantly lower than that of DESI. The increased sample loss is likely due to the lower ability to transfer ions and potentially also due do a different ionization mechanism which frequently causes increased fragmentation. It is also important to note that, while the yields for DESI analysis are the highest amongst the sources, the deviation from run to run is also quite high, which is indicative of potentially poor reproducibility in signal strength and detection, especially at levels near the limit of detection.

In addition to the three sources which were analyzed in this chapter, Table 3.8 also highlights the yields from a number of other techniques. When the sources are compared to the other ambient technique, DART, it can be seen that DESI, DEFFI, and LTP have yields that exceed those of DART. The increased yields are likely due to a combination of differences in the source and the mass spectrometer. The DART source desorbs samples at a much faster rate than any of the other sources because of its high temperature and high flow rates. Since nearly the entire sample is consumed within the first few seconds, instead of several minutes like DESI, DEFFI, and LTP, less ions will be successfully transported and analyzed by the mass spectrometer. The high flow rates of gas coupled with transmission mode analysis also may cause significant sample loss as a large part of the sample is carried away from the mass spectrometer inlet. The use of a time-of-flight (TOF) mass spectrometer may also hinder the yield as a faster scan rate (0.05 s versus 1 s) leads to increased dead time.

Table 3.8 Comparison of the obtained useful yields measurements of the various ionization sources for TNT, RDX, and PETN.

	TNT	RDX	PETN
DESI			
Useful Yield	3.0×10^{-5}	8.5×10^{-6}	$3.8 \times \times 10^{-5}$
% RSD	88.0 %	24.5 %	22.1 %
DEFFI			
Useful Yield	3.4×10^{-7}	1.0×10^{-7}	2.6×10^{-7}
%RSD	23.1 %	22.4 %	20.0 %
LTP			
Useful Yield	7.7×10^{-7}	1.0×10^{-6}	1.0×10^{-6}
% RSD	13.0 %	30.2 %	22.0 %
DART			
Useful Yield	2.3×10^{-8}	2.3×10^{-8}	1.2×10^{-8}
% RSD	25.5 %	22.8 %	35.5 %
GC-MS			
Useful Yield	2.2×10^{-7}	3.4×10^{-7}	1.2×10^{-8}
% RSD	12.5 %	14.8 %	10.5 %
SIMS			
Useful Yield	1.0×10^{-8}	3.8×10^{-8}	5.0×10^{-8}
% RSD	5.0 %	6.4 %	3.2 %

Comparison of the useful yields of the ambient sources to other techniques like GC-MS and SIMS are fairly similar as far as total number of analyte ions detected per neutral molecule. The difference between these techniques lies in the relative standard deviation amongst samples runs. The high vacuum techniques, such as SIMS has

extremely high transfer efficiency, which equates to much lower loss of ionized analyte molecules and therefore there is significantly less deviation from run to run when compared to the ambient techniques. This translates to more reproducible results, especially at low concentration levels. Sample loss is also minimized in a technique like GC-MS, where the column directly introduces the sample into the mass spectrometer.

One of the potential uses for useful yields measurements is to help optimize methods for analysis as well as determine which portion of the sampling and analysis scheme would be most beneficial to focus research efforts on. An example of how useful yields can be used to aid in method optimization is presented in Table 3.9, which presents the useful yields under various parameters for the analysis of TNT by DART-MS. By using the yields for different parameters it is possible to see which portions of the optimization provide the best enhancement in signal or are the most detrimental to detection. In this instance, it is seen that increasing the gas stream temperature results in a two-fold loss of analyte ions and approximately a two fold increase in variability between sample runs. Removal of the dopant species is another area which is shown to greatly affect the variability of sample-to-sample runs. Similarly, the yields can be used to look at the ability of different examiners to complete the analysis, in a casework setting. For the experiment described here, a second examiner from DFSC was asked to complete the identical useful yield experiment using the optimized method. The useful yield of the second examiner fell within 6 % of the yield for the analysis, indicating that the sampling methods between the two examiners are nearly equal and do not represent a major area for method improvement.

Table 3.9 Representation of how altering method or sampling parameters can affect the useful yield.

TNT	Optimized Method	Higher Gas Temperature (300 °C)	Lower Gas Temperature (150 °C)
Useful Yield	2.27×10^{-8}	1.26×10^{-8}	2.84×10^{-8}
% RSD	25.5%	45.7%	25.6%

TNT	Increased Orifice Voltage (-60 V)	Removal of Dopant	Second Examiner
Useful Yield	2.78×10^{-8}	1.90×10^{-8}	2.41×10^{-8}
% RSD	26.2%	88.2%	34.3%

.

Section 3.4 Conclusions

Optimized methods for a wide range of traditional explosive compounds have been established for DESI-MS, DEFFI-MS, and LTP-MS. These methods allow for successful detection of explosives in both negative and positive modes with sensitivities similar to those reported for DART-MS. While each source has its own particular strength, in terms of explosives it is best suited for detect, all have been shown to be effective in detecting the entire range of compounds. DEFFI has been shown to be particularly sensitive in the detection of nitramines and other nitrate adduct forming explosives, likely due to the in-source production of nitrate. LTP has the highest sensitivity for nitrate esters, and offers the best run-to-run reproducibility. DESI had a difficult time detecting multiple explosives in a mixture, but offers the greatest opportunity to alter ionization chemistry. Reproducibility of the sources has been shown to exceed 98% in all cases. The three sources have also been shown to effectively discriminate the majority of the components of complex mixtures, with difficulties detecting volatile explosives molecules such as EGDN. Finally, useful yields have

shown that DESI is the most efficient technique at ionizing samples, though it is hindered by high variability from sample run to run.

Chapter 4: Development of a Standard Artificial Fingerprint Material

Section 4.1 Introduction

Several of the studies that are described in this thesis deal with the development or application of new analytical techniques capable of spatially resolved chemical analysis of latent fingerprints. One of the difficulties in conducting such research is that the chemical composition of fingerprints is extremely variable, both throughout the population and even for an individual. Since the composition of a fingerprint residue is affected by a number of factors including but not limited to health conditions, medications, diet, use of cosmetic products, age, gender and race, it is nearly impossible to have two fingerprints which have identical chemical make-up. Other factors that make obtaining two similar fingerprints more difficult are differences in the force used to deposit the fingerprint and the spatial distribution of sebaceous and eccrine secretions throughout the finger, prior to deposition. This variability presents a number of issues that arise in fingerprint research, and have only recently been recognized by the forensic community.[82] There is currently significant interest in developing standardized practices to allow for direct comparison across research groups and projects. One way to address this need is by developing a standard artificial fingerprint material, which has a known composition, in addition to developing a standard artificial fingerprint. This chapter focuses on the development of such an artificial fingerprint. This process has already been adopted and is currently being validated by the Defense of Forensic Science Center

(DFSC), for use in research and the validation of the latent fingerprint development techniques.

Subsection 4.1.1 Composition of Typical Latent Fingerprint Residue

There are over three hundred chemicals that have been identified in fingerprints that are excreted from either eccrine or sebaceous glands.[83] While there is considerable variability in the exact composition and concentration of each individual component within a fingerprint, there are major constituents that are present in nearly all fingerprints at approximately equal proportions. It is important to note that the exact concentrations of these chemicals and the amount of fingerprint material deposited vary widely and may be dependent on gender, age, and some medical conditions.

The first, and most common, type of secretion found in fingerprint material is the eccrine secretion. More commonly known as sweat, these materials are excreted by eccrine glands and contain 98% to 99% water by weight.[84] The additional 1% to 2% of the eccrine excretion contains numerous inorganic and organic compounds. Major inorganic components that are present in sweat include ammonia, iodide, bromide, fluoride, sodium, iron, sulfate, magnesium, phosphate, potassium, and calcium.[28,83] The average concentrations of these ions in sweat are listed in Table 4.1. Inorganic components that are present at trace levels include zinc, copper, cobalt, lead, manganese, molybdenum, mercury, sulfur, and tin.[28,83]

Table 4.1 Typical concentrations of the inorganic components of eccrine secretions.

Inorganic Component	Concentration (mg / L)
Cl^-	520 – 7,000
HCO_3^-	915 – 1,220
SO_4^{2-}	7 – 190
PO_4^{3-}	10 – 17
F^-	0.2 – 1.18
Br^-	0.2 – 0.5
I^-	0.005 – 0.012
Na^+	750 – 6,100
K^+	190 – 340
Ca^{2+}	100 – 150
NH_4^+	10 – 150
NH_4^+	9 – 144
$Fe^{2+/3+}$	1 – 70
Mg^{2+}	Trace
Zn^{2+}	Trace
$Cu^{+/2+}$	Trace
Co^{2+}	Trace
Mn^{2+}	Trace
Mo^{2+}	Trace
$Sn^{2+/4+}$	Trace
$Hg^{1+/2+}$	Trace

Aside from the inorganic components present in eccrine secretions, there are also a number of organic components, which are comprised of mostly amino acids and proteins. The concentration of amino acids present in a typical fingerprint has been found to range between 0.3 mg/L and 2.5 mg/L.[83] Several different studies have been completed that explored the relative concentrations of individual amino acids, and it was found that the percent abundance was largely uniform.[28,83,85] All of the studies found that

the most abundant amino acid in the eccrine secretion is serine. Glycine (present at a concentration by mass of 54% to 67% that of serine) and ornithine (present at a concentration by mass of 32% to 45% that of serine) are typically the second and third most abundant amino acids.[85] Other amino acids which have been detected in fingerprints at concentrations greater than ten weight percent that of serine include alanine (30%), aspartic acid (18%), threonine (15%), histidine (15%), valine (10%), and leucine (10%).[85,86]

Proteins comprise the other major organic component of eccrine secretions, and are found at concentrations ranging from 0.15 g/L to 0.25 g/L.[28] The identities of the proteins present in a fingerprint are extremely varied. A study that characterized proteins in fingerprints using 2-D electrophoresis was able to identify over 400 different polypeptide components, including albumin, glycoproteins, lysozymes, and lipoproteins.[28] Additional organic compounds that can be present in the eccrine secretions of fingerprints at trace levels include lipids, enzymes, immunoglobins, and vitamins. Certain drugs, and their metabolites, can also be excreted through the eccrine glands.[87–89]

In conjunction with eccrine secretions, sebaceous secretions are also commonly found in fingerprints. Sebaceous secretions, also known as sebum, are excreted by the sebaceous glands, located next to hair follicles. The sebaceous glands are most concentrated on the face and scalp and are widely absent from the palms of the hands and the soles of the feet. Even though sebaceous glands are not present on fingers and palms, sebum can represent a significant fraction of fingerprint components because of the tendency to touch areas of the body where sebaceous glands are concentrated. The

components in sebum can be broken down into six main classes, as highlighted in Table 4.2. Free fatty acids, which are the largest constituent, are present due to the hydrolysis of a number of wax esters and triglycerides.[83] Both saturated and unsaturated fatty acids are present in sebum, at roughly equal amounts. The most abundant saturated fatty acids are octadecanoic acid ($C_{18:0}$), hexadecanoic acid ($C_{16:0}$), and tetradecanoic acid ($C_{14:0}$).[28,86] The most common unsaturated fatty acids are monoenes, accounting for nearly all of the unsaturated fatty acid make-up, with (9Z)-hexadecenoic acid ($C_{16:1}$) and (9Z)-octadecenoic acid ($C_{18:1}$) being the most common.[28] Several multiple unsaturated fatty acids, including cis-9,12-octadecadienoic acid ($C_{18:2}$) and cis-9,12,15-octadecatrienoic acid ($C_{18:3}$), as well as several branched chain fatty acids, are also present in sebaceous secretions.

Wax esters are the second most abundant class of compounds, containing a fatty acid esterified to a fatty alcohol. These wax esters range in size from 18 carbons to 27 carbons, with 20 carbon esters being the most common.[28] Like free fatty acids, a variety of wax esters exist, most all of which have at least one unsaturation, and roughly 25 % of which are branched.

Cholesterol and its related compounds represent the remaining portions of sebaceous secretions. While the amount of cholesterol present in an adult's fingerprint is low (approximately 1% by weight), its precursor, squalene, is abundant in much higher amounts. Also, though trace in an adult fingerprint, cholesterol has been shown to be a larger component of children's fingerprints, accounting for up to 10% of the sebaceous secretion by weight.[90] In addition to cholesterol and squalene, the other major cholesterol-related constituents are cholesterol esters. Cholesterol esters are present in

sebaceous secretions because of bacterial esterification of free cholesterol and the release of free sterols from the lower skin layers.[28] Like the free fatty acids and wax esters, there is a wide range of cholesterol esters present in sebaceous secretions.

Table 4.2 Typical weight percentages of the various components of sebaceous secretions. The first six categories represent the main classes of constituents.

Sebaceous Component	**Concentration (wt%)**
Free Fatty Acids	30 - 40%
Glycerides	15-25%
Wax Esters	20 - 25%
Squalene	10 - 12%
Cholesterol Esters	2 - 3%
Cholesterol	1 - 3%
Aldehydes	Trace
Ketones	Trace
Amines	Trace
Amides	Trace
Alkanes	Trace
Alkenes	Trace
Alcohols	Trace
Phospholipids	Trace
Pyrroles	Trace
Pyridine	Trace
Piperidines	Trace
Pyrazines	Trace
Furans	Trace
Haloalkanes	Trace
Mercaptans	Trace
Sulfides	Trace

Subsection 4.1.2 Factors that Affect Fingerprint Composition

There are a variety of factors that can affect the chemical composition of individual fingerprints. Most prominent, is the effect of donor age, which is correlated to sebaceous gland activity. These glands are nearly inactive throughout childhood, yet become very active and peak in activity during puberty, with a gradual decrease with age after that.[91] Therefore, the fingerprint of a child is typically absent of sebaceous secretions and is composed almost solely of eccrine secretions. Furthermore, the amount of sebaceous secretions deposited tends to vary between male and female, with males depositing up to ten times more fingerprint material than females.[92] Bacteria are another factor that can affect fingerprint composition, especially in regards to sebaceous secretions. Studies have shown the presence of bacteria present in soils can degrade squalene and unsaturated fatty acids on the hands.[93] Drugs and medications can also alter the chemical composition by changing the rate of excretion of either of the two glands.[94] A number of drugs and their metabolites are excreted through sweat and therefore can be detected in a fingerprint.[94] The presence of any cosmetic product or lotion on the hand will also affect the chemical make-up of the fingerprint.[95] Finally, there is some evidence to suggest that changing diet will alter the composition. One such study reported significant differences in amino acid concentrations between vegetarians and omnivores.[85]

Subsection 4.1.3 The Need for an Artificial Fingerprint Material

While it would be extremely difficult to replicate the entire chemical composition of a human fingerprint due to the inherent complexity and variability, it is possible to develop

an artificial fingerprint material containing a number of the most abundant and chemically relevant fingerprint components. Commercial products do exist, however they only incorporate a handful of components at physiologically irrelevant concentrations. Also, previous studies have been completed to create artificial sweat and sebum[96–99], however this is the first attempt to incorporate both excretion types into one inclusive material.

The development of this material was focused on the chemicals present in fingerprints that are at concentrations that can be detected by a number of different analytical techniques such as secondary ion mass spectrometry (SIMS), ambient ionization mass spectrometry (AI-MS), gas chromatography mass spectrometry (GC-MS), and Fourier transform infrared spectroscopy (FTIR). From an extensive literature search and the compilation of the chemical compositions of actual fingerprints, a list of the prevalent and readily detected fingerprint constituents was established. This provided the basis for several iterations of artificial sebum and artificial eccrine secretions to be developed to formulate a mixture that most closely mimics the chemical composition of actual human fingerprints. Since a number of different compositions were attempted, each iteration was compared, using SIMS, AI-MS, and FTIR, to the collection of real human fingerprints spectra. Furthermore, the artificial fingerprint material was also compared to other artificial fingerprint materials, both commercially available and from literature.

The ability to make a chemically relevant fingerprint material can have wide ranging applications. It could allow for a reproducible sample set for any type of latent fingerprint research, or as a standard for development in casework analysis. Research opportunities involving the study of the chemical changes in fingerprints and

opportunities in increasing the understanding of the chemical reactions of fingerprint development techniques could benefit from such a material. Furthermore, reproducible fingerprints could be used to test a forensic examiner's ability to visually develop fingerprints and possibly be used for proficiency testing in the forensic laboratories. Also, since the substance is made in-house, the chemical composition can be altered to remove individual components or to add additional ones. This can allow for inclusion or exclusion of components which could be useful in a number of different applications such as trace detection.

Section 4.2 Materials and Methods

Subsection 4.2.1 Instrumental Parameters

In order to compare the chemical signature of the artificial fingerprint material to that of actual fingerprints, a number of analytical techniques were used. These techniques include FTIR, desorption electrospray ionization mass spectrometry (DESI-MS), and SIMS. Each of these techniques required a separate method of sample preparation as well as individual analysis parameters.

For analysis with FTIR, fingerprints were deposited directly onto IR-reflective slides purchased from MirrIR (Kevley Technologies, Chesterland, OH, USA). Analysis was completed with a Smiths IlluminatIR II microscope (Watford, UK) using the attenuated total reflectance (ATR) objective. Additional run parameters included the summing of 128 scans per sample analysis, a resolution of 8 cm^{-1}, and an analysis window of 4000 cm^{-1} to 650 cm^{-1}. All samples were analyzed in triplicate, and the data was

processed using Grams AI Spectroscopy Software (Thermo Scientific, Waltham, MA, USA).

DESI-MS analysis was completed by depositing fingerprints directly onto clean glass microscope slides (VWR, Radnor, PA, USA). The ionization source used was a Prosolia DESI source (Indianapolis, IN, USA) coupled to an ABSciex 4000 Q Trap mass spectrometer (Framington, MA, USA). Source parameters included a spray voltage of ±4000 V, N_2 carrier gas at a pressure of 80 psi (550 kPa), an incidence angle of approximately 40 ^{0}, and a solvent flow rate of 5 µL/min. The solvent used was a 50:50 methanol-water mixture. Mass spectrometer parameters included an inlet temperature of 200 ^{0}C and a scan range of 100 *m/z* to 800 *m /z*, with an integration of one second per scan. Both positive and negative ion mass spectra were collected.

Preparation of samples for analysis by SIMS was completed by depositing the sample onto a 2.54 cm circular silicon wafers. Analysis of the samples was completed on a CAMECA IMS-4f (Madison, WI, USA) equipped with an IonOptika C_{60} primary ion source (Gennevilliers Cedex, France). Instrument parameters included a primary ion accelerating voltage of 10 keV, a 500 µm by 500 µm raster size, a 250 µm by 250 µm imaging field, and a primary current of 1 x 10^{-10} A. Mass spectrum parameters included a scan range of 0 *m/z* to 300 *m/z* with 900 cycles and an integration time of 0.1 s/cycle. Like DESI-MS analysis, both positive and negative ion scans were completed.

Subsection 4.2.2 Emulsion Development

To prepare the sweat solution, the components listed in Table 4.3 (total of 19) were dissolved into 990 mL of deionized water, in a volumetric flask. The sample was then

sonicated for fifteen minutes to ensure complete mixing. After mixing, the solution was adjusted to a pH of approximately 5.5 using 5.0 M NaOH and 12 M HCl. Once the pH was adjusted, the solution was brought to a final volume of 1000 mL and sonicated for an additional fifteen minutes.

The chemicals that were used to create the sebum, the amount used, and the supplier from where they were purchased from are listed in Table 4.4 (total of 23). The sebum was produced by mixing the compounds listed in Table 4.4 in a 20 mL amber vial using sonication. The heat produced from sonication (which raised the temperature of the mixture to approximately 35 °C) was sufficient to liquefy all solid components and allow for complete mixing. It was also found, during the first attempts, that mixing time can be reduced by adding a small amount (approximately 1 mL) of heptane to the sebum mixture. The heptane can then be evaporated off once the mixture has combined.

The goal of this work was to create a single fingerprint material that incorporated the major components of both eccrine and sebaceous secretions. In order to accomplish this, it was determined that producing an emulsion was the most easily implemented approach. In order to make the emulsion, equal amounts (by weight) of artificial sebum and sweat were sonicated together and an emulsifying agent, Steareth-20, (Sigma-Aldrich, St. Louis, MO, USA) was added at approximately 0.5% by weight. Steareth-20 is a common emulsifying agent found in cosmetics and creams and is a plausible exogenous material that could be found in actual fingerprints. The final emulsion has the consistency of a cosmetic lotion, allowing it to be easily applied to surfaces, fingers, or artificial fingers. If a dilute emulsion is desired, the material could be diluted in water.

Table 4.3 Chemicals, and their amounts, used to create the artificial eccrine secretion.

Chemical	Amount (mg)	Supplier
Inorganic Salts		
Potassium Chloride	1,400	Sigma- Aldrich
Sodium Chloride	1,300	Sigma- Aldrich
Sodium Bicarbonate	250	Sigma- Aldrich
Ammonium Hydroxide	175	Sigma- Aldrich
Magnesium Chloride	40	Sigma- Aldrich
Amino Acids		
Serine	275	Carolina
Glycine	135	Carolina
Ornithine	110	Carolina
Alanine	80	Carolina
Aspartic Acid	40	Carolina
Threonine	40	Carolina
Histidine	40	Carolina
Valine	30	Carolina
Leucine	30	Carolina
Other Components		
Lactic Acid	1,900	Sigma- Aldrich
Urea	500	Sigma- Aldrich
Pyruvic Acid	20	Sigma- Aldrich
Acetic Acid	5	J.T. Baker
Hexanoic Acid	5	Sigma- Aldrich

Table 4.4 Chemicals, and their amounts, used to create artificial the sebaceous secretion.

Chemical	Amount (mg)	Supplier
Free Fatty Acids		
Hexanoic Acid	50	Sigma-Aldrich
Heptanoic Acid	50	Sigma-Aldrich
Octanoic Acid	50	Sigma-Aldrich
Nonanoic Acid	50	Sigma-Aldrich
Dodecanoic Acid	50	Sigma-Aldrich
Tridecanoic Acid	50	Sigma-Aldrich
Myristic Acid	50	Sigma-Aldrich
Pentadecanoic Acid	50	Sigma-Aldrich
Palmitic Acid	55	Sigma-Aldrich
Stearic Acid	55	KIC
Arachidic Acid	50	Sigma-Aldrich
Linoleic Acid	55	Fluka
Oleic Acid	55	Sigma-Aldrich
Triglycerides		
Triolein	275	Sigma-Aldrich
Tricaprylin	20	Supelco
Tricaprin	20	Supelco
Trilaurin	20	Supelco
Trimyristin	20	Supelco
Tripalmitin	20	Supelco
Other Components		
Squalene	120	Fluka
Cholesterol	30	Sigma-Aldrich
Cholesterol n-Decanoate (Cholesterol Ester)	40	Sigma-Aldrich
Cetyl Palmitate (Wax Ester)	155	Sigma-Aldrich

Subsection 4.2.3 Artificial Fingers

Production of artificial fingers was accomplished using dental stone and ballistics gelatin.[100] To prepare the cast for the ballistics gelatin, dental stone was prepared, as per the manufacturer's instructions, and poured into 50 mL plastic beakers. A human finger was then placed in the dental stone and allowed to cure for approximately ten minutes. Once cured, the finger was removed and heated ballistics gelatin was poured into the mold. After the gelatin had solidified, the artificial finger was carefully removed. This produces a positive image of the original fingerprint. The dental stone mold can be reused to create multiple artificial fingers. Additionally, 3-D printed artificial fingerprint stamps were created by Matthew Staymates at the National Institute of Standards and Technology (NIST), using Auto-CAD software. These artificial fingerprints were based upon a real fingerprint where ridge details within the computer generated model were altered to make the fingerprint biometrically different from anyone, thus removing any concerns of personal identifiable information. Artificial fingerprints were produced by depositing a known amount of the emulsified mixture (typically 1 µL to 10 µL) onto a glass slide. The artificial finger was then swiped over the fingerprint material to load the finger with the emulsion and then subsequently pressed down onto the surface of interest to produce a fingerprint. Real fingerprints were prepared by loading the finger with sebaceous material by rubbing the subject's forehead, followed by deposition onto the surface of interest.

Subsection 4.2.4 Fingerprint Development Techniques

Traditional analysis of latent fingerprints involves the use of physical and/or chemical developing techniques to better visualize the fingerprint. Therefore, to evaluate the ability to develop artificial fingerprints and compare them to actual fingerprints, a number of development techniques were tested. The techniques explored include: black fingerprint powder, fluorescent fingerprint powder, cyanoacrylate fuming followed by treatment with rhodamine 6G, ninhydrin, crystal violet, and 1,2-indanedione. Latent prints deposited on glass microscope slides were developed using black fingerprint powder and fluorescent fingerprint powders (Sirchie Co., Youngsville, NC, USA)

Latent prints deposited on bond paper (Navigator premium multipurpose ultrabright) were developed using solutions of ninhydrin or 1,2-indanedione. To prepare the ninhydrin working solution, 5 g of ninhydrin (Evident Crime Scene Products, Union Hall, VA, USA) was mixed into 45 mL ethanol (Fisher Chemical, Pittsburgh, PA, USA), 2 mL ethyl acetate (Fisher Chemical, Pittsburgh, PA, USA), and 5 mL glacial acetic acid (Sigma Aldrich, St. Louis, MO, USA); to this solution, 1 L of Novec™ HFE7100 (3M, St. Paul, MN, USA) was added for the final dilution step. The 1,2-indanedione working solution was prepared by dissolving 2 g of 1,2-indanedione (Sirchie Co.) in 70 mL ethyl acetate and mixing with 930 mL Novec™ HFE7100 (3M). These working solutions were applied individually to the bond paper by spraying the surface until it was wetted thoroughly. After air-drying, the papers were placed in a drying oven at 90 °C for 20 minutes.

Latent prints deposited on clear packing tape (Scotch Brand, 3M) were developed using superglue or gentian violet. To develop with superglue, the tapes were hung in a

0.05 m^3 cabinet with 150 mg superglue (Adhesive Systems RP100, Frankfort, IL, USA) in an aluminum dish on a hot plate heated to 110 °C. The tapes were allowed to fume for 10 minutes, and the cabinet was vented for 10 additional minutes prior to opening. After development with superglue, the developed prints were rinsed with a methanol-based solution of rhodamine 6G for enhanced visualization. The rhodamine 6G working solution consisted of 5 mg rhodamine 6G (Sigma-Aldrich) in 500 mL methanol (Fisher Chemical). The gentian violet working solution was prepared by adding 1 g gentian violet to 1 L distilled water. The tapes were dipped into a shallow bath of gentian violet working solution, and then rinsed with a gentle stream of water.

The developed fingerprints were photographed using a Nikon Af-5 Micro (Nikon, Toyko, Japan) camera under a light source suitable for the developer used. A 532 nm laser (Coherent TracER, Santa Clara, CA, USA) was used to illuminate fingerprints developed with 1,2-indanedione and rhodamine 6G. When using the 532 nm laser, an orange filter was placed over the camera lens (Promaster YA2 filter, 62 mm, filter factor 2.5, exposure factor 1.3 stops). A white light source (Spex Crimescope CS15-400, Edison, NJ, USA) was used to illuminate fingerprints developed by ninhydrin and gentian violet.

Section 4.3 Results and Discussion

Subsection 4.3.1 Chemical Comparison of the Artificial Fingerprint Material to Real Fingerprints

To evaluate the chemical relevance of the emulsion to actual fingerprints, chemical analysis of the two samples was completed using FTIR, SIMS, and DESI-MS. All three

of the techniques showed that the emulsion is chemically similar, though not chemically identical, to actual fingerprints that were also analyzed. The FTIR comparison, which is presented in Figure 4.1, shows that a number of characteristic peaks are shared amongst the two samples. These common peaks include the C-H doublet peak at 2800 cm^{-1}, and the C-C bond peaks in the 1600 cm^{-1} region. Two peaks that show significant differences in intensity are the –OH peak at 3300 cm^{-1} and the C-O peak at 1100 cm^{-1}. The increase in the C-O bond peak in the actual fingerprint is likely attributed to a fingerprint with a greater sebum to sweat ratio than is present in the emulsion (which is 1:1 w/w).

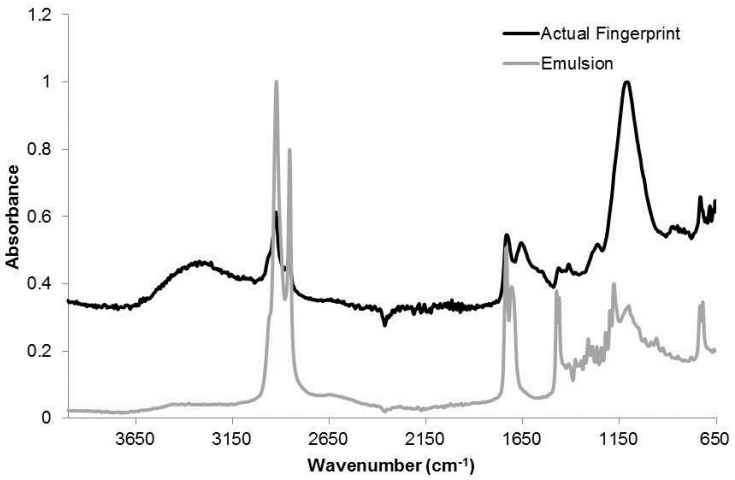

Figure 4.1 FTIR spectral comparison of the artificial fingerprint material (grey) to a real fingerprint (black).

Figures 4.2 and 4.3 illustrate the similarities between the actual fingerprint and emulsion when analyzed by SIMS in positive and negative modes, respectively. The benefit of analyzing samples via SIMS instead of more traditional mass spectrometry based techniques is that it allows for simultaneous analysis of organics and inorganics. The positive ion mass spectrum provides information predominantly on the inorganics,

such as sodium and potassium, which are found in both the fingerprint and the emulsion. While there are some differences between the two positive ion mass spectra, almost all peaks present in the fingerprint are also present in the emulsion. Furthermore, the mass spectrum of the emulsion has additional peaks present in the 200 *m/z* to 600 *m/z* range. These peaks have been identified as being related to the emulsifying agent Stereath-20, and can be subtracted out if necessary. The negative ion mass spectra provide more in-depth information on the anionic species present in the samples, as well as amino acids and fatty acids. The make-up of the longer chain fatty acids (mass range 200 *m/z* to 350 *m/z*) is nearly identical with the exception of heptadecanoic acid ($[M-H]^-$ at 269 *m/z*), which is present in actual fingerprints but not in the emulsion. Amino acids, which are present in the 70 *m/z* to 150 *m/z* range, are also similar between the fingerprint and the emulsion.

A comparison of the chemical compositions via negative ion DESI-MS is presented in Figure 4.4 and shows similar agreement to SIMS. Stronger peaks for the glycerides present in the range beyond 400 *m/z* are present and are likely due to a larger amount of sample deposited with the emulsion when compared to the fingerprint. Overall, the three analytical techniques used here show that the chemical composition of the sebum-sweat emulsion very closely resembles the composition of real human fingerprints.

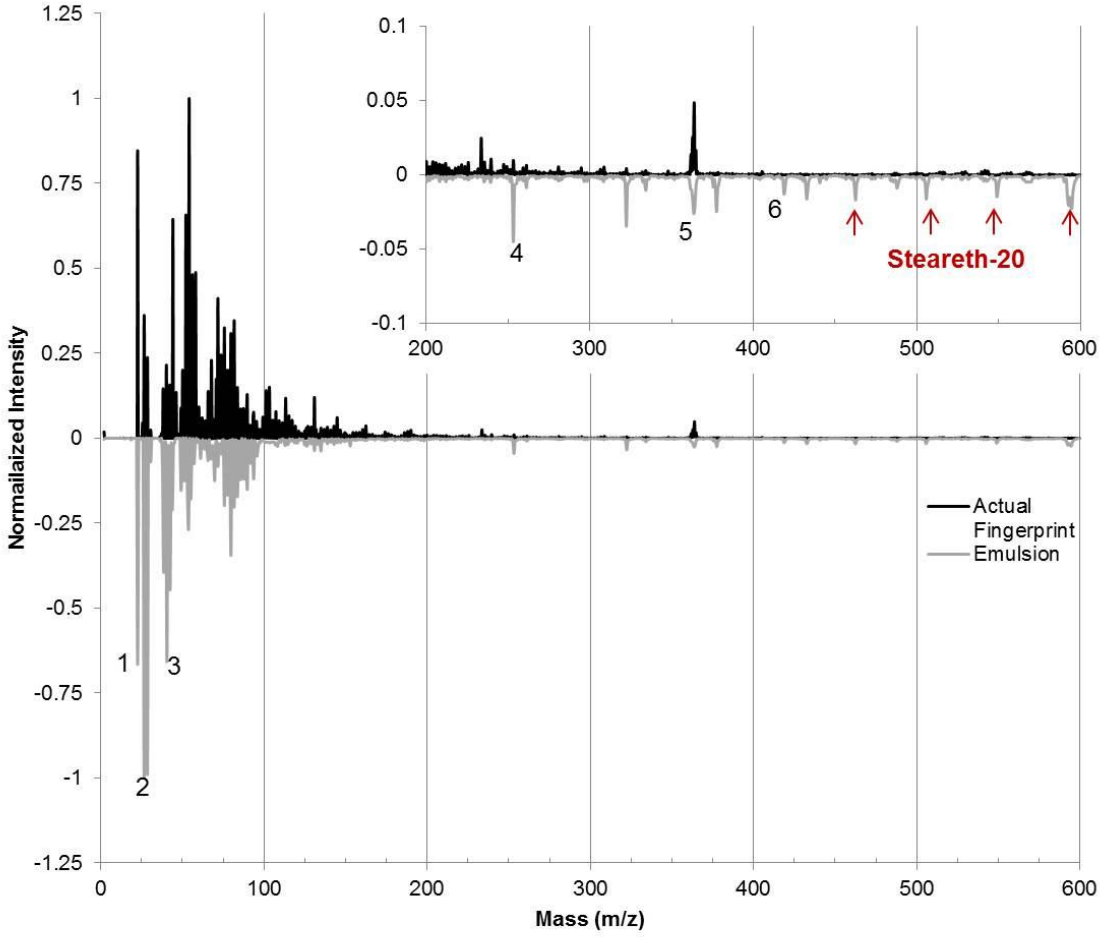

Peak #	Nominal Mass	Compound	Peak #	Nominal Mass	Compound
1	23	Sodium	4	257	Palmitic Acid $[M+H]^+$
2	24	Magnesium	5	369	Cholesterol $[M-OH]^+$
3	39	Potassium	6	410	Squalene $[M+H]^+$

Figure 4.2 Comparison of the positive mode SIMS mass spectrum of the artificial fingerprint material (grey) and an actual fingerprint (black). Representative peaks are also identified.

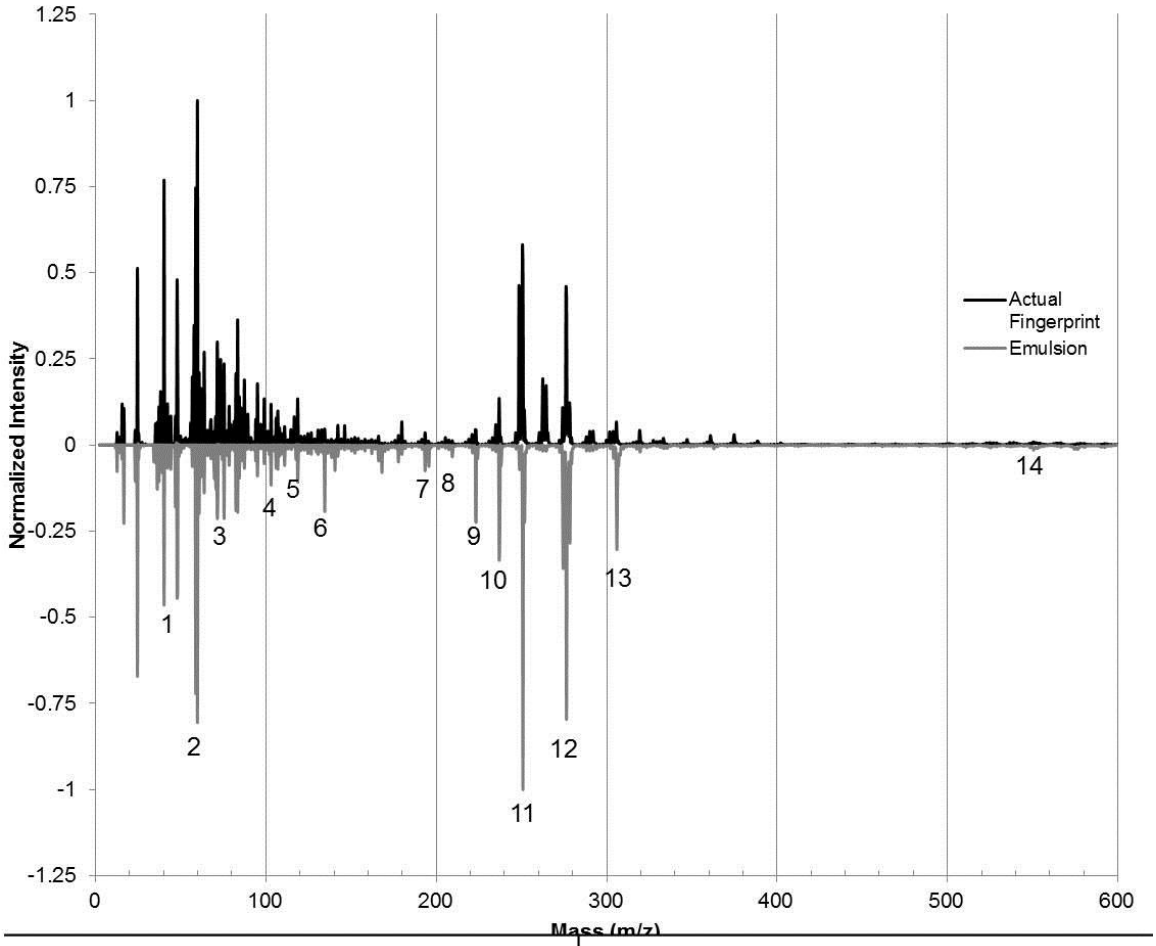

Peak #	Nominal Mass	Compound	Peak #	Nominal Mass	Compound
1	35	Chloride	8	213	Tridecanoic Acid $[M-H]^-$
2	59	Urea $[M-H]^-$	9	227	Tetradecanoic Acid $[M-H]^-$
3	74	Glycine $[M-H]^-$	10	241	Pentadecanoic Acid $[M-H]^-$
4	104	Serine $[M-H]^-$	11	255	Hexdecanoic Acid $[M-H]^-$
5	116	Valine $[M-H]^-$	12	269	Octadecanoic Acid $[M-H]^-$
6	131	Ornithine $[M-H]^-$	13	283	Eicosanoic Acid $[M-H]^-$
7	199	Dodecanoic Acid $[M-H]^-$	14	553	Tricaprin $[M-H]^-$

Figure 4.3 Comparison of the negative mode SIMS mass spectrum of the artificial fingerprint material (grey) and an actual fingerprint (black). Representative peaks are also identified.

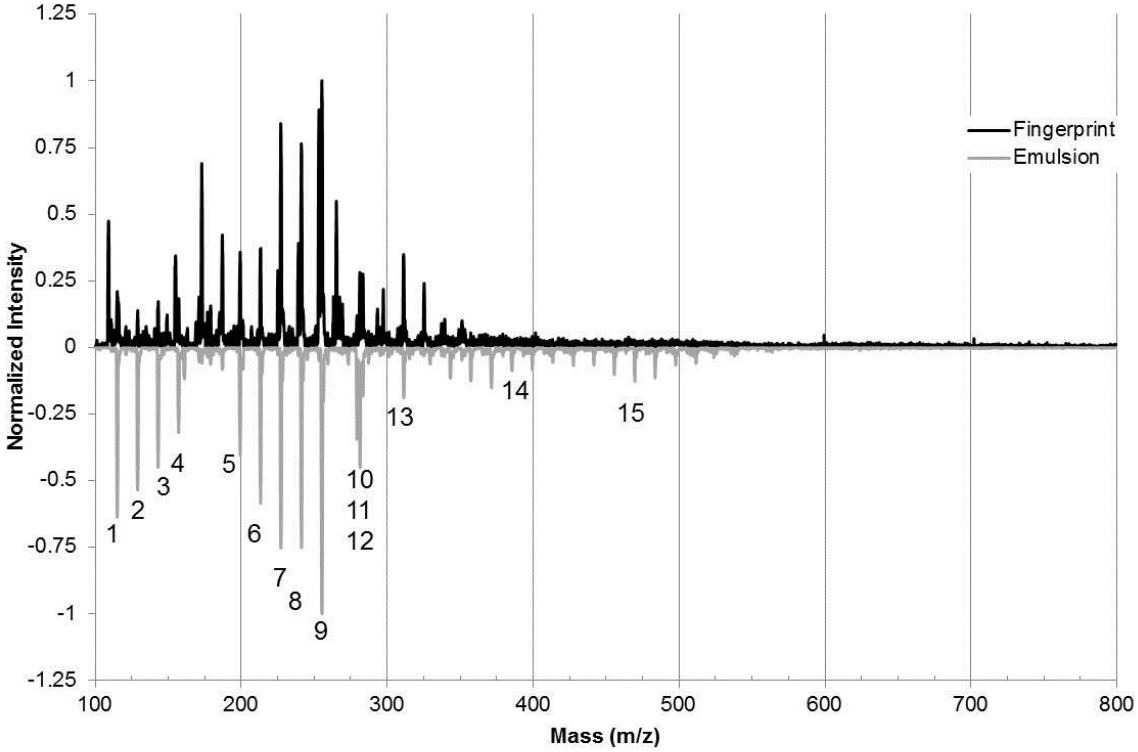

Peak #	Nominal Mass	Compound	Peak #	Nominal Mass	Compound
1	115	Hexanoic Acid $[M-H]^-$	9	255	Hexdecanoic Acid $[M-H]^-$
2	129	Heptanoic Acid $[M-H]^-$	10	279	Linoleic Acid $[M-H]^-$
3	143	Octanoic Acid $[M-H]^-$	11	281	Oleic Acid $[M-H]^-$
4	157	Nonanoic Acid $[M-H]^-$	12	283	Stearic Acid $[M-H]^-$
5	199	Dodecanoic Acid $[M-H]^-$	13	312	Eicosanoic Acid $[M-H]^-$
6	213	Tridecanoic Acid $[M-H]^-$	14	386	Cholesterol $[M-H]^-$
7	227	Tetradecanoic Acid $[M-H]^-$	15	469	Tricparylin $[M-H]^-$
8	241	Pentadecanoic Acid $[M-H]^-$			

Figure 4.4 Comparison of the negative mode DESI mass spectrum of the artificial fingerprint material (grey) and an actual fingerprint (black). Representative peaks are also identified.

Subsection 4.3.2 Stability of the Artificial Fingerprint Material

To establish the stability of the artificial fingerprint material the emulsion was allowed to age six months under storage at -4 °C and then re-analyzed using the mass spectrometry based techniques under identical parameters used for the initial analysis. Figure 4.5 shows the negative ion SIMS comparison of the fresh emulsion to the aged emulsion. While the constituents which were initially present are still detectable at six months, it was noted that the relatively fatty acid signal is lower, indicating a potential loss or degradation of the fatty acid constituents as the sample was aged. These results were supported by the negative ion DESI-MS spectrum, shown in Figure 4.6. The negative ion DESI-MS spectra show a noticeable decrease in the more volatile shorter chained fatty acids (shorter than fourteen carbons) as well as a marked decrease in the larger chained unsaturated fatty acids. Degradation of the triglycerides was also noted in the aged emulsion. Future work will focus on quantifying this relative loss using sandwich injection GC-MS methods as well as determining a shelf life for material as well as optimal storage conditions.

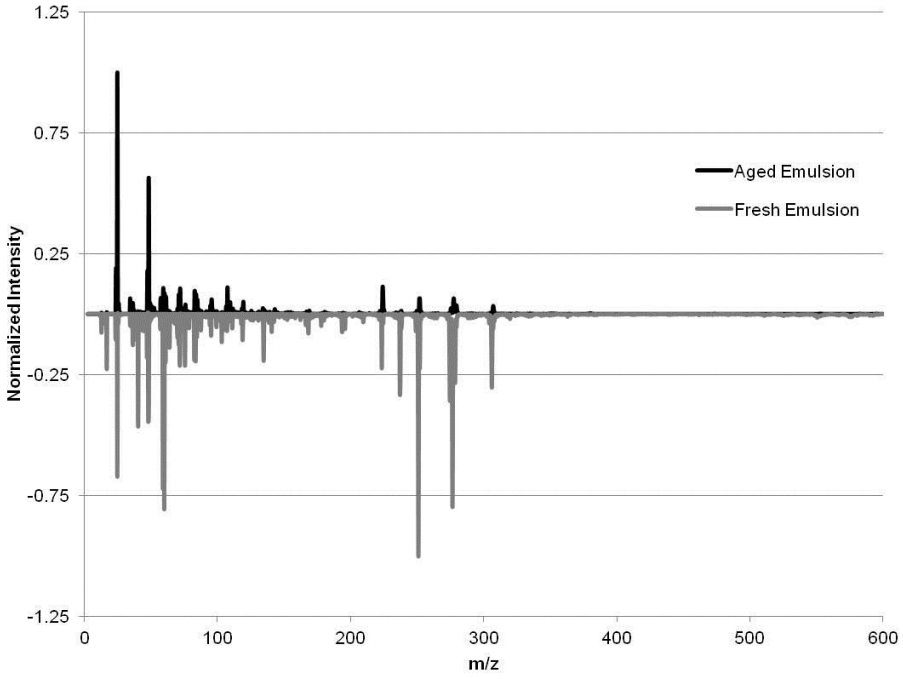

Figure 4.5 Negative ion SIMS mass spectral comparison of the 6 month aged emulsion (black) to freshly made emulsion (grey).

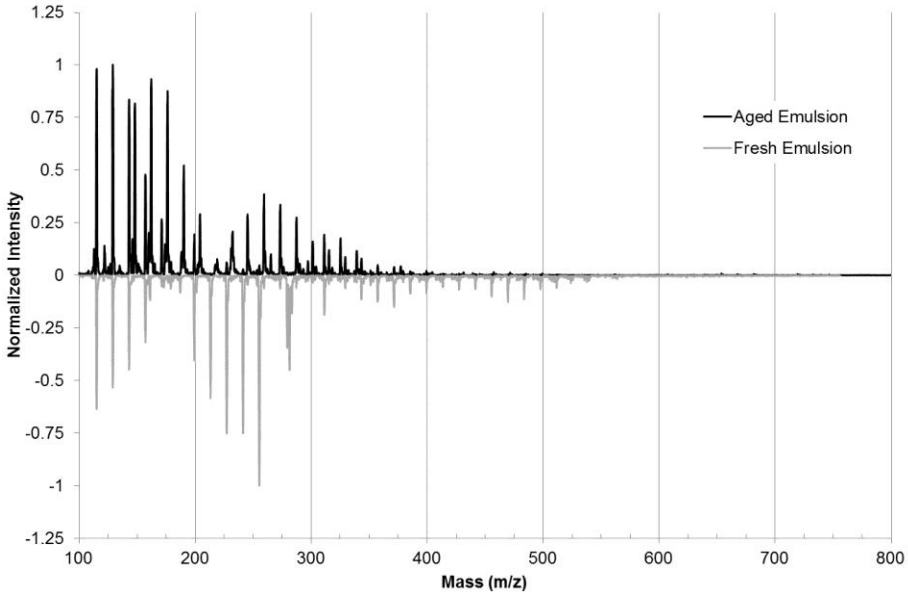

Figure 4.6 Negative ion DESI-MS mass spectral comparison of the 6 month aged emulsion (black) to freshly made emulsion (grey).

Subsection 4.3.3 Comparison to Commercially Available Materials

Another important comparison of the emulsion which was completed was determining if the emulsion more accurately represented the chemical composition of a latent fingerprint when compared to commercial products. Currently, only one set of commercial products are available and marketed as artificial fingerprint material. These pads are sold by Sirchie Co. and are available as an amino acid pad and a sebaceous pad. Using a clean artificial fingerprint stamp, artificial fingerprints comprised of these materials were deposited, as per the manufacturer's instructions, and analyzed using the same methods and conditions as the emulsion. Figures 4.7 and 4.8 shows the positive and negative ion SIMS mass spectral comparison of the two commercial products, and how they compare to an actual fingerprint. The amino acid pad was not found to contain any amino acids at detectable concentrations. Furthermore, the sebaceous pad was found to have a large peak pertaining to phenoxyethanol which the MSDS listed as a major ingredient of the pad. Neither pad was found to contain common components of latent fingerprints, including inorganic salts, fatty acids, cholesterol, or amino acids. While these products are able to test physical developing techniques, they are not chemically similar to actual fingerprints. The artificial fingerprint material presented herein is more chemically similar to an actual fingerprint than the current commercial products.

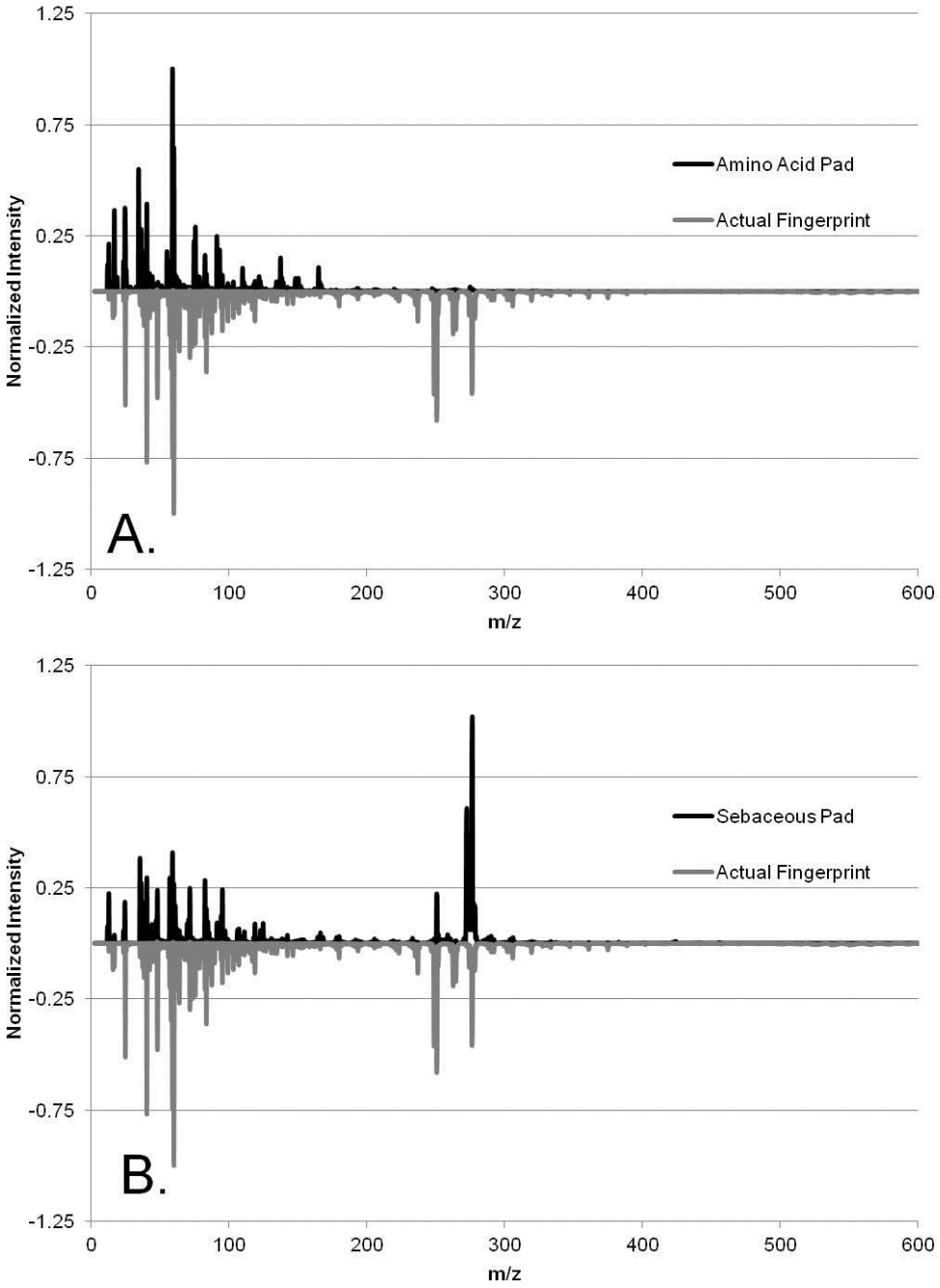

Figure 4.7 Negative ion SIMS comparison of an actual fingerprint (grey) to the commercially available amino acid pad (A. black) and commercially available sebaceous pad (B. black).

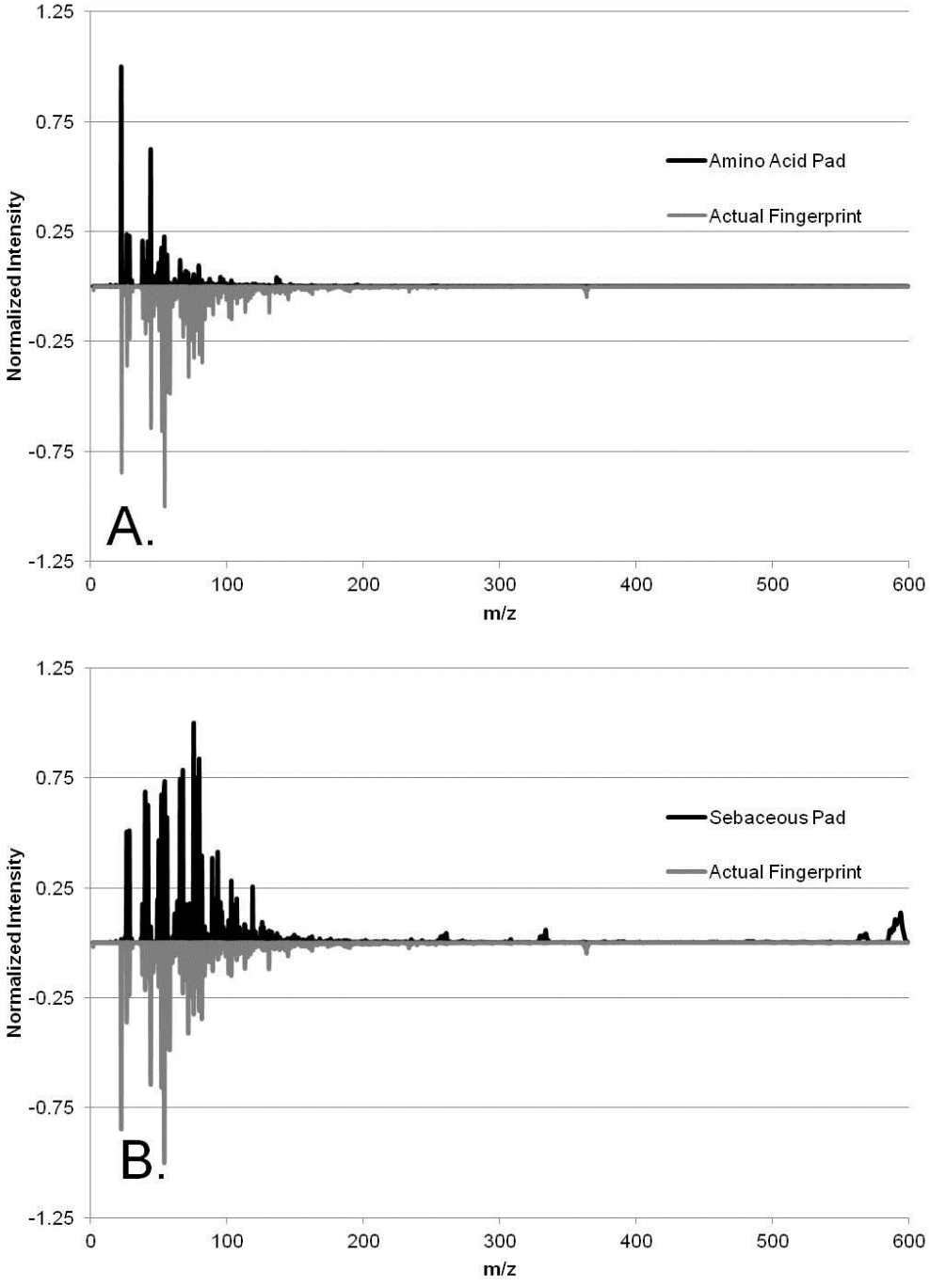

Figure 4.8 Positive ion SIMS comparison of an actual fingerprint (grey) to the commercially available amino acid pad (A. black) and the commercially available sebaceous pad (B. black).

Subsection 4.3.4 Comparison of the Ability to Develop Latent Prints

In order to evaluate the ability of the emulsion to be developed in a manner similar to actual fingerprints, artificial fingerprints were deposited onto surfaces, next to actual human fingerprints and subjected to a number of different latent fingerprint development techniques. The techniques chosen included black powder, fluorescent powder, cyanoacrylate fuming followed by rhodamine 6G treatment, crystal violet, ninhydrin, and 1,2-indandione. The first three techniques were explored because of their widespread use in the field. Crystal violet was tested because it reacts with the sebaceous components of fingerprints while ninhydrin and 1,2-indandione were chosen to test the reaction with amino acids.[2] Fingerprints (both real and artificial) that were developed by these techniques were deposited onto a variety of surfaces and developed with appropriate developers as discussed in Subsection 4.2.2.

Figure 4.9 shows the results of developing both the real and artificial fingerprints with each of the development techniques. Examination of the visual fingerprint quality of the real versus the artificial fingerprints was completed by a certified latent fingerprint examiner at the DFSC and the quality of the artificial fingerprint was determined to be equal to or better than that of the real fingerprint in all cases. This indicates that the ability to use the emulsion as a method to study fingerprint development is possible.

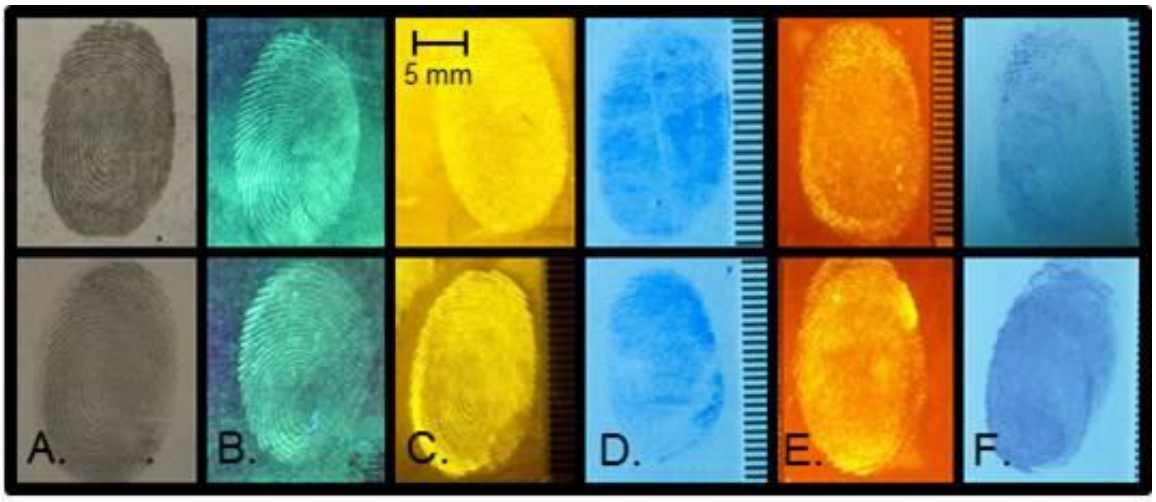

Figure 4.9 Comparison of real (top) and artificial (bottom) fingerprints developed using black fingerprint powder (A.), fluorescent fingerprint powder (B.), cyanoacrylate fuming followed by treatment with Rhodamine 6G (C.), gentian violet (D.), 1,2-indanedione (E.), and ninhydrin (F.).

Subsection 4.3.5 Incorporation of Additional Chemicals & Particles

One of the possible benefits of the emulsion is the fact that additional chemicals can be incorporated into the emulsion at desired concentrations to allow for the production of doped fingerprints. A proof-of-concept exercise to illustrate this capability was completed using florescent microspheres as the doping agent (Fluoro-Max Green Fluorescent Poly Microspheres - 24 µm diameter) (Thermo Scientific, Waltham, MA, USA). Doping was completed by mixing approximately 0.1 mg of the fluorescent microspheres into approximately 5 mg of the emulsion followed by subsequent application onto the ballistics finger and deposition onto a glass microscope slide. To determine the efficacy of this technique, the fingerprint was imaged using a Leica microscope (Leica Microsystems, Buffalo Grove, IL, USA), with a 1x objective. Individual images were stitched together in an automated fashion to produce a comprehensive image of the doped fingerprint, which is shown in Figure 4.10. The

bright spheres dispersed in the fingerprint ridges are the fluorescent microspheres, showing that doping of the emulsion is possible. Similar doping techniques could be used to produce explosive or narcotic containing fingerprints, which could be useful in a wide range of applications, especially in trace contraband standards development.

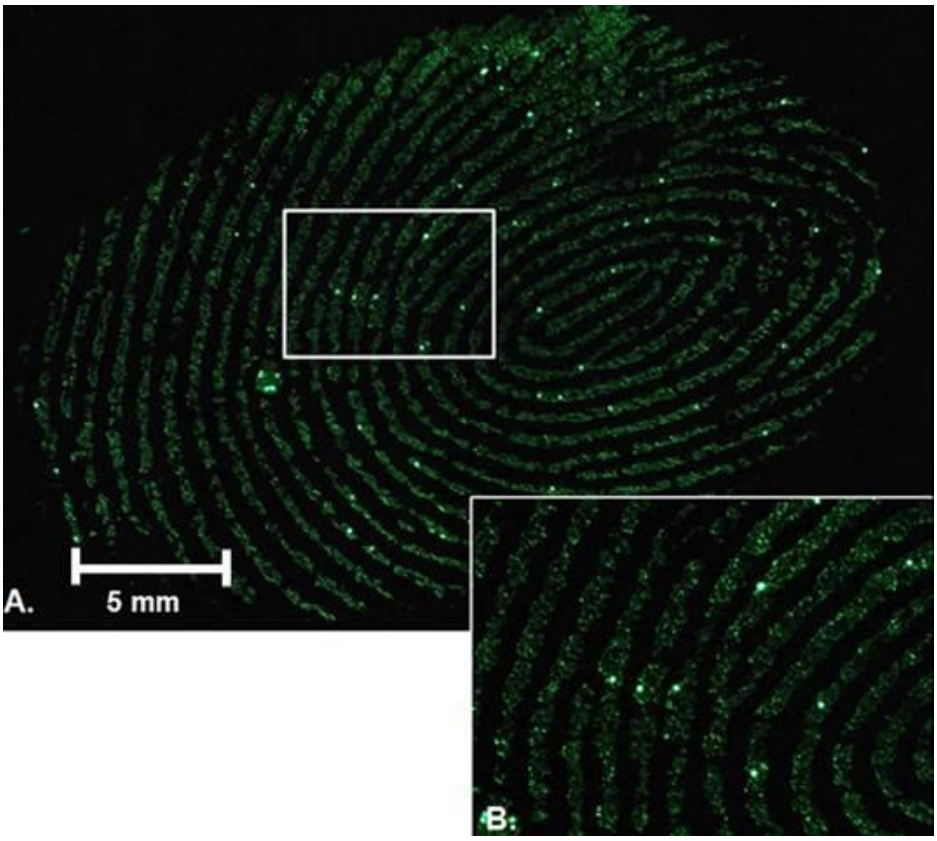

Figure 4.10 Fluorescence image of an artificial fingerprint which was doped with 10 µm fluorescent microspheres. The cutout (B.) is a magnified portion of the highlighted area in (A.).

Section 4.4 Conclusions

A chemically relevant artificial fingerprint material has been developed. Unlike prior work to create such a material, and available commercial products where only one type of secretion is present, this method combined the sebaceous and eccrine solutions using an

emulsification process. The material contains the major chemical components of actual fingerprints at similar concentrations. Furthermore, the material can be developed using a number of different latent fingerprint development techniques that target different classes of chemicals. Another benefit of this material is that it is made in-house which allows for the ability to incorporate additional materials to create a doped fingerprint. Additional work is being completed to better quantify a method of doping the material, to understand the stability of the material, and explore ways to enhance the precision of deposits to create a more reproducible fingerprint.

Chapter 5: Imaging using Desorption Electro-Flow Focusing Ionization Mass Spectrometry for the Analysis of Fingerprints and Trace Chemicals

Adapted from:

Forbes, T.; Sisco, E. *Analyst*. **2014**, In Press, DOI: 10.1039/C4AN00172.

Section 5.1 Introduction

Mass spectrometry imaging (MSI) allows for the spatial distribution of molecules or elements within sample to be mapped with resolution ranging from a few hundred micrometers to a few hundred nanometers. While this process has been in use for many years, over the last decade it has begun to see increasing popularity in the field of forensic science. Traditional MSI analyses were and are completed using high vacuum mass spectrometry such as secondary ion mass spectrometry (SIMS). Though these techniques still offer the potential for a wealth of information, recent use of ambient ionization mass spectrometry (AI-MS) systems to analyze samples in atmosphere greatly increases the potential applications of MSI. By utilizing AI-MS platforms, vacuum sensitive samples can be easily analyzed as can samples with geometries or substrates that are not conducive to SIMS analysis. Furthermore, a lower cost may allow AI-MS techniques to more easily reach the hands of forensic laboratories, and can be used for a number of different analysis types such as screening evidence for explosives or narcotics. The drawbacks to the AI-MS techniques, however, include lower spatial resolution and increased background, when compared to a traditional SIMS imaging experiment.[101]

MSI has begun to find its way into the forensic science field. Several studies have been published which highlight the ability of SIMS to image fingerprints, as well as trace chemicals, i.e. explosives and narcotics, which are located within the fingerprint.[32,102] Furthermore, SIMS has shown the ability to analyze and differentiate overlapping fingerprints as well as provide a method to enhance the visualization of poor quality fingerprints.[103–105] Other areas of forensic science where SIMS imaging has been shown to be useful include gunshot residue analysis,[106,107] questioned documents,[108] and nuclear forensics.[109,110] Imaging using AI-MS techniques in forensic science began with the demonstration of fingerprint imaging using desorption electrospray ionization mass spectrometry (DESI-MS).[34] Other techniques have also been shown to provide imaging capabilities for the analysis of fingerprints, namely matrix assisted laser deosprion ionization mass spectrometry (MALDI-MS)[111–113] and DESI-MS.[114–117] As spatial resolution increases with improved techniques and procedures, so will these potential applications.

This chapter focuses on the development of the imaging capabilities of desorption electro-flow focusing ionization mass spectrometry (DEFFI-MS), the proof of concept for DEFFI MSI, and what potential benefits it has over other similar techniques. The DEFFI source operates in a manner similar to DESI source, but with a few major differences. Foremost to imaging, the spot size of the DEFFI source is significantly smaller than that of the DESI source, as the DEFFI source uses a focused gas stream. A smaller spot size should lead to increased spatial resolution. The ability to form nitrate ions in the source may also help increase the sensitivity of certain materials which will

readily adduct with that ion. Also, the applied voltage and gas flow rates used are less than those of by DESI, which would lead to lower operating costs in the real world.

Section 5.2 Materials and Methods

Subsection 5.2.1 The DEFFI Imaging Set-up

The DEFFI source used in these studies is identical to the one used in Chapter 3 and was developed by Thomas Forbes at NIST. The stage that was used for moving the samples was constructed by mounting two linear motorized translational stages from Thor Labs (Newton, NJ) perpendicularly to allow for automated movement in the x and y directions. The automated sample stages were then mounted to a three-axis manual stage, controlling the DEFFI source orientation and position, to allow for manipulation in the z direction, as well as movement of the stage away from the mass spectrometer when needed. A picture of this setup is shown in Figure 5.1. In order to control the stages, scan patterns, and triggering of the mass spectrometry, a custom LabVIEW program was written by Dr. Thomas Forbes and Matthew Staymates at NIST. The program allowed for the input of scan type, step-size, scan velocity, scan dimensions, delay times, and dwell times. Possible scan types for the setup included unidirectional, serpentine, point-to-point, or constant scan velocity. The code also allowed for triggering mass spectrum data acquisition within the Analyst software (the software that controls the mass spectrometer) by sending a TTL signal through the auxiliary interface on the QTrap 4000 instrument.

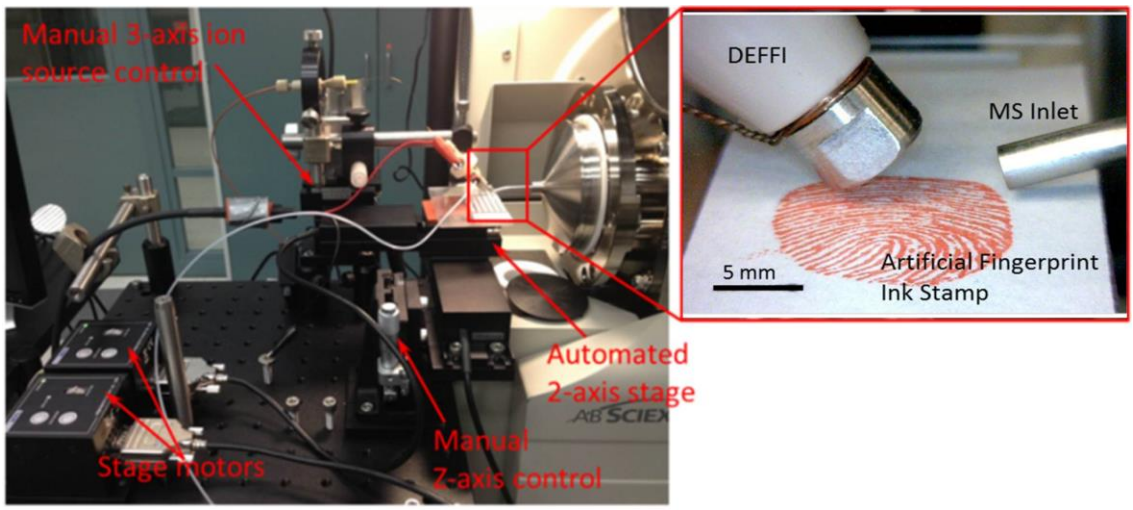

Figure 5.1 The DEFFI imaging setup.

Subsection 5.2.2 Imaging Parameters

For all images obtained in this chapter, the constant scan velocity method was the scan method used to collect data. Also, a flyback scan pattern, in which the sample is returned to the "home" position after each row so that scans were completed in the same direction every time, was used, as shown in Figure 5.2. Scan velocities varied from

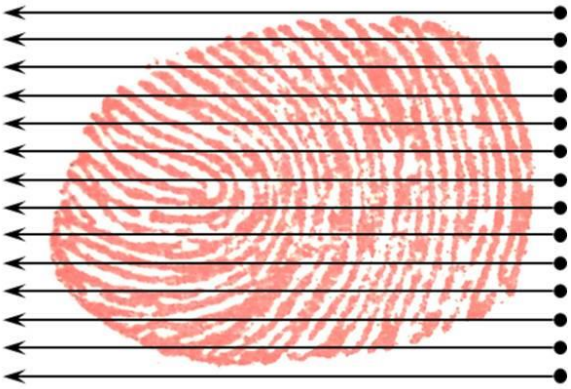

Figure 5.2 Pictorial representation of the scan pattern for fingerprint imaging.

100 µm/sec to 400 µm/sec with pixel sizes ranging from 50 µm by 50 µm to 200 µm by 200 µm. For data collection using a constant scan velocity, each scanned row was collected as a series of mass spectra within one data file, where one mass spectrum was the equivalent of one pixel. In order to calculate the appropriate scan time per mass range per pixel, the following equation (eq. 5.1) was used:

$$MS\ scan\ time = \frac{(Pixel\ size\ in\ \mu m)(Number\ of\ Scan\ Windows)}{\left(Scan\ Rate\ in \frac{\mu m}{sec}\right)} - \ 0.005\ sec \quad \text{(eq. 5.1)}$$

The additional 0.005 seconds is the required dead time to switch between mass ranges and could be changed if desired. The number of cycles, or mass spectral scans, completed within each file was equal to that of the number of pixels in that particular run. Each file is triggered by the LabVIEW software by sending a 500 ms pulse through the auxiliary interface of the mass spectrometer that queued the start of data collection in Analyst. The mass windows that were chosen for individual runs were dependent upon what the analyte(s) of interest were and the amount of time per scan was defined by the scan rate and pixel size. For individual runs, up to three separate mass windows were chosen to scan within a single pixel.

Other parameters of the mass spectrometer that were kept constant were the use of a 36 mm, 15 ° inlet tube, a curtain gas pressure of 17 psi (115 kPa), an ion source gas pressure of 7 psi (50 kPa), no ion source gas 2, an inlet temperature of 150 °C, an entrance potential of ±10 V, and a declustering potential of ±75 V. For the DEFFI source, nitrogen was always used as the spray gas, and an incidence angle of 50 ° with respect to the sample surface was always used. In all cases, the DEFFI source was

positioned within 1 mm of the sample in order to obtain the smallest spot size possible. In order to obtain an image of an entire fingerprint, which comprised a total scan area of 18 mm by 23 mm, multiple batches had to be created within the Analyst software (which only allows for a maximum queue of 100 samples).

Subsection 5.2.3 Data Conversion

In order to obtain the image from the raw mass spectra files, a series of data conversions were required. The data collected from the Analyst software was saved in AbSciex's proprietary .wiff format, which contained an entire batch of samples within a single file. The first conversion that was completed required the "AbSciex MS Data Converter", provided by the manufacturer, which took the single .wiff file and converted it into a series of .mzML files, where each scanned row was given its own file. The series of .mzML files were then converted into a single .imzML file using "imzML Converter" (http://www.cs.bham.ac.uk/~ibs/imzMLConverter/). Within this converter it was crucial that the proper scan settings were chosen under the "Scan" tab. Once the .mzML files were converted into a single .imzML file, it could be opened by an imaging software program. The program used in this analysis was "MSiReader".[118] Within "MSiReader" various color scales are available, including RGB overlays.

Subsection 5.2.4 Sample Preparation

For this study, an artificial fingerprint, and the artificial fingerprint material discussed in Chapter 4 were used to obtain samples. The 3-D printed artificial fingerprint stamp, discussed in Chapter 4 was used. The fingerprint it created measured 16 mm by

21 mm, which is similar in size to an actual human fingerprint,[83] and the stamp itself was composed of a rubber–plastic mixture. To prepare a sample, 5 µg of artificial fingerprint material and 5 µg of a target compound were deposited onto the fingerprint mold and allowed to dry. The 5 µg sample lead to a spatial coverage of approximately 15 ng/mm^2. Target analytes included a range of explosives (AccuStandard), narcotics (Sigma Aldrich), and hand lotion (Gold Bond Hand Sanitizing Lotion). Once the fingerprint material and analytes dried, the stamp was then deposited onto a number of surfaces. Surfaces onto which a fingerprint was deposited included glass microscope slides (VWR, Radnor, PA), fingerprint lift tape (Sirchie, Youngsville, NC), and a simulated car panel. The simulated car panel was an aluminum panel coated with black automotive paint and a clear coat top layer. Fingerprints that were deposited on surfaces other than the fingerprint lift tape were lifted, in most instances, from their respective surfaces using the lift tape, prior to imaging.

In order to evaluate the quality of the fingerprint post analysis, were developed using cyanoacrylate fuming. Fuming was completed by placing the fingerprints, with a weigh boat containing 1 mL of Omega-Print Cyanoacrylate fuming compound (Sirchie Co.), and a weigh boat containing approximately 1 mL of water into a sealed plastic bag and allowed to develop for 24 hours. The cyanoacrylate reacts with the fingerprint to form a polymeric coating on the fingerprint that is easily imaged. Imaging of the developed fingerprints was completed with a Nikon D90 DSLR camera.

Section 5.3 Results & Discussion

Subsection 5.3.1 Optimization of Imaging Methods

Before optimization of the imaging parameters was completed, mass spectra were taken of the artificial fingerprint material and target analytes to identify where mass windows of interest would be located, and to identify any potential issues with overlap of peaks from target analytes and the fingerprint material. Figure 5.3 shows the negative ionization mode mass spectrum of the artificial fingerprint material, with identification of the various components within the fingerprint. Detection of the compounds in the artificial fingerprint material was not readily achieved in the positive ionization mode. Representative mass spectra of the target analytes can be found in Appendix 5.

Optimization of the imaging parameters for the analysis of fingerprints was completed on a trial and error basis. Parameters that were found to play a significant role in the quality of the obtained image include: solvent flow rate, scan rate, sample substrate, pixel size, and sample age. The most important parameter for sample analysis was found to sample substrate. Initial analyses were completed on fingerprints that had been deposited directly onto glass microscope slides. It was found, however, that the fingerprint material was easily pushed around on the glass slides. This problem was compounded by the fact that some material was pushed backward, which caused analysis of subsequent rows to be compromised by the buildup of fingerprint material behind the solvent spray. This caused the fingerprint ridges and valley of the chemical image to be irresolvable. Other smooth surfaces were attempted and all produced the same issue with sample buildup. Since fingerprint imaging has been shown to be completed using DESI off of smooth surfaces[34,53] leaving the possibility of the artificial fingerprint material

being more “wet” than traditional fingerprints as one potential factor behind why this build-up occurs. Fingerprint lift tape was then chosen as a possible realistic alternative, and was shown to not be affected by the same issues as those presented with smooth surfaces. The adhesive of the tape was strong enough to maintain sample integrity, even with the bombardment of the solvent spray. Furthermore, there were no significant background peaks attributed to the lift tape that were present in the mass windows of interest. Major background peaks in negative ion mode are 297 *m/z*, 311 *m/z*, 325 *m/z*, and 339 *m/z*. Positive mode background peaks occur at 245 *m/z*, 261 *m/z*, 462 *m/z*, and 483 *m/z*.

While fresh artificial fingerprints were unable to be analyzed on smooth surfaces, it was found that aged fingerprints could be. Figure 5.4 shows an image of a seven day old artificial fingerprint that was deposited onto a glass microscope and analyzed directly off of the surface. As the samples age, dehydration of the fingerprint occurs, and after a length of time as long as one week, little remains, which more tightly adheres the fingerprint to the glass surface. The lack of water in the sample allows for the maintenance of the sample position during a sample run. The issue with aged fingerprints, however, is lateral movement of other chemicals occurs over time, which complicates images, as can be seen in Figure 5.4. While this is more realistic, the movement of material makes it more difficult to optimize the parameters in order to obtain the best possible image.

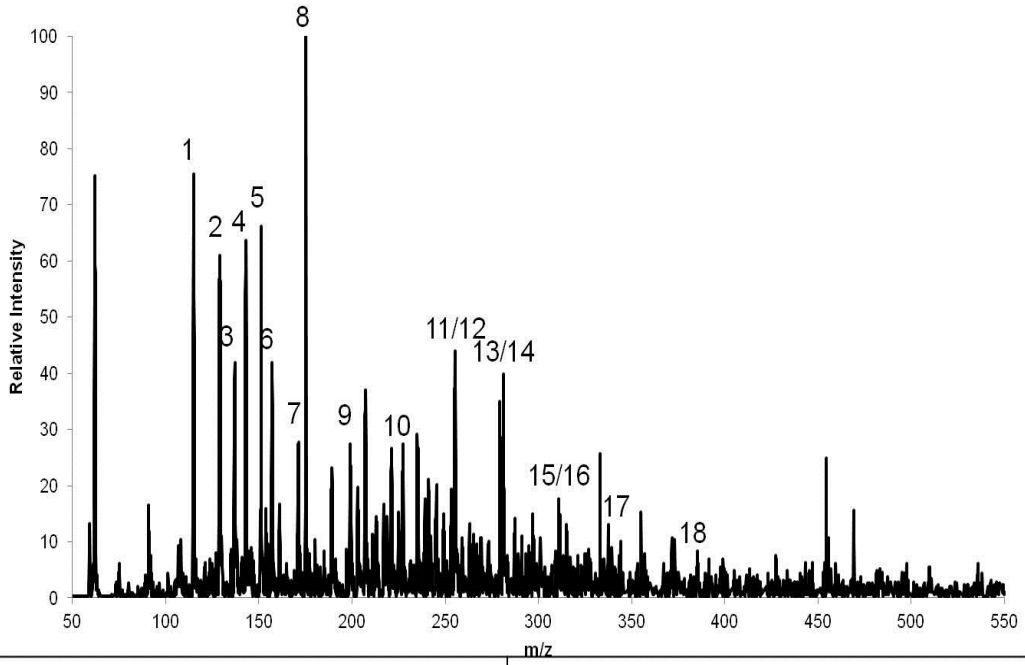

Peak	Nominal Mass	Assignment	Peak	Nomnial Mass	Assignment
1	115	Hexanoic Acid $[M-H]^-$	10	227	Tetradecanoic Acid $[M-H]^-$
2	129	Heptanoic Acid $[M-H]^-$	11	253	Palmitoleic Acid $[M-H]^-$
3	137	Glycine $[M+NO_3]^-$	12	255	Hexadecanoic Acid $[M-H]^-$
4	143	Octanoic Acid $[M-H]^-$	13	281	Oleic Acid $[M-H]^-$
5	151	Alanine $[M+NO_3]^-$	14	283	Octadecanoic Acid [M-H]-
6	157	Nonanoic Acid $[M-H]^-$	15	311	Eicosanoic Acid $[M-H]^-$
7	171	Decanoic Acid $[M-H]^-$	16	316	Palmitoleic Acid $[M+NO_3]^-$
8	175	Pyruvic Acid $[2M-H]^-$	17	344	Hexadecanoic Acid $[M+NO_3]^-$
9	199	Dodecanoic Acid $[M-H]^-$	18	385	Cholesterol $[M-H]^-$

Figure 5.3 DEFFI negative ion mass spectrum, and representative constituents, of the artificial fingerprint material.

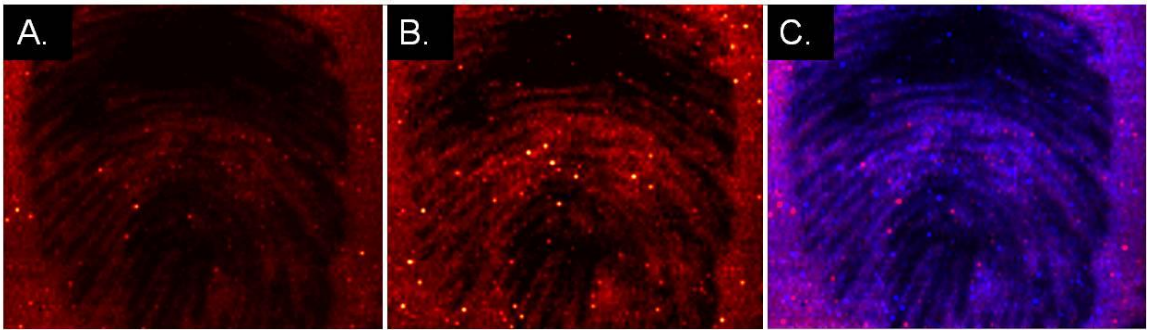

Figure 5.4 DEFFI-MS image of a one week old artificial fingerprint, laden with TNT, on a glass microscope slide. The images depict the spatial distribution of lauric acid (199 m/z $[M-H]^-$) (A.), TNT (227 *m/z* $[M]^-$) (B.) and colocalization map (C.). In (A.) and (B.), a lighter color indicates higher intensity. In (C.) lauric acid is shown in blue and TNT in red.

Another parameter, solvent flow rate, was shown to have a significant effect on the resolution of the image that was obtained. At high solvent flow rates, puddling of the solvent occurred, which significantly hindered the ability to resolve ridges and valleys within the fingerprint. Appendix 5 contains an example of how high flow rates (on the order of 3 µL/min) cause poor resolution within the sample. It was found that flow rates between 1.5 µL/min and 2.0 µL/min allowed for optimal resolution. Flow rates below 1.5 µL/min were unstable and there was difficulty maintaining a constant spray, especially at higher spray voltages.

Scan rate and pixel size were the other parameters that were optimized to obtain the best image. However, with these parameters it was also necessary to take into account a balance between image quality and time required for analysis. Initial scan rates of 100 µm/sec were used, as the slower scan rate lead to a longer integration time per mass by the mass spectrometer, which could have potentially increased sensitivity at low concentrations. However, it was found that at scan rates this slow, resolution of the image suffered, as both puddling of the solvent and movement of the sample in the

backwards direction were occurring simultaneously. The scan rate of the sample was then increased in order to obtain the optimal balance between integration time and resolution. It was found that at a scan rate of 350 µm/sec there was minimal sample pushback and puddling, while still allowing enough time to obtain sufficient signal counts from the analytes of interest. Similarly, it was found that a 100 µm by 100 µm pixel size was the optimal pixel size. A pixel size of 200 µm by 200 µm was found to be too large to differentiate the details of ridges versus valleys within the fingerprint. Dropping the pixel size to 50 µm by 50 µm provided only a marginal increase in resolution when compared to the 100 µm by 100 µm pixel size. Also, the decreased scan time of the 50 µm by 50 µm pixel lead to intermittent detection of analyte targets and also lead to increased file sizes, since there were four times as many scans required to cover a 100 µm wide row. It was found that the optimal scan parameters were 100 µm by 100 µm pixels obtained at a scan rate of 350 µm/sec with a solvent flow rate of 1.75 µL/min when analyzing a sample off of fingerprint lift tape.

Subsection 5.3.2 Examples of Mass Spectral Imaging

A number of different target analytes and fingerprint components have been interrogated to simulate a wide range of potential situations in a forensic environment. One such situation would be in a case where someone was handling explosives. To simulate this, 5 µg of artificial fingerprint material and 5 µg of HMX were deposited onto the fingerprint stamp and directly stamped onto fingerprint lift tape. Using the optimized method for analysis, signals for both HMX and (9Z)-octadecenoic acid (a component of the artificial fingerprint material were monitored. HMX produced a strong nitrated

molecular ion peak at 358 *m/z*, whereas oleic acid produced a deprotonated molecular ion peak at 281 *m/z* and a nitrated molecular ion peak at 344 *m/z*. A scan window of 340 *m/z* to 360 *m/z* was chosen, and the resulting image is shown in Figure 5.5. The distribution of both the (9Z)-octadecenoic acid and HMX are clearly delineated to the ridges of the fingerprint, and both show significant areas of overlap that can be seen in the color composite of the two individual images. Furthermore, under these optimal settings, minimal redistribution, or pushback, of the sample occurs, allowing for an image that closely resembles that of the actual fingerprint stamp. An additional example of an explosive-laden fingerprint is shown in Figure 5.6, where RDX was used as the target

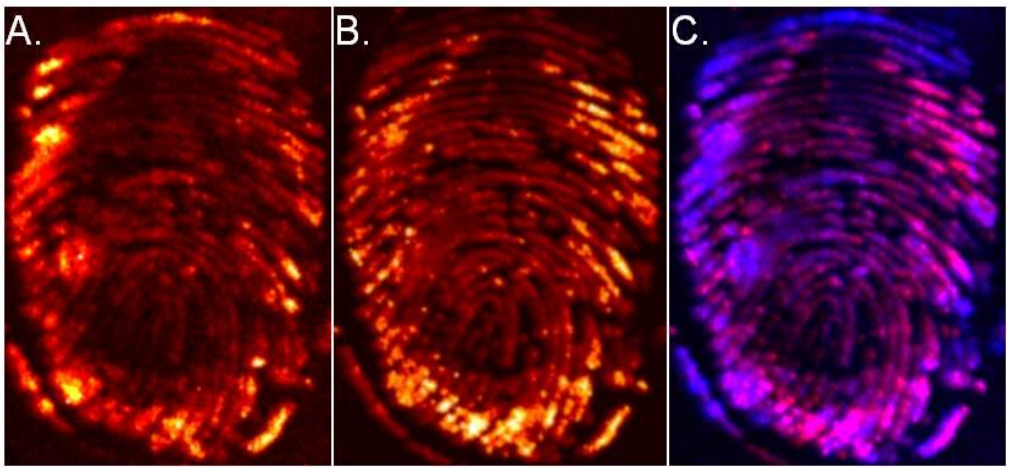

Figure 5.5 DEFFI-MS image of an HMX laden artificial fingerprint deposited directly onto fingerprint lift tape. The images depict the spatial distribution of (9Z)-octadecenoic acid (344 *m/z* $[M+NO_3]^-$) (A.), HMX (358 *m/z* $[M+NO_3]^-$) (B.) and colocalization map (C.). In (A.) and (B.), a lighter color indicates higher intensity. In (C.) (9Z)-octadecenoic acid is shown in blue and HMX in red.

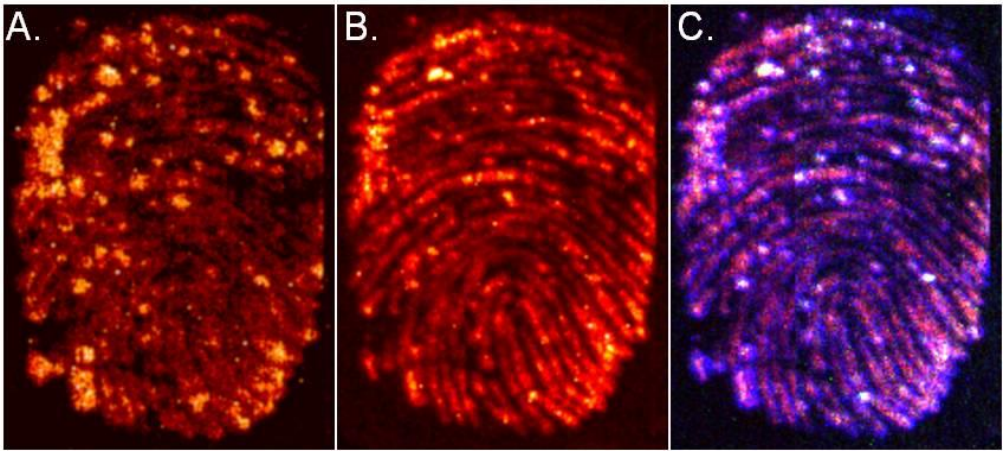

Figure 5.6 DEFFI-MS image of an RDX laden artificial fingerprint deposited directly onto a simulated automobile panel and the lifted off of the surface using fingerprint lift tape. The images depict the spatial distribution of (9Z)-hexadecenoic acid (253 *m/z* $[M-H]^-$) (A.), RDX (284 *m/z* $[M+NO_3]^-$) (B.) and colocalization map (C.). In (A.) and (B.), a lighter color indicates higher intensity. In (C.) (9Z)-hexadecenoic acid is shown in blue and RDX in red.

analyte and (9Z)-hexadecenoic acid was used as the target fingerprint constituent. In this instance, instead of stamping onto the fingerprint lift tape directly, the stamp was applied to a simulated car panel and the fingerprint was then lifted off of the panel and analyzed. This scheme provides a more realistic approach for how real-world samples would be collected. The results of this image are nearly identical to that of the HMX-laden fingerprint. It is important to note that TNT was also attempted as a potential explosive of interest, however the base peak of TNT at 226 *m/z* overlaps with that of tetradecanoic acid, a component of the artificial fingerprint material and a common component in actual fingerprints. This issue, however, could be mitigated with the use of MS/MS scan types.

Another potential situation where imaging of a fingerprint would be useful would be for the detection of narcotics within a fingerprint. Since narcotics are generally easily ionized in positive mode, it was necessary that a fingerprint constituent peak in positive

mode also be established. Several endogenous compounds of interest were attempted, however none produced sufficient signal to be able to obtain a useful chemical image of the fingerprint. Therefore, a different approach for the detection of a fingerprint compound was undertaken. Instead of targeting a component of the artificial fingerprint material, hand lotion was applied to the fingerprint stamp as well, and a component found in the lotion was targeted in addition to the narcotic. Figures 5.7 and 5.8 represent two examples of detection and imaging of narcotics in fingerprints. In these samples, 5 µg of artificial fingerprint material, hand lotion, and the respective narcotic were deposited onto the stamp and then directly stamped onto fingerprint lift tape, for methamphetamine, or lifted off of the car panel, for cocaine. The lotion component that was monitored in both instances was benzethonium, a quaternary ammonium salt and common anti-bacterial agent. The ability to analyze components in both positive and negative mode allow for the potential of a host of different compounds, both endogenous and exogenous, to be interrogated.

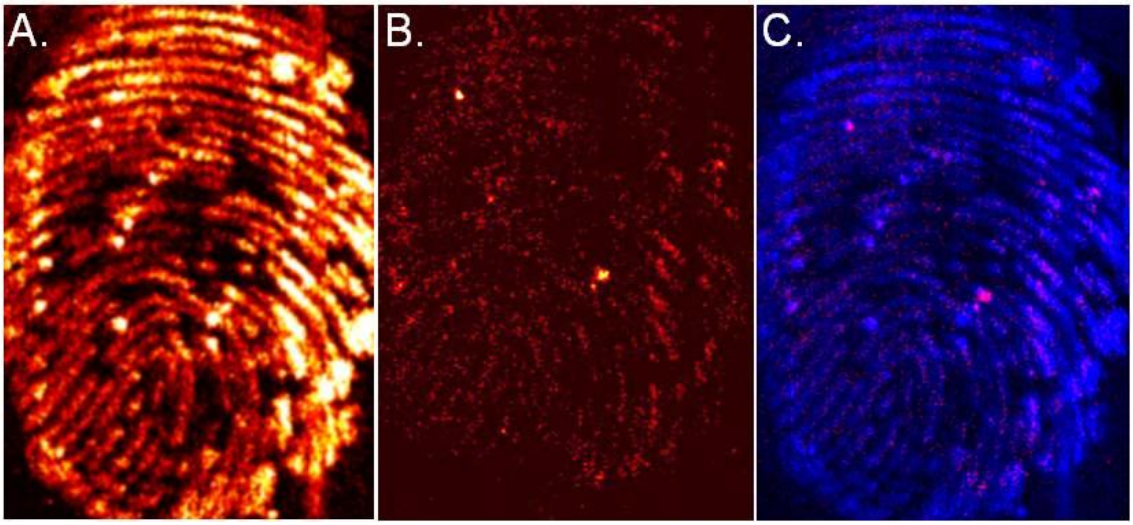

Figure 5.7 DEFFI-MS images of a methamphetamine and hand lotion laden artificial fingerprint deposited directly onto fingerprint lift tape. The images depict the spatial distribution of benzethonium (412 m/z $[M]^+$) (A.), a component of the lotion, methamphetamine (150 *m/z* $[M+H]^+$) (B.), and a colocalization plot of the lotion and drug component (C.) where the lotion is represented in blue and the methampetamine in red. In all cases a brighter color indicates a higher signal.

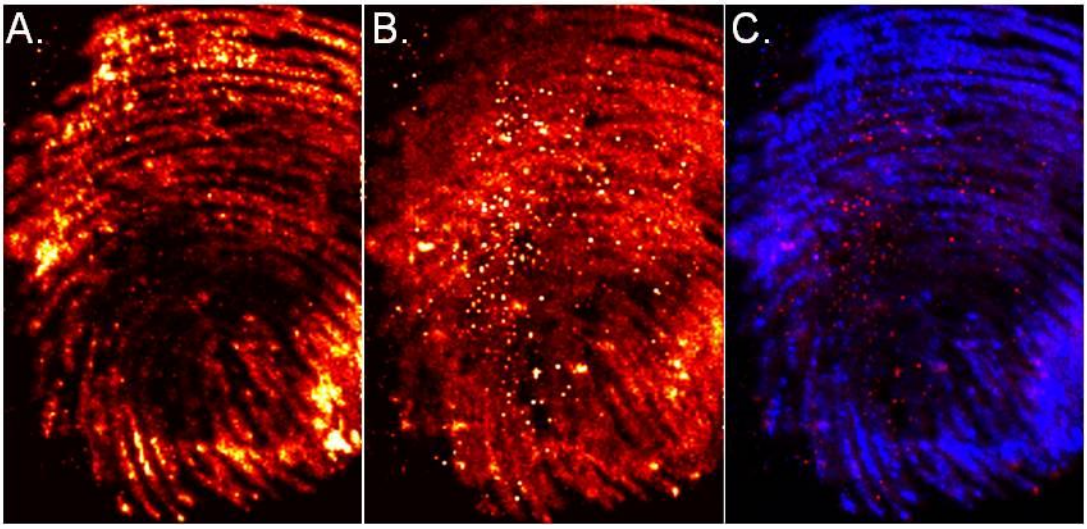

Figure 5.8 DEFFI-MS images of a cocaine and hand lotion laden artificial fingerprint deposited directly onto a simulated car panel and then lifted with fingerprint lift tape. The images depict the spatial distribution of benzethonium (412 m/z $[M]^+$) (A.), a component of the lotion, cocaine (304 *m/z* $[M+H]^+$) (B.), and a colocalization plot of the lotion and drug component (C.) where the lotion is represented in blue and the cocaine in red. In all cases a brighter color indicates a higher signal.

Subsection 5.3.3 Retention of Fingerprint Material

The final parameter which was tested was the ability to develop a fingerprint post-analysis. Since the fingerprints were deposited onto tape, utilization of a developing method that exist for fingerprints on adhesives was necessary. The easiest and most widely used of these techniques is cyanoacrylate fuming. Figure 5.9 shows developed fingerprints on tapes that were and were not analyzed by DEFFI. While DEFFI does decrease the integrity of the fingerprint post-analysis, it is still possible to develop the fingerprint for biometric or identification purposes, post analysis. This is key to any technique that could be used in a forensic setting.

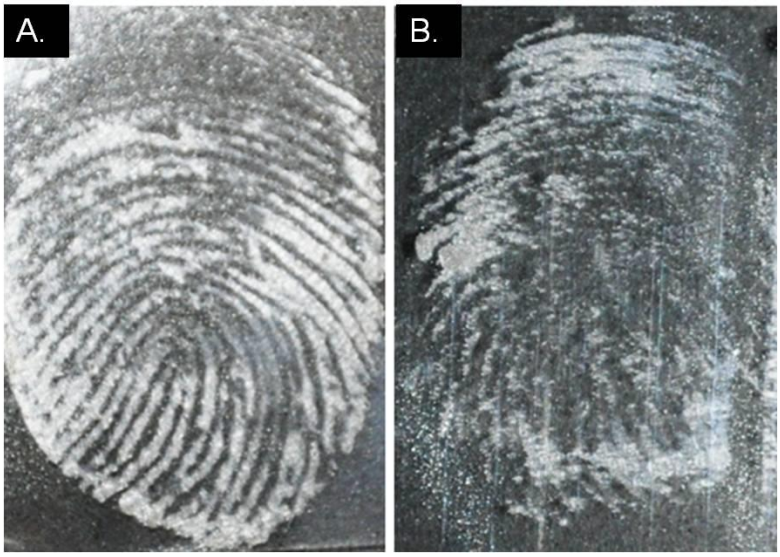

Figure 5.9 Comparison of a cyanoacrylate developed fingerprint not exposed to DEFFI-MS imaging (A.) to one that was exposed to DEFFI-MS imaging (B.).

Section 5.4 Conclusions

DEFFI-MS is capable of chemical imaging latent fingerprints that have been lifted off of a surface using fingerprint lift tape. Because of puddling and the movement of sample on a smooth surface, imaging of fresh fingerprints off of smooth surfaces is

problematic unless the fingerprint has aged. The images produced by DEFFI MSI are sufficient to resolve fingerprint ridges versus valleys. Furthermore, the actual fingerprint is able to be developed using traditional development techniques after analysis, allowing for potential biometric identification post-run. Detection of a number of exogenous compounds including explosives, narcotics, and lotion components has been demonstrated. Current research is looking into how to enhance the resolution of the chemical images as well as methods to allow for simultaneous imaging of organic and inorganic components in a fingerprint, quantitation of components in fingerprint images, and reactive solvent spray imaging.

Chapter 6: Imaging and other Applications of C_{60}^+ Secondary Ion Mass Spectrometry for the Analysis of Fingerprints and Trace Chemicals

Adapted from: Sisco, E.; Demoranville, L.; Gillen, G. *Forensic Sci. Int.* **2013**, *231* 263–269.

Section 6.1 Introduction

This chapter outlines the use and capabilities of a C_{60}^+ secondary ion mass spectrometry (SIMS) instrument to obtain chemical information and chemical images of fingerprints. There are several potential benefits to the use of SIMS for forensic analysis of human fingerprints. One beneficial aspect of SIMS is the potential for low limits of detection. The low detection limits are coupled with higher spatial resolution than other mass spectrometry imaging techniques such as desorption electrospray ionization mass spectrometry (DESI-MS).[101] Additionally, the evidentiary value of fingerprints is more likely to be maintained since minimal sample, as few as several monolayers, is consumed during analysis. This is unlike other techniques, such as DESI-MS, where the fingerprint ridges are dissolved due to the solvent spray. Loss of volatile components in ultra high vacuum would, however, need to be considered for the SIMS experiment. Research has shown that there are notable changes in lipid concentration and the lipid profile of fingerprints that have been exposed to vacuum for prolonged periods of time[119]. Images of the fingerprint can also be acquired using characteristic molecular ions of either exogenous or endogenous components. Furthermore, SIMS allows for the simultaneous

detection of organic and inorganic species. Finally, SIMS allows for the ability to depth profile fingerprint ridges, which provides insight into the chemical composition of a fingerprint ridge with respect to the depth of the ridge. Depth profiling could allow for the differentiation of surface compositional changes from bulk changes in a fingerprint ridge. This chapter evaluates the capabilities of C_{60}^+ SIMS for the chemical analysis of fingerprints. More specifically it describes the compounds that have been detected by SIMS, the effects of fingerprint development techniques on the chemical analysis, the imaging capabilities of the technique, and proof of concept of the ability to depth profile fingerprint ridges.

Section 6.2 Materials & Methods

Subsection 6.2.1 Instrumentation

A Cameca IMS 4f SIMS instrument (Cameca Instruments, Genneviller Cedex, France) fitted with an Ionoptika C_{60}^+ primary ion source (Ionoptika LTD, Hampshire, United Kingdom) was used in these experiments. Primary C_{60}^+ ions were created by heating powdered fullerene to a vapor state with subsequent ionization via electron impact from a tungsten filament.[61] C_{60}^+ ions were selected using a Wein filter and accelerated to 10 keV. A primary ion current of approximately 5.0×10^{-12} A was used for all mass spectral analyses. A focused ion beam of approximately 25 µm in diameter was rastered over a 500 µm by 500 µm area. Under these conditions, an ion dose of approximately 4×10^{12} ions/cm^2 was delivered during a typical mass spectrum. The ion dose is calculated using the equation:

$$Ion\ Dose = \frac{Primary\ Ion\ Flux \times Analysis\ Time}{Bombared\ Surface\ Area} \quad \text{(eq. 6.1)}$$

$$4 \times 10^{12} ions / cm^2 = \frac{(5.0\times10^{-12}\text{A})\left(\frac{1\text{ C}}{1.6\times10^{-19}\text{A}}\right)(300\text{ sec})}{(250000\ \mu m^2)\left(\frac{1 cm^2}{10^8 \mu m^2}\right)} \quad \text{(eq 6.2)}$$

The secondary ion accelerating voltage for positive ion mode was ±1.12 kV, which allowed for a secondary ion mass range of 0 *m/z* – 1200 *m/z* to be analyzed. For positive ion mass spectra, a range of 0 *m/z* – 800 *m/z* was chosen, however, due to lack of signal intensity in the region greater than 800 *m/z*. A mass range of 0 *m/z* – 600 *m/z* for negative mode was chosen due to lack of signal in the region greater than 600 *m/z*. For each mass spectrum there were 1800 to 2400 recorded data points, depending on the mass range, with 0.1 s integration time per scan point. A ∓10 kV post acceleration voltage was applied to the electron multiplier to compensate for the lower secondary accelerating voltage. Mass spectra were taken by using a 500 µm by 500 µm raster size with a 150 µm by 150 µm image field. In order to correct for day-to-day instrument variation resulting from differences in secondary ion focusing and primary bream current stability, mass spectra were normalized to the total ion count of the individual spectra.

Images were obtained in microbeam imaging mode by rastering the primary ion beam over a 500 µm by 500 µm area while detecting secondary ions using an electron multiplier detector with a 1 s to 20 s integration time per image, depending on the analyte signal intensity. To image an entire fingerprint, a 40 x 40 close packed array of images was collected using automated stage control with individual x and y steps of 500 µm. Individual images were then stitched together into rows and manually aligned using ImagePro software (Media Cybernetics, PA, USA).

Depth profiles of fingerprints were obtained by rastering the beam over a 500 µm by 500 µm area with a 250 µm by 250 µm image field. A 60 µm diameter field aperture

was also used to minimize crater wall effects. Sample and substrate masses were monitored on the electron multiplier detector with 1 s signal integration per mass. Ion intensities were monitored until secondary ion signals from all species were approximately constant for at least 30 s. A primary ion current of 3 x 10^{-10} A was used for the depth profiles, which delivers an ion dose of approximately 4 x 10^{12} ions/cm^2 for a 500 s depth profile.

For comparison of chemical images to the actual fingerprint, optical images were obtained using a Zeiss Discovery.V9 SteREO microscope with a 1x objective. An automated stage was used to step the image, and the total fingerprint image was stitched together using ImagePro software.

Subsection 6.2.2 Sample Preparation

Fingerprint samples were obtained at the University of Maryland, without recording identifiable information, by loading the finger with sebaceous secretions from the bridge of the nose before deposition. No other grooming technique or hand washing was completed. This was done to allow for the simultaneous analyses of eccrine and sebaceous components.

All fingerprints and neat analyte compounds were deposited onto 2.54 cm diameter silicon wafers which had been cleaned with ethanol. All pure compounds were purchased from Sigma-Aldrich (St. Louis, MO, USA) in 95% purity or greater. For deposition of the compounds onto silicon wafers, approximately 0.1 g of the analyte was dissolved into 5 mL of n-heptane or methanol using sonication. A 20 µL aliquot of the solution was then deposited onto the silicon wafer, and the solvent was allowed to

evaporate before analysis. This provided approximately 400 μg of sample spread over the entirety of the silicon wafer. For the analysis of fingerprints after development, the development materials used were Sirchie (Youngsville, NC, USA) Hi-Fi Volcano Latent Print Powder (Black Powder), Sirchie Magnetic Latent Print Powder, and Sirchie Fluorescent Invisible Detection Powder (Pale Yellow). Fingerprints were developed using the manufacturer's recommended procedures.

Section 6.3 Results & Discussion

Subsection 6.3.1 Identification of Fingerprint Constituents

The first goal of the study was to identify the constituents of fingerprints that can be detected using C_{60}^+ SIMS. Using SIMS, a number of these sebaceous and eccrine components have been identified. Identification of all compounds was confirmed by comparison of the fingerprint spectrum to that of pure compounds. A representative positive ion mass spectrum of a fingerprint is shown in Figure 6.1. Of the components that were identified in the positive spectrum, free fatty acids are the most prevalent, with saturated fatty acids between twelve and twenty carbons being identified. Both squalene and cholesterol are also detectable, however the signal from these compounds rapidly diminish with time since deposition. This reduction is likely due to a combination of high volatility in vacuum and environmental degradation.[120,121] The fatty acids and squalene produce $[M+H]^+$ ions while cholesterol produces both a minor $[M+H]^+$ peak and a major $[M-OH]^+$ peak. Also present in the positive ion scans is an exogenous compound, dimethyldioctadecylammonium (551 *m/z*, $[M]^+$), which has been found in nearly all of the fingerprints analyzed. This compound is commonly found in hand soaps

and lotions and has been previously reported to be found in fingerprints.[122] The signal from the silicon substrate is also detectable. The peaks in the higher mass range (500 *m/z* to 700 *m/z*) are believed to be a number of different diglycerides, which represent a major component of sebaceous secretions.[123] Due to the large variation in glyceride composition, identification of specific diglycerides was not been attempted using C_{60}^{+} SIMS. Identification of these compounds is based on literature comparisons.

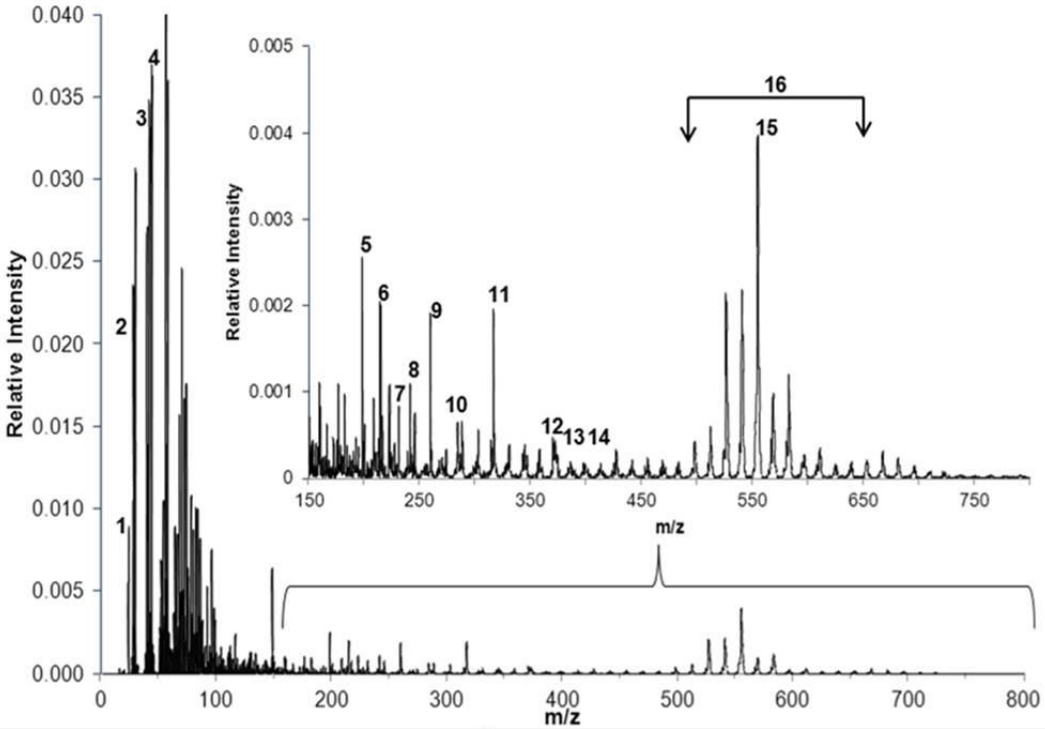

Peak #	Nominal Mass	Assignment	Peak #	Nominal Mass	Assignment
1	23	Sodium Na^+	9	257	Hexadecanoic Acid $[M+H]^+$
2	28	Silicon Si^+	10	285	Octadecanoic Acid $[M+H]^+$
3	39	Potassium K^+	11	313	Eicosanoic Acid $[M+H]^+$
4	40	Calcium Ca^+	12	369	Cholesterol $[M-OH]^+$
5	201	Dodecanoic Acid $[M+H]^+$	13	387	Cholesterol $[M+H]^+$
6	215	Tridecanoic Acid $[M+H]^+$	14	411	Squalene $[M+H]^+$
7	229	Tetradecanoic Acid $[M+H]^+$	15	551	Dimethyldioctadecylammonium $[M]^+$
8	243	Pentadecanoic Acid $[M+H]^+$	16	500 - 600	Glycerides

Figure 6.1 Representative C_{60}^+ SIMS positive ion mass spectrum of the chemical composition of a fingerprint. Nominal positions of some of the identified components are highlighted.

In the negative ion spectrum, shown in Figure 6.2, fewer compounds of interest have been identified compared to the positive ion spectrum. As with the positive ion spectrum, the negative ion shows a number of the free fatty acids as well as some of the anions present in eccrine secretions. Free fatty acids, which are present as the $[M-H]^-$ ion, have a much stronger relative signal in the negative ion mode than in the positive ion mode. Glycine, an amino acid, has also been identified in this mode, unlike positive mode, where an elevated background in the 80 *m/z* to 120 *m/z* region may have prevented identification. One other group of compounds that SIMS can detect in both the positive and negative modes is the eccrine salts. A number of both cations and anions have been identified. This could provide additional information that other techniques, such as GC-MS could not provide.

Of the donors whose fingerprints were analyzed in this study, the variation both inter- and intra-person is minimal. The noticeable differences in the mass spectra included the presence or absence of cholesterol and squalene, and in one instance the absence of dimethyldioctadecylammonium. Also, though free fatty acids are detected in every fingerprint, the relative intensity of fatty acids amongst one another varied both between donors and within different fingerprints from the same donor. Blank silicon wafers were run to ensure that the peaks that were detected and identified were not due to the substrate background or cluster ions formed from the substrate background.

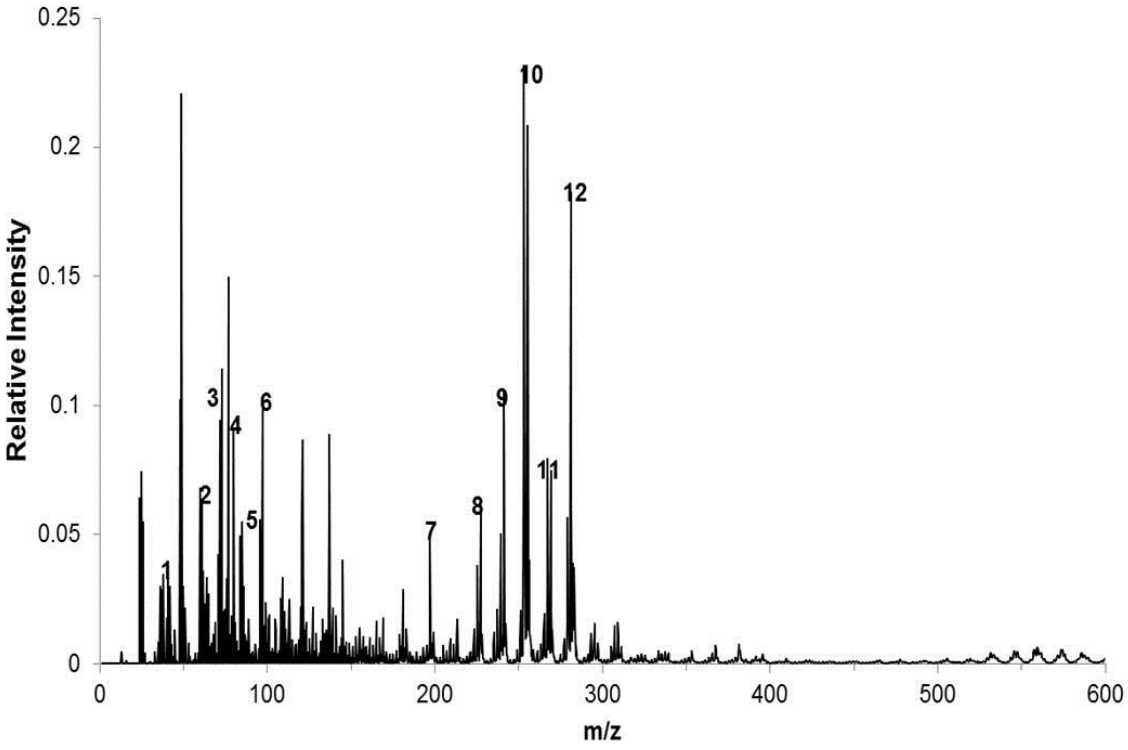

Peak #	Nominal Mass	Assignment	Peak #	Nominal Mass	Assignment
1	35 & 37	Chloride Cl^-	7	199	Dodecanoic Acid $[M-H]^-$
2	59	Urea $[M-H]^-$	8	227	Tetradecanoic Acid $[M-H]^-$
3	74	Glycine $[M-H]^-$	9	241	Pentadecanoic Acid $[M-H]^-$
4	80	Bromide Br^-	10	255	Palmitic Acid $[M-H]^-$
5	95	Phosphate PO_4^-	11	269	Heptadecanoic Acid $[M-H]^-$
6	96	Sulfate SO_4^-	12	283	Stearic Acid $[M-H]^-$

Figure 6.2 A representative C_{60}^+ SIMS negative ion mass spectrum of the chemical composition of a fingerprint. Nominal positions of some of the identified components are highlighted.

Subsection 6.3.2 Effects of Fingerprint Developing Techniques

To determine the effect of fingerprint development techniques on the SIMS analysis of fingerprints, three different powders including black fingerprint powder, fluorescent powder, and magnetic powder were examined. Mass spectra of the fingerprints were taken before and after application of a developer, and compared. It was found that, in all cases, when a fingerprint was analyzed before and after application of a development technique, the mass spectrum remained largely unchanged except for an increase in the relative signal intensity in the 0 *m/z* – 150 *m/z* range. Examples of the differences in the mass spectra are shown in Figure 6.3. In all instances, background from the powders was minimal in the scanned mass range in the 150 *m/z* – 600 *m/z* mass range. While all of the components that were detected in the fingerprint are present both before and after application of the development technique, a change in signal intensities is seen in all cases. In the post-150 *m/z* mass range, signal intensities are approximately equal before and after application of the powders. The intensities in sub-150 *m/z* mass range are shown to increase in all instances and can be attributed to the increase in background in this mass region caused by the powders. Even with these changes in the mass spectra, however, all compounds that were originally detectable are still readily observed. This persistence in the detection of fingerprint components shows that C_{60}^{+} SIMS may be utilized for the qualitative chemical analysis of fingerprints both before and after development techniques are applied, making it a more practical technique for analysis than techniques like DESI-MS which are hindered by the presence of fingerprint developing powders.

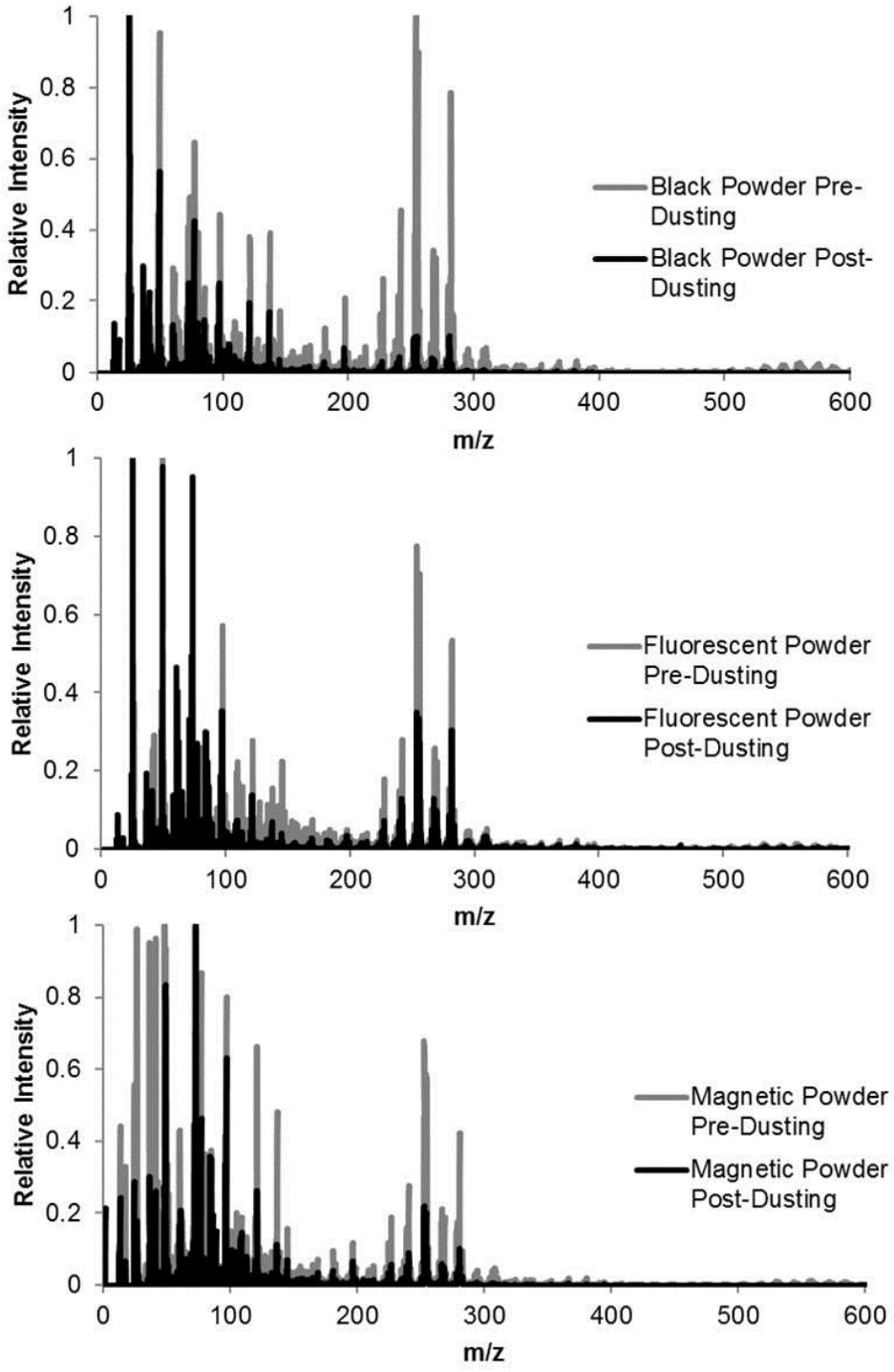

Figure 6.3 Effect of fingerprint developing powders on the SIMS mass spectrum of a fingerprint. Powders used are black powder (Top), fluorescent powder (Middle), and magnetic powder (Bottom).

Subsection 6.3.3 Chemical Fingerprint Imaging

One of the most significant advantages of SIMS is the ability to obtain high spatial resolution images of the chemical composition of the sample in addition to mass spectra. Obtaining both images and mass spectra allows for the correlation of the presence of specific analytes to particular locations in the fingerprint and allows for discrimination from background. Furthermore, site specific imaging allows for the mitigation of the influence of the substrate by either subtracting out the background signal or comparing the image of a sample to that of the background. Imaging of fingerprints using SIMS has been completed with time-of-flight secondary ion mass spectrometry (TOF-SIMS) techniques before[32,102], but never using a C_{60}^+ source nor a double focusing magnetic sector (DFMS) SIMS instrument. Imaging of the fingerprint with C_{60}^+ SIMS is possible using a number of different secondary ion signals, where the time required for acquisition is dependent upon the intensity of the signal. Analytes with strong signals, such as sodium and potassium in the positive mode, or the fatty acids in negative mode, can be imaged with an integration time as short as 1 s per image. Compounds that have weaker secondary ion signals can require 10 s to 20 s integration time per image. To image an entire fingerprint requires stitching together hundreds of individual images. In negative ion mode, with the relatively strong hexadecanoic acid signal, an analysis time of approximately one hour is required for a complete fingerprint image.

To determine if the SIMS images were correlated with the fingerprint valleys or the ridges, a mosaic of 5 by 5 images of the negative hexadecanoic acid ion (255 *m/z*), was acquired using a three second integration time and a 3 second pre-sputter time.

Hexadecanoic acid was chosen because it is the organic compound that produces the greatest intensity, allowing for the lowest integration time. Furthermore, it is reported as being the most abundant saturated fatty acid in fingerprints.[28] Once the hexadecanoic acid image was compiled, it was compared to a reflected light stereomicroscope image of the same area. This comparison is presented in Figure 6.4. From this image it was determined that the hexadecanoic acid ion distribution was correlated with the fingerprint ridges. Once the correlation was determined, an entire fingerprint was imaged. Figure 6.5 shows a fingerprint image collected from the negative hexadecanoic acid ion signal using the SIMS technique, as well as an optical image obtained from the same fingerprint. In this case, each image was integrated for 1 s, with a 1 s pre-sputter period. Similar SIMS images have been obtained using the sodium, potassium, chloride, tetradecanoic acid, and octadecanoic acid signals. Because of the lengthy collection times, conventional optical microscopy is still superior for routine imaging of fingerprint morphology where chemical imaging is not necessary. In cases where chemical information or correlation of compounds with the fingerprint or background is desirable, imaging mass spectrometry such as SIMS may offer important benefits. Also, imaging using SIMS, or another imaging mass spectrometry technique, could allow for the identification of exogenous traces, such as narcotics or explosives, in a fingerprint.

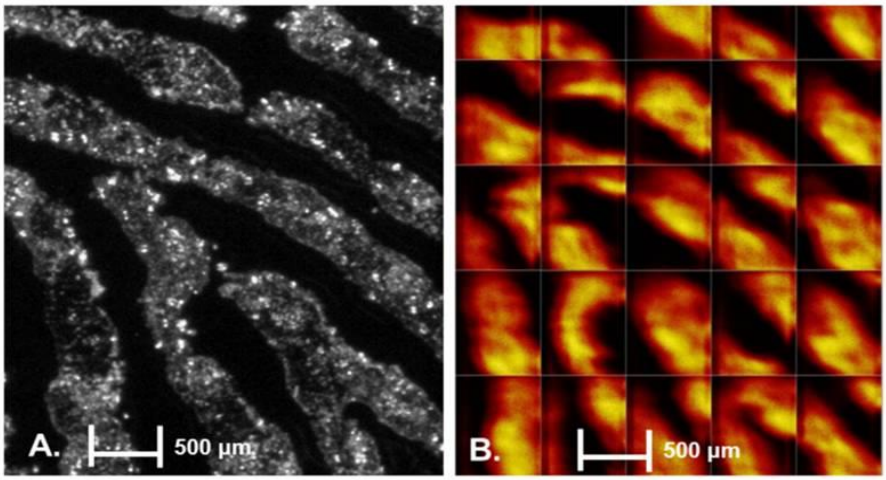

Figure 6.4 Determination of fingerprint ridges and valleys. The optical microscope image (A.) is compared to the SIMS chemical image (B.) of the hexadecanoic acid $[M-H]^-$ ion signal (255 *m/z*).

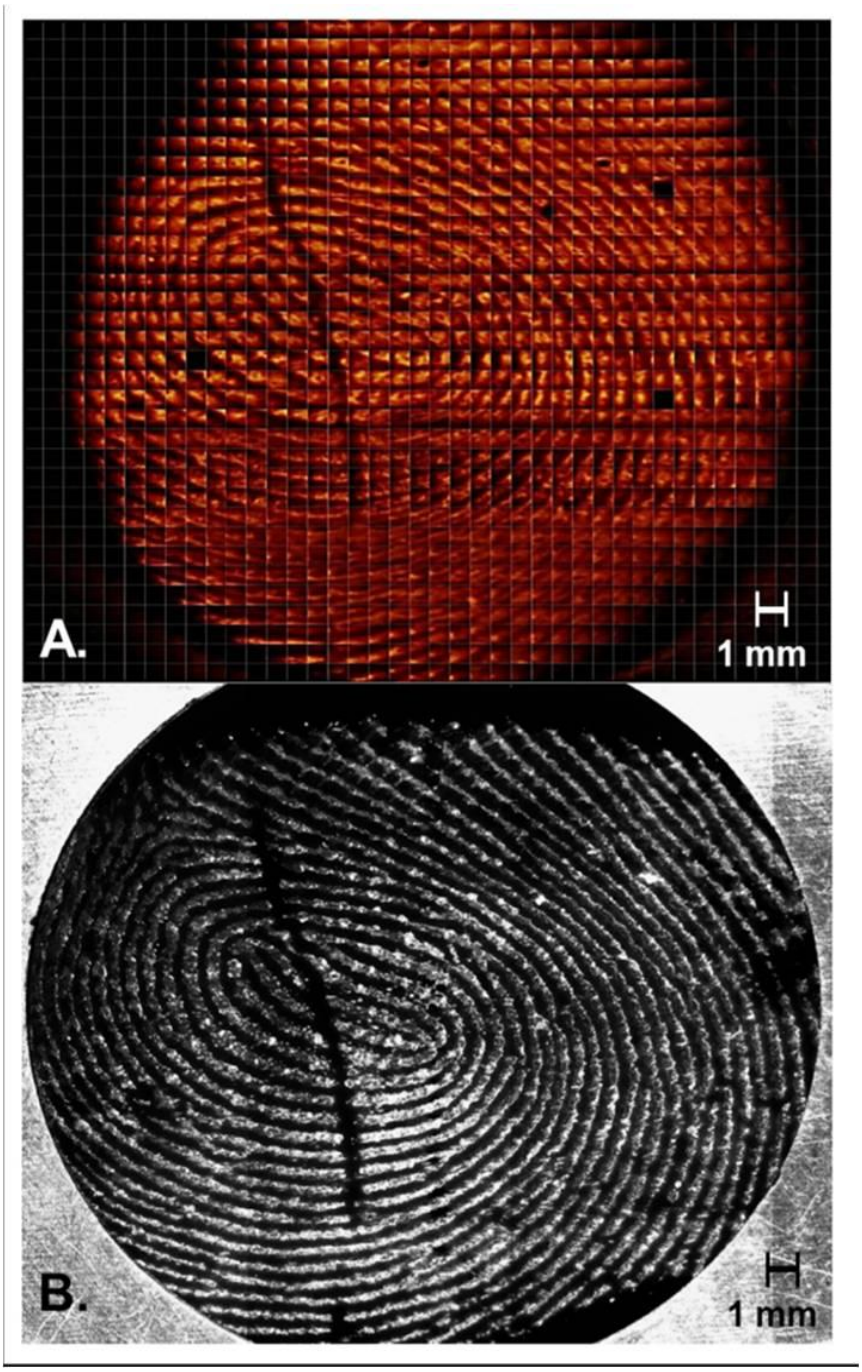

Figure 6.5 Comparison of a SIMS chemical image of a fingerprint (A.) to the optical image of the same fingerprint (B.). Individual SIMS images were collected in negative mode using the signal from the hexadecanoic acid ion. A 1 second pre-sputtering period was completed before each 1 second integration.

Subsection 6.3.4 Depth Profiling

Molecular SIMS depth profiling using C_{60}^{+} cluster ion bombardment is a novel technique for forensic applications that may provide a method for monitoring changes in the chemical composition of an organic sample with respect to depth. This has potential to be useful in a number of different applications by allowing for the determination of surface versus bulk effects, or whether an exogenous analyte, such as an explosive or narcotic particle, is located on the surface of the fingerprint ridge or embedded inside the ridge. Such identification may provide information regarding the order of deposition, allowing the assessment of whether an analyte was originally on the finger or was detected due to prior or subsequent contamination.

It was unclear if molecular depth profiling would be feasible due to the heterogeneity and thickness of fingerprint ridges, however, the ability to depth profile a fingerprint ridge is presented in Figure 6.6. The signal of the fatty acids is shown to decrease in intensity as the ridge is profiled, while the signal of the silicon background is shown to increase in intensity, indicating that the fingerprint ridge is gradually being eroded. The time at which the silicon and fatty acids signals level out indicating the time at which the entirety of the ridge has been sputtered through. This is a method of analysis that is currently not possible using ambient techniques.

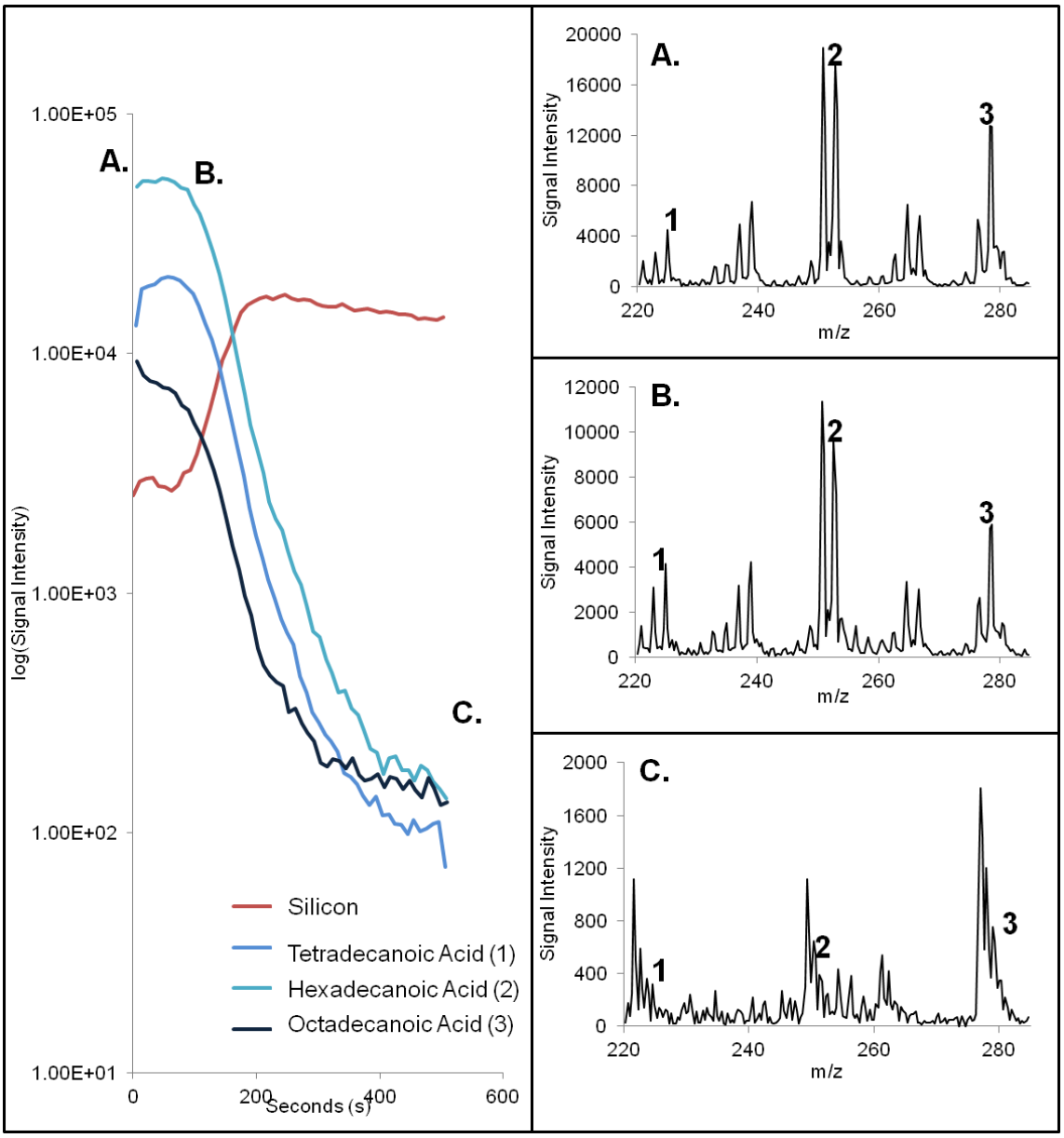

Figure 6.6 Depth profile of tetradecanoic acid, hexadecanoic acid, and octadecanoic acid in a fingerprint ridge versus the silicon substrate (left). The mass spectra of the fatty acids at three time points during the depth profile are also shown (right). The mass spectra shown represent before depth profiling (A.), at the beginning of the decrease in fatty acid signal (B.), and after depth profiling (C.). Both depth profile and mass spectrum were obtained in negative ion mode.

A second example of how depth profiling could be beneficial to fingerprint analysis is shown in Figure 6.7. In this case approximately 1 μg of the explosive RDX was crystallized onto a silicon wafer, after which a fingerprint was deposited on top of it.

A depth profile of the fingerprint was then completed, this time monitoring the silicon background signal, the hexadecanoic acid signal, and the RDX signal. Since the RDX is initially present underneath the fingerprint, the signal produced from the explosive is relatively low. As the fingerprint ridge is sputtered through, the RDX signal gradually increases indicating that the explosive is indeed underneath the fingerprint. This type of depth profiling could be extremely useful in identifying the series in which events occurred.

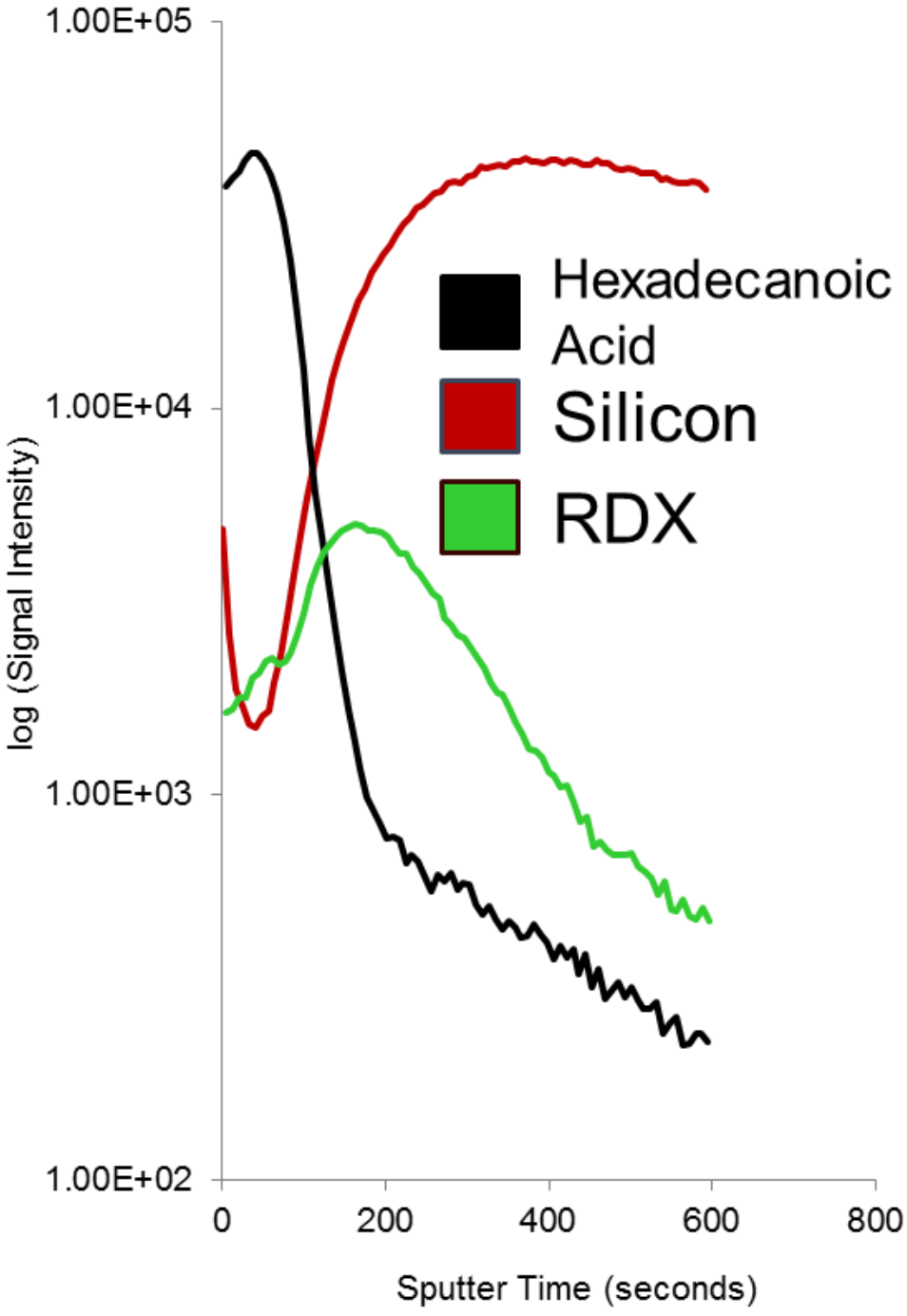

Figure 6.7 Depth profile of a fingerprint deposited on top of RDX crystals.

Section 6.4 Conclusions

C_{60}^+ SIMS has been shown to be a viable mass spectrometry technique for the chemical analysis of fingerprints. SIMS is able to detect a number of compounds commonly encountered in fingerprints, including both eccrine and sebaceous components. Further research is being completed to identify which glycerides can be detected as well to identify additional eccrine components. It is believed that a number of compounds are also undetectable, such as short chain unsaturated fatty acids and lactic acid, due to their volatility under vacuum conditions. Furthermore, the chemical composition appears to be largely unaffected by latent print development techniques including black fingerprint powder, fluorescent powder, and magnetic powder, which is expected with the powders since they do not chemically react with the fingerprint constituents. Chemical imaging of fingerprints using SIMS is possible, and provides complimentary information to conventional optical microscopy. SIMS imaging may be beneficial for the detection of trace amounts of explosives, narcotics, or other exogenous components, that are not optically detectable under a microscope. Also, dynamic SIMS provides the ability to depth profile fingerprint ridges in order to probe changes in the chemical composition throughout the ridge of a fingerprint – something that has not be reported to date.

One potential limitation of the approach is the current inability of SIMS to detect all of the expected species in a fingerprint. While it is unlikely that any one technique will be able to detect all of the components, other work has suggested that derivatization of fingerprints or the use of AI-MS techniques may be able to provide additional information. We are currently exploring the viability of several of these ambient

ionization techniques for fingerprint component identification. A second issue is the potential loss of more volatile components that could be addressed by using a cooled sample stage, or the ambient ionization techniques like DESI-MS. However, even with these limitations, C_{60}^{+} SIMS is a viable technique for both chemical analysis and imaging of fingerprints.

Chapter 7: Imaging and other Applications using Time-of-Flight Secondary Ion Mass Spectrometry for the Analysis and of Fingerprints and Trace Chemicals

Section 7.1 Introduction

It has been shown through these studies, and previously published studies, that chemical imaging of latent fingerprints can be completed using a variety of techniques, and can be applied to a number of different situations. Specifically, secondary ion mass spectrometry (SIMS) has been shown to provide capabilities outside those of other chemical imaging techniques. While C_{60}^+ SIMS may not provide rapid high spatial resolution images, it can provide the ability to complete depth profiling. Time-of-flight secondary ion mass spectrometry (TOF-SIMS), however, is a platform that allows for both rapid and high spatial resolution chemical imaging. TOF-SIMS imaging of small portions of fingerprints has been shown to be possible, though full scan mass spectral imaging (MSI) of fingerprints has not been discussed.[32,102] This work aims to show a proof of concept as to the types of chemical images that can be obtained using this technique. Furthermore, it explores another potential application of fingerprint research, age dating.

Age dating of fingerprints has been researched for many years as it is believed that being able to determine the age of a fingerprint may provide significant information to a criminal investigation. Two potential benefits to knowing the age of a fingerprint found at a crime scene are that the approximate time of crime could be determined, or that the age of a fingerprint could confirm the presence of a suspect at the crime scene at

a given time. While a number of different studies have looked into how fingerprints age, nearly all have been concerned with how individual components found in a fingerprint degrade as a function of time. Previous work has shown that the degradation of unsaturated organic constituents in a fingerprint degrade significantly faster when exposed to light.[120,121] They have also identified a number of the degradation components into which the starting materials form, as unsaturations along the carbon are broken and form peroxides.[121] Cholesterol is another compound present in fingerprints which has been identified as easily degraded by environmental exposures, such as ozone.[124,125]

While there is inherent benefit in understanding the degradation processes that occur in an aging fingerprint, there is a wide variation in which these compounds appear in fingerprints. A number of studies have concluded that variation in composition and amount deposited is vast,[90,92,126,127] which may make the use of degradation products as a method for age dating more difficult. Therefore, it is important to explore other potential routes for age dating. One such route is monitoring bulk viscous flow of chemical constituents of latent fingerprints as a function of time, surface, and environmental exposure. This type of analysis requires the high spatial resolution offered by TOF-SIMS analysis. This chapter aims to show a proof of concept of high resolution chemical imaging, as well as identifying changes in the chemical image of a latent fingerprint as a function of the parameters stated above – age, surface, and environmental exposure.

Section 7.2 Materials and Methods

Subsection 7.2.1 Instrumental Methods

Analysis by TOF-SIMS was completed using an IONTOF IV instrument (IONTOF, Munster, Germany) equipped with a 25 kV Bi_n^+ analysis gun. The gun was oriented at a 45 ° incidence angle. A low energy electron flood gun was used, when necessary, to aid in eliminating charge build-up on the sample surface during analysis. For sample analysis, a Bi_3^+ primary ion beam was used in high mass resolution mode and rastered inside 500 µm by 500 µm squares to obtain individual chemical images. The individual images had a pixel density of 64 pixels by 64 pixels and were stitched together to obtain the entire chemical image. For all analyses, the ion dose was approximately 1×10^{12} ions/cm^2.

For the time lapse photography of lateral fingerprint changes, a Leica microscope (Leica Microsystems, Buffalo Grove, IL, USA), with a 1 x objective and attached camera was interfaced with ImagePro Plus software (Media Cybermetrics, Rockville, MD, USA). The ImagePro software triggered the camera to take a photograph once every twenty minutes over a 72 hour period. Individual images were then extracted out of the time lapse.

To understand the aging of fingerprints as a result of environmental exposure, several different exposure setup ups were used. To simulate exposure to sunlight, a Luzchem five light UV panel was utilized (Gloucester, ON, Canada). The light panel contained four UV-A lamps (centered at 350 nm) and one UV-B lamp (centered at 300 nm, with a peak at 313 nm). Exposure was calibrated against the degradation of TNT left in actual sunlight, and it was found that 24 hours of exposure under the light panel was

approximately equal to eight hours of actual sunlight. For exposure to elevated levels of ozone, a Jenesco PT101-2K (Amherst, NH, USA) ozone generator was used. The generator was triggered to turn on for one minute ever ninety minutes. By completing this cycle, the average ozone concentration in the chamber was 1 ppm, as measured continuously by an Ozone Solutions S-200 portable ozone monitor (Hull, IA, USA). An ozone concentration of 1 ppm is approximately thirteen times higher than the average ozone concentration, as reported by EPA in the "National Ambient Air Quality Standards", of 0.075 ppm.[128] For exposure to elevated levels of heat and/or humidity, an Associated Environmental LH Series Environmental Test Chamber was used (Ayer, MA, USA).

Subsection 7.2.2 Chemicals and Materials

For this study, real fingerprints were used for analyses. The fingerprints were obtained by loading the fingerprint with sebaceous materials through rubbing the bridge of the nose with the finger and then depositing onto a surface. The surfaces that were used include 2.54 cm round silicon wafers, glass microscope slides, a simulated car panel, copy paper, and a piece of aluminum metal.

Section 7.3 Results & Discussion

Subsection 7.3.1 Identifiable Compounds and Imaging Optimization

A sebaceous loaded fingerprint was deposited onto a silicon wafer and analyzed directly, in both positive and negative ionization modes, using the method described above, to determine which compounds were detected as well as to determine if

fingerprint imaging was feasible. Figures 7.1 and 7.2 represent the positive and negative TOF-SIMS mass spectra of latent fingerprints respectively. Like C_{60}^{+} SIMS, TOF-SIMS was able to detect a number of different fatty acids, inorganic salts, and other common fingerprint components. Furthermore, the negative ion scan also produced a greater number of identifiable peaks. Using these parameters, fingerprints were also found to be easily imaged using the pre-existing conditions. Examples of chemical fingerprint imaging are shown throughout the remainder of the chapter.

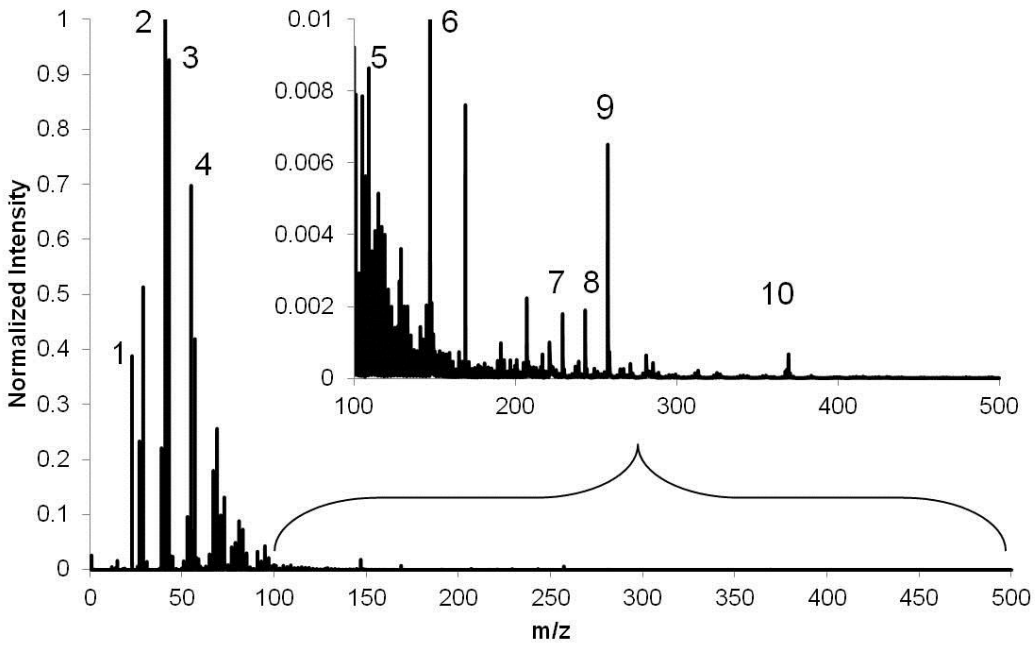

Peak	Nominal Mass	Assignment	Peak	Nomnial Mass	Assignment
1	23	Sodium Na^+	6	147	Lysine $[M+H]^+$
2	39	Potassium K^+	7	229	Tetradecanoic Acid $[M-H]^-$
3	40	Calcium Ca^+	8	243	Pentadecanoic Acid [M-H]-
4	55	Iron Fe^+	9	257	Hexadecanoic Acid $[M+H]^+$
5	107	Serine $[M+H]^+$	10	369	Cholesterol $[M-OH]^+$

Figure 7.1 Representative positive ion mass spectrum of a fingerprint analyzed by TOF-SIMS.

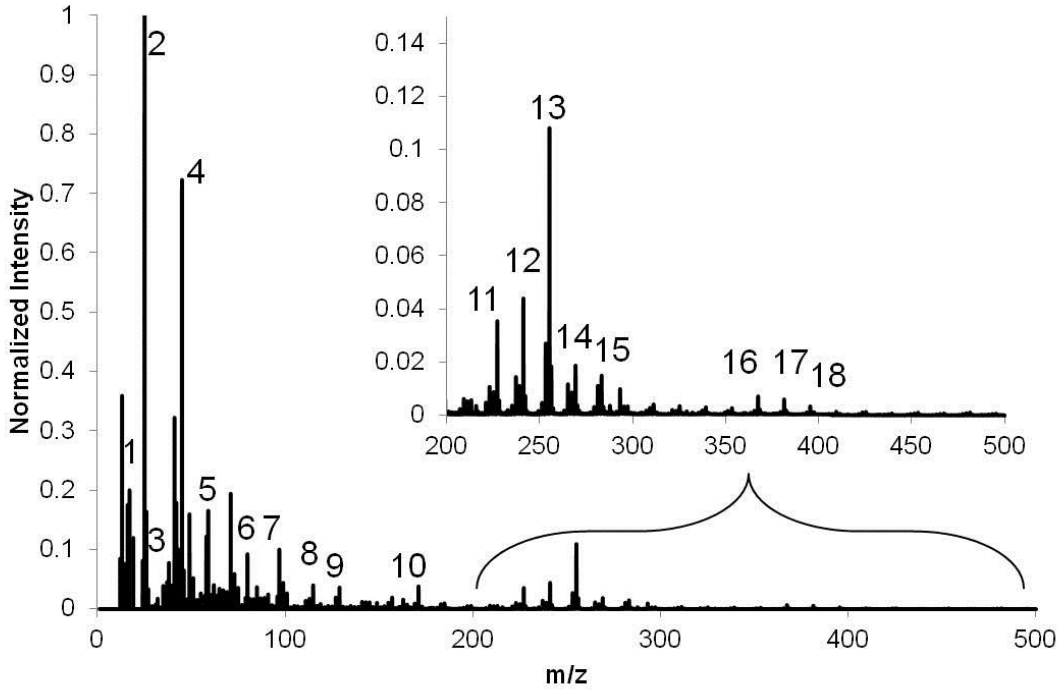

Peak	Nominal Mass	Assignment	Peak	Nomnial Mass	Assignment
1	19	Fluorine F^-	10	171	Decanoic Acid $[M-H]^-$
2	26	Cyanide CN^-	11	227	Tetradecanoic Acid $[M-H]^-$
3	35 / 37	Chlorine Cl^-	12	241	Pentadecanoic Acid $[M-H]^-$
4	46	Nitrite NO_2^-	13	255	Hexadecanoic Acid $[M-H]^-$
5	60	Urea $[M]^-$	14	269	Heptadecanoic Acid $[M-H]^-$
6	79	Bromine Br^-	15	283	Octadecanoic Acid [M-H]-
7	97	Sulfate $[SO_4+H]^-$	16	367	Tetracosanoic Acid $[M-H]^-$
8	115	Hexanoic Acid $[M-H]^-$	17	381	Pentacosanoic Acid $[M-H]^-$
9	129	Heptanoic Acid $[M-H]^-$	18	395	Hexacosanoic Acid $[M-H]^-$

Figure 7.2 Representative negative ion mass spectrum of a fingerprint analyzed by TOF-SIMS.

Subsection 7.3.2 Potential for Age Dating – Effect of Age on Samples

The benefits to TOF-SIMS analysis of fingerprints are the parallel detection, high chemical specificity, and the rapid acquisition of high spatial resolution images, allowing for a unique approach to the analysis of fingerprints and fingerprint aging. It is believed that by measuring the viscous flow of components out of fingerprint ridges it may be possible to obtain a more accurate and robust determination of age over other, more traditional methods such as monitoring degradation components. Flow out of fingerprint ridges should be less dependent on the amount of particular constituents present and thus not require the quantification of materials necessary for other methods that have been explored.

The idea of viscous flow of fingerprint constituents began with a time lapse photo taken of a fingerprint deposited on a silicon wafer. Figure 7.3 shows stills from the time-lapse of a fingerprint. Initially, all material is visibly isolated to the ridges of the fingerprints. However, after four hours movement of some material is already seen occurring out of the fingerprint ridges and into the valleys. By eighteen hours the material has nearly traversed the majority of the ridges within the fingerprint, and by the end of the seventy two hour period complete coverage across every valley in the frame can be seen. It is important to note that this time-lapse occurred under laboratory conditions (22 °C, 20% relative humidity, and ambient lighting). This process, and the speed at which it occurs, would vary depending on surface and environmental exposure.

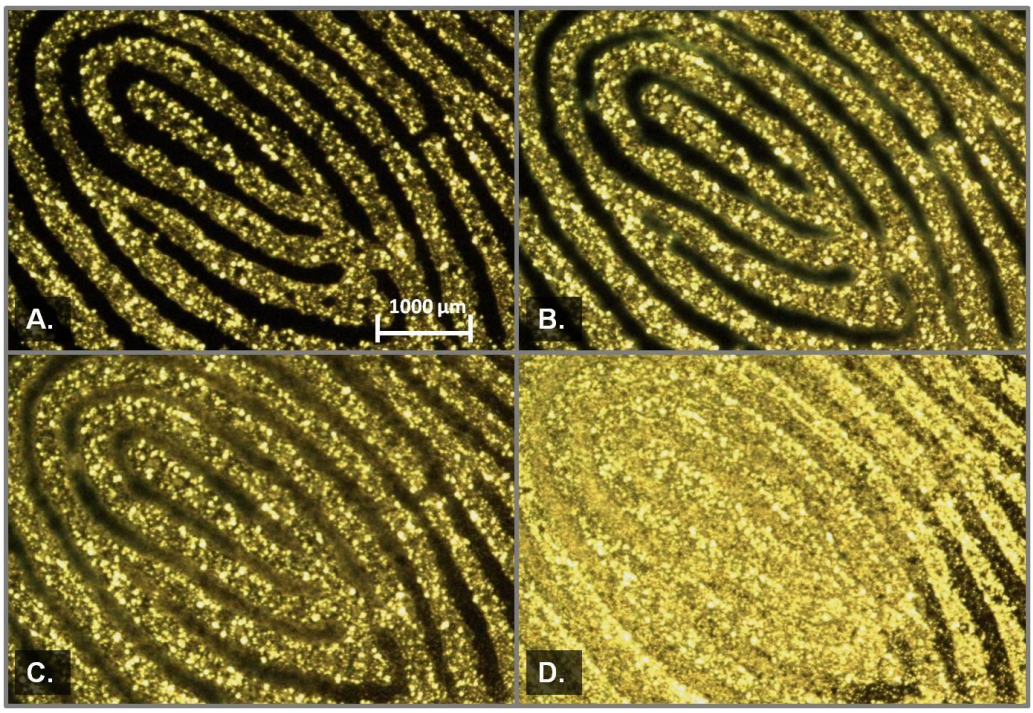

Figure 7.3 Time lapse stills of the visible lateral movement of a fingerprint deposited onto a silicon wafer obtained using an optical microscope. Times are 0 hours (A.), 4 hours (B.), 18 hours (C.), and 72 hours (D.).

In order to identify what constituents of the fingerprint were flowing out of the ridges in the short time frame, a number of fingerprint samples were deposited on the same day and imaged using TOF-SIMS at varying time intervals. Figure 7.4 shows the short-term study that looked at how the chemical distribution of the fingerprint changed within the first 72 hours after deposition. It was thought that the constituents flowing out of the ridges were likely all related to one type of constituent, either sebaceous or eccrine. Figure 7.4 shows the negative ion chemical image of one chemical from each type of constituent (hexadecanoic acid is a sebaceous component and sulfate is an eccrine component). As is mirrored in the time-lapse photography, the initial fingerprint exhibits co-location of all components of the fingerprint, as well defined valleys can be seen. After 24 hours, the chemical imaging shows movement of compounds out of the

fingerprint ridges corresponding to the sebaceous components in the fingerprint. The movement of hexadecanoic acid and other sebaceous compounds, continues, and by the end of the 72 hour study, movement of hexadecanoic acid has occurred across nearly all fingerprint valleys, whereas the sulfate ion has remained located in fingerprint ridges.

To better understand which sebaceous fingerprint components were diffusing, and to determine if different sebaceous components diffuse more rapidly than others, a series of fingerprints were deposited and imaged over the first 14 days after deposition. Figure 7.5 shows identical portions of a small part of the fingerprint as well as the location of six unsaturated fatty acids with chain lengths between ten and twenty carbons long. The flow of the shorter length fatty acids appears to proceed more rapidly than those of the longer lengths. Eicosanoic acid ($C_{20:0}$) does not show any signs of flow until day fourteen, while decanoic acid ($C_{10:0}$) shows signs of nearly immediate flow. It may be possible to follow the age of a fingerprint by using high resolution chemical imaging to identify which of these fatty acids has begun to diffuse out of the fingerprint ridges and which have not.

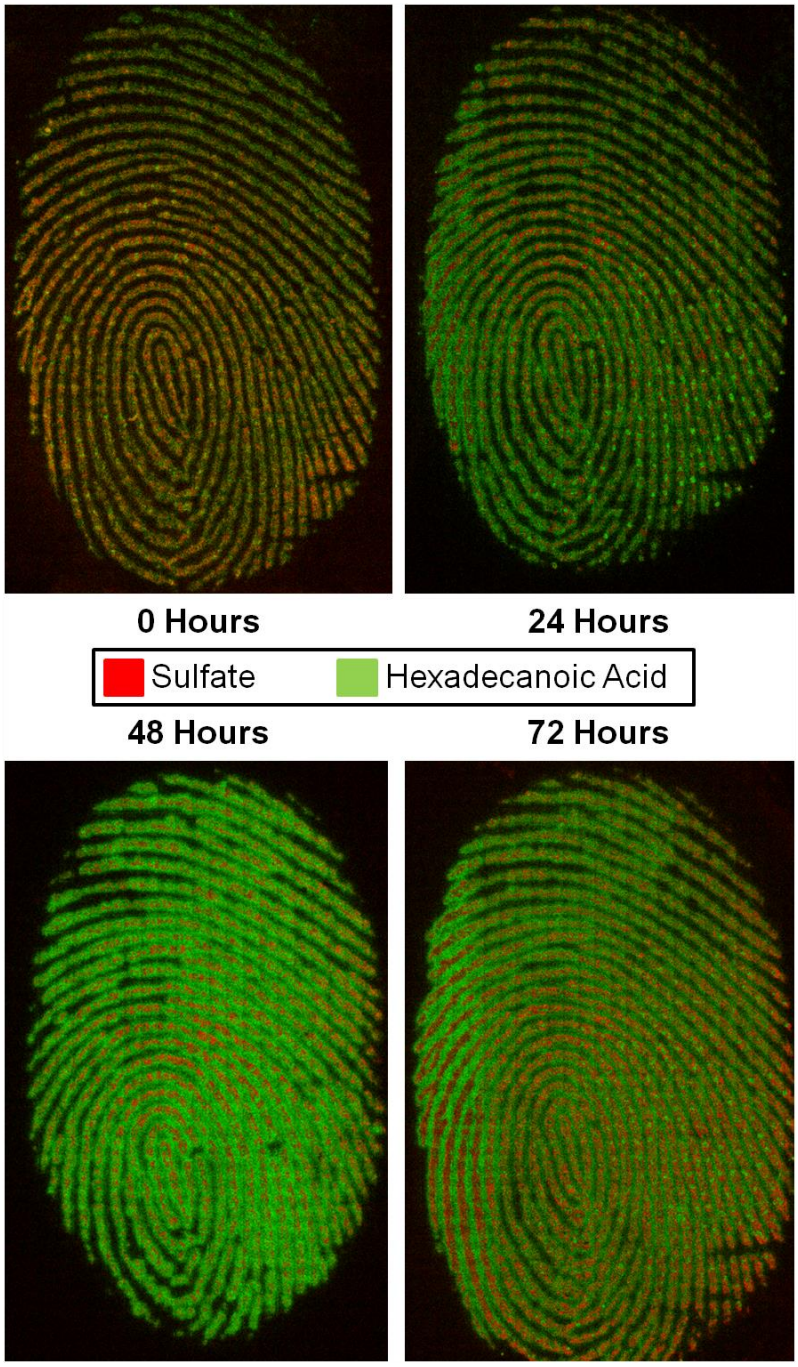

Figure 7.4 Chemical images of the sulfate ion (red) and hexadecanoic acid deprontonated molecular ion signal (green) within latent fingerprints over the first 72 hours after deposition.

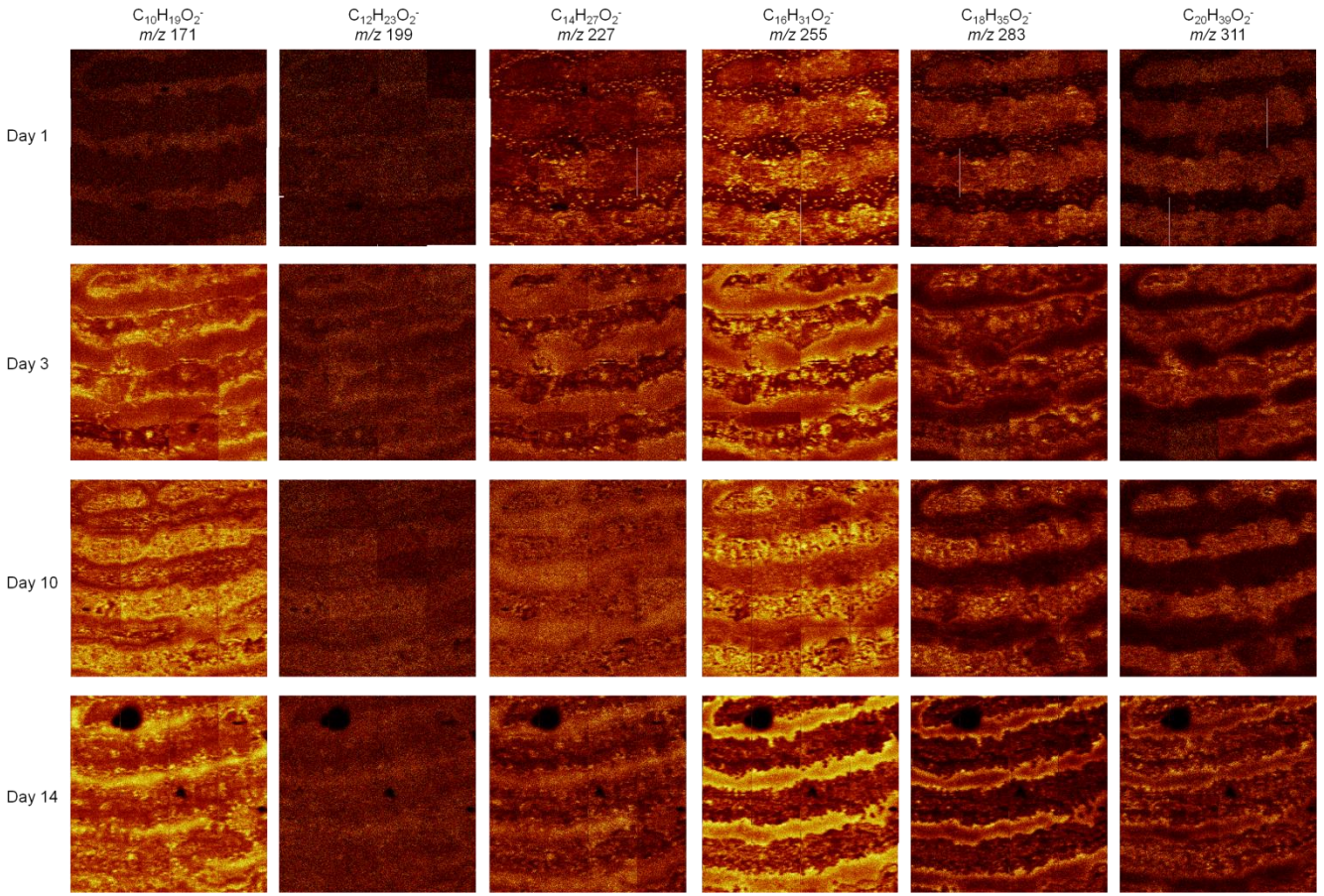

Figure 7.5 Chemical images of the location of several fatty acids in latent fingerprints between Day 0 and Day 14. The fatty acids are decanoic acid (A.), dodecanoic acid (B.), tetradecanoic acid (C.), hexadecanoic acid (D.), octadecanoic acid (E.), and eicosanoic acid (F.). In all images a lighter color indicates higher intensity.

To identify viscous flow characteristics of fingerprint materials beyond the first two weeks, additional studies were carried out in which fingerprints were aged up to twelve months before analysis and imaging using TOF-SIMS. Figure 7.6 shows identical portions of fingerprints at timeframes from fresh to one year old. As expected, fresh fingerprints show excellent co-location amongst constituents and the silicon background represents the negative image of the fingerprint ridges. After three months of aging, there were significant changes to the chemical distribution within the fingerprint. Not only had the hydrocarbons and lipids diffused out of the fingerprint ridges, so had the salts. This indicated that there was some timeframe at which the eccrine components of the fingerprint would also begin diffusing out of the fingerprint ridges. Identifying this time point would be crucial as it could allow for the determination of a rough age of fingerprint, depending on whether one or both of the types of fingerprint constituents had begun diffusing. By month twelve, movement had occurred to the point where the chemical image could no longer discriminate the fingerprint ridges from valleys. While the chemical image was no longer resolvable, the optical image of the fingerprint still allowed for differentiation of ridges versus valleys, as shown in Figure 7.7. This is another potentially useful marker as it would allow for another time stamp for the approximate age of a fingerprint.

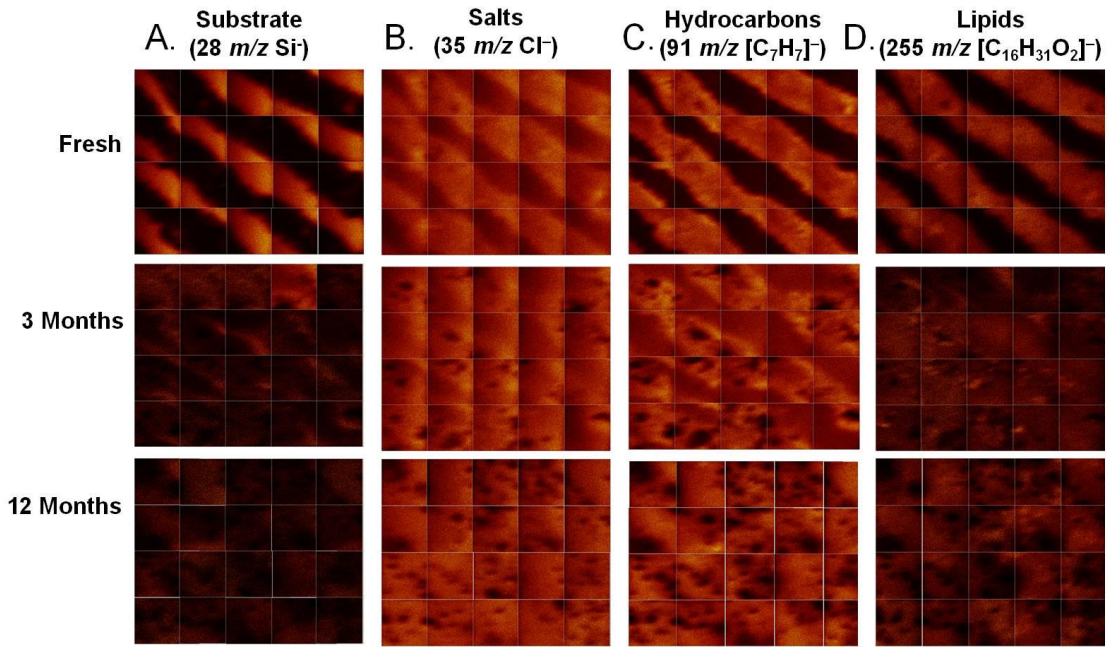

Figure 7.6 Chemical images of several different fingerprint constituents and the silicon background at Day 0, 3 Months, and 12 Months after deposition. Constituents imaged are the silicon background (A.), chloride (B.), a hydrocarbon fragment (C.), and the deprotonated molecular ion of hexadecanoic acid (D.). In all images lighter color indicates higher intensity.

Figure 7.7 Optical image of a one year old fingerprint. Note that the ridges and valleys are still visibly distinguishable.

Subsection 7.3.3 Potential for Age Dating - Effect of Environmental Exposure

In addition to time, it is expected that the environment to which a fingerprint is exposed would play a critical role in determining the extent of viscous flow of fingerprint components. To better understand what effects certain environmental factors have on chemical composition, fingerprints deposited on silicon wafers were exposed to UV light and ozone for a period of three months and then chemically imaged using TOF-SIMS. The UV exposure was constant and was determined to be approximately one day of full sun per twenty four hour period. The ozone exposure was also constant at a concentration of approximately one part per million. Figure 7.8 shows how these environmental factors can affect the chemical distribution in latent fingerprints. In these

images the blue represents the silicon background, green represents hexadecanoic acid, a sebaceous compound, and red represents sulfate, an eccrine compound.

The fingerprint that was kept in a laboratory environment shows the flow of fingerprint material, both eccrine and sebaceous, out of the valleys and into the ridges. It also shows the halo of eccrine salts that appear to accumulate around the edges of the fingerprints after approximately two months of age. A stark contrast to this image is seen when the UV or ozone exposed fingerprints are analyzed.

The UV exposed fingerprint shows that little remains of the sebaceous compounds, as they are likely degraded by the UV exposure. The hexadecanoic acid that did remain was located in the valleys of the fingerprints and therefore did show that movement occurred prior to or during degradation of the compound. Furthermore, no movement of the eccrine components is seen. This was likely due to the increased rate of evaporation of water from the fingerprint that is a combination of the UV exposure and the slightly elevated temperature (approximately 32 °C) inside the UV chamber.

For the fingerprint that was exposed to an elevated ozone environment, the chemical distribution is also much different than that of the other two exposure environments. The presence of ozone appears to inhibit the flow of sebaceous materials out of the fingerprint valley, while still allowing the flow of eccrine components. Preferential movement of the eccrine components of the fingerprints may have been caused by the rapid ozonolysis of sebaceous secretions as they diffuse into thin layers in the fingerprint valleys. This hypothesis is still being investigated.

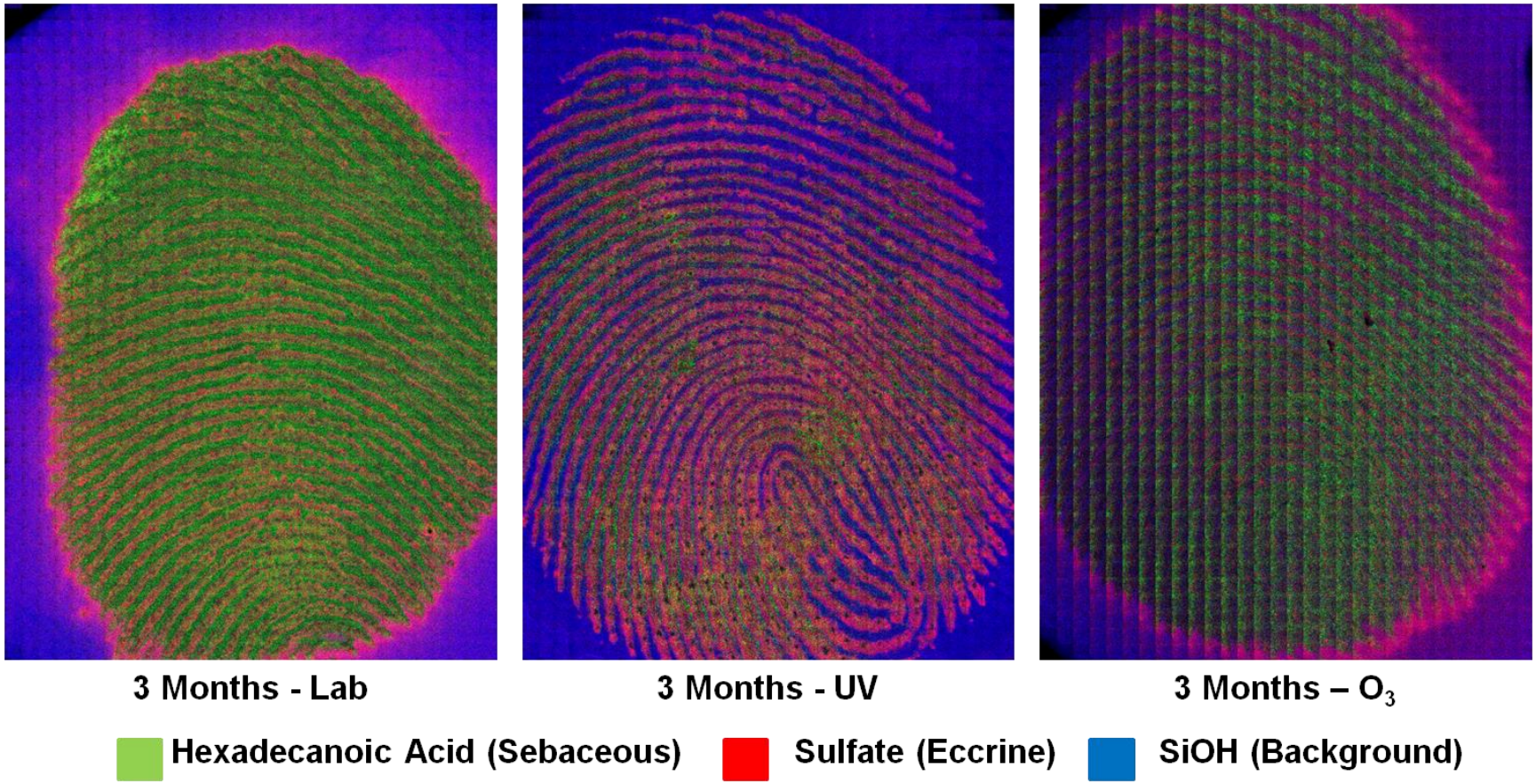

Figure 7.8 Chemical images of fingerprints exposed to different environmental conditions for 3 months. The three conditions were laboratory (A.), simulated UV (b.), and elevated ozone (c.).

Subsection 7.3.4 Potential for Age Dating – Effect of Surfaces

Another set of experiments were completed to determine if fingerprints could be imaged off of a variety of different surfaces as well evaluate how the viscous flow of constituents compares to those identified on the silicon substrate. In total, for different surfaces were tested and included a glass microscope slide, an aluminum plate, a sheet of plastic, and a piece of copy paper. Fingerprints were deposited as normal, and aged for up to one week before being imaged. Imaging of these fingerprints was identical to those of other imaging tests discussed in this chapter with the exception of the additional use of an electron gun to help mitigate charging of the non-conductive samples. Both negative and positive ionization images were obtained. Figure 7.9 shows an exemplary negative and positive ion chemical image of the fingerprints off of the four different surfaces. In all cases, chemical imaging was possible off of the surfaces. The paper substrate had the greatest charging effect, and because of that, low abundance constituents were not well resolved. Comparison of the location of eccrine and sebaceous components between Day 0 and Day 7 can be seen in Figure 7.10. The lateral movement of fatty acids was seen to occur on the glass and steel surfaces. On plastic surfaces it appeared that the movement was actual reverse, with eccrine components diffusing out of the fingerprint ridges, and the sebaceous components staying in place. The paper charged too much to obtain reasonable identification of which, if any, components were diffusing.

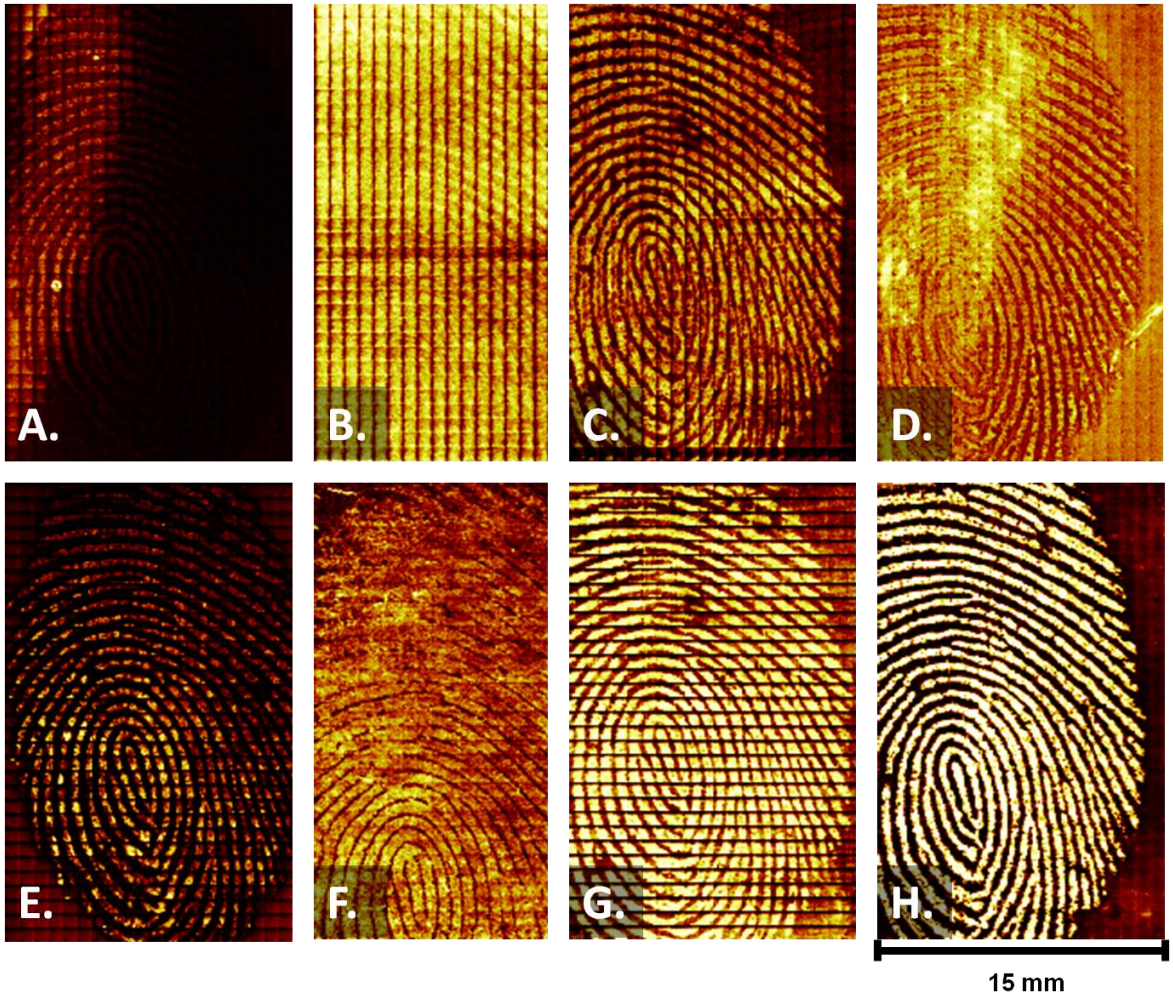

Figure 7.9 TOF-SIMS images of sulfate (negative mode) (A. – D.) and potassium (positive mode) (E. – H.). Surfaces are glass (A. & E.), paper (B. & F.), Plastic (C. & G.), and steel (D. & H.). In all images, a brighter color is indicative of higher signal intensity.

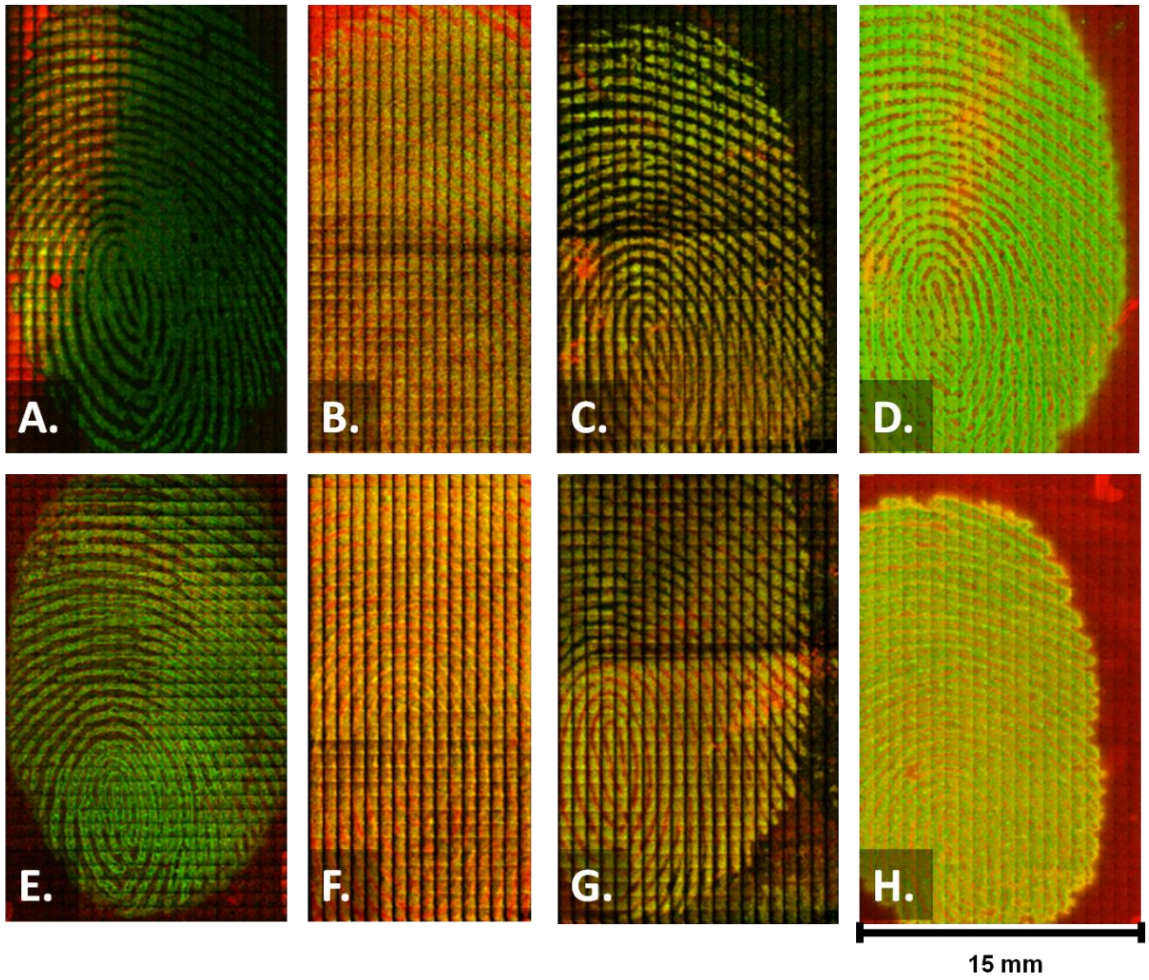

Figure 7.10 Comparison of fresh fingerprints (A. - D.) and 1 week old fingerprints (E. – H.). In all cases red is indicative of sulfate (eccrine) and green is indicative of palmitic acid (sebaceous). The surfaces are glass (A. & E.), paper (B. & F.), plastic (C. & G.), and steel (D. & H.).

Section 7.4 Conclusions

High resolution chemical imaging with the ability to identify and visualize the distribution of virtually all chemical components of latent fingerprints can be achieved using TOF-SIMS. An image of a complete fingerprint can be obtained, in under one hour, with a complete mass spectrum in each pixel of the image. This is in contrast to C_{60}^{+} SIMS, which requires approximately 4 hours and each pixel contains information for select masses, or DEFFI-MS that takes approximately three hours and contains only a small mass range in each pixel. The rapid throughput of this technique is advantageous; however, it is limited to small samples and vacuum compatible materials. TOF-SIMS is also the optimal technique for mapping and better understanding the lateral movement of fingerprint constituents. It has been shown that viscous flow of various fingerprint constituents occur at different rates, with sebaceous compounds flowing more rapidly than eccrine components. It has also been shown that different environmental exposures affect the movement of these chemicals. By enhancing the understanding of this phenomena, and expanding the range of surfaces that have been examined, gaining a better understanding of fingerprint aging through viscous flow may be possible.

Chapter 8: Conclusions & Future Areas of Research

Section 8.1 Trace Explosives Analysis – Conclusions

Methods for the analysis of trace explosives by direct analysis in real time mass spectrometry (DART-MS), desorption electrospray ionization mass spectrometry (DESI-MS), desorption electro-flow focusing ionization mass spectrometry (DEFFI-MS), and low temperature plasma mass spectrometry (LTP-MS) have been developed and optimized. The method using DART-MS, developed as part of this thesis, has now been adopted for the routine examination of evidence at the Defense Forensic Science Center (DFSC). Each of the above mentions techniques has been shown to provide rapid analysis of a wide range of organics and explosives at sensitivities equal to or exceeding those of confirmatory techniques such as gas chromatography mass spectrometry (GC-MS). Furthermore, these methods were shown to have the capability to detect a majority of the studied explosives in a mixture simultaneously, with the exception of ethylene glycol dinitrate (EGDN) and 2,6-Bis(picrylamino)-3,5-dinitropyridine (PYX). Sensitivities for explosives in mixtures were found to decrease, in nearly all cases, by a factor of two or more. Characteristic mass spectra produced by the explosives are reproducible and can be used to identify the explosive(s) present. Isomeric explosives, such as 2,4-DNT and 2,6-DNT were shown to produce nearly identical mass spectra. In terms of implementation of these techniques into a screening scenario, where the goal is simply to detect the presence or absence of explosives at trace levels, these sources show great promise. High throughput and sensitive analysis of both nitro-containing and peroxide based explosives can be achieved without the need for sample preparation. This

type of analysis could greatly reduce the time required by forensic scientists to analyze evidence, as it is possible to screen ten or more pieces of evidence in the time required to complete one confirmatory sample run on the GC-MS. In an airport or other security screening environment, these techniques will allow for a larger range of detectable compounds than currently deployed instrumentation, though it is likely that significantly more user training would be required.

Section 8.2 Trace Explosives Analysis – Future Directions

Even with the development of methods for the screening of explosives by DART-MS, DESI-MS, DEFFI-MS, and LTP-MS, there are many questions remaining to be explored. Additional ambient ionization sources, such as matrix assisted laser desorption ionization (MALDI), thermal desorption ionization (TDI), or atmospheric pressure glow discharge ionization (APGDI), could be validated and optimized for explosives screening to understand each techniques strengths and limitations. Additionally, while utilization of AI-MS techniques in a forensic laboratory is relatively straightforward and would be compatible with existing protocols, this may not be the case for deployment at security checkpoints. Methods would have to be developed to sample different surfaces types, for instance luggage and hands, and a reproducible way for sample introduction needs to be developed. Furthermore, for deployment in a checkpoint screening scenario, routine instrument maintenance may be more problematic, additional operator training would be necessary, and the instrumentation would need to be ruggedized.

Another potential area of future work to explore would be the development of confirmatory methods for the forensic analysis of trace explosives. Significant work has

been completed by Robetr Steiner *et al* at the Virginia Department of Forensic Science to show how DART-MS can be utilized as both a screening and confirmatory technique for the analysis of narcotics.[64] It was shown that by rapidly switching the orifice voltage of the time-of-flight (TOF) mass spectrometer, it was possible to obtain both the parent ion of the narcotic, at a low orifice voltage, in addition to characteristic fragment ions, at a high orifice voltage. The combination of the exact mass of the parent ion and the characteristic fragment ion patterns was determined to be sufficient to confirm the identity of the analyte of interest.

In addition to work which would be completed for the deployment of these instruments into the field, whether for screening or confirmatory purposes, there is still a need to better understand the fundamentals of these techniques and continued research is required to improve sensitivity and reproducibility. Desorption and ion transport mechanisms into and through the ambient mass spectrometer interface would be one area for future work. A better understanding of the unique capabilities of DEFFI, with the combination of corona discharge occurring concurrently with electrospray, and how to best utilize this distinct phenomena would also be important to study. Finally, further exploring the potential benefits of the addition of a pre-separation technique, such as ion mobility or differential mobility prior to sample entering the mass spectrometer should be completed. Though some work has been done in this field already,[129–133] this type of instrumentation has not been accepted in a criminal justice setting.

Section 8.3 Next Generation Chemical Analysis of Latent Fingerprints - Conclusions

The use of AI-MS and secondary ion mass spectrometry (SIMS) for forensic science applications is feasible and will likely continue to develop over the coming years. In this work, it was shown that the chemical analysis and imaging of spatial distributions of a number of exogenous and endogenous components is possible within latent fingerprints using both techniques. Understanding the chemical makeup of latent fingerprints provides new possibilities for forensics and trace screening, including the potential ability to age date a fingerprint or to determine characteristics of a person from the chemical makeup of their fingerprint.

The use of standards for fingerprint analysis can take several forms including an artificial material used to test the ability of visual fingerprint development techniques, a standard fingerprint to aid in competency testing, or development of a background matrix to mimic the handling of trace contraband. The artificial fingerprint material that was discussed in Chapter 4 is currently being evaluated for use in all of these settings.

Though being able to probe the chemical constituents in latent fingerprints is important, this can, and has, been demonstrated using a number of techniques such as GC-MS, high performance liquid chromatography mass spectrometry (HPLC-MS), and other AI-MS techniques.[120,121,134,135] The work detailed in Chapters 5 through 7 described the ability of both AI-MS techniques (DEFFI in particular) and SIMS to produce spatially resolved chemical images of fingerprints. There are a number of potential cases in which this type of analysis could prove invaluable. Foremost is the potential to monitor the lateral movement of fingerprint constituents in order to potentially determine the age of the fingerprint. High resolution chemical imaging with time-of-flight secondary ion mass

spectrometry (TOF-SIMS) has shown that a number of chemicals within the fingerprint ridges will diffuse into the valleys over a time frame of days to weeks. It has also been shown that this process appears to be dependent on the environmental exposure of the sample, and is likely also dependent upon the surface of deposition, the force of deposition, and the degree to which the fingerprint was smudged upon deposition. Another benefit of the chemical imaging of fingerprints is to better understand how to appropriately construct standards and test materials. Using chemical images to determine the area coverage, as well as the location and concentration of exogenous materials in a fingerprint could lead to the development of more realistic test materials for trace contraband detection. The final application that may show promise as a next generation forensic science technique is that of depth profiling. Being able to determine the location of particles relative to the fingerprint, whether the particle was present below or deposited on top of the fingerprint, could help to establish a potential order of events.

Section 8.4 Next Generation Chemical Analysis of Latent Fingerprints – Future Areas of Study

Mass spectral imaging (MSI) is still in the early stages of development in this arena and thus there is a large amount of work to be completed in order to fully realize the impact of this technique on forensic science. With regards directly to latent fingerprint analysis, future work could focus on the improvement of imaging resolution of AI-MS techniques by reducing the primary beam size or decreasing the required scan times by increasing the scan rate per pixel. The potential application of MSI to age dating needs to certainly be researched further, as only preliminary data has been

discussed. Additional work should focus on understanding the effects of time, environmental exposure, deposition surface, and the combination that the three have on the lateral movement of chemicals. These studies could be completed in a highly reproducible fashion through the utilization of an artificial fingerprint prior to or concurrent with a study using actual fingerprints.

One future direction of MSI likely lies in spatially resolved sample quantification. Initial work using AP-MALDI has shown that a drop case residue could be used to generate calibration curves for site specific quanification of a chemical image.[136,137] This methodology could be easily combined with current inkjet printing technologies to allow for the printing of well-defined calibration curves directly onto or next to a sample. This would allow for the ability to simultaneously complete multiple analysis types, and negate the need to completely dissolve the sample for quantification using techniques such GC-MS or HPLC-MS. If quantification is to be pursued, another area which must be studied is the removal efficiency of the imaging techniques, or what percentage of the sample is consumed during analysis. Understanding the total amount of material consumed in an imaging scan could be completed by dissolving and quantifying a marker within the sample using a technique such as GC-MS or HPLC-MS, and to determine the amount of sample removed, which can thus be related back to quantification using the chemical image. The benefits of quantification using chemical imaging could be numerous, and include the potential to determine if a person of interest directly or secondarily handled explosives, whether the amount and location of trace contraband is maintained after hand washing or after a certain handling time, and the quantification of trace narcotics and/or metabolites to determine a handler from a user. Though this work

has shown the capability of chemical imaging of latent fingerprints, the potential implications of this application have just only begun to be explored.

Appendix 1: Search List and Representative Mass Spectra for the Analysis of Explosives by DART-MS

Appendix 1 provides information to support Chapter 2, the validation of a direct analysis in real time mass spectrometry (DART-MS) for trace explosives analysis. Included in this appendix is a copy of the search lists (one for negative ionization mode and one for positive ionization mode) which were used in determining the explosives which were detectable in mixtures, blind sampling, and post-blast materials. These search lists were constructed from representative mass spectra of each explosive, which are also presented in the appendix.

Table A1.1 A copy of the negative ionization mode DART-MS search list developed for the explosives validation study.

Chemical Formula	Exact Mass	Assignment(s)
C6H5N1O2	123.032029	Nitrobenzene (NB) [M]
C3H3N3O3	129.017442	Cyclotetramethylene Tetranitramine (HMX) Fragment
C3H5N4O2	129.041251	Cyclotrimethylene Trinitramine (RDX) [M-H-2NO2] / Ethylene Glycol Dinitrate (EGDN) Fragment
C7H6N1O2	136.039854	2(3)(4)-Nitrotoluene (2-NT, 3-NT, 4-NT) [M-H]
C7H7N1O2	137.047679	2(3)(4)-Nitrotoluene (2-NT, 3-NT, 4-NT) [M]
C6H4N1O3	138.019119	1,3-Dinitrobenzene (1,3-DNB) [M-NO]
C7H8N1O2	138.055504	3(4)-Nitrotoluene (3-NT, 4-NT) [M+H]
C7H8N1O2	138.055504	Nitrobenzene (NB) [M+CH3]
C8H9N1O2	151.063329	2(4)-Nitrotoluene (2-NT, 4-NT) [M-H+CH3]
C7H6N1O3	152.034769	2,6(2,4)-Dinitrotoluene (2,6-DNT / 2,4-DNT) [M-NO]
C8H10N1O2	152.071154	2-Nitrotoluene (2-NT) [M+CH3]
C7H4N1O4	166.014034	2,6(2,4)-Dinitrotoluene (2,6-DNT / 2,4-DNT) [M-NH2]
C6H4N2O4	168.017108	1,3-Dinitrobenzene [M] / 2,6(2,4)-Dinitrotoluene (2,6-DNT / 2,4-DNT) [M-CH3]
C3H6N5O4	176.041980	Cyclotrimethylene Trinitramine (RDX) [M-NO2]
C7H5N2O4	181.024933	2,6(2,4)-Dinitrotoluene (2,6-DNT / 2,4-DNT) [M-H]
C7H6N2O4	182.032758	2,6(2,4)-Dinitrotoluene (2,6-DNT / 2,4-DNT) [M]
C6H3N2O5	183.004198	1,3-Dinitrobenzene (1,3-DNB) [M-H+O] / 1,3,5-Trinitobenzene (1,3,5-TNB) [M-NO]
C7H7N2O4	183.040583	2,6(2,4)-Dinitrotoluene (2,6-DNT / 2,4-DNT) [M+H]
C7H5N3O4	195.028007	2-Amino-4,6-Dinitrotoluene [M-2H] / 4-Amino-2,6-Dinitrotoluene [M-2H]

C7H6N3O4	196.035832	4-Amino-2,6-Dinitrotoluene [M-H] / 2-Amino-4,6-Dinitrotoluene [M-H]
C7H5N2O5	197.019848	Trinitrotoluene (TNT) [M-NO] / 2,6(2,4)Dinitrotoluene (2,6-DNT / 2-4-DNT) [M-H+O]
C7H7N3O4	197.043657	4-Amino-2,6-Dinitrotoluene [M] / 2-Amino-4,6-Dinitrotoluene [M]
C2H4N3O8	197.999842	Ethylene Glycol Dinitrate (EGDN) [M+NO2]
C6H3N2O6	198.999113	Ammonium Picrate (AP) [M-NO2-NH4+OH] / Picric Acid (PA) [M-NOH2]
C3H7N2O8	199.020243	Nitroglycerin (NG) [M-NO2+H2O]
C4H7N6O4	203.052879	Cyclotetramethylene Tetranitramine (HMX) [M-H-2NO2]
C7H4N3O5	210.015097	Tetryl [M*-NO2-CH3+COH] / Trinitrotoluene (TNT) [M-OH]
C6H2N3O6	211.994362	Ammonium Picrate (AP) [M-ONH4] / Picric Acid (PA) [M-OH]
C2H3N3O9	212.986932	Ethylene Glycol Dinitrate (EGDN) [M+NO3-H]
C6H3N3O6	213.002187	Ammonium Picrate (AP) [M-ONH3] / 1,3,5-Trinitrobenzene (1,3,5-TNB) [M] / Trinitrotoluene (TNT) [M-CH3]
C2H4N3O9	213.994757	Ethylene Glycol Dinitrate (EGDN) [M+NO3]
C3H5N6O6	221.027059	Cyclotrimethylene Trinitramine (RDX) [M-H]
C7H4N3O6	226.010012	Trinitrotoluene (TNT) [M-H]
C8H8N3O5	226.046397	Tetryl [M*-NO2+COH2]
C7H5N3O6	227.017837	Trinitrotoluene (TNT) [M]
C6H2N3O7	227.989277	Ammonium Picrate (AP) [M-NH4] / Picric Acid (PA) [M-H] / Tetryl [M*-NCH3+O]
C3H6N3O9	228.010407	Nitroglycerin (NG) [M+H]
C7H5N3O6(i)	228.020452	Trinitrotoluene (TNT) [M] isotope
C4H8N2O9	228.022983	Diethylene Glycol Dinitrate (DEGDN) [M+O2]
C7H6N3O6	228.025662	Trinitrotoluene (TNT) [M+H] / 2-Amino-4,6-Dinitrotoluene [M-H+O2]
C6H3N3O7	228.997102	Ammonium Picrate (AP) [M-NH4+H] / Picric Acid (PA) [M] / Tetryl [M*-NCH3+O+H]
C7H5N4O6	241.020911	Tetryl [M*-H]
C4H8N3O9	242.026057	Ethylene Glycol Dinitrate (EGDN) [M+M-NO3] / Diethylene Glycol Dinitrate (DEGDN) [M+NO2]
C7H6N4O6	242.028736	Tetryl [M*]
C7H5N3O7	243.012752	Tetryl [M*-NCH3+OCH3] / Trinitrotoluene (TNT) [M+OH]
C7H7N4O6	243.036561	4-Amino-2,6-Dinitrotoluene [M+NO2] / 2-Amino-4,6-Dinitrotoluene [M+NO2]
C7H5N4O7	257.015826	Tetryl [M*-H+O]
C4H8N3O10	258.020972	Ethylene Glycol Dinitrate (EGDN) [M+M-NO2] / Diethylene Glycol Dinitrate (DEGDN) [M+NO3]
C7H6N4O7	258.023651	Tetryl [M*+O]
C4H9N3O10	259.028797	Diethylene Glycol Dinitrate (DEGDN) [M+NO3+H]
C7H7N4O7	259.031476	4-Amino-2,6-Dinitrotoluene [M+NO3]
C3H6N7O8	268.027788	Cyclotrimethylene Trinitramine (RDX) [M+NO2] / Cyclotetramethylene Tetranitramine (HMX)
C3H6N7O9	284.022703	Cyclotrimethylene Trinitramine (RDX) [M+NO3] / Cyclotetramethylene Tetranitramine (HMX) [M-CH2N+O]
C3H5N4O12	288.990401	Nitroglycerin (NG) [M+NO3]
C3H6N4O12	289.998226	Nitroglycerin (NG) [M+NO3+H]
C4H7N4O12	303.006051	Erythritol Tetranitrate (ETN) [M+H]
C5H7N4O12	315.006051	Pentaerythritol Tetranitrate (PETN) [M-H]
C4H7N4O13	319.000966	Erythritol Tetranitrate (ETN) [M+NO3]
C5H10N9O8	324.065236	Cyclotrimethylene Trinitramine (RDX) [M+NO2NCH2NCH2]
C4H8N9O10	342.039416	Cyclotetramethylene Tetranitramine (HMX) [M+NO2]
C7H5N6O11	349.001634	Tetryl [M+NO3]
C4H8N9O11	358.034331	Cyclotetramethylene Tetranitramine (HMX) [M+NO3]
C5H8N5O14	362.006780	Pentaerythritol Tetranitrate (PETN) [M+NO2]
C4H6N5O15	363.986045	Erythritol Tetranitrate (ETN) [M+OH]

C4H6N6O15	377.989119	Erythritol Tetranitrate (ETN) [M+NOH]
C5H8N5O15	378.001695	Pentaerythritol Tetranitrate (PETN) [M+NO3] / Erythritol Tetranitrate (ETN) [M+CH2OH]
C14H14N6O8	394.087314	4-Amino-2,6-Dinitrotoluene [M+M]
C6H12N11O10	398.076864	Cyclotetramethylene Tetranitramine (HMX) [M+NO2NCH2NCH2]
C6H12N13O14	490.062672	Cyclotrimethylene Trinitramine (RDX) [M+M+NO2]
C17H6N11O6	619.999403	2,6-Bis(picrylamino)-3,5-dinitropyridine [M-H]-
C17H7N111O16	621.301589	2,6-Bis(picrylamino)-3,5-dinitropyridine [M]-

Table A1.2 A copy of the positive ionization mode DART-MS search list developed for the explosives validation study.

Formula	**Exact Mass**	**Assignment(s)**
C3H8O1N1	74.060589	Triacetone Triperoxide (TATP) / Hexamethylene Triperoxide Diamine (HMTD) Fragment
C4H7N2	83.060923	Triacetone Triperoxide (TATP) / Hexamethylene Triperoxide Diamine (HMTD) Fragment
C4H9O1N2	101.071488	Triacetone Triperoxide (TATP) / Hexamethylene Triperoxide Diamine (HMTD) Fragment
C5H11O1N2	115.087138	Triacetone Triperoxide (TATP) / Hexamethylene Triperoxide Diamine (HMTD) Fragment
C8H14O2	142.099380	Triacetone Triperoxide (TATP) fragment
C5H9O3N2	145.061318	Hexamethylene Triperoxide Diamine (HMTD) [M-CH3O3]
C5H11O5N2	179.066798	Hexamethylene Triperoxide Diamine (HMTD) [M-OCH2+H]
C6H12O5N2	192.074623	Hexamethylene Triperoxide Diamine (HMTD) [M-O]
C6H13O6N2	209.077363	Hexamethylene Triperoxide Diamine (HMTD) [M+H]

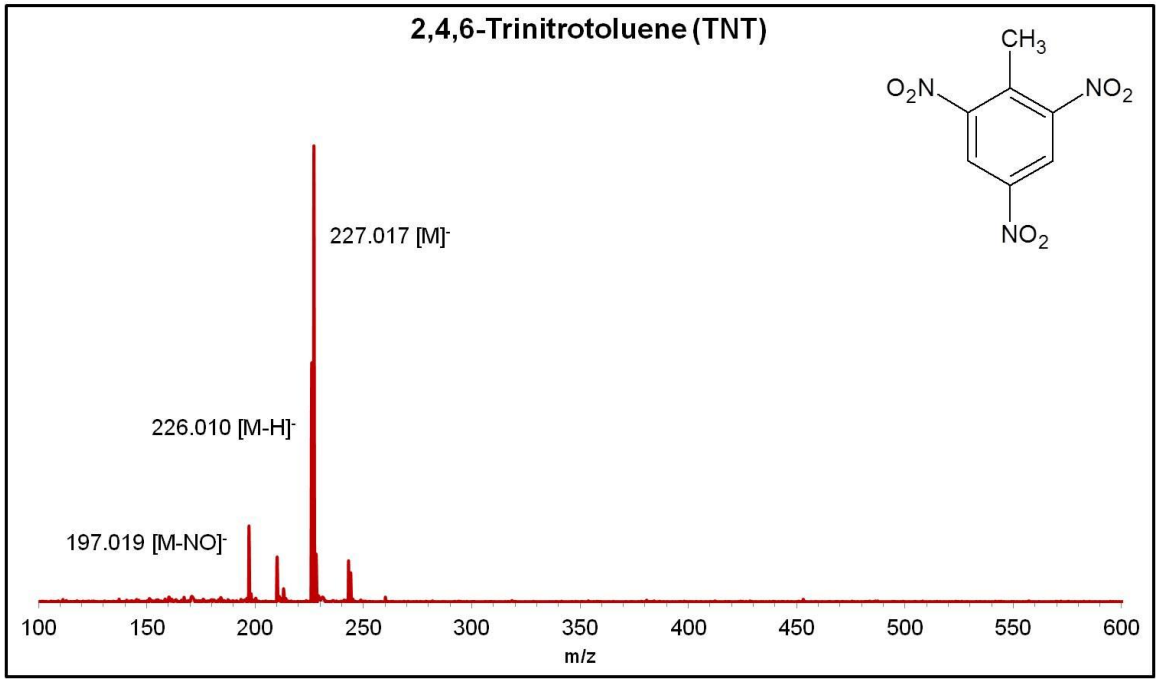

Figure A1.1 A representative mass spectrum of TNT analyzed under the optimized parameters for negative mode.

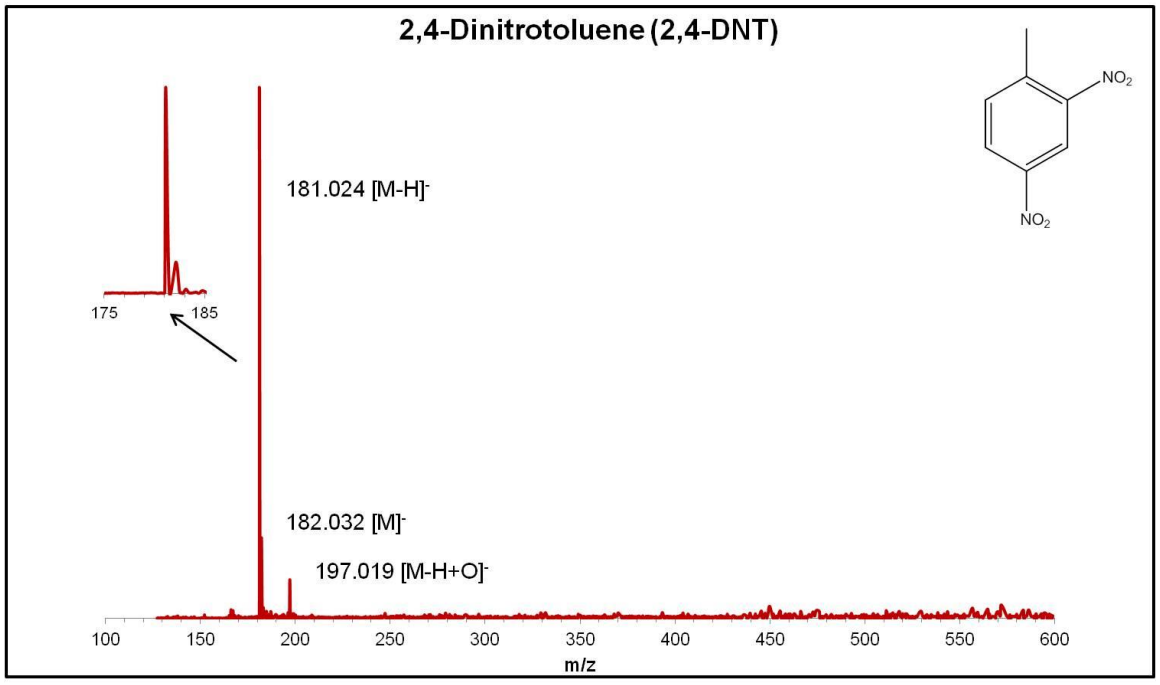

Figure A1.2 A representative mass spectrum of 2,4-DNT analyzed under the optimized parameters for negative mode.

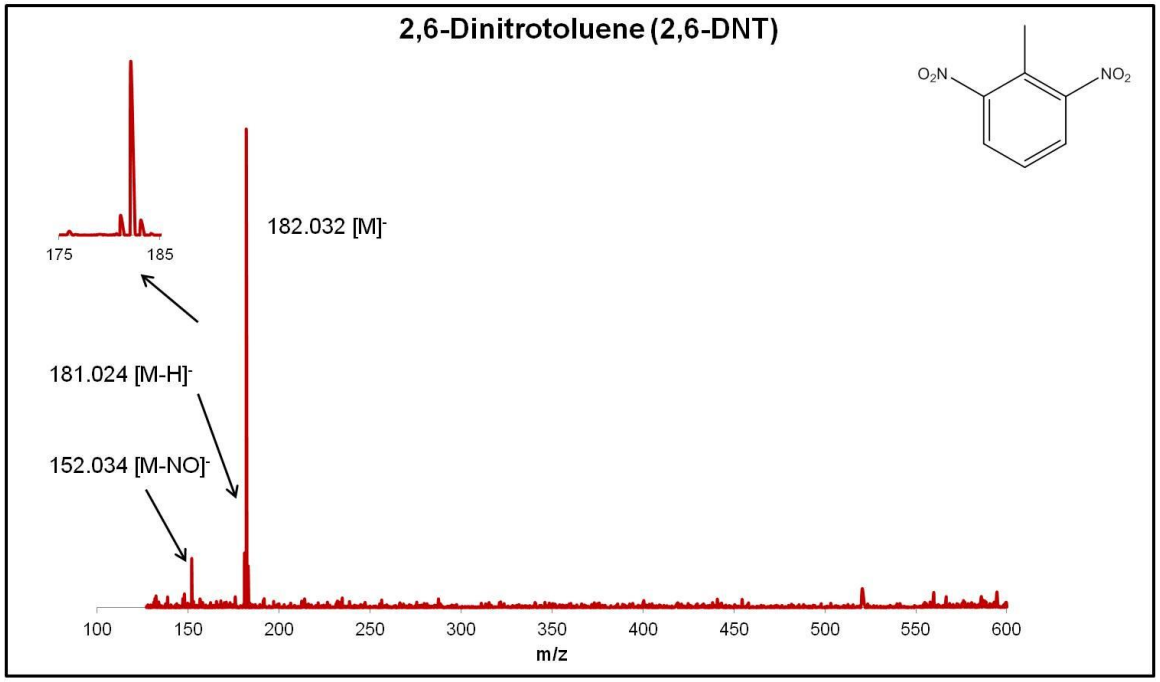

Figure A1.3 A representative mass spectrum of 2,6-DNT analyzed under the optimized parameters for negative mode.

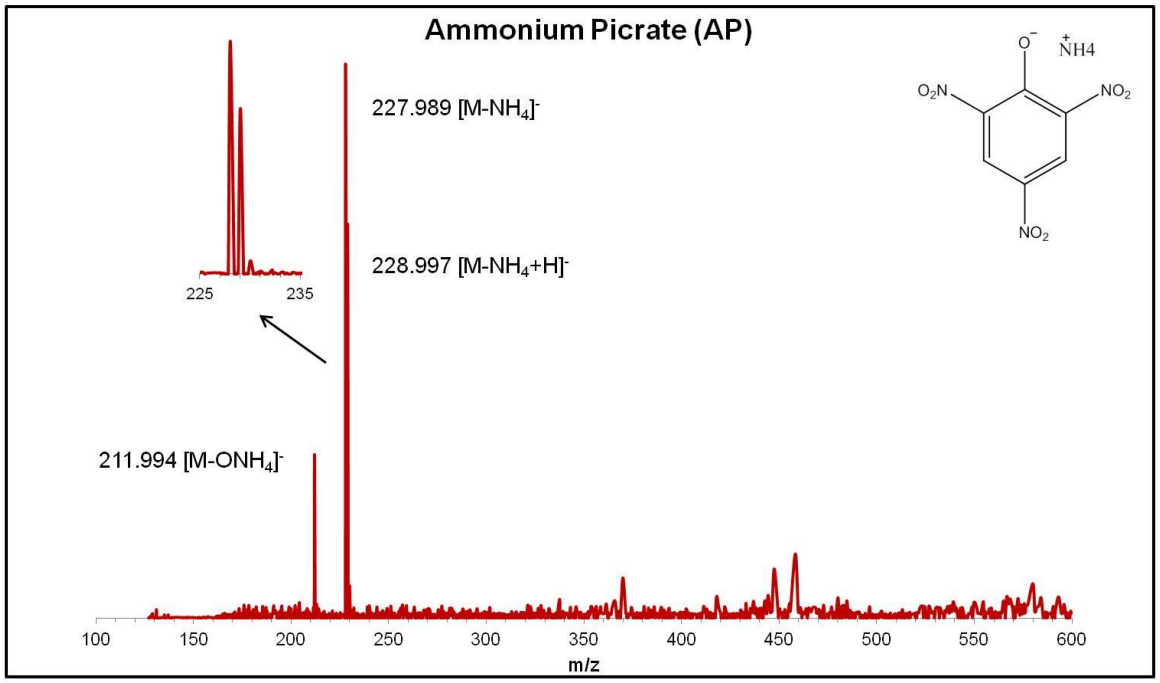

Figure A1.4 A representative mass spectrum of AP analyzed under the optimized parameters for negative mode.

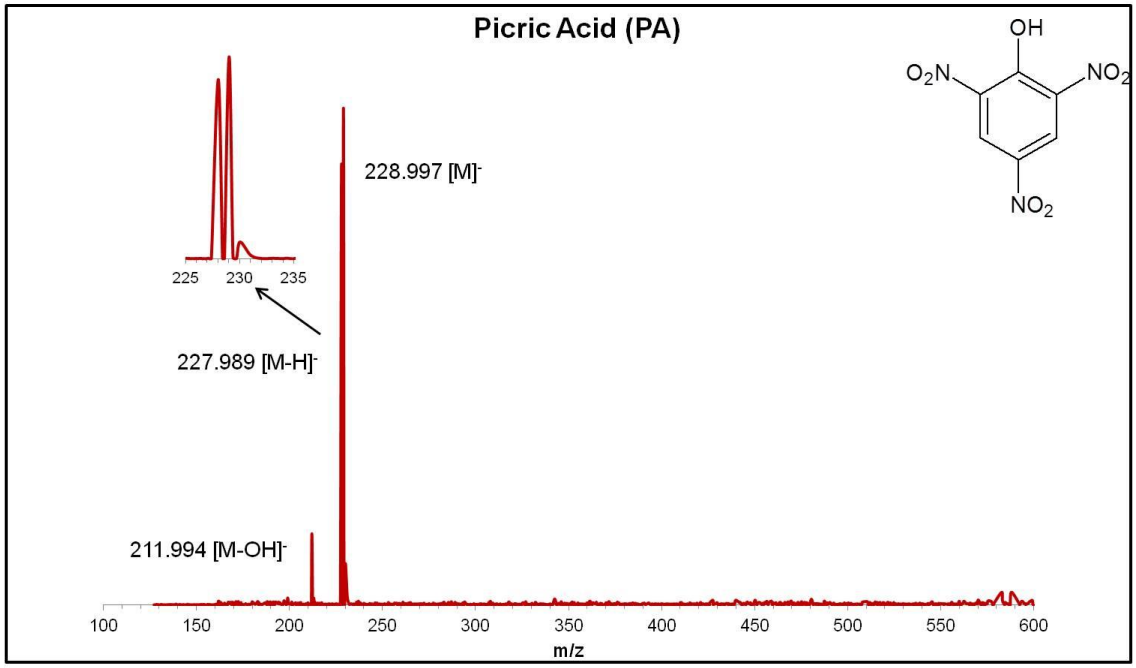

Figure A1.5 A representative mass spectrum of PA analyzed under the optimized parameters for negative mode.

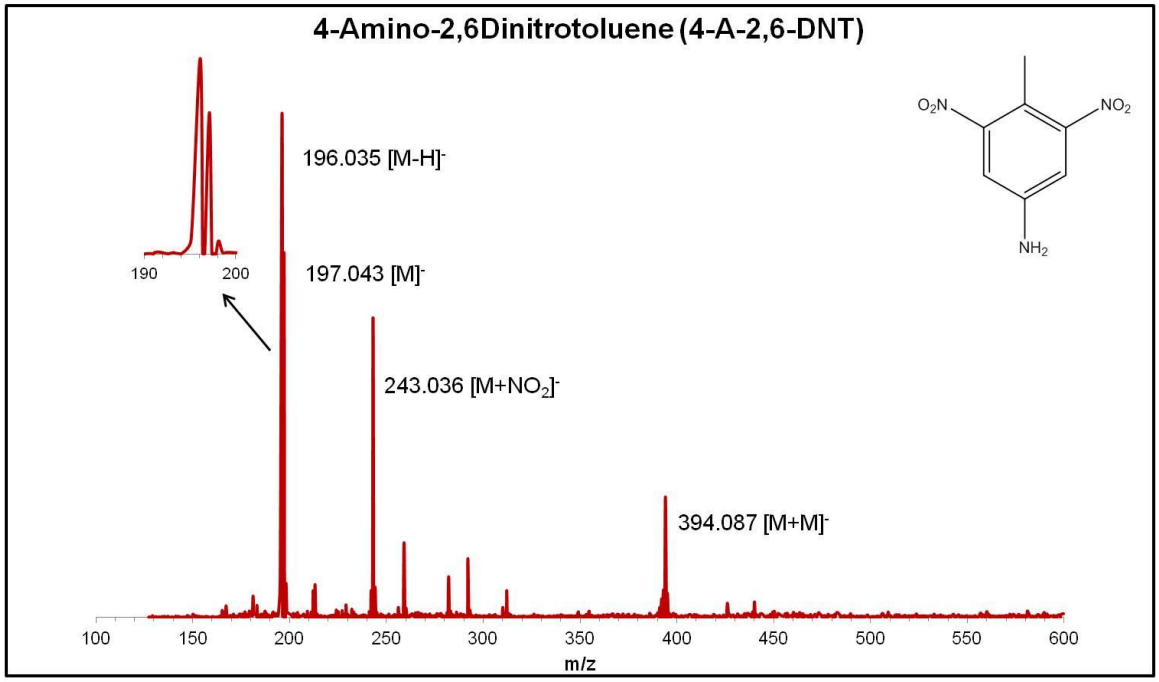

Figure A1.6 A representative mass spectrum of 4-A-2,6-DNT analyzed under the optimized parameters for negative mode.

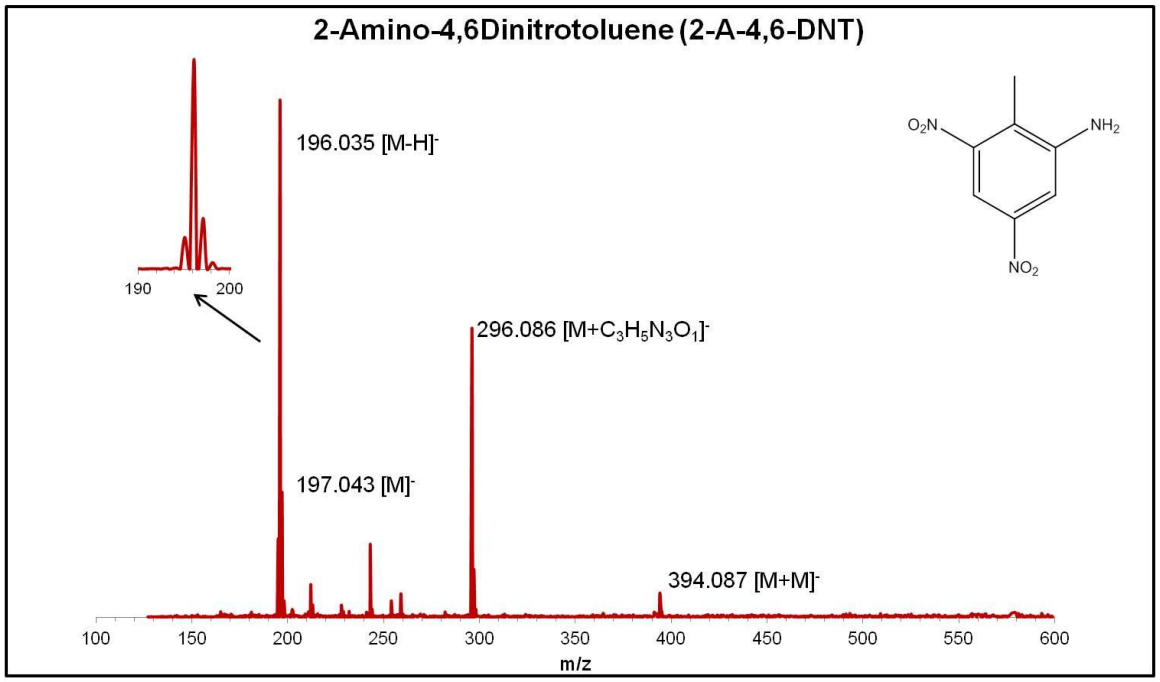

Figure A1.7 A representative mass spectrum of 2-A-4,6-DNT analyzed under the optimized parameters for negative mode.

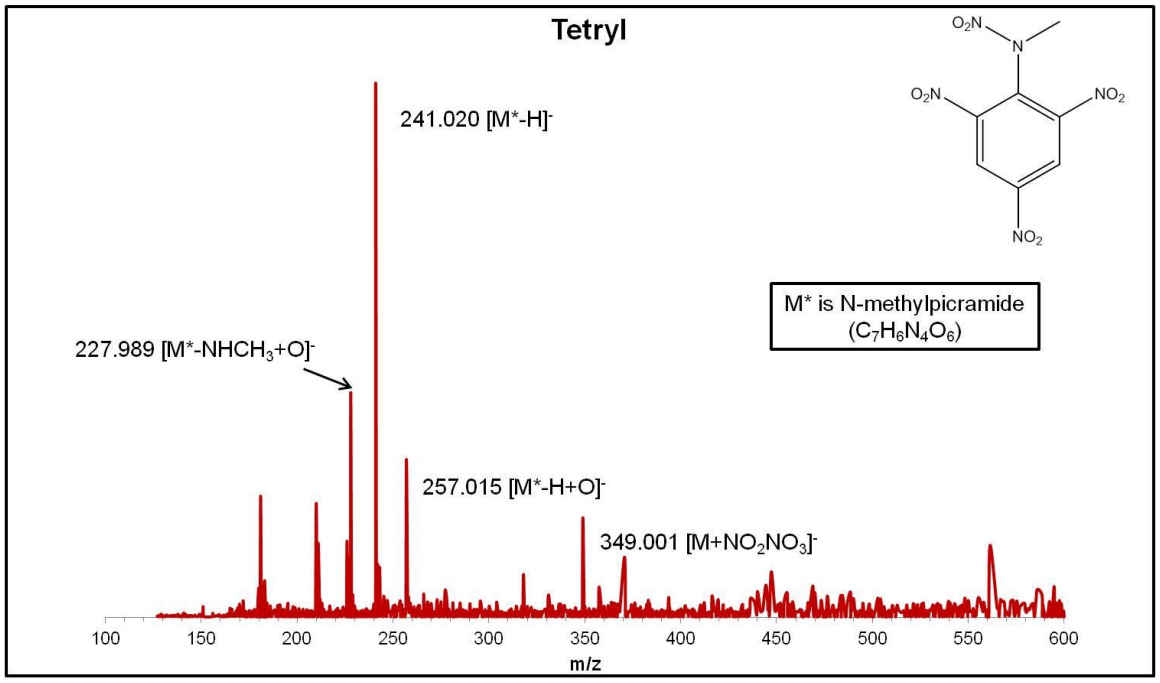

Figure A1.8 A representative mass spectrum of Tetryl analyzed under the optimized parameters for negative mode.

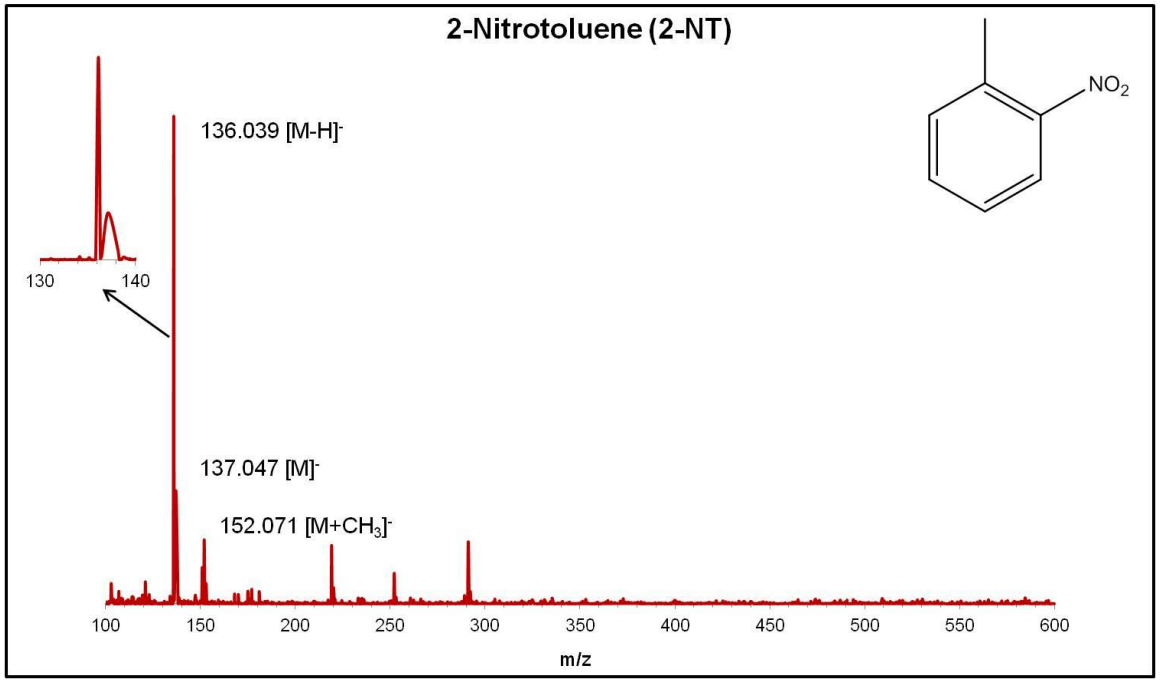

Figure A1.9 A representative mass spectrum of 2-NT analyzed under the optimized parameters for negative mode.

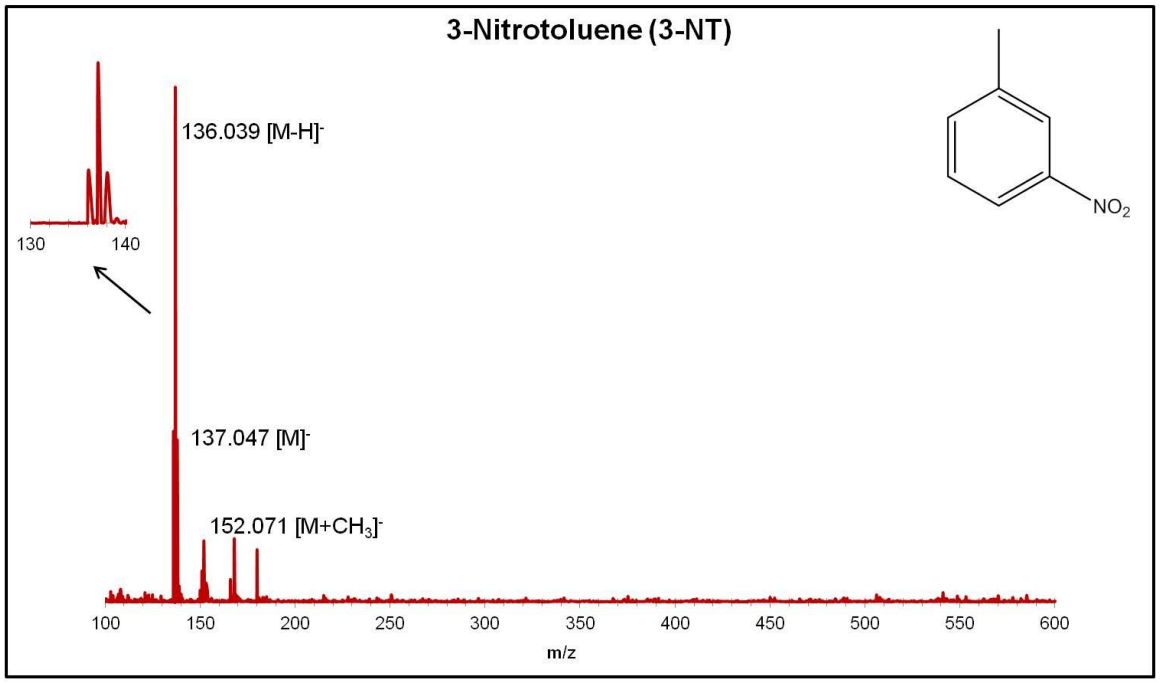

Figure A1.10 A representative mass spectrum of 3-NT analyzed under the optimized parameters for negative mode.

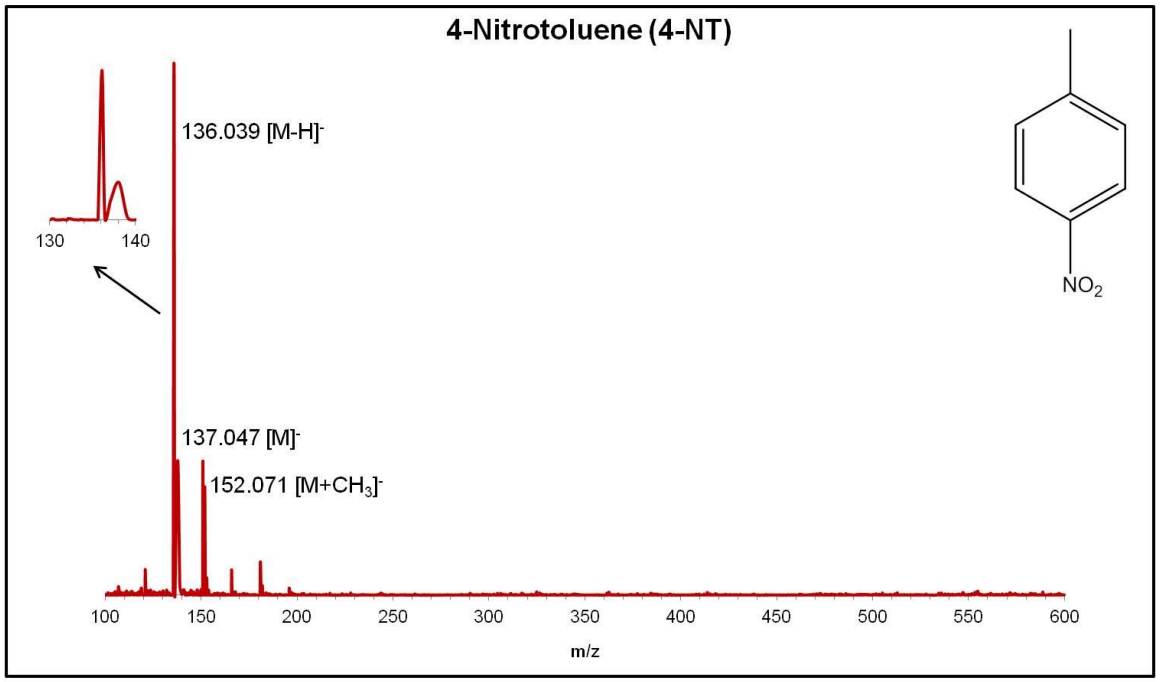

Figure A1.11 A representative mass spectrum of 4-NT analyzed under the optimized parameters for negative mode.

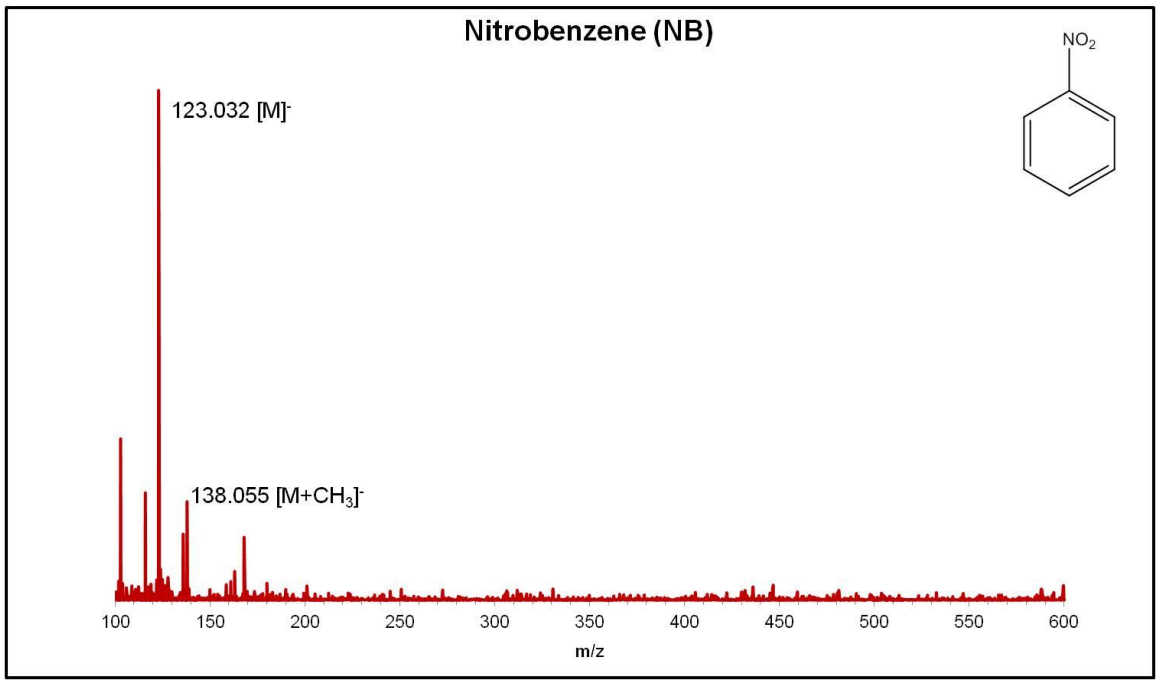

Figure A1.12 A representative mass spectrum of NB analyzed under the optimized parameters for negative mode.

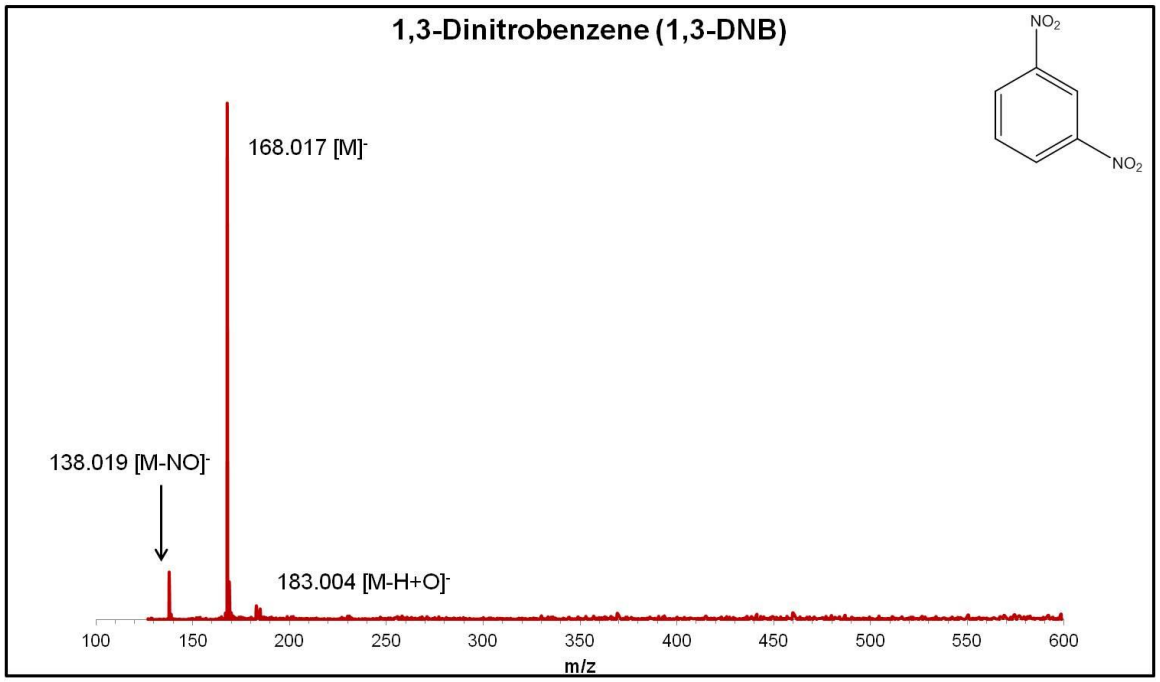

Figure A1.13 A representative mass spectrum of 1,3-DNB analyzed under the optimized parameters for negative mode.

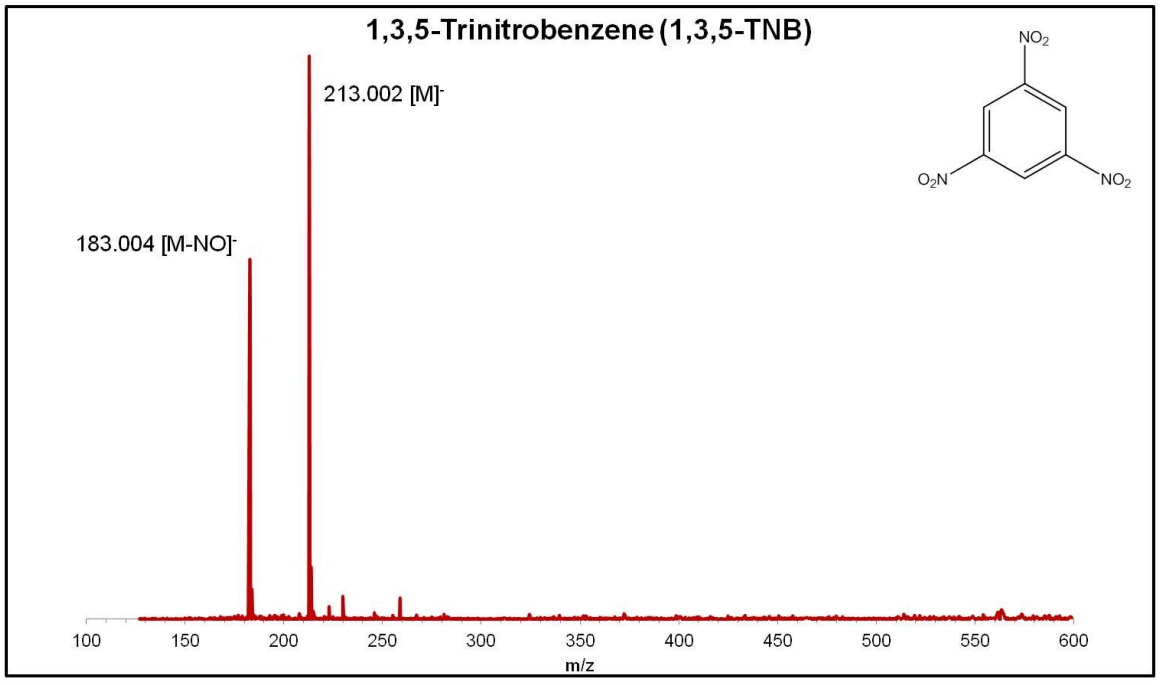

Figure A1.14 A representative mass spectrum of 1,3,5-TNB analyzed under the optimized parameters for negative mode.

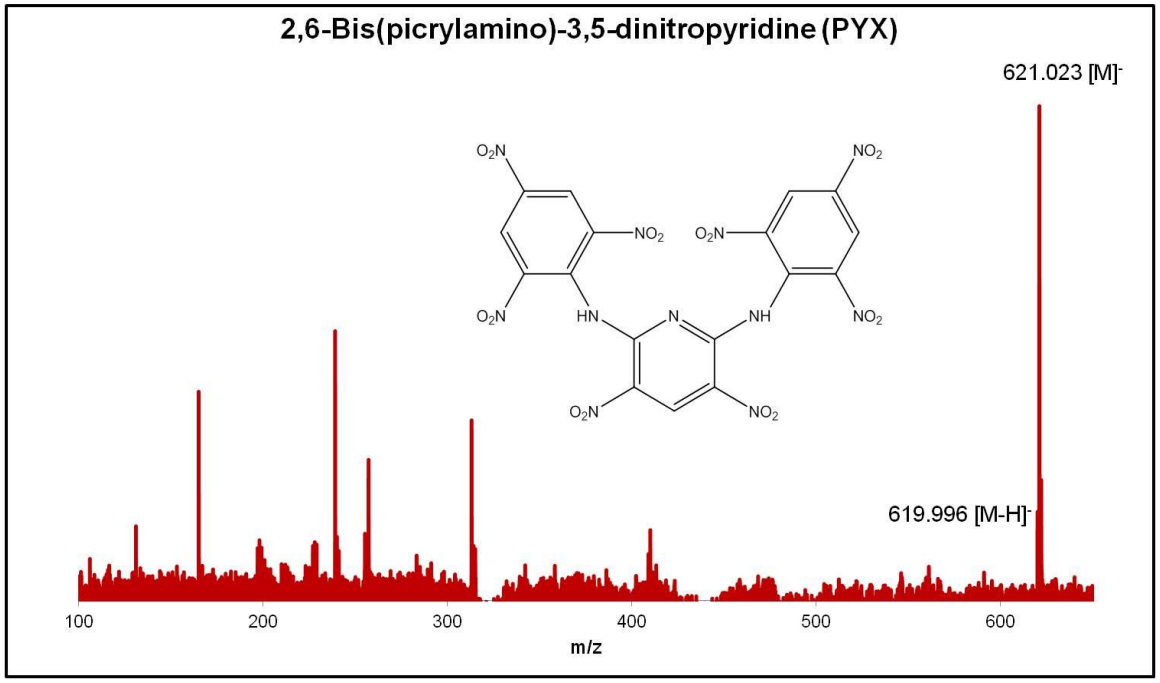

Figure A1.15 A representative mass spectrum of PYX analyzed under the optimized parameters for negative mode.

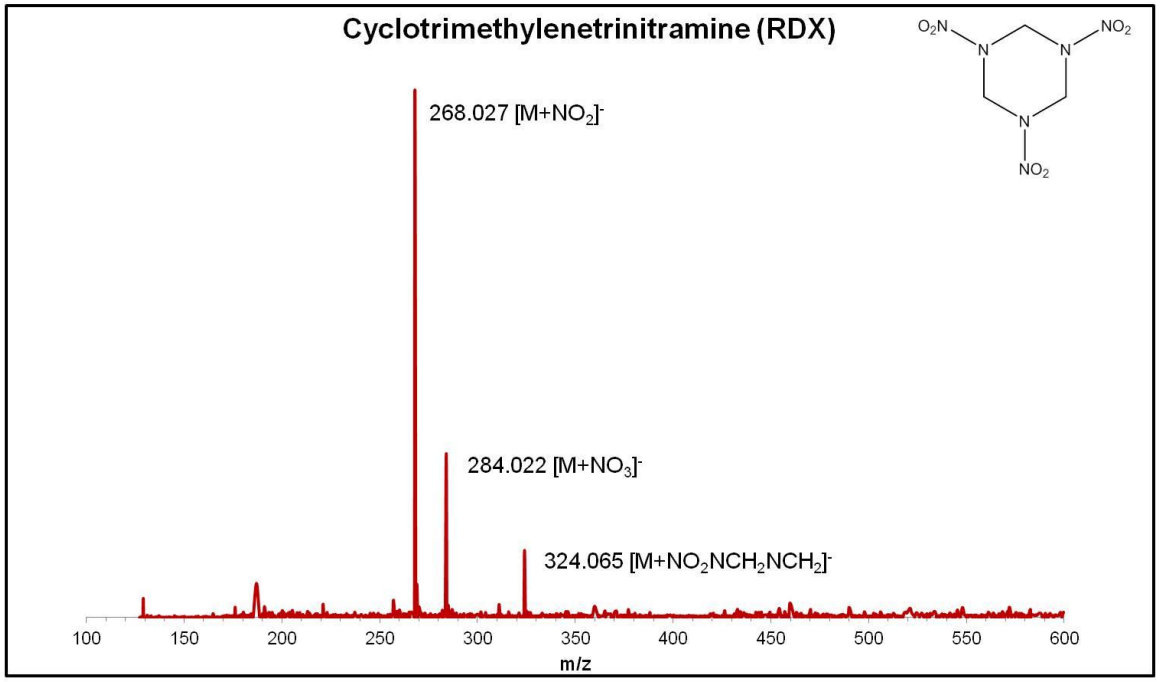

Figure A1.16 A representative mass spectrum of RDX analyzed under the optimized parameters for negative mode.

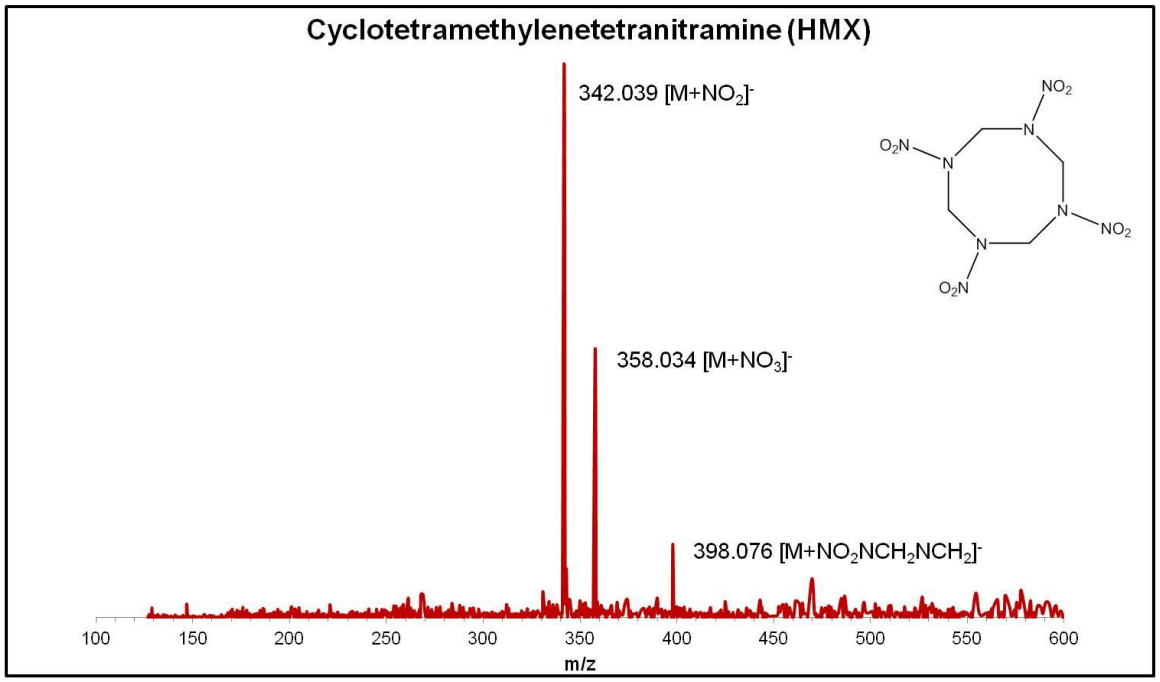

Figure A1.17 A representative mass spectrum of HMX analyzed under the optimized parameters for negative mode.

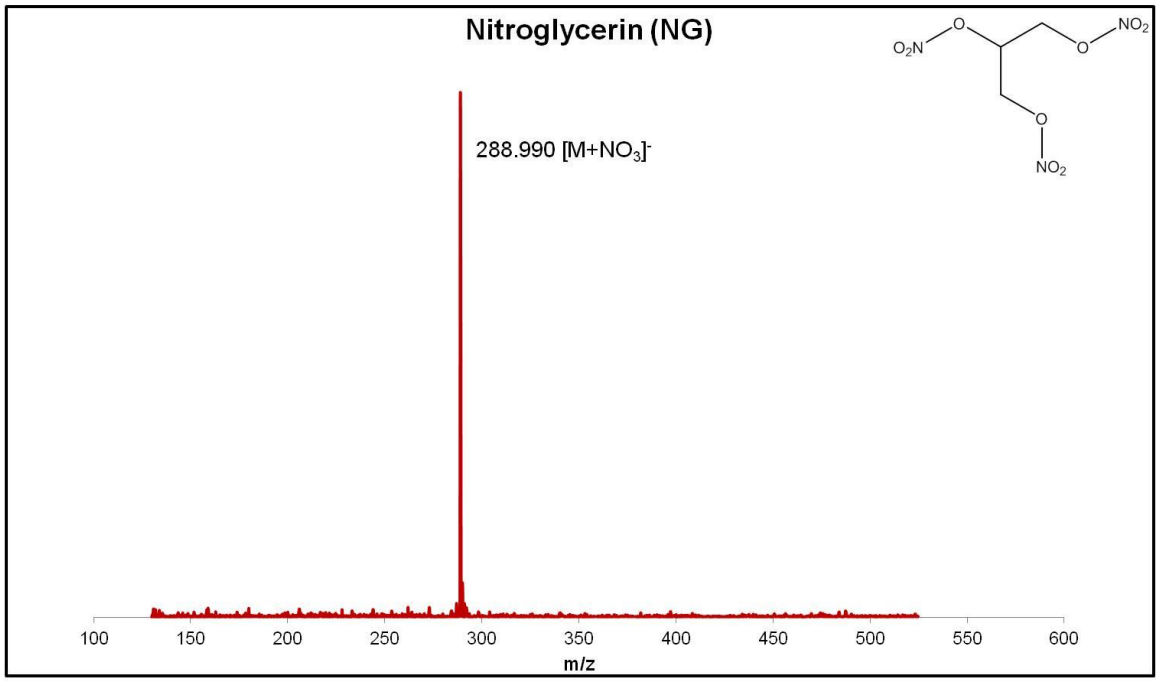

Figure A1.18 A representative mass spectrum of NG analyzed under the optimized parameters for negative mode.

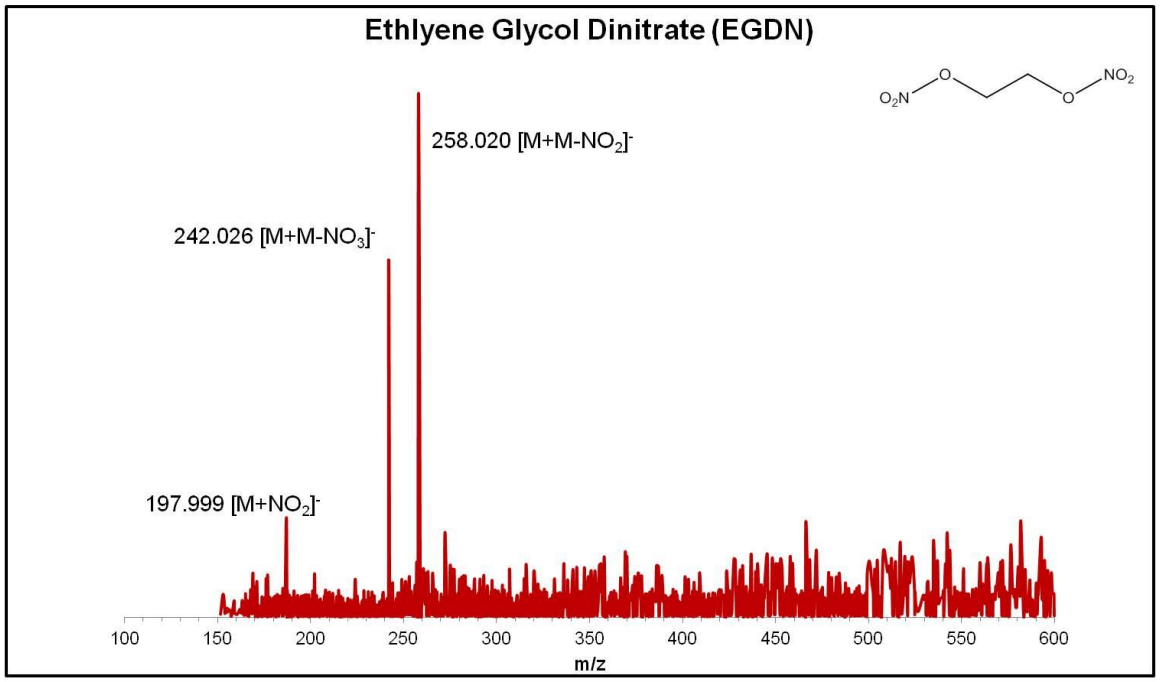

Figure A1.19 A representative mass spectrum of EGDN analyzed under the optimized parameters for negative mode.

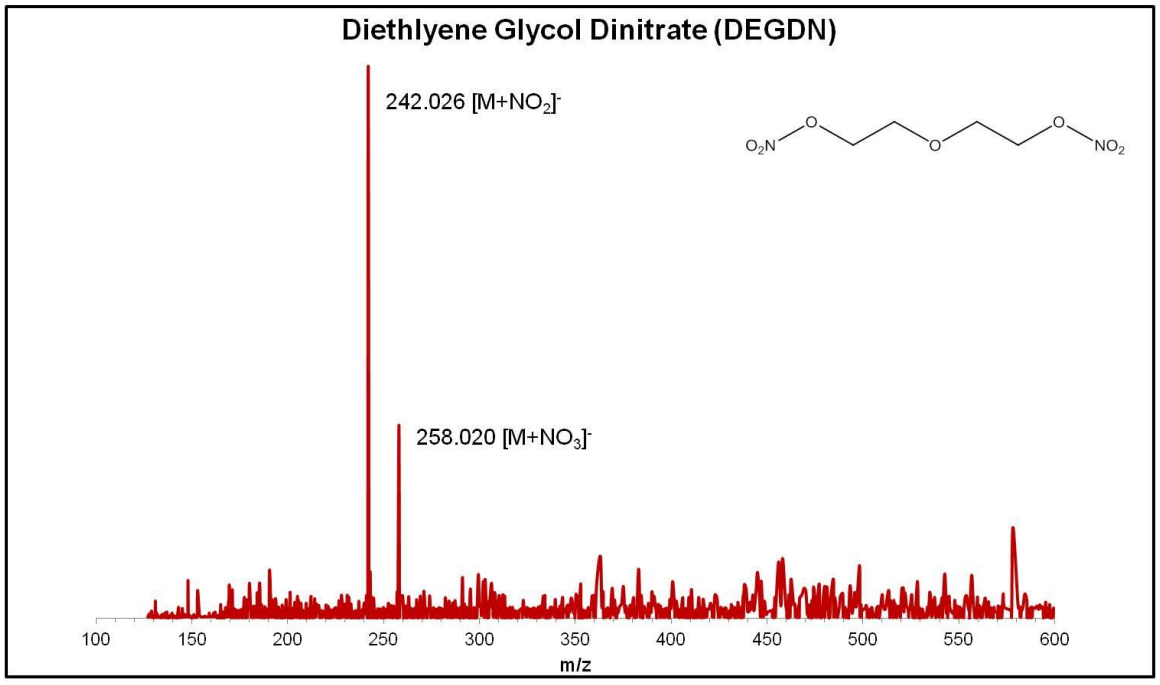

Figure A1.20 A representative mass spectrum of DEGDN analyzed under the optimized parameters for negative mode.

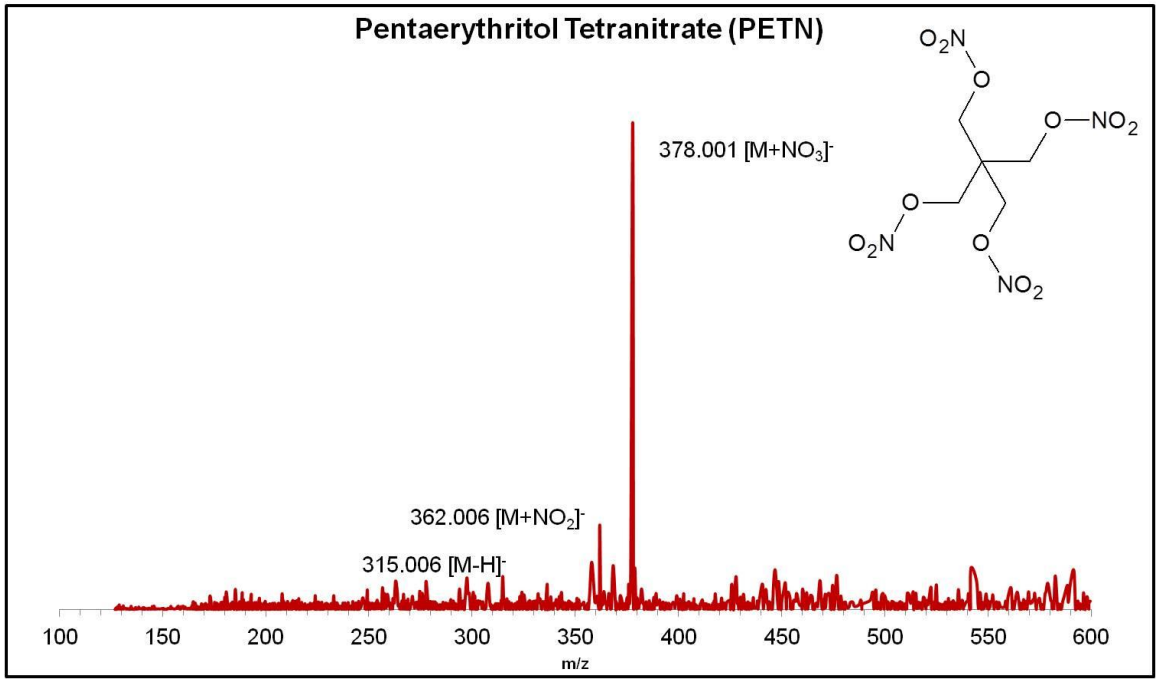

Figure A1.21 A representative mass spectrum of PETN analyzed under the optimized parameters for negative mode.

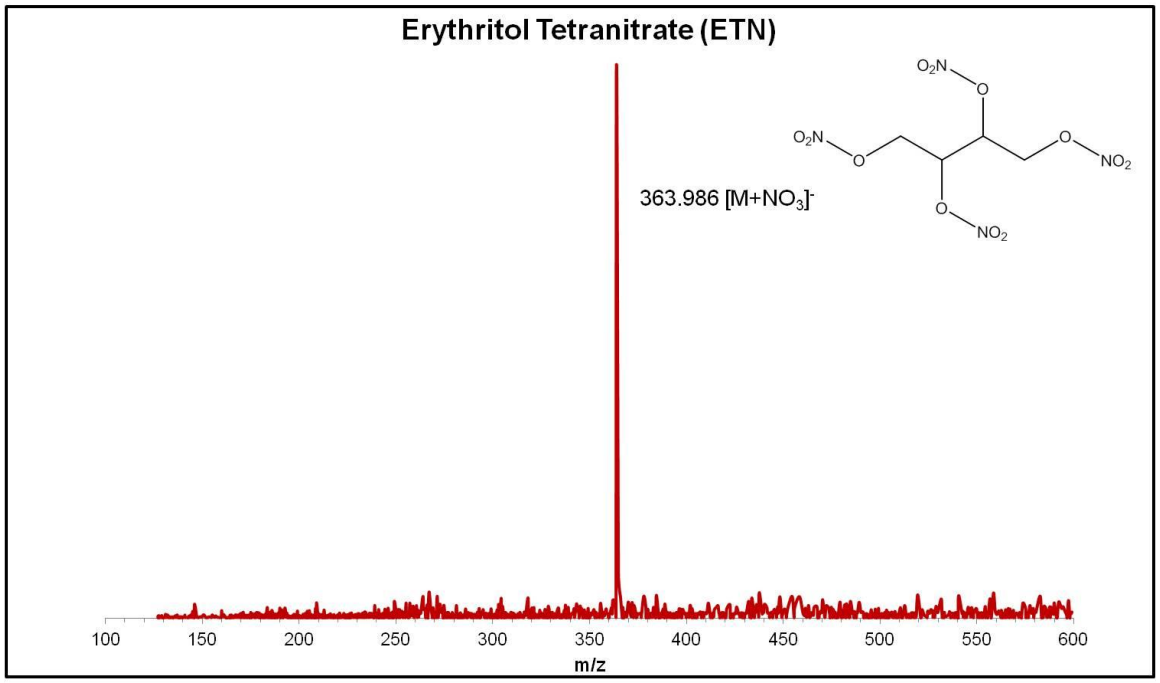

Figure A1.22 A representative mass spectrum of ETN analyzed under the optimized parameters for negative mode.

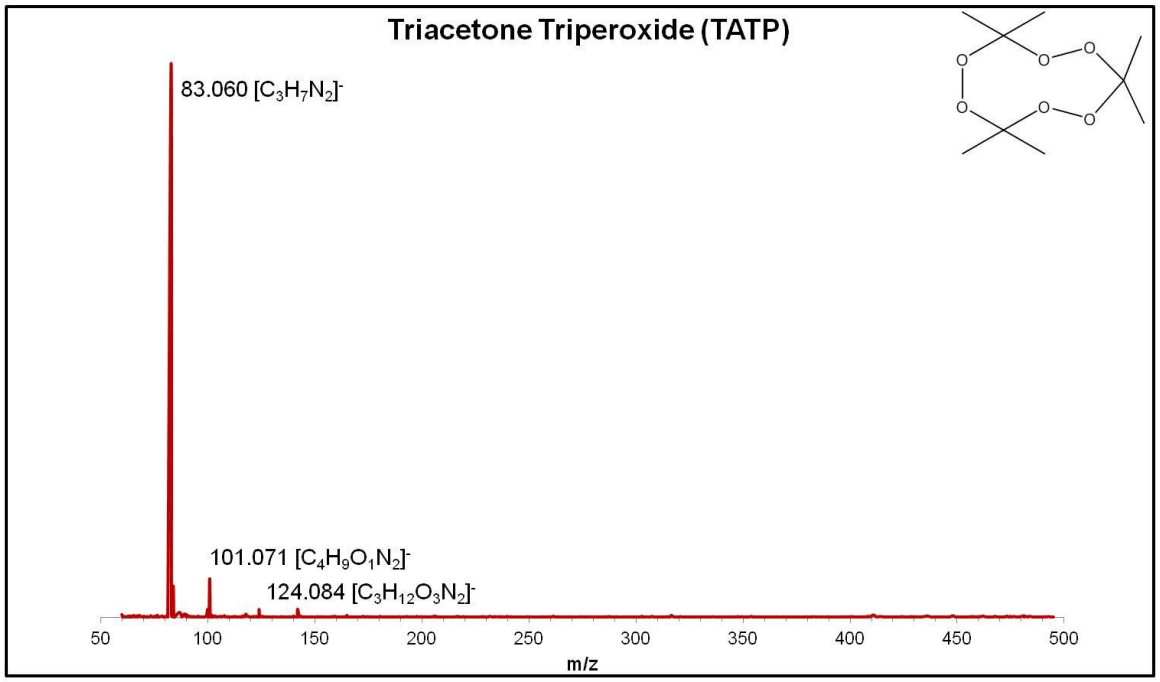

Figure A1.23 A representative mass spectrum of TATP analyzed under the optimized parameters for negative mode.

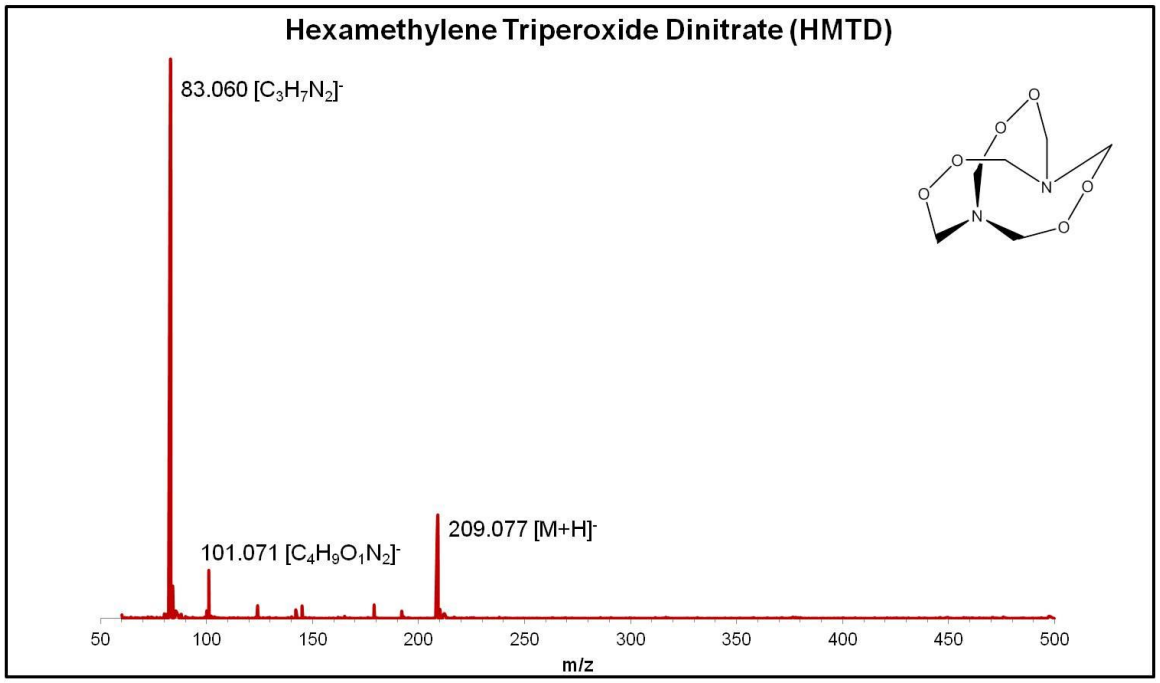

Figure A1.24 A representative mass spectrum of HMTD analyzed under the optimized parameters for negative mode.

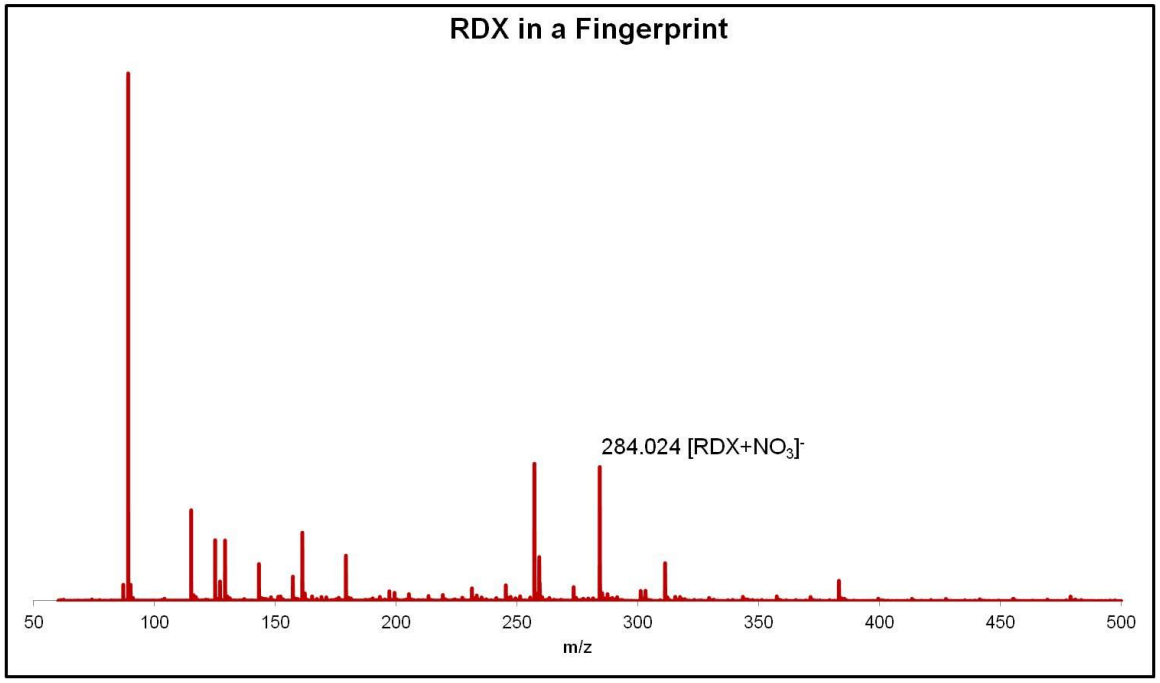

Figure A1.25 A DART-MS mass spectra of RDX in a fingerprint.

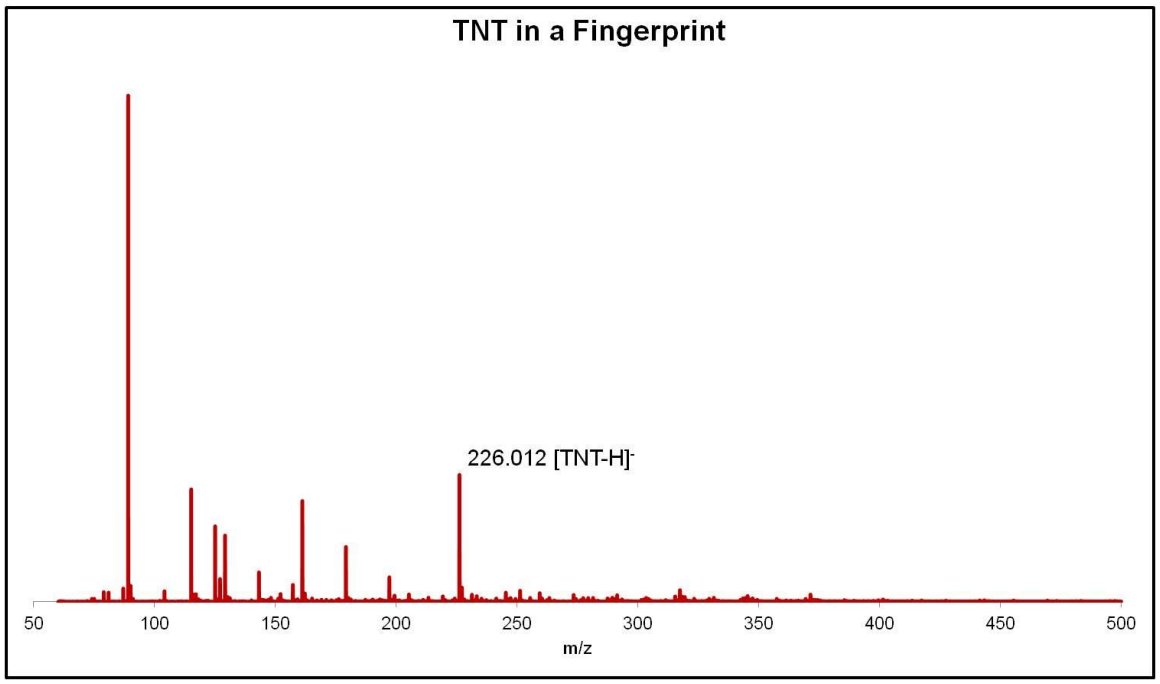

Figure A1.26 DART-MS mass spectra of TNT in a fingerprint.

Appendix 2: Method Optimization and Validation for the Analysis of Adulterants in Solution by DART-MS

The following provides details on another major validation and optimization study completed using direct analysis in real time mass spectrometry (DART-MS). In this study, a method was developed and optimized for the detection of common low molecular weights adulterants in complex solutions.

Section A2.1 Introduction

The adulteration of beverages is a potential issue in a number of different fields, including forensics, food safety, and overall industry quality control. Furthermore, adulteration can be an issue from the time of manufacturing (such as instances where the producer will knowingly or unknowingly contaminate their product) up until just prior to consumption (as may be encountered in typical criminal cases). The introduction of unknown and potentially unsafe compounds into beverages can cause a number of dangerous side effects including poisoning or death.[138] Therefore, it is important to have a method that is able to detect these adulterants in beverages rapidly, efficiently, and effectively. This paper aims to demonstrate the use of a technique that has been widely applied to the fields where adulteration is an issue, in providing a useful screening technique for the detection of these types of compounds.

DART-MS is a technique which has been widely applied to areas of forensic analysis and quality control. It has been shown to be a viable tool in screening for a number of compounds ranging from explosives and narcotics to phthalates and pesticides.[16,70,71,139,140] The DART-MS source utilizes a stream of heated metastable gas

molecules to ionize a sample under atmospheric conditions.[44] By performing sampling under atmospheric conditions, minimal to no sample preparation is required. This is especially beneficial in the analysis of aqueous beverages that cannot be directly analyzed by techniques such as gas chromatography mass spectrometry (GC-MS) without extraction or sample preparation techniques. Furthermore, since there is no chromatographic element to the technique, analysis time is a on the order of seconds, allowing for rapid screening which could significantly lower the time required to complete an analysis.

This paper focuses on nine low molecular weight adulterants which are commonly used to adulterate beverages. The chemicals which were analyzed include: methanol, ethanol, 1-propanol, 2-propanol, 1-butanol, acetone, ethylene glycol, ammonia, and hypochlorite. Methanol is a common laboratory solvent as well as a component in windshield washer fluid, and has been used to adulterate wines to give them a more bitter taste.[138] 1-Propanol is a component of brake fluid, employed as an antiseptic, and also used as the solvent in making vegetable oils and waxes. 2-Propanol, similarly, is a common antiseptic found in most hand sanitizer products. 1-Butanol is a widely used industrial solvent, a component of hydraulic fluid, and a component of paint thinner. Acetone, a constituent of nail polish remover and superglue, can also be used as a food additive. Ethylene glycol is a major component of radiator fluid and ammonia and hypochlorite (the active component of bleach) are common household cleaners.

Detection of these compounds has been completed in the past using a number of different techniques. GC-MS has been used for detection of alcohols, acetone, and ethylene glycol in a number of different applications.[16,44] It has been shown to be

selective and specific, but requires sample runs on the order of minutes, as well as sampling the headspace of aqueous components but not the liquid itself. Liquid chromatography has also been used to detect these types of compounds, with the added benefit of being able to directly analyze aqueous solutions but with analysis times similar to GC-MS.[143] Bleach has been analyzed using gas chromatography coupled to flame ionization detection, but requires derivatization and long sample runs.[144] Previous work has also shown that detection of alcohols by DART-MS is possible with sample derivatization.[145] A number of other techniques have also been explored.[146–148] This work shows that DART-MS can be used to analyze all nine of these potential adulterants without derivatization as both neat samples, and in the complex solutions of several common beverages. This is aided by the addition of a dopant material to the sampling rod to allow for the formation of adducts to help increase the sensitivity and selectivity of the technique.

Section A2.2 Materials and Methods

Subsection A2.2.1 Solvents, Standards, and Sampling Materials

Methanol, 1-propanol, and acetone were purchased from Fisher Scientific (Waltham, MA, USA) in LC-MS grade or better. 2-Propanol, 1-butanol, and ethylene glycol were purchased from Sigma-Aldrich in LC-MS grade or better (St. Louis, MO, USA). Ethanol, 190 proof, and 5 N ammonia were purchased from Sigma-Aldrich. Clorox® (Oakland, CA, USA) bleach was used to obtain the hypochlorite ion, and was present at a concentration of 6.15% v/v. All samples were diluted in either deionized water, or in one of four beverages. The beverages which were used in these experiments were Coca-Cola

Classic®, Red Bull® Red Edition, Gatorade® Fierce, and 13th Colony Southern Corn Whiskey. Several dopants (hexanoic acid, linoleic acid, and methyl pentadecanoate), all purchased from AccuStandard (New Haven, CT, USA), were also used in these experiments either neat or dissolved in hexane purchased from Fisher Scientific. Additionally a mass calibrant and independent quality assurance quality control (QA/QC) compounds were run with each sample set to ensure mass accuracy of ±0.005 Da. The mass calibrant used was polyethylene glycol (PEG) 600 (Acros Organics, Geel, Belgium) which was dissolved in methanol. The independent QA/QC compounds which were used were reserpine, which was purchased from Sigma-Aldrich, and cis-9,12-octadecadienoic acid. Both compounds were diluted in methanol.

Glass microcapillaries were used to introduce the samples into the DART gas stream. The 90 mm closed capillaries were purchased from Corning Incorporated (Corning, NY, USA). Before analysis, the capillaries were introduced into the gas stream to burn off any contaminants which may have been present on the rods.

Subsection A2.2.2 Development of Mass Calibration Mixtures

In these studies a solution of PEG 600 (50 µL dissolved in 10 mL of methanol) was used to calibrate the mass spectrometer for each run. PEG600 provided a series of $[M+H]^+$ and $[M+H_3O]^+$ ions in positive mode, allowing for tuning peaks in the range of 61 *m/z* to 679 *m/z*. In negative mode $[M+OH]^-$ peaks were used, providing a tuning range of 75 *m/z* to 675 *m/z*. Acceptable calibration was determined if a residual value of 9×10^{-12} or lower was obtained. To ensure proper calibration, a solution of reserpine (5 mg dissolved in 10 mL of methanol) or cis-9,12-octadecadienoic acid (20 µL diluted in

10 mL of hexane) was analyzed subsequent to the PEG 600 in every sample run. Reserpine produces a protonated molecule peak at 609.281 *m/z* in positive mode and a deprotonated molecule peak at 607.265 *m/z* in negative mode. Additionally, cis-9,12-octadecadienoic acid, which produces a deprotonated molecule peak at 279.232 *m/z* was also used in negative mode to ensure accurate calibration in the low mass range. Calibration was deemed sufficient if the mass of the above listed peaks fell within ±0.005 Da of the theoretical value.

Subsection A2.2.3 Parameters for AccuTOF-DART

The instrument which was used in the study was a JEOL (Toyko, Japan) AccuTOF™ mass spectrometer (JMS-T100LC) coupled with an IonSense (Saugus, MA, USA) DART® source. Ultra-pure helium was used as the ionizing gas with a flow rate of 1.75 L/min. For all analyses the DART® source was set to a needle voltage of -3,000 V. Electrode 2 and grid electrode voltages were set to +200 V and ±225 V respectively. Mass spectrometer settings which were kept constant include an orifice 2 voltage of ±5 V and a ring lens voltage of ±3 V.

Two separate methods were developed for detection of these compounds by DART-MS, one method for the detection of alcohols, acetone, ethylene glycol, and ammonia in positive mode and one for the detection of the hypochlorite ion in negative mode. Additional parameters for the positive mode method include an orifice 1 voltage of +10 V, a peaks voltage of 300 V, and a mass range of 30 *m/z* to 650 *m/z* at 0.5 seconds per scan. A helium gas stream temperature of 325 °C was also employed. For the negative mode, additional parameters included a gas stream temperature of 375 °C, an

orifice 1 voltage of -10 V, a peaks voltage of 600 V, and a mass scan range of 65 *m/z* to 650 *m/z* at 0.5 seconds per scan.

Subsection A2.2.4 GC-MS Methods

In order to compare the limits of detection for the DART-MS to current confirmatory techniques, solutions were also analyzed by HS-GC-MS. The instrument used was an Agilent 6890N gas chromatograph equipped with an Agilent 30 m by 0.25 mm DB-1MS column coupled to an Agilent 5975B quadrapole mass spectrometer (Santa Clara, CA, USA). A 1 mL manual injection of the headspace was completed using a Hamilton airtight syringe (Reno, NV, USA). The inlet was set to a temperature of 265 ^{0}C and the sample was split 30:1 with a split flow of 29.0 mL/min and a total flow of 32.7 mL/min. Ultra pure helium was used as the carrier gas. An isothermal GC temperature of 40 ^{0}C was used. A mass range of 10 *m/z* to 120 *m/z* was scanned. The source temperature in the mass spectrometer was set to 230 ^{0}C, and the quadrapole temperature was set to 150 ^{0}C.

Subsection A2.2.5 Limit of Detection Determinations

In order to determine the limit of detection for each of the adulterants by DART-MS and headspace gas chromatography mass spectrometry (HS-GC-MS), serial dilutions of the pure compounds were prepared in increments ranging from 1% to 0.001% by volume in de-ionized water. Each of these dilutions was then run in triplicate on both DART-MS and HS-GC-MS. Analysis by DART-MS was completed by depositing 1 µL of both the dopant and sample onto a clean glass sampling rod, followed by introduction of the rod

into the gas stream, where it was held until the signal was no longer present. All samples runs were then examined for the presence of the adduct ion (with the exception of ethylene glycol, where the dimer ion was monitored). The limit of detection was defined as the lowest concentration at which the peak of interest was present at a signal-to-noise ratio of at least 3:1 in all three replicates. Analysis of HS-GC-MS was completed by sampling 1 mL of the headspace of each vial followed by direct injection onto the column of the GC-MS. The limit of detection was defined as the level that the chromatographic peak had a signal-to-noise ratio of at least 3:1 in all replicates.

Section A2.3 Results and Discussion

Subsection A2.3.1 Method Optimization and Specificity

A number of different parameters were varied in order to determine the optimal conditions for the detection of these compounds. All nine of the compounds (acetone, methanol, ethanol, 1-propanol, 2-propanol, 1-butanol, ethylene glycol, ammonia, and hypochlorite) were optimized individually and those with like optimal parameters were grouped together for further testing. Parameters which were optimized included: ion polarity, gas stream temperature, orifice voltage, and needle voltage. It was found that although the alcohols responded in both positive and negative modes, the signal intensity was stronger (with less background contributions in the low mass region) using the positive mode. Signal intensities were up to an order of magnitude higher in positive mode than in negative mode. Similar results were seen for acetone and ethylene glycol. Hypochlorite was only detected in negative mode and ammonia was only detected in positive mode. The temperature of the helium gas stream was shown to greatly affect the

detection of ammonia and hypochlorite. For all chemicals, gas temperatures were tested between 250 ºC and 450 ºC. It was found that in order for hypochlorite to be desorbed into the gas stream a gas temperature of at least 375 ºC was required. However, beyond 375 ºC there was negligible increase in signal. Similarly, a gas temperature of at least 300 ºC was required for ammonia to be desorbed and detected. Maximum signal for the signal of the remaining compounds was found to occur in the 300 ºC to 350 ºC range. The orifice 1 voltage, which can produce additional fragmentation at high voltages, was found to increase the number of background peaks in the low mass region of the mass spectra for both positive and negative mode, without providing any additional peaks relating to the chemicals tested, and therefore an orifice 1 voltage of ±10 V was used for analysis. Also, an increase in orifice 1 voltage was shown to decrease the signal of dimers and trimers which were readily formed when a low orifice 1 voltage was used. The needle voltage, which was varied from -2,500 V to -4,500 V and was found to have negligible effect across the range of chemicals tested.

Subsection A2.3.2 DART Mass Spectra and Dopant Introduction

The mass spectra that are produced by the nine adulterants differ depending on whether an organic or inorganic compound is being analyzed. For the organic compounds (alcohols, acetone, and ethylene glycol) the mass spectra are dominated by protonated molecules, dimers and in some cases trimers, as we all as $[n\text{M}–\text{OH}]^+$ ions. Figure 1 shows representative mass spectra for each of the compounds of interest. With the exception of acetone, the dimer ion was identified as the strongest signal in all samples. For the two inorganic compounds, detection of the ions was difficult due to

their low molecular weight and potential lack of desorption without complexation with an organic constituent.

While the organic chemicals produced suitable mass spectrum when analyzed in pure form, it was found that detection of the compounds was complicated when they were mixed with a common beverage or present at low concentrations (less than 1% v/v). To enhance detection of these compounds in complex mixtures, the addition of a dopant to the sample was employed. The method used to incorporate the dopant into the sampling scheme was to dip the glass sampling rod directly into a vial of the diluted dopant (at a concentration of approximately 5 mg/mL in hexane) followed by pipetting 1 µL to 2 µL of the sample onto the rod. This method minimizes contamination of the dopant vials. Furthermore, the addition of the dopant onto the rod first was shown to be necessary to get adduct formation of the hypochlorite solution. This is potentially due to desorption of the cis-9,12-octadecadienoic acid molecules underneath the hypochlorite ions, which allows the fatty acid to adduct with the hypochlorite ions upon transfer from the rod into the gas stream.

A number of dopants were tested and included: fatty acids, fatty acid methyl esters, and glycol ethers. These candidate dopants were chosen because they are easily accessible, inexpensive, ionize readily in their respective modes, and would likely not cause any adverse effects if they contaminated the sample (unlike using narcotics or explosives as a candidate dopant which could cause issues in a criminal investigation). It was found that for different chemicals, different dopants helped to provide maximum signal. For the organic components it was found that short chain fatty acids such as hexanoic acid and heptanoic acid provided the best response. Larger chain fatty acids,

such as hexadecanoic acid and octadecanoic acid, did not easily form adducts with the larger alcohols like 1-butanol, or with acetone. The adduct which is formed when a short chain fatty acid is incorporated onto the sampling rod is an $[M+adduct–OH]^+$ ion for the straight chain alcohols and an $[M+adduct+ H]^+$ ion for the branched alcohol and acetone. This also allowed for a way to discriminate between isomers such as 1-propanol and 2-propanol, as different adducts are formed. For ethylene glycol, there was no dopant which was tested whose adduct was of greater intensity then the ethylene glycol dimer peak, and therefore, no adduct was used in the analysis of this compound. Table A2.1 shows the molecular formula and exact masses for the various adducts that are formed. Figure A2.1 shows the mass spectra of the chemicals of interest and their dopants. For ammonia it was found that long chain fatty acid methyl esters provided the best signal, while for hypochlorite only unsaturated fatty acids produced adducts. Adduct formation was used in the determination of limits of detection and analysis of complex mixtures.

Table A2.1 Adulterants and the dopants that were used to form adduct ions. The molecular formula was derived from the accurate mass of the adduct ion, which allowed for an assignment of each to be made. Under the assignment of adducts column "HA" stands for hexanoic acid, "MP" stands for methyl pentadecanoate, and "LA" for cis-9,12-octadecdienoic acid, the dopants used in the analysis.

Compound	Adduct Used	Mass of Adduct	Molecular Formula of Adduct	Assignment of Adduct
Methanol	Hexanoic Acid	131.1072	$C_7H_{15}O_2$	[HA+Methanol-OH]+
Ethanol	Hexanoic Acid	145.1228	$C_8H_{17}O_2$	[HA+Ethanol-OH]+
1-Propanol	Hexanoic Acid	159.1385	$C_9H_{19}O_2$	[HA+Propanol-OH]+
2-Propanol	Hexanoic Acid	173.1541	$C_9H_{19}O_2$	None
Butanol	Hexanoic Acid	173.1541	$C_{10}H_{21}O_2$	[HA+Butanol-OH]+
Acetone	Hexanoic Acid	175.1334	$C_9H_{19}O_3$	[HA+Acetone+H]+
Ammonia	Methyl Pentadecanoate	274.2746	$C_{16}H_{36}O_2N_1$	$[MP+NH_4]^+$
Hypochlorite	Cis-9,12-octadecadienoic Acid	315.2090 (^{35}Cl) 317.2067 (^{37}Cl)	$C_{18}H_{32}O_2Cl_1$	$[LA+ClO-O]^-$
Ethylene Glycol	None	None	None	None

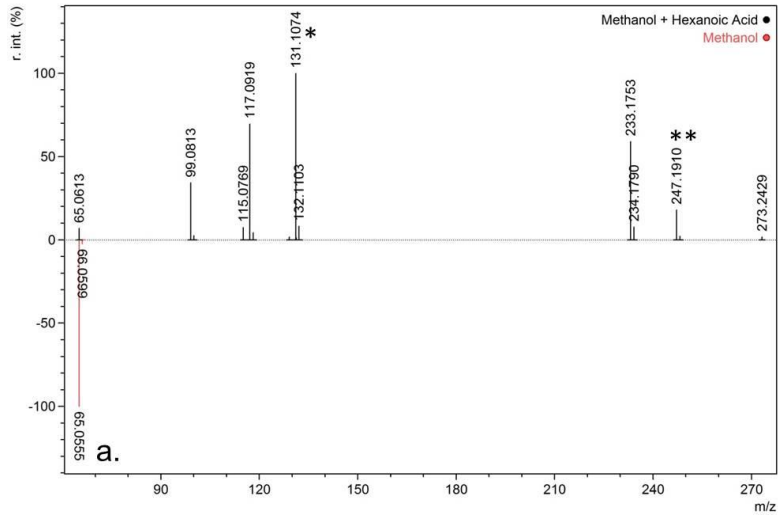
Methanol + Hexanoic Acid
Methanol
r. int. (%)
a.
m/z

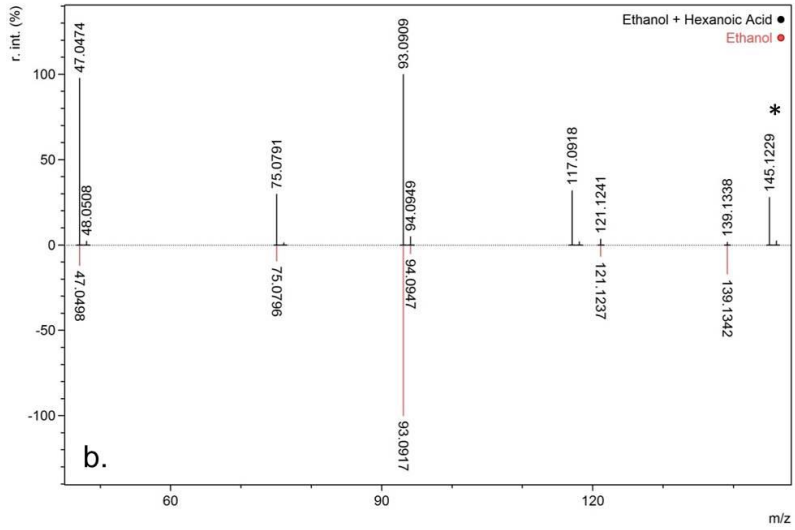
Ethanol + Hexanoic Acid
Ethanol
r. int. (%)
b.
m/z

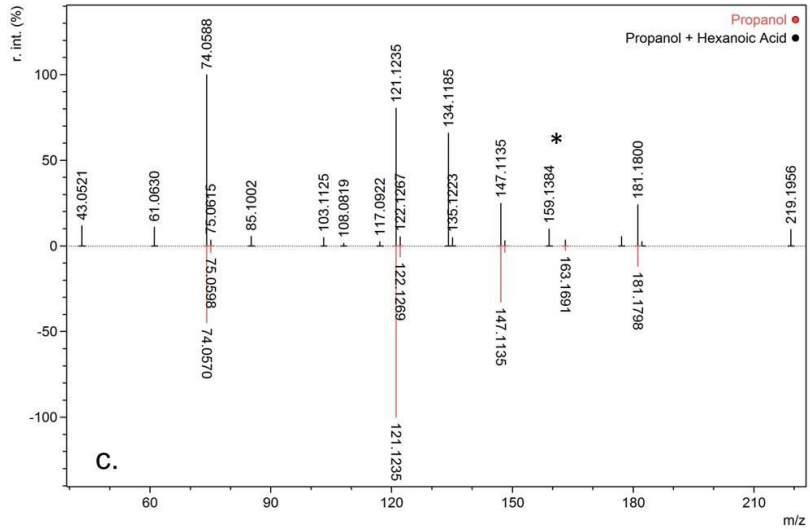
Propanol
Propanol + Hexanoic Acid
r. int. (%)
c.
m/z

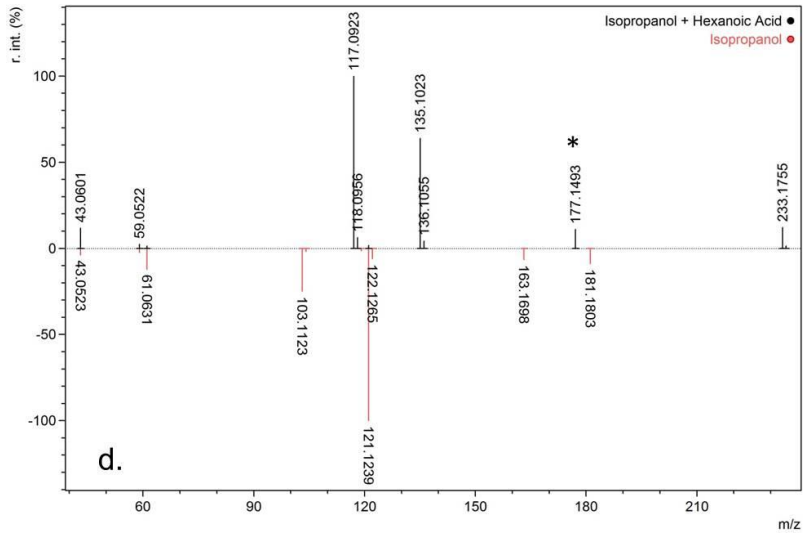
Isopropanol + Hexanoic Acid
Isopropanol
r. int. (%)
d.
m/z

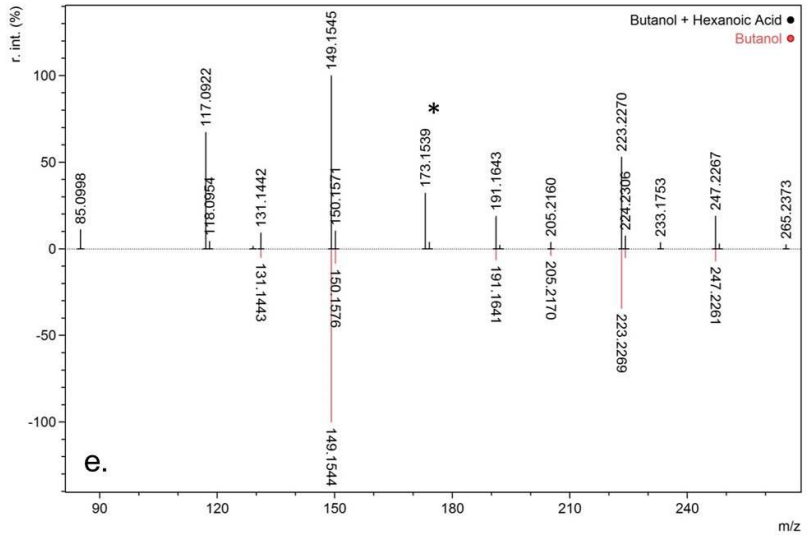
Butanol + Hexanoic Acid
Butanol
r. int. (%)
e.
m/z

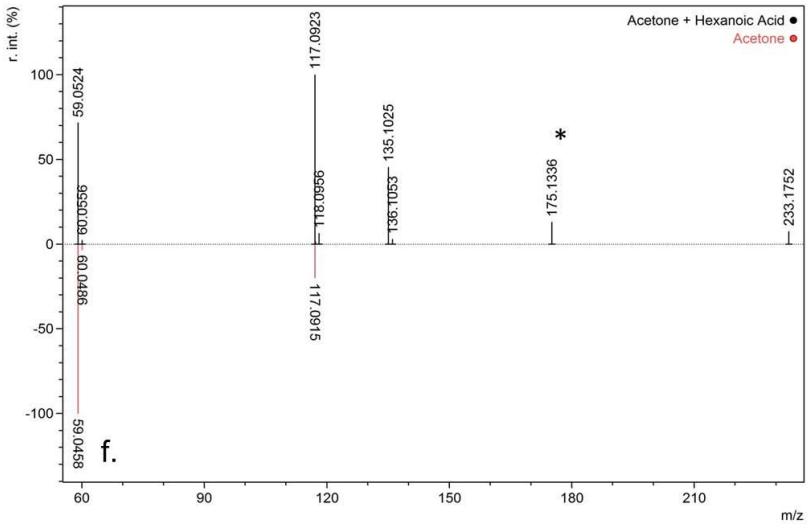
Acetone + Hexanoic Acid
Acetone
r. int. (%)
f.
m/z

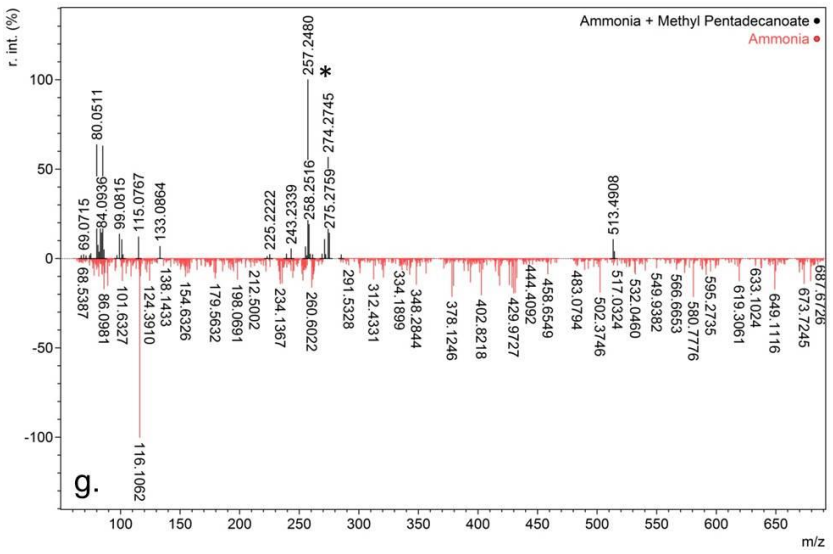
Ammonia + Methyl Pentadecanoate
Ammonia
r. int. (%)
m/z
g.

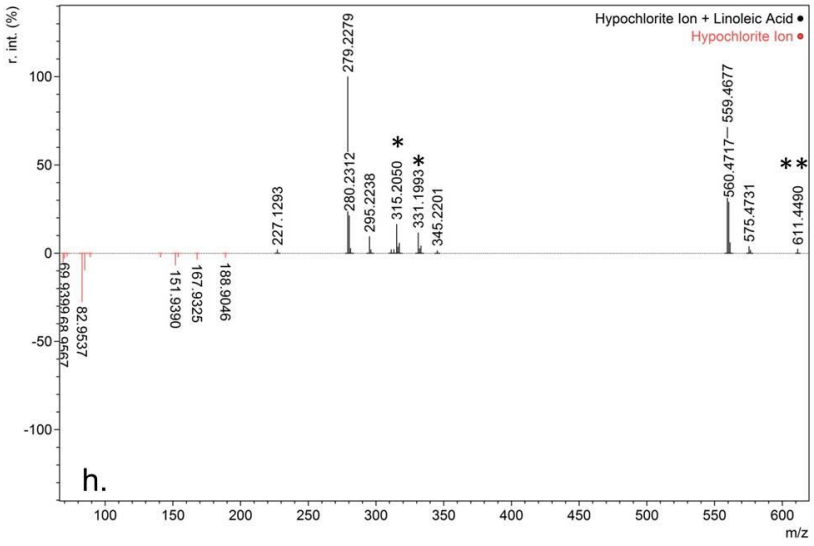
Hypochlorite Ion + Linoleic Acid
Hypochlorite Ion
r. int. (%)
m/z
h.

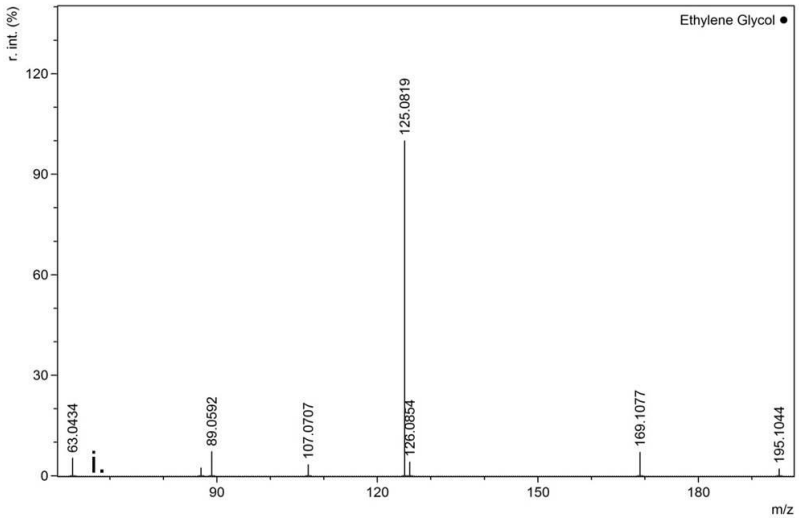
Ethylene Glycol
r. int. (%)
m/z
i.

Figure A2.1 Mass spectra of the pure adulterant (red) and the adulterant with the addition of the respective dopant (black) for methanol (A.), ethanol (B.), propanol(C.), isopropanol (D.), butanol (E.), acetone (F.), ammonia (G.), hypochlorite (H.), and ethylene glycol (I.). In all spectra, the adduct which is formed is indicated with an asterisk (*) and the dimer of the adduct is indicated with a double asterisk (**).

The formation of the chlorine adduct in the hypochlorite solution was further tested for specificity to the hypochlorite ion. To test this, 1% by volume solutions of hypochlorite, sodium chloride, potassium chlorate, and ammonium perchlorate were analyzed, with the addition linoleic acid as a dopant, for the presence of the adduct ions. Figure A2.2 shows the mass spectra of the samples of these four chlorine-containing ions. It was found that the adduct peaks at nominal masses 315 *m/z*, 317 *m/z*, 331 *m/z*, and 333 *m/z* were specific to the hypochlorite ion.

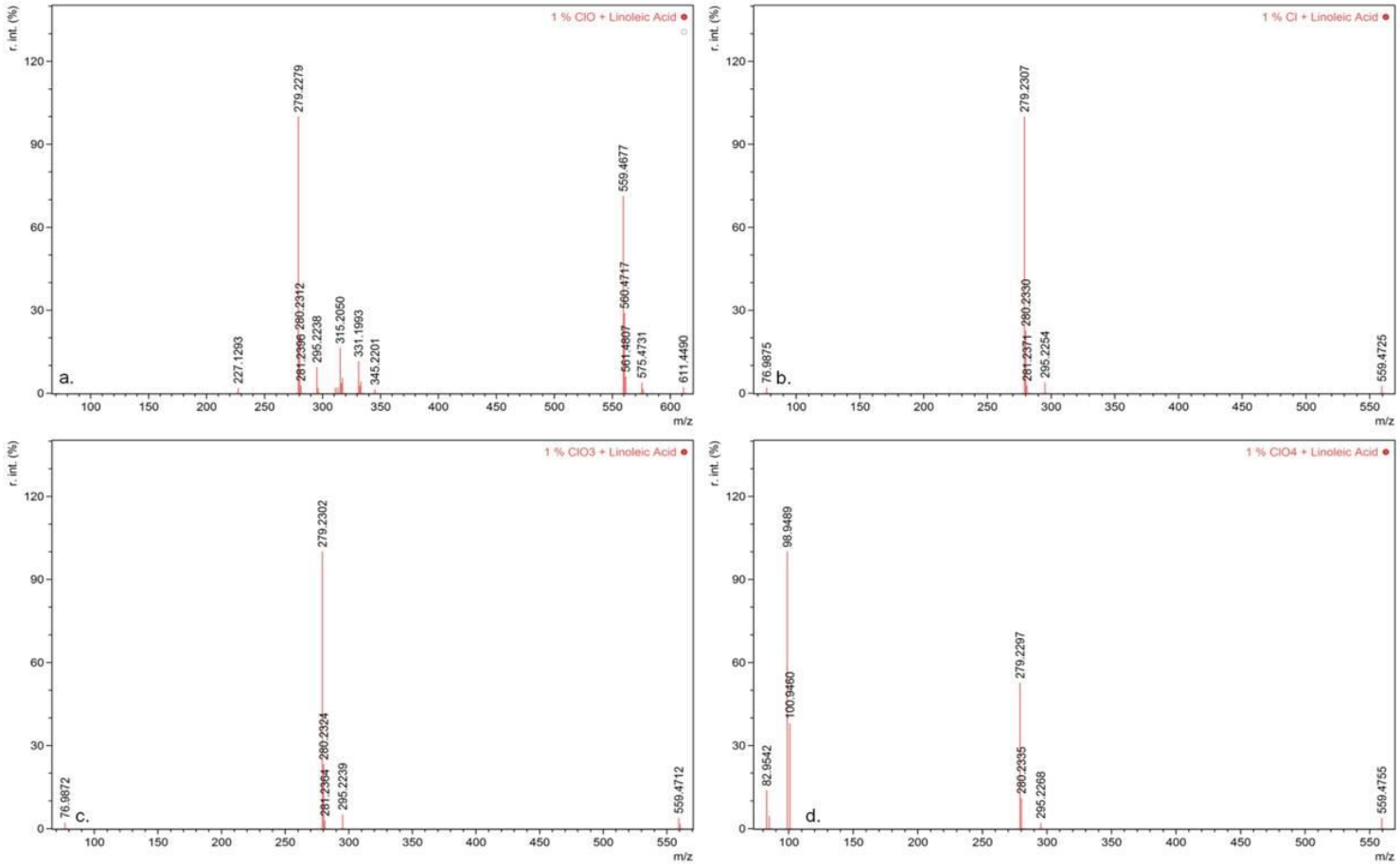

Figure A2.2 Mass spectra of a cis-9,12-octadecadienoic acid dopant with hypochlorite (A.), chloride (B.), chlorate (C.), and perchlorate (D.).

Subsection 2.3.3 Limits of Detection

The limit of detection of the adulterants diluted in deionized water was determined for both DART-MS and HS-GC-MS. Table A2.2 depicts the limits of detection for all species analyzed by both techniques. No limit of detection exists for analysis of the ammonia and hypochlorite solutions by HS-GC-MS due to the inability to detect inorganic compounds with such a technique. The limits of detection reported for DART-MS were determined for the adduct peak in all adulterants, with the exception of ethylene glycol (in which the dimer was monitored). With all adulterants, the limit of detection for analysis by DART-MS was found to be lower than that of HS-GC-MS. Coupled with the rapid analysis time and a wider range of chemicals able to be detected, this increased sensitivity further highlights the use of DART-MS as a viable screening tool.

Table A2.2 Limits of detection for the nine adulterants when analyzed on DART-MS and HS-GC-MS. The limits of detection are expressed as percent by volume when diluted in de-ionized water. An asterisk (*) indicates that the adulterant was not capable of being analyzed by HS-GC-MS and thus no limit of detection is available.

Compound	DART-MS LOD (% v/v)	HS-GC-MS LOD (% v/v)
Methanol	0.01 %	0.5 %
Ethanol	0.01 %	0.5 %
1-Propanol	0.01 %	0.5 %
2-Propanol	0.01 %	0.5 %
Butanol	0.01 %	0.5 %
Acetone	0.001 %	0.5 %
Ammonia	0.001 %	N/A*
Hypochlorite	0.001 %	N/A*
Ethylene Glycol	0.01 %	0.01 %

Subsection A2.3.4 Analysis of Complex Mixtures

In order to establish the feasibility of this method for real-world casework, mock samples were made, each containing one of the nine adulterants at a 1% by volume level in one of four beverages. The beverages which were chosen were: Coca-Cola, Gatorade, Red Bull, and 13th Colony Southern Corn Whiskey. By doping the beverages with the adulterants it could be determined whether or not the presence of sugar, salts, preservatives, and flavoring compounds would hinder detection or specificity of the technique. Also, the Corn Whiskey was chosen to evaluate whether or not the adulterants could be detected in solutions containing a high concentration of ethanol. Each sampling was run in triplicate and the centroided mass spectra were searched against an in-house search list developed, from the peak identities of both the adducted and non-adducted solution. Search parameters which allowed for detection of a particular peak required it to be greater than 1% relative intensity in respect to the base peak of the mass spectra and with an actual measured mass within ± 0.005 Da of the theoretical mass.

Figure A2.3 shows representative mass spectra of Coca-Cola, Gatorade, and Red Bull, each containing 1% by volume of ethanol. It was determined that none of the four beverages produced a peak which overlapped with any of the adduct peaks. The background spectra from Coca-Cola did produce a peak at 145 *m/z*, the same nominal mass as the ethanol-hexanoic acid adduct, but the accurate mass of that peak is sufficiently outside of the 5 mDa mass tolerance as to not be falsely identified as the adduct ion. All adulterant adducts, and ethylene glycol, were detected in Coca-Cola,

Gatorade, and Red Bull, at the 1% by volume level. The adduct peaks were also typically well above the 1 % relative intensity threshold.

Detection of adulterants in corn whiskey was shown to be more difficult than in the non-alcoholic beverages. Since the concentration of ethanol in the whiskey was much higher than the concentration of the adulterant, in the case of the organic compounds where the same dopant is used, the dopant preferentially adducted with the ethanol molecules. This led to lack of detection of the methanol and 2-propanol in the whiskey. However, detection of the other organics 1-propanol, 1-butanol, and acetone, was possible though the adduct ion signal was suppressed in comparison to that of non-ethanol containing beverages. Detection of ethylene glycol was possible in the whiskey as well, likely because no dopant is necessary to detect this compound. Also, detection of ammonia and hypochlorite were possible, likely because different dopants are used.

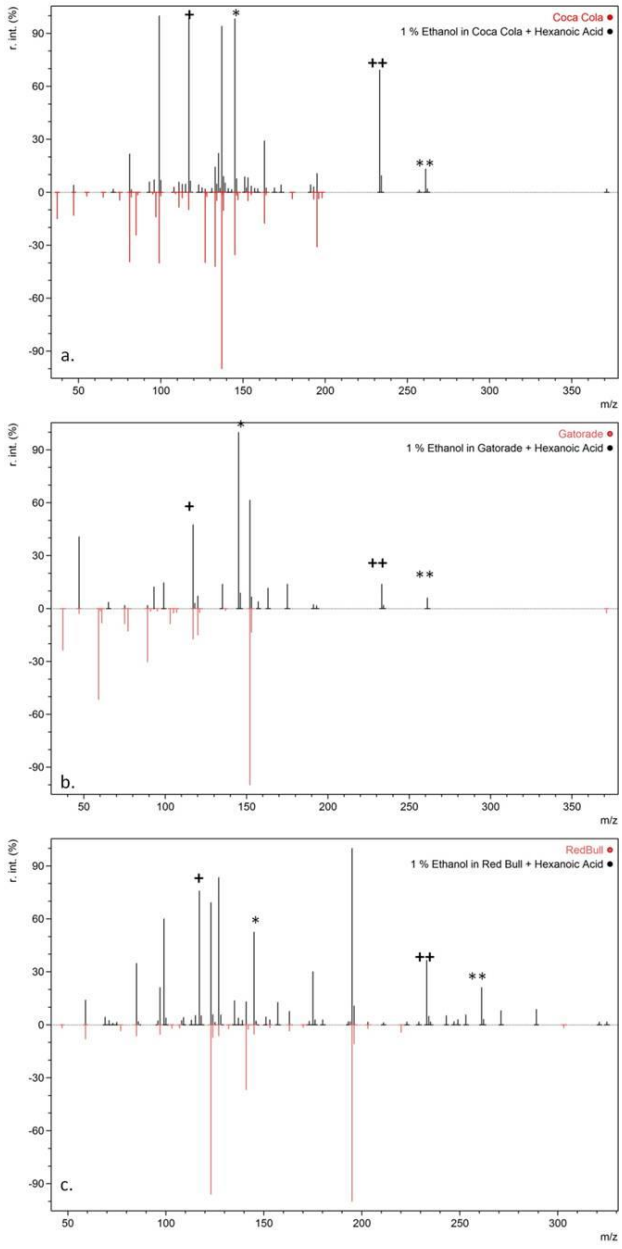

Figure A2.3 Mass spectra of a 1 % by volume ethanol mixture in Coca Cola (A.), Gatorade (B.), and RedBull (C.) with the addition of hexanoic acid as a dopant (black), versus a 1 % solution of ethanol in water with the addition of hexanoic acid as a dopant (red). The + and ++ indicate the monomer and dimer of hexanoic acid, respectively, while the * and ** indicate the monomer and dimer hexanoic acid ethanol adduct, respectively.

Subsection A2.3.5 Potential Method for Handling Unknown Samples

Since the methods described herein employed several different dopants, and different ionization modes, a method for the handling of unknown samples would be useful in order to minimize sample consumption, opportunities for loss/contamination, and analysis time. The proposed method of analysis, as outlined in Figure A2.4, first involves the analysis of the neat sample in positive ionization mode without the addition of a dopant. This would allow the examiner to determine if ethylene glycol, acetone, or an alcohol was present. If ethylene glycol was present, no further analysis would be necessary. If acetone or an alcohol was present, an additional run doped with hexanoic acid would determine the type of alcohol which was present or to confirm the presence of acetone. If no compounds of interest were detected, the sample could then be doped with methyl pentadecanoate and run to evaluate for the presence of ammonia. Finally, the ionization mode could be switched and the sample doped with cis-9,12-octadecadienoic acid to determine if the hypochlorite ion was present. The total analysis time would be approximately 10 minutes and consume less than 15 µL of sample. Additional dopants and analysis methods could be added onto this chain to further enhance the suite of chemicals which are being screened.

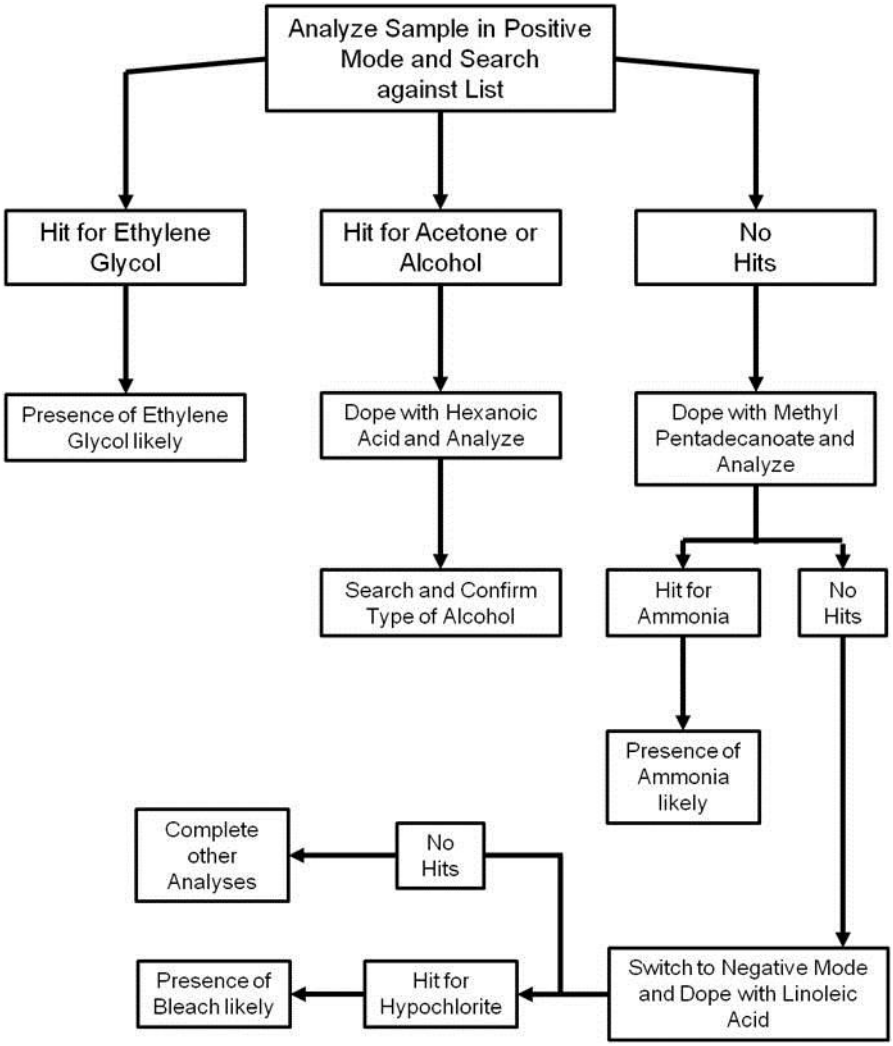

Figure A2.4 Potential analytical scheme for the analysis of an unknown beverage by DART-MS.

Section A2.4 Conclusions

Rapid, sensitive, and specific detection of adulterants has been shown to be possible using DART-MS. By introducing a dopant and allowing for adduct formation, these potential adulterants, both organic and inorganic, can be detected in a number of common beverages. If the beverage contains ethanol at a higher concentration than another adulterant, detection of the adulterant could be hindered. This is particularly true with organic compounds of a similar or lower molecular weight than ethanol. The technique was also shown to be more sensitive than HS-GC-MS for detection of the

organic adulterants, and could also detect inorganic components such as ammonia and hypochlorite, which HS-GC-MS could not detect. Differentiation of isomeric compounds was also possible due to different pathways for adduct formation. Future work will focus on expanding the adulterants which can be screened for, as well as establishing at what, if any, ethanol to adulterant ratio would allow for the successful detection of adulterants like methanol in an ethanol-containing beverage.

Appendix 3: Method Development and Validation for the Detection of Bank Dye (MAAQ) by DART-MS

Section A3.1 Introduction

An additional method development and validation study was completed for the analysis of bank dye, 1-Methylaminoanthraquinone (MAAQ), by direct analysis in real time mass spectrometry (DART-MS). Bank dye, a red aerosolized powder that rapidly and permanently stains substrates when wetted, is a component of the explosive dye pack commonly found in banks that can be used to thwart bank robberies. Other components of a bank dye pack include an explosive charge and, typically, a tear gas compounds such as capsaicin. The method developed in the section looked at optimization of parameters, defining a limit of detection, reproducibility, analysis off of different substrates, and potential false positives. This work builds upon work published by Steiner *et al*. who completed a validation of DART-MS for this type of analysis at their crime lab at the Virginia State Police.[65] Additional validations which have been completed but are not discussed in this thesis include analysis of lotions, pepper spray, hair dye components, sugars, automotive fluids, and detergents by DART-MS.

Section A3.2 Materials and Methods

A JEOL AccuTOF™ mass spectrometer coupled to a IonSense DART source was used in these analyses. Parameters of the instrument which were kept constant throughout the study include a needle voltage of -3000 V, a ring lens voltage of +3 V, an orifice 2 voltage of +5 V, helium carrier gas with a flow rate of 1.75 L/min, and a mass

scan range of 100 *m/z* to 800 *m/z* integrated at 0.5 second per scan. Polyethylene glycol (PEG) 600 was used as the mass calibrant, and was prepared by dissolving 50 µL of PEG 600 (Acros, Lot: A0211373001) into 10 mL of methanol (Fisher). Two quality assurance quality control (QA/QC) compounds were also used. These were methyl decanoate, that was prepared by diluting 50 µL of a 10 mg/mL stock solution (AccuStandard) into 10 mL of methanol, and reserpine, that was prepared by dissolving 0.5 mg of reserpine (Sigma) into 10 mL of methanol. MAAQ was purchased from SPI (SPI Supplie, West Chester, PA) and used both as a powder and dissolved in methanol.

Section A3.3 Results and Discussion

Subsection A3.3.1 Method Optimization

While many parameters may be varied on the AccuTOF™-DART system, there are four parameters which are commonly varied for individual analyses. These include the orifice 1 voltage, the detector voltage, the orifice temperature, and the addition of a dopant. The orifice 1 voltage affects the amount of fragmentation of the molecules that are sampled, with a higher voltage typically increasing the amount of fragmentation. The detector voltage affects the instrument sensitivity, with a higher voltage providing a higher sensitivity but also potentially increasing instrumental noise. The gas stream temperature can have a range of effects on the types of compounds which are sampled, with lower temperatures being effective on lower vapor pressure molecules and higher temperatures being effective on higher vapor pressure molecules. The presence of a dopant, which is an independent chemical compound introduced into the gas stream, can be used to generate adduct ions.

In this study, three orifice 1 voltages (+10 V, +30 V and +60 V), six gas temperatures (150 °C, 200 °C, 250 °C, 300 °C, 325 °C, and 350 °C), and one dopant (ammonium hydroxide) were examined to determine what parameters would be most effective for the analysis of MAAQ, which readily undergoes positive ionization. A matrix of all possible instrumental parameters was completed to determine that optimal operating conditions. The detector voltage was set to 2500 V and was not changed, as this parameter had been optimized in a prior validation study.

From the data collected, MAAQ was readily detected using all permutations of these parameters. A higher orifice 1 voltage did increase the amount of fragmentation which was noticed, providing additional peaks at nominal masses 220 *m/z* and 223 *m/z*. Furthermore, the increased voltage caused a significant increase in signal intensity, with a base peak twice as intense for a +60V orifice 1 voltage, when compare to the +10 V orifice 1 voltage. Voltages greater than + 60 V were not chosen because usable PEG mass calibration curves could not be obtained. Increasing the DART temperature from 150 °C to 325 °C provided a substantial increase in signal intensity for MAAQ, in which the intensity was increased approximately two-fold when the temperature was raised from 200 °C to 325 °C. Increasing the temperature beyond 325 °C provided no additional increase in signal intensity, and therefore a gas temperature of 325 °C was chosen.

The other variable which could be manipulated was the presence of a dopant. Since positive mode is being used for analysis, a chemical which would readily produce vapors that are ionized or ionizable in positive mode was chosen. The dopant was introduced by placing a capped GC-MS vial with a microcapillary through the cap

directly underneath the gas stream. The dopant, ammonium hydroxide, provides a cloud of NH_4^+ ions in the gas stream that can allow for the potential production of ammonium adducts. In the case of MAAQ, there proved to be no adduct formation and no noticeable increase in signal intensity. Because of these factors, it was decided that a dopant would not be used.

The final parameter which was evaluated was to switch the voltages during analysis. Switching the voltages allows for analysis by both a high and low voltage which can then produce a mass spectrum which contains the information from both the soft lower voltage and the increased fragmentation of the higher voltage. When the voltage switching was applied (switching between +30 V and +60 V) it was found that the signal intensity was actually decreased by a factor of three. Since the protonated molecular ion was still abundant in the +60 V analysis, voltage switching was not applied to the optimized method. A representative mass spectrum of MAAQ analyzed by the optimized method, with peak assignments, is presented in Figure A3.1.

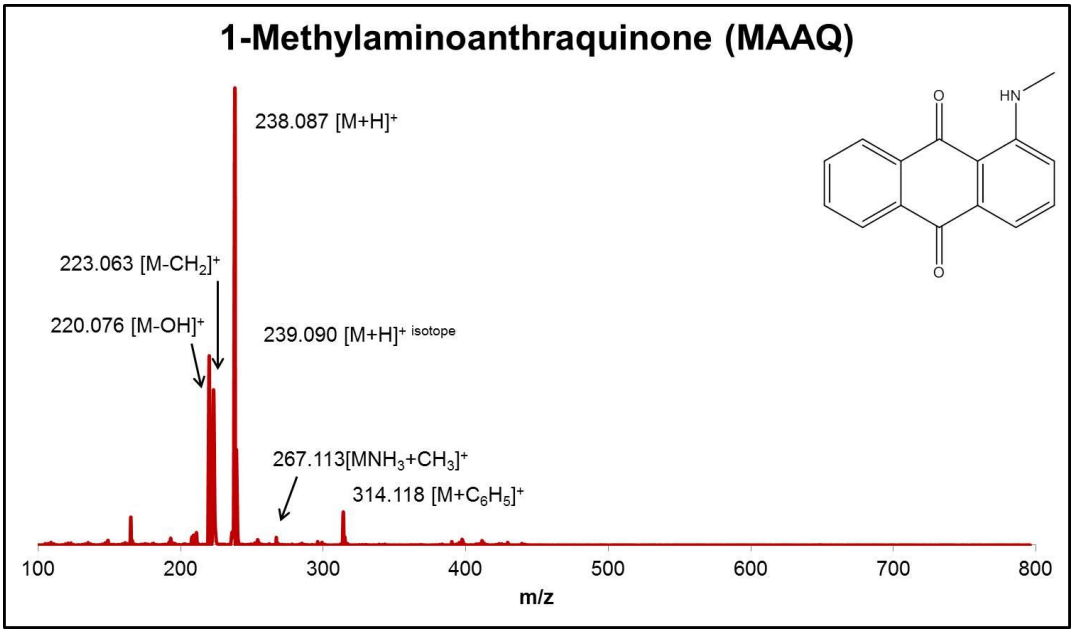

Figure A3.1 Representative mass spectrum of MAAQ.

Subsection A3.3.2 Limit of Detection

Once an optimized method for MAAQ detection was completed, the limit of detection by both DART-MS, and electron impact gas chromatography mass spectrometry (EI-GC-MS), the current validated technique, were determined. The limit of detection was defined as the amount of material which produced a base peak with a signal-to-noise ratio of at least three to one for all three replicates of analysis. Since no standard solution of MAAQ was available, a solution was made by dissolving 9.33 mg of MAAQ in 8.5 mL of methanol (Fisher, Lot #107165), giving of solution concentration of ~ 1097 ng/µL. This was the "Stock" solution. Serial dilutions of MAAQ were then prepared in the following manner:

From the "Stock" solution of MAAQ:

- A 100 ng/µL dilution was made by pipetting 100 µL of the stock solution and 900 µL of methanol into a GC-MS vial and vortexing for 10 seconds.
- A 10 ng/µL dilution was made by pipetting 100 µL of the 100 ng/µL dilution and 900 µL of methanol into a GC-MS vial and vortexing for 10 seconds.
- A 1 ng/µL dilution was made by pipetting 100 µL of the 10 ng/µL dilution and 900 µL of methanol into a GC-MS vial and vortexing for 10 seconds.
- A ~0.1 ng/µL dilution was made by pipetting 100 µL of the 1 ng/µL dilution and 900 µL of methanol into a GC-MS vial and vortexing for 10 seconds.

Each of the dilutions was tested in triplicate on the AccuTOF-DART using the following sequence:

PEG 600 > Methyl Decanoate > Reserpine > Replicate 1 > Replicate 2 > Replicate 3

For each replicate, 1 µL of the solution was placed on a clean glass rod, using a micro-syringe, and sampled. Separate rods were used for each replicate to prevent concentration changes between replicates due to residual materials. The dilutions were also run on the EI-GC-MS to compare the sensitivity of the DART technique to a technique which is being utilized in casework.

It was found that the DART technique provided increased sensitivity to that of the GC-MS. The limit of detection for DART was found to be 100 pg whereas the limit of detection on the GC-MS was found to be the 100 ng/µL solution, which equates to 10 ng when the split of the method is accounted for. The increased sensitivity of the DART technique allows for it to be used as an efficient screening technique for MAAQ

Subsection A3.3.3 Analysis off of Substrates

A study was performed on the AccuTOF™-DART to determine if interferences would be observed on this instrument if MAAQ was analyzed directly off of a number of different substrates. To test this, the 5 µL of the 1 µg/µL solution was deposited onto 15 different substrates, which are listed in Table A3.1. A number of different substrate types and substrate colors were used to simulate those which may be encountered in casework. The stain that was created on each substrate was cut in half, with one half being extracted into 1 mL of methanol. The remaining half of each substrate was used to analyze the stain directly in the DART source. This allowed for comparison of the extracted samples to the direct analysis of the stain on the substrate. Each substrate and its corresponding extracts were analyzed in triplicate.

For the methanol extracted samples, separate rods were used for each replicate to prevent concentration changes between replicates due to residual materials. Once analyzed, each spectra was searched against the MAAQ search list to determine whether or not MAAQ was successfully detected.

To ensure the substrate was not interfering with the detection of MAAQ due to peak overlap, a clean piece of each substrate was also analyzed, in a separate run. Of the fifteen blank substrates analyzed, only one substrate (#11 – Grey Fabric Swatch) produced a hit for an MAAQ peak. In this substrate only one peak was present (at nominal mass 238 *m/z*) with an intensity well below 1,000, making it too low to be significant.

In the case of the samples extracted into methanol, MAAQ was readily detected in all of the replicates of all of the runs. Furthermore, in every replicate at least four of the six peaks were detected with the molecular ion peak at nominal mass 238 *m/z* being the most abundant peak. For the samples which were analyzed directly in the DART source, MAAQ was detected in all replicates of all runs as well. Samples #6 (synthetic leather) and #12 (blue fabric swatch) both had significant background which made obtaining a useable spectra and completing replicate runs difficult. These two fabrics also had fewer MAAQ peaks detected, though the base peak was still present. Samples which were analyzed directly in the DART source did have the potential to melt if the fabrics were left in the gas stream for more than a few seconds. Caution should be used when analyzing materials directly in the DART source to prevent contamination of the system.

Table A3.1 A list of sample substrates used in analysis.

Sample #	Name	Color	Fiber Type (if applicable)
1	Cotton Cloth	White	Cotton
2	Dollar Bill	Green	Unknown
3	Printer Paper	White	Celluose
4	100% Cotton Underwear	White	Cotton
5	100% Cotton Underwear	Black	Cotton
6	Synthetic Leather	Purple	Unknown
7	Synthetic Suede	Tan	Cotton
8	Red Fabric Swatch (1)	Red	Unknown
9	Orange Fabric Swatch	Orange	Polyester
10	Red Fabric Swatch (2)	Red	Nylon
11	Grey Fabric Swatch	Grey	Nylon
12	Blue Fabric Swatch	Blue	Cotton
13	Brown Fabric Swatch	Brown	Cotton
14	Purple Fabric Swatch	Purple	Polyester
15	Cardboard	White / Brown	Unknown

Subsection A3.3.4 Potential False Positives

As the possibility exists that red stains which are analyzed for the presence of MAAQ may be a substance other than MAAQ, testing was performed on common items which contain red dye to analyze if there are any components which could interfere with the screening of MAAQ by providing false positives. A total of eight items containing red dye which could create red stains in realistic situations were analyzed, as well as two samples of MAAQ – one which was dissolved in methanol and one which was applied as a dry compound. Table A3.2 lists the items chosen for testing.

To test the items, they were applied directly to white cloths, each labeled with the appropriate sample number. Six spots, each consisting of one drop, were applied. Once dry, three of the six spots were cut out and placed in individual test tubes, while the other three spots were kept intact. The spots which were cut out were then extracted with 1 mL

of methanol. Extraction was completed by vortexing each sample for 20 seconds. The extractions and the samples on the cloth were then analyzed using the optimized method for MAAQ detection. Extracted samples were analyzed by dipping a glass micro capillary in the sample and waving it front of the gas stream. Direct analysis off of the cloth was completed by folding along the red spot and placing the sample on the edge of the gas stream. Each mass spectrum was then searched against the MAAQ search list.

Table 3.2 Potential false positives tested.

Sample #	Item Name
1	Sharpie CD/DVD Marker
2	Skilcraft Permanent Impression Marker
3	Skilcraft Liquid Magnus Rollerball Pen
4	Revlon Red Nail Polish (#680)
5	Trodat Printy 4913 "Cancellation" Stamp
6	Cake Mate Writing Icing
7	Kroger Naturally & Artificially Flavored Fruit Punch
8	Cherry Kool Aid
9	3SI MAAQ dissolved in MeOH
10	3SI MAAQ

From this testing, it was found that 7 of the 8 samples which were not MAAQ were found to have no peaks which are characteristic of MAAQ. One of the samples, #7 Kroger Fruit Punch, contained one of the peaks characteristic of MAAQ (nominal mass 267 *m/z*). No other characteristic peaks for MAAQ (including the base peak at nominal mass 238 *m/z*) were detected. The abundance of this one peak was low in sample, and therefore would not be a strong indication of MAAQ. Further tests could discriminate

fruit punch from MAAQ as well. The two samples of MAAQ had positive hits in all cases, and each sampling had at least 5 of the 6 MAAQ peaks present.

Three other useful items were noticed in this study. First, the dye present in samples #1 and #2 turned a fluorescent orange/pink when extracted into methanol. This color was easily distinguishable from the red/pink of MAAQ. Secondly, the dye present in sample #3 could not be extracted using methanol. Thirdly, in the MAAQ samples, there were often more peaks relating to MAAQ with direct sampling.

Subsection A3.3.5 Reproducibility and Blind Sampling

A robust study of the reproducibility of the MAAQ method was performed. The sample set which was used consisted of the following compounds in order of analysis:

PEG 600 > Methyl Decanoate > Reserpine > MAAQ1 > MAAQ2 > MAAQ3

The compound of interest was analyzed in triplicate within each sample set to ensure that the measured masses were consistent with theoretical masses.

Sampling took place once daily over six days, with an additional sample runs being performed on two of the six days. Each sample run consisted of three replicates of MAAQ, as listed above. This data was used to determine that the method provided reproducible and accurate data for the analysis of the compounds of interest, as well as validating the use of methyl decanoate as an independent QA/QC standard. For the purposes of validation, accuracy was defined as providing a measured mass that was within ± 0.005 Da of the theoretical value, which is the instrumental tolerance recommended by the manufacturer. Additionally, the tuning curve generated from the

polyethylene glycol had to have a correlation coefficient that was of the order of 10^{-12} or lower in order to be an effective curve.

The PEG 600 had very reproducible peaks between nominal masses 107 *m/z* and 767 *m/z*. This provides the working range for this analytical method. Samples with masses inside of this range can be accurately measured as this range of PEG is both accurate and reproducible. This provides an effective range for MAAQ, as all peaks lie within this range. Additionally, the molecular ion for both methyl decanoate and reserpine fall within this range, giving effective independent QA/QC standards.

From the data collected, it was found that all peaks which were monitored fell within the ±0.005 Da tolerance that was set. This includes masses from both the PEG at the beginning and end of the run, methyl decanoate, reserpine, and the triplicate runs of MAAQ. It was noticed that accurate mass measurements were observed in peaks with resolutions greater than 4300, having Gaussian shapes with sharp inclines to apex and smooth declines back to the baseline.

The reproducibility testing in this phase clearly demonstrated that within the effective range of this method (107 *m/z* – 767 *m/z*), the data collected for both the independent quality control standards and the compound of interest were both accurate and reproducible.

An additional test of the capabilities of the AccuTOF™-DART to screen for bank dye samples in a realistic setting was completed with blind sampling study. For this study, two sets of unknown samples, which encompassed the types of samples analyzed in Subsection A3.3.4, were prepared without knowledge of the constituents by the examiners. Two samples sets, each consisting of 6 samples, were provided to two

examiners. All samples were provided as single spots on white cotton cloths which were individually heat sealed in plastic to prevent contamination.

In order to analyze the samples, the spots were cut in half. Half of the spot was then extracted in methanol and analyzed in triplicate, while the other half was analyzed directly in the DART source. After the samples were run, the mass spectra were searched using the in house built search library to determine the presence of MAAQ. The results which were obtained are highlighted in Table A3.3. A compound in green text indicates that at least 4 of the peaks for MAAQ were identified well above background in all replicates. Orange text indicates that less than four peaks which correspond to MAAQ were detected ***and*** the abundance of these peaks was below 1,000 counts for at least one of the replicates of the run. Red text indicates that peaks which correspond to MAAQ were not detected in any of the replicates of the run. From this summation, a few points were observed:

1. In all cases when MAAQ was present, at least four of the six MAAQ peaks were detected in all replicates of all runs, regardless of whether it was the extraction that was analyzed or the sample was analyzed directly.
2. For samples that did not contain MAAQ, except for those that were possibly contaminated, any peaks that did produce hits for MAAQ were below 1,000 counts – putting them at or below background levels. These peaks could be ruled out as MAAQ due to their low counts, poor resolution, and the lack of four or more hits. Furthermore, in nearly all of the runs where one or two MAAQ peaks were detected, the 238 *m/z* peak was not that which was detected. This is,

however, the peak which is most predominant in all runs where MAAQ was detected – both in this section and previous sections.

3. There appears to be no benefit in extracting the samples versus direct analysis. Results were nearly identical between the two in all runs.
4. No false negatives were detected in any replicate of any run.

The data supports the ability of the AccuTOF-DART to be a useful screening tool to examine sample types that may be encountered in casework.

Table A3.3 Results of the blind sampling study. It was found that sample 10 contaminated the tweezers which were used to introduce samples into the DART source thereby contaminating samples 11 and 12.

Sample	Sample Identity	Methanol Extraction	Direct Analysis
1	Skillcraft Rollerball Liquid MAGNUS	No Peaks Detected	No Peaks Detected
2	Writing Icing	3 or less Peaks Detected – All Replicates	No Peaks Detected
3	Kroger Fruit Punch	One Peak Detected – All Replicates	One Peak Detected – One Replicate
4	MAAQ Liquid	4+ Peaks Detected – All Replicates	4+ Peaks Detected – All Replicates
5	DVD Marker	No Peaks Detected	No Peaks Detected
6	Revlon Red	No Peaks Detected	No Peaks Detected
7	Cherry Kool Aid	No Peaks Detected	One Peak Detected – One Replicate
8	Skillcraft Rollerball Liquid MAGNUS	No Peaks Detected	No Peaks Detected
9	Revlon Red 680	No Peaks Detected	No Peaks Detected
10	MAAQ Powder	4+ Peaks Detected – All Replicates	4+ Peaks Detected – All Replicates
11	Kroger Fruit Punch	2 or Less Peaks Detected – Two Replicates	***4 Peaks Detected – All Replicates***
12	Writing Icing	One Peak Detected – Two Replicates	***One Peak Detected – One Replicate***

Section A3.4 Conclusions

DART-MS is readily capable of detecting MAAQ in a variety of circumstances. A method has been optimized to achieve limits of detection below 100 pg, which far exceeds that of EI-GC-MS. The method also obtained excellent repeatability. MAAQ was shown to be capable of analyzed both from a methanol extraction and directly off of a surface. A number of surfaces were tested and none posed any significant issues with detection of MAAQ or presence of a number of peaks associated with MAAQ. Furthermore, a number of other red dyes were tested and again there were no issues in differentiated between MAAQ and other compounds.

Appendix 4: Additional Information for the Cross-Comparison of Ambient Ionization Techniques for the Analysis of Explosives

This appendix is intended to supplement Chapter 3, cross-comparison of ambient ionization mass spectrometry (AI-MS) techniques for the analysis of explosives. Included in this section are search lists for and representative mass spectra, with assignments, for the analysis of the explosives used in the study. Data for DESI-MS, LTP-MS, and DEFFI-MS are present. Mass spectra of the two mixtures analyzed in this study are also presented.

Section A4.1 DESI-MS Search Lists and Representative Mass Spectra

Table A4.1 A copy of the negative ionization mode DESI-MS search list developed for the explosives cross-comparison study.

Mass	Formula	Assignment
120	C7H6N1O1	2,4-DNT [M-NO3] / 2,6-DNT [M-NO3]
136	C7H6N1O2	2,4-DNT [M-NO2] / 2,6-DNT [M-NO2]
181	C7H5N2O4	TNT [M-NO2] / Tetryl [M*-NO2-CH3] / 2,4-DNT [M-H] / 2,6-DNT [M-H]
182	C6H2N2O5	AP[M-N2H4O2]
185	C6H4N1O2	NB [M+NO3]
196	C7H6N3O4	2-A-4,6-DNT [M-H] / 4-A-2,6-DNT [M-H]
197	C7H5N2O8	TNT [M-NO]
198	C2H4N3O8	EGDN [M+NO2]
212	C6H2N3O6	1,3,5-TNB [M-H]
213	C6H3N3O6	1,3,5-TNB [M]
214	C2H4N3O9	EGDN [M+NO3]
226	C7H4N3O6	TNT [M-H]
227	C3H5N3O9	NG [M]
228	C6H2N3O7	AP[M-NH4] / Tetryl [M*-NHCH3+O]
232	C7H7N3O4Cl1	2-A-4,6-DNT [M+Cl] / 4-A-2,6-DNT [M+Cl]

242	C4H8N3O9	DEGDN [M+NO2]
243	C7H7N4O6	2-A-4,6-DNT [M+NO2] / 4-A-2,6-DNT [M+NO2]
248	C6H3N3O6Cl1	1,3,5-TNB [M+Cl]
257	C3H6N6O6Cl1	RDX [M+Cl]
258	C4H8N3O10	DEGDN [M+NO3]
259	C7H7N4O7	2-A-4,6-DNT [M+NO3] / 4-A-2,6-DNT [M+NO3]
262	C3H5N6O9Cl1	NG [M+Cl]
262	C5H6N4O7	PYX Fragment
268	C3H6N7O8	RDX [M+NO2]
275	C6H3N4O9	1,3,5-TNB [M+NO3]
284	C3H6N7O9	RDX [M+NO3]
287	C7H5N5O8	Tetryl [M]
289	C3H5N4O12	NG [M+NO3]
289	C7H5N4O9	TNT [M+NO3]
301	C4H5N4O12	ETN [M-H]
303	C4H7N4O12	EGDN [2M-H]
315	C5H7N4O12	PETN [M-H]
331	C4H8N8O8Cl1	HMX [M+Cl]
337	C4H6N4O12Cl1	ETN [M+Cl]
342	C4H8N9O10	HMX [M+NO2]
347	C4H5N5O14	ETN [M+NO2-H]
349	C7H5N6O11	Tetryl [M*+NO2+NO3-H]
351	C5H8N4O12Cl1	PETN [M+Cl]
358	C4H8N9O11	HMX [M+NO3]
362	C5H8N5O14	PETN [M+NO2]
363	C7H11N4O8	2,4-DNT [2M-H] / 2,6-DNT [2M-H]
364	C4H6N5O15	ETN [M+NO3]
378	C5H8N5O15	PETN [M+NO3]
391	C8H15N2O14	DEGDN [2M-H]
393	C14H13N6O8	2-A-4,6-DNT [2M-H] / 4-A-2,6-DNT [2M-H]
429	C14H14N6O8Cl1	2-A-4,6-DNT [2M+Cl] / 4-A-2,6-DNT [2M+Cl]
440	C14H14N7O10	2-A-4,6-DNT [2M+NO2] / 4-A-2,6-DNT [2M+NO2]
451	C10H16N8O24	PETN [2M-H]
456	C14H14N7O11	2-A-4,6-DNT [2M+NO3] / 4-A-2,6-DNT [2M+NO3]
479	C6H12N12O12Cl1	RDX [2M+Cl]
489	C6H10N6O6Cl1	NG [2M+Cl]
490	C6H12N13O14	RDX [2M+NO2]
506	C6H12N13O15	RDX [2M+NO3]
620	C17H6N11O16	PYX [M-H]

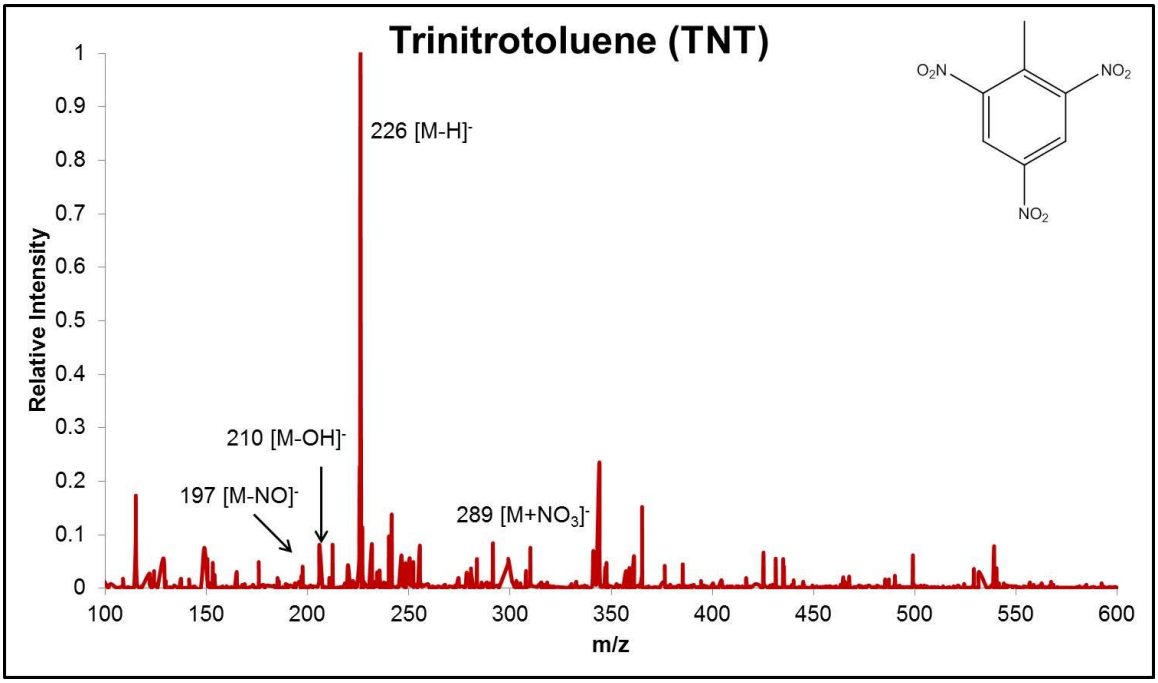

Figure A4.1 A representative mass spectrum of TNT analyzed by DESI-MS under the optimized parameters for negative mode.

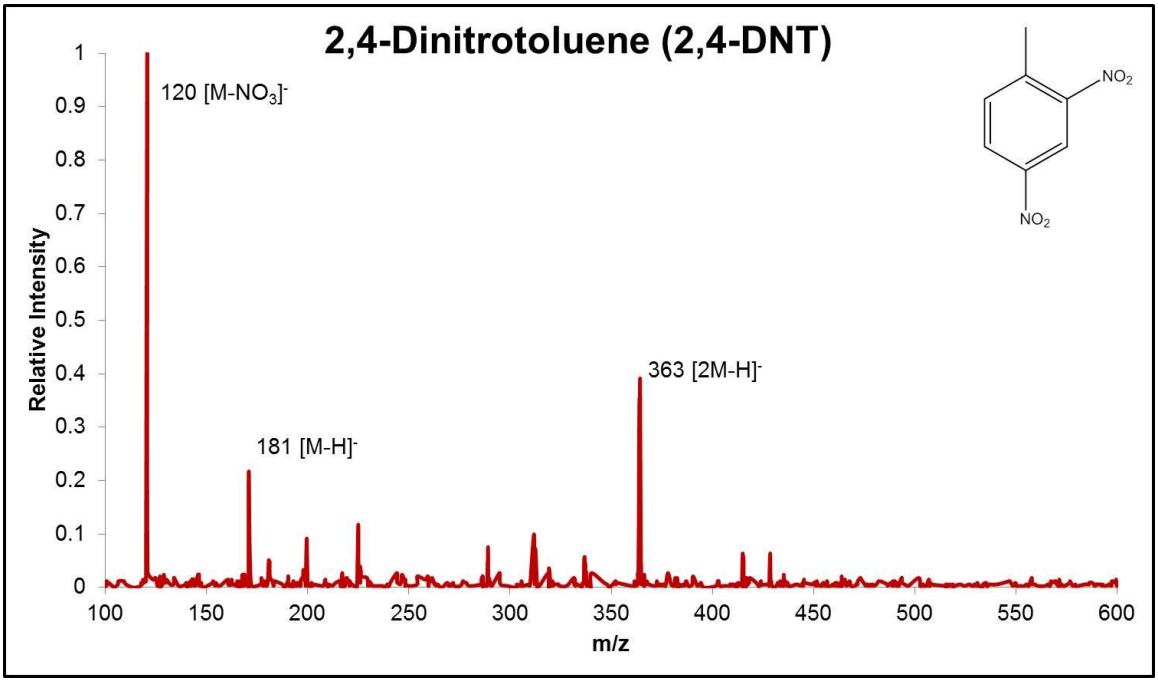

Figure A4.2 A representative mass spectrum of 2,4-DNT analyzed by DESI-MS under the optimized parameters for negative mode.

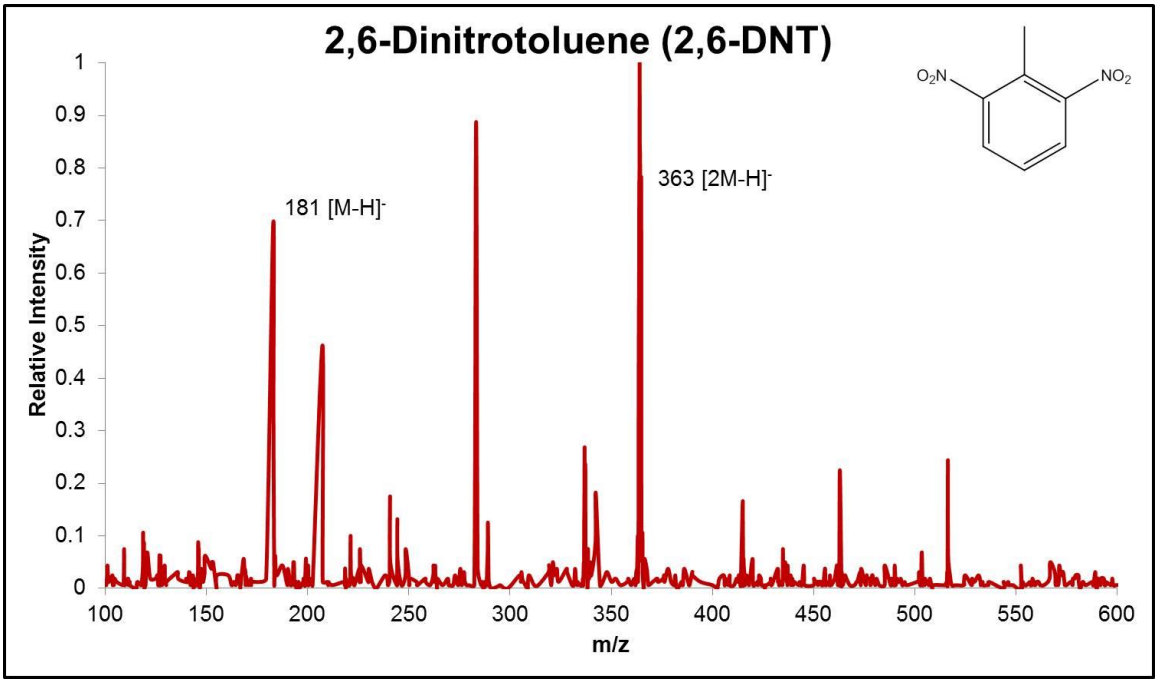

Figure A4.3 A representative mass spectrum of 2,6-DNT analyzed by DESI-MS under the optimized parameters for negative mode.

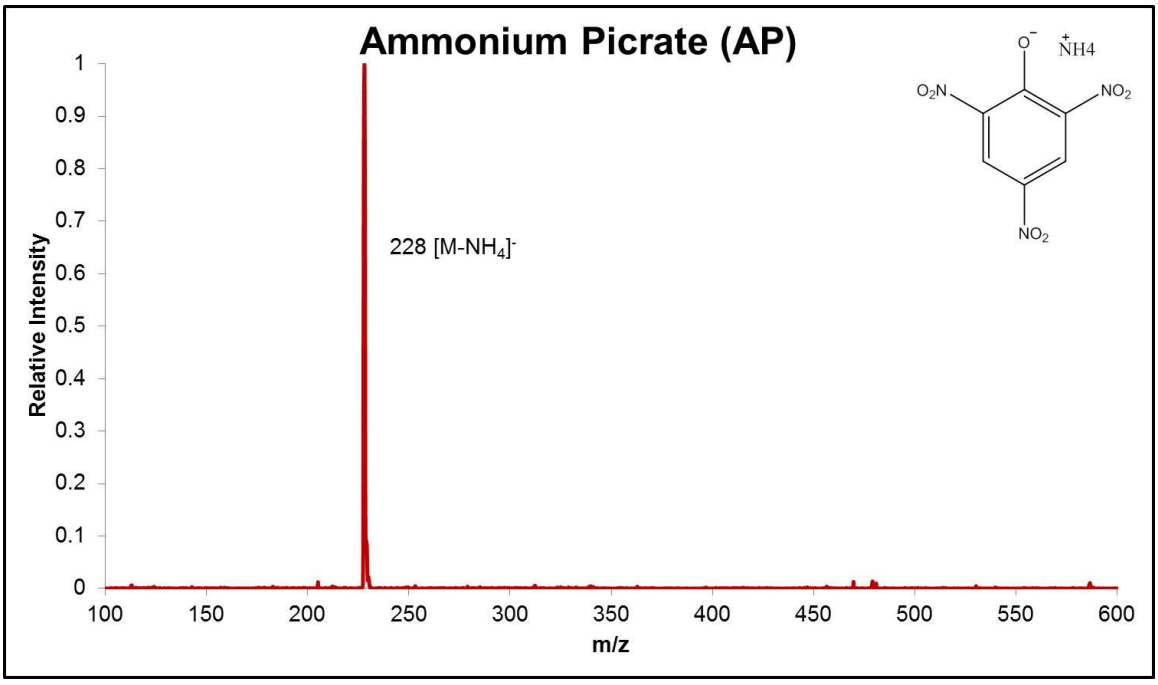

Figure A4.4 A representative mass spectrum of AP analyzed by DESI-MS under the optimized parameters for negative mode.

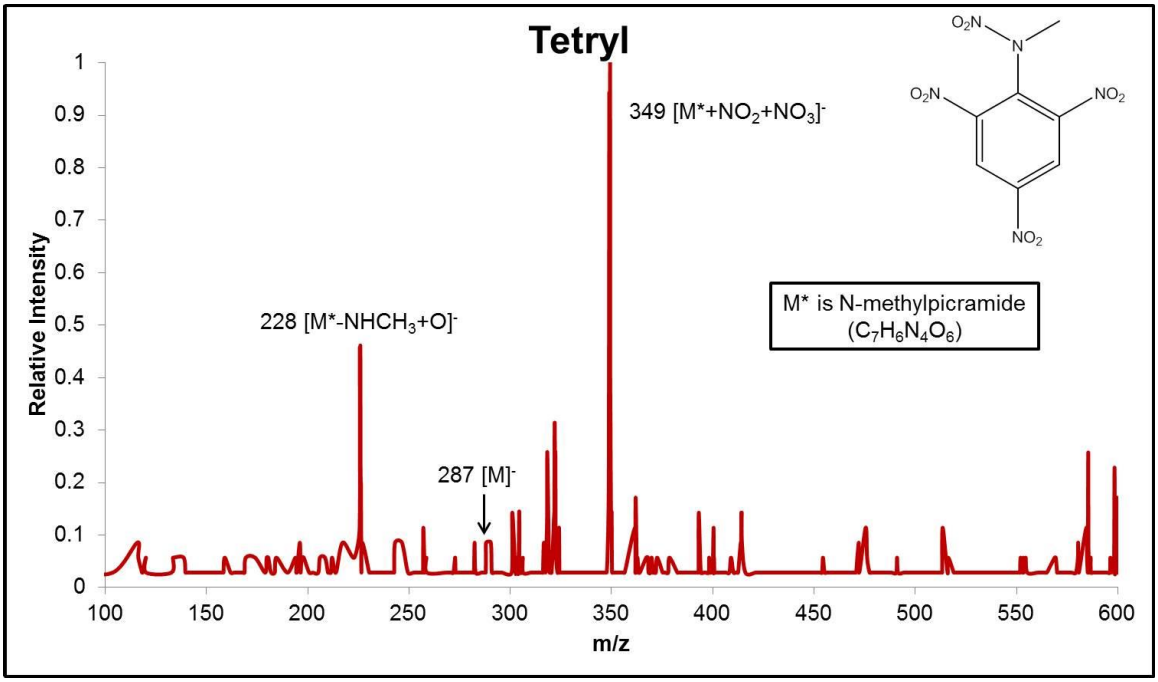

Figure A4.5 A representative mass spectrum of Tetryl analyzed by DESI-MS under the optimized parameters for negative mode.

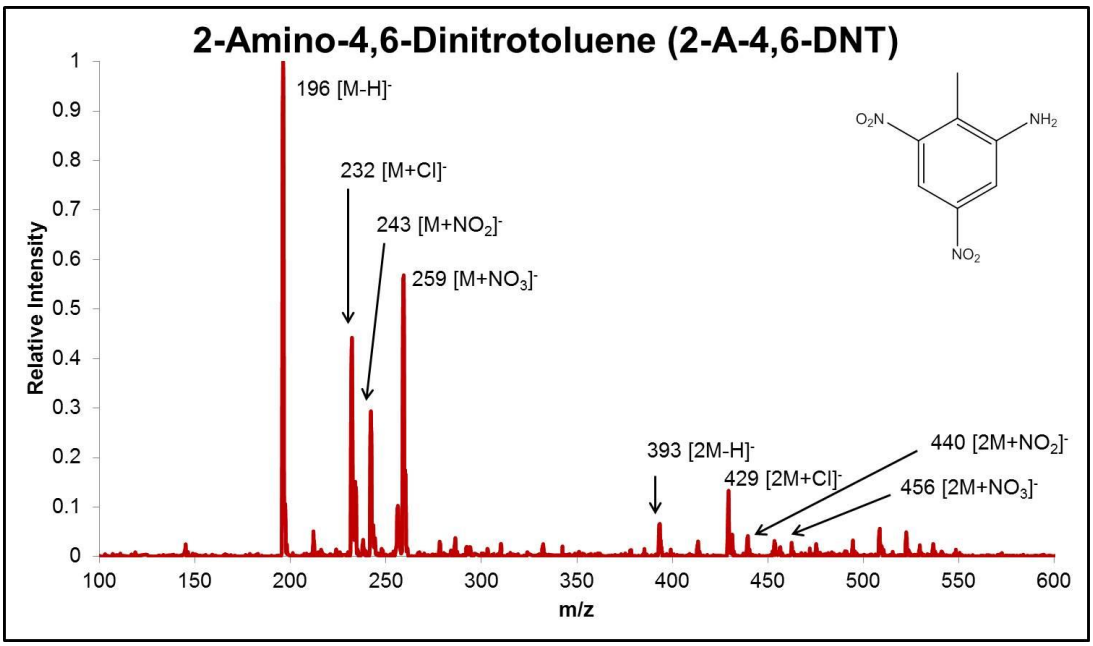

Figure A4.6 A representative mass spectrum of 2-A-4,6-DNT analyzed by DESI-MS under the optimized parameters for negative mode.

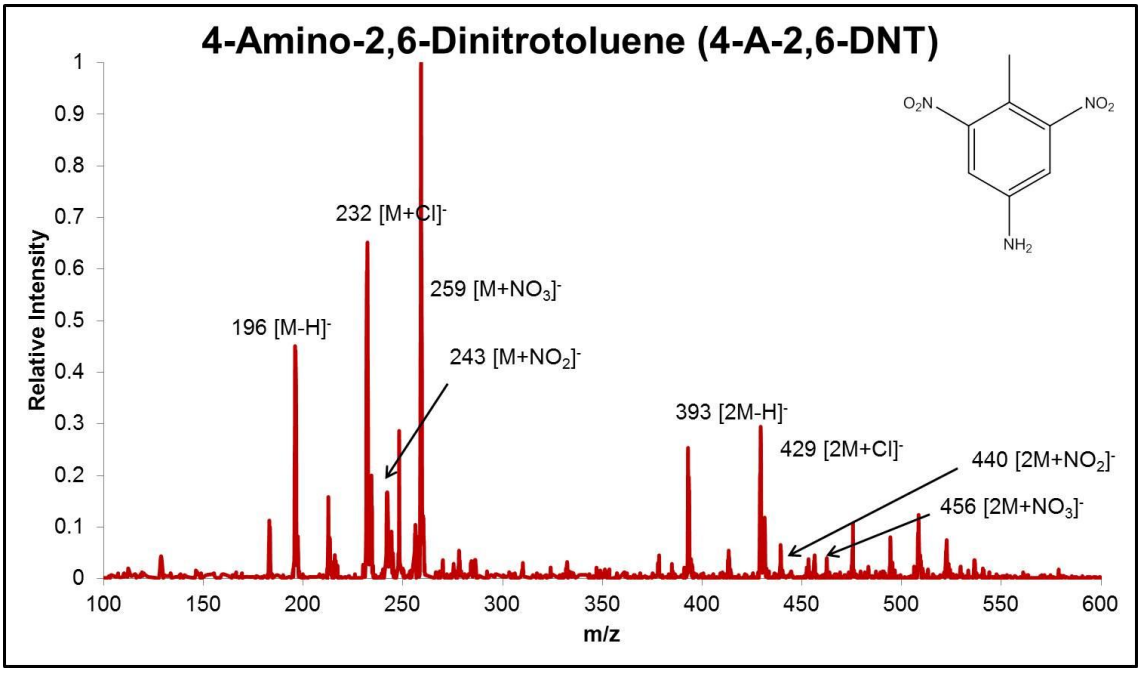

Figure A4.7 A representative mass spectrum of 4-A-2,6-DNT analyzed by DESI-MS under the optimized parameters for negative mode.

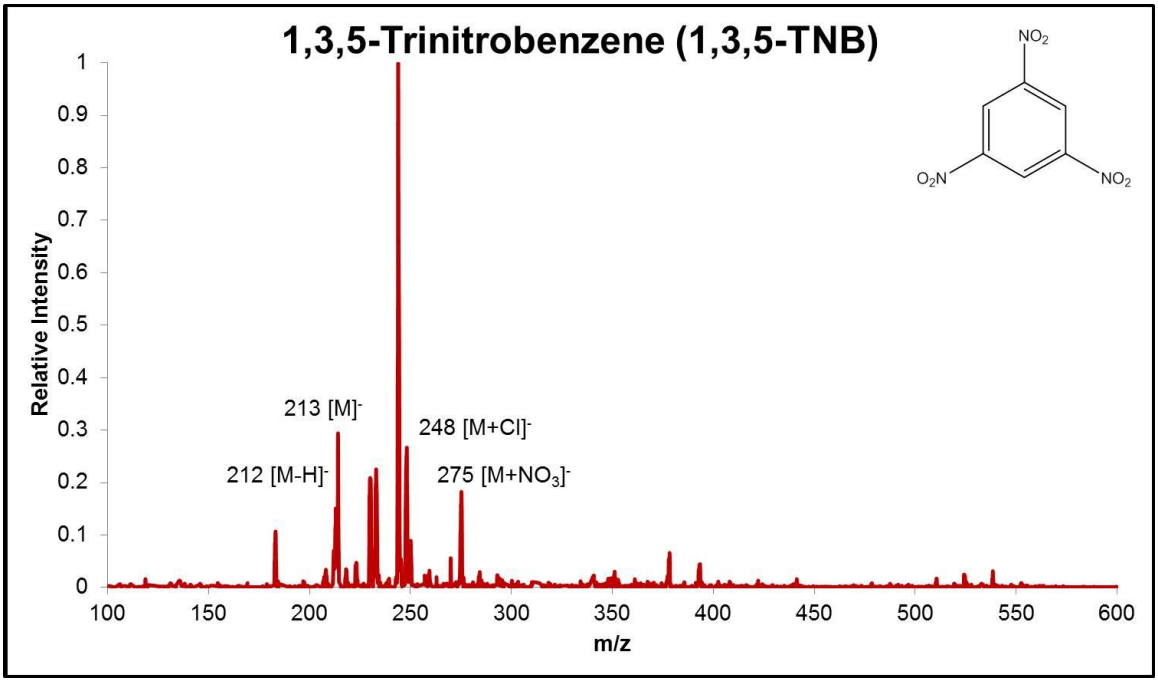

Figure A4.8 A representative mass spectrum of 1,3,5-TNB analyzed by DESI-MS under the optimized parameters for negative mode.

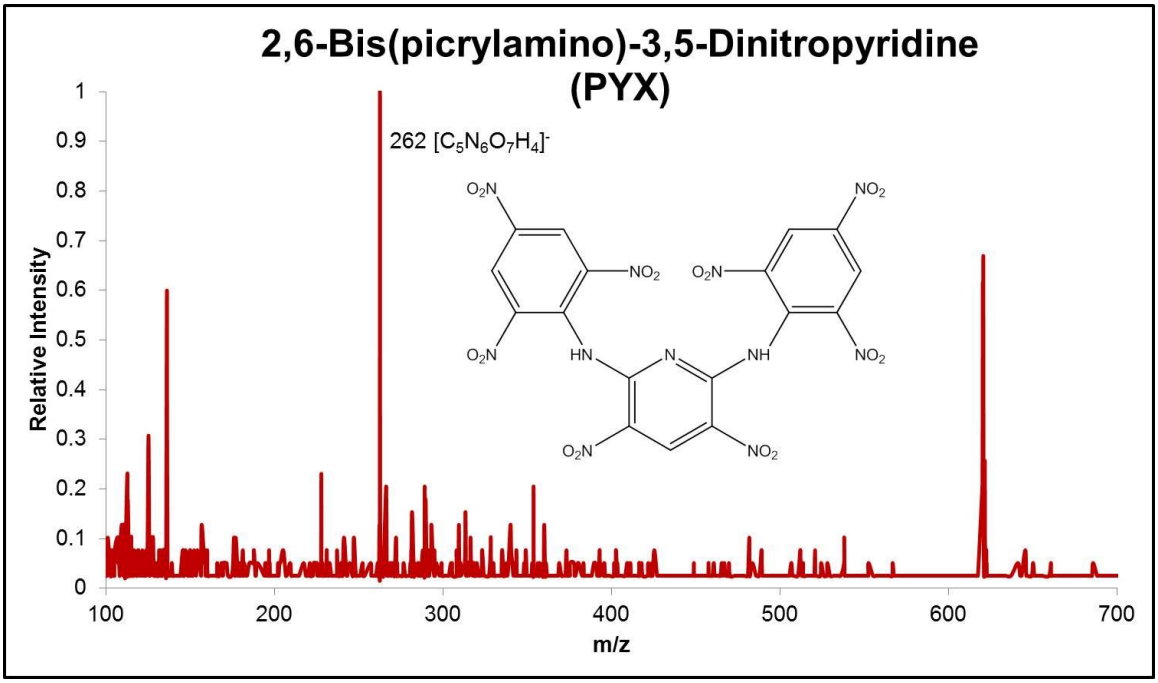

Figure A4.9 A representative mass spectrum of PYX analyzed by DESI-MS under the optimized parameters for negative mode.

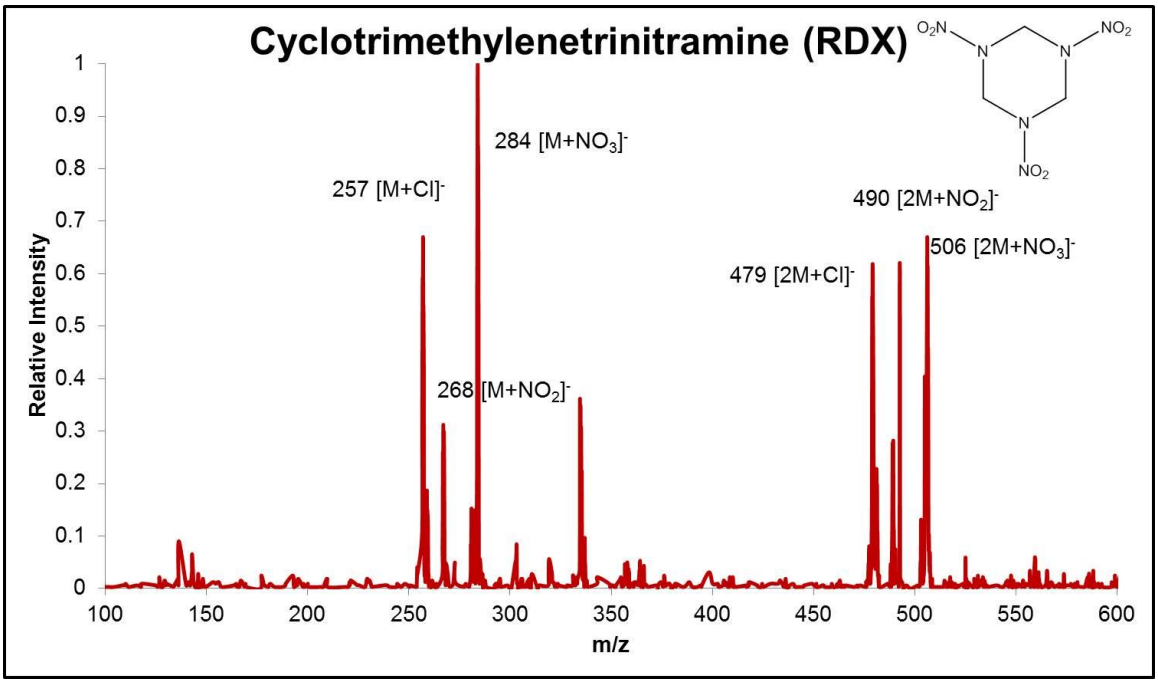

Figure A4.10 A representative mass spectrum of RDX analyzed by DESI-MS under the optimized parameters for negative mode.

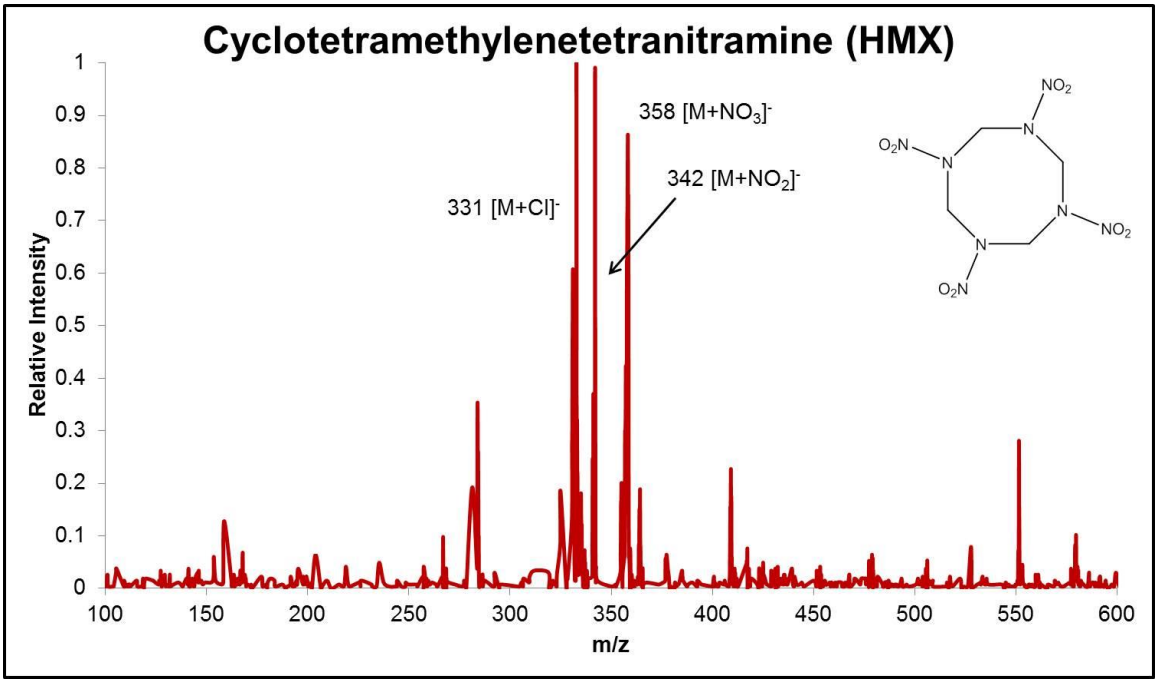

Figure A4.11 A representative mass spectrum of HMX analyzed by DESI-MS under the optimized parameters for negative mode.

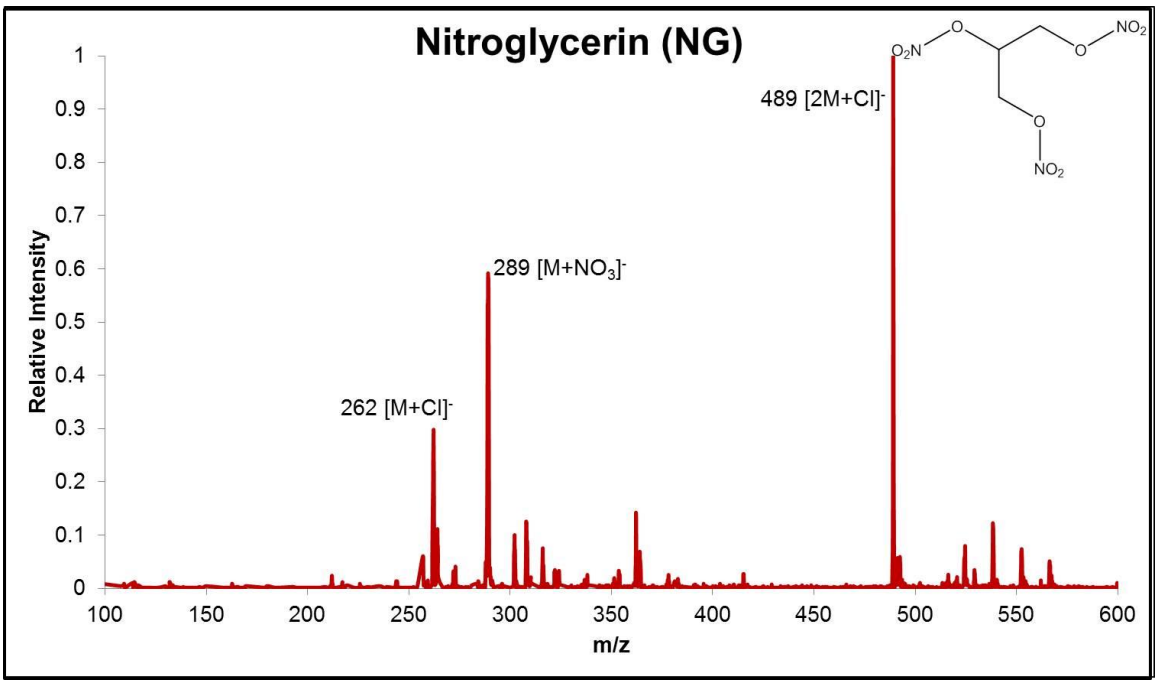

Figure A4.12 A representative mass spectrum of NG analyzed by DESI-MS under the optimized parameters for negative mode.

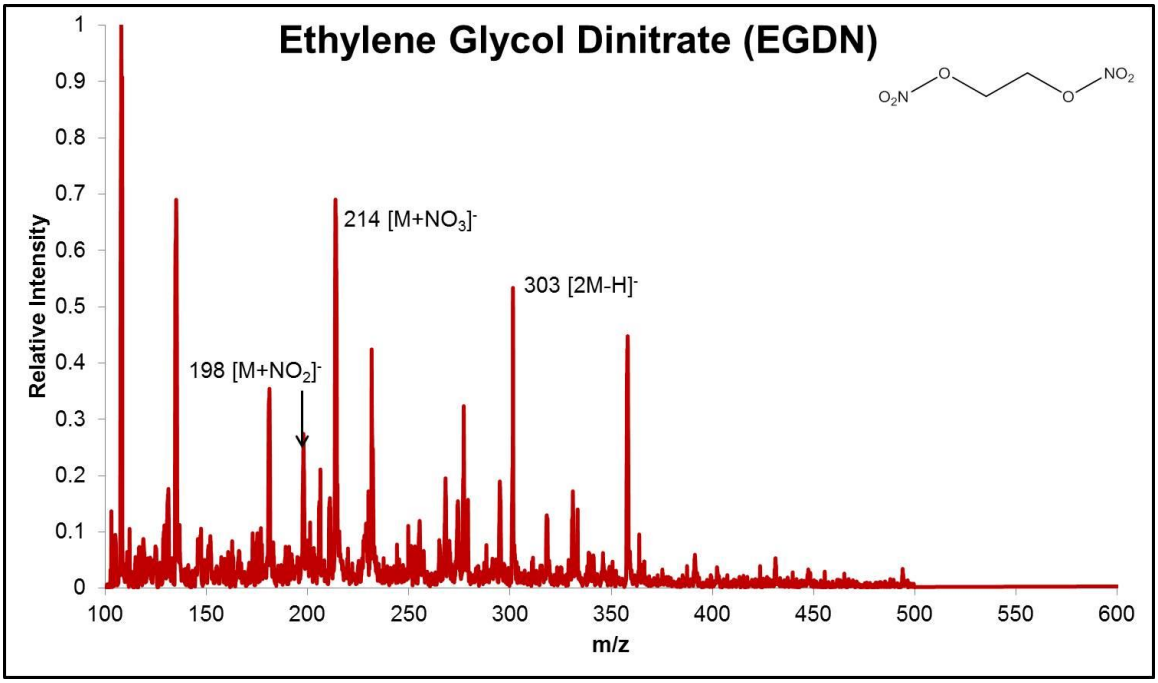

Figure A4.13 A representative mass spectrum of EGDN analyzed by DESI-MS under the optimized parameters for negative mode.

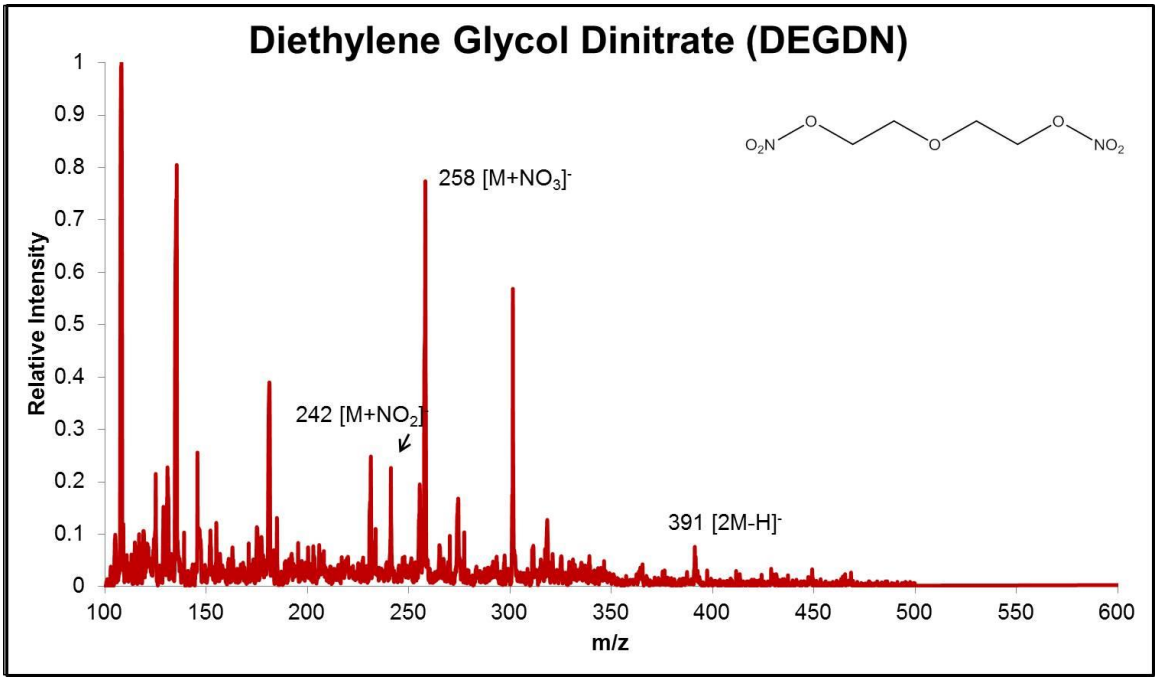

Figure A4.14 A representative mass spectrum of DEGDN analyzed by DESI-MS under the optimized parameters for negative mode.

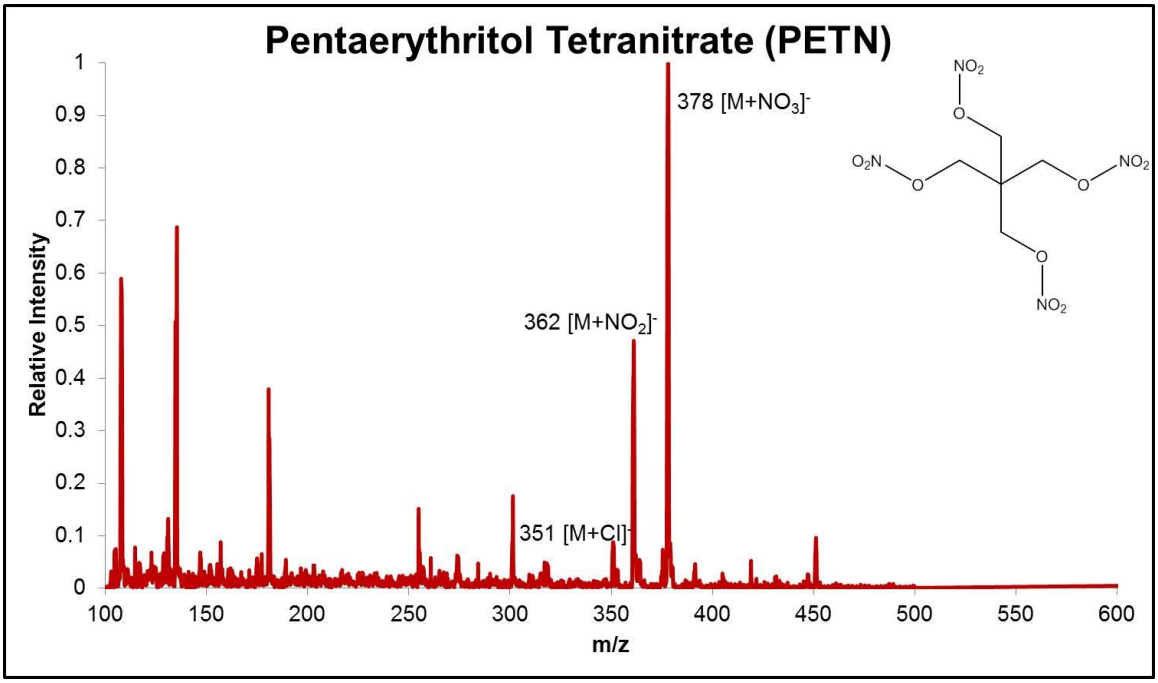

Figure A4.15 A representative mass spectrum of PETN analyzed by DESI-MS under the optimized parameters for negative mode.

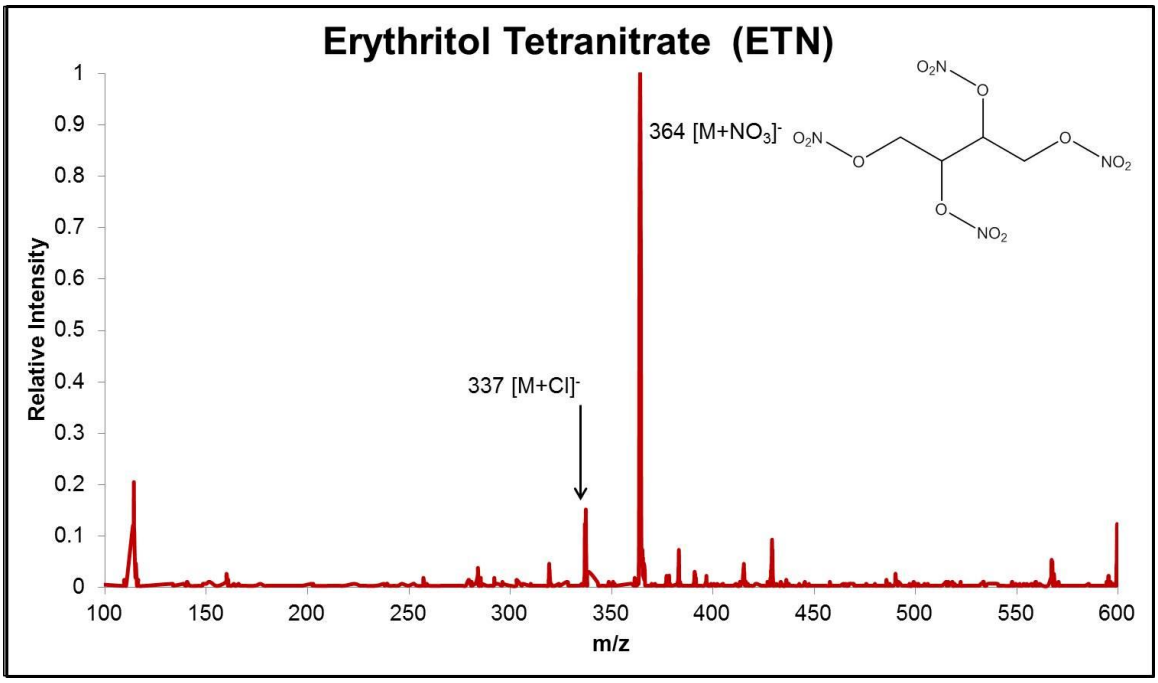

Figure A4.16 A representative mass spectrum of ETN analyzed by DESI-MS under the optimized parameters for negative mode.

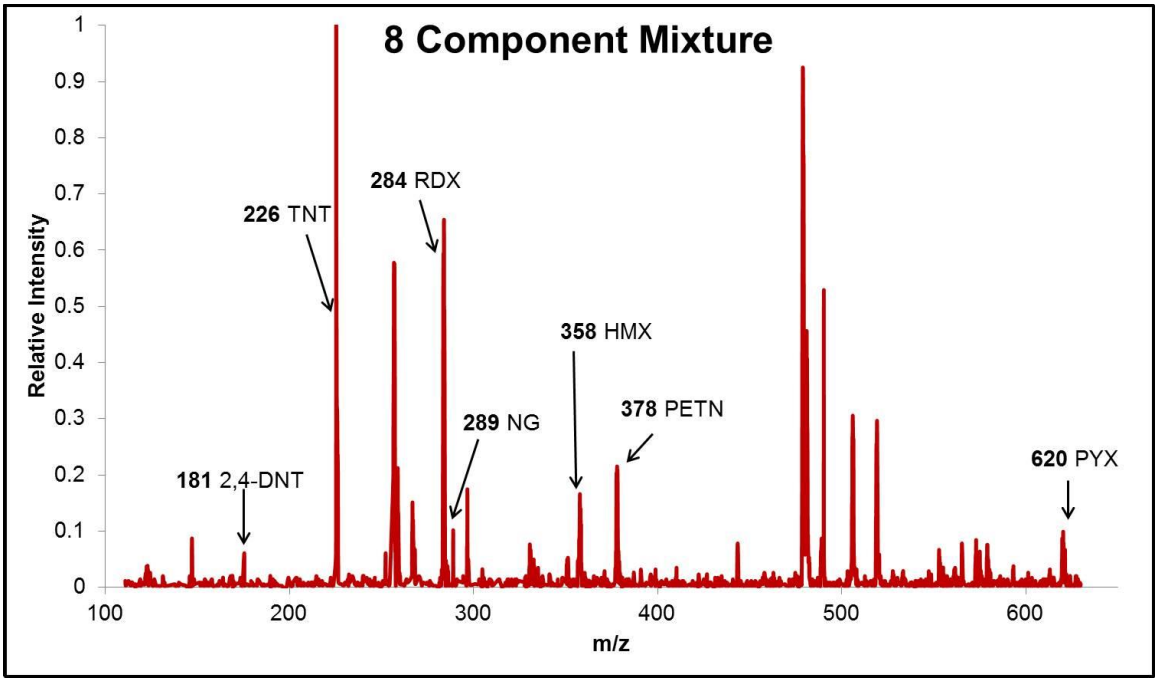

Figure A4.17 A representative mass spectrum of 8 component mixture used for determining normalized yields by DESI-MS under the optimized parameters.

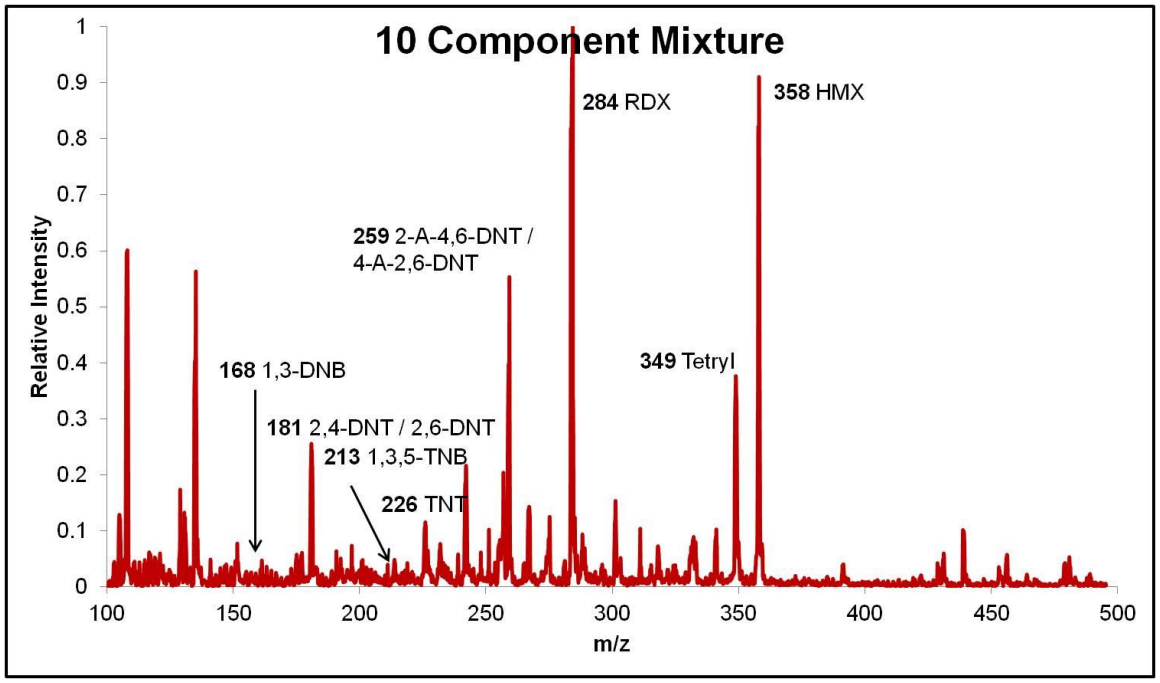

Figure A4.18 A representative mass spectrum of 10 component mixture analyzed by DESI-MS under the optimized parameters for negative mode.

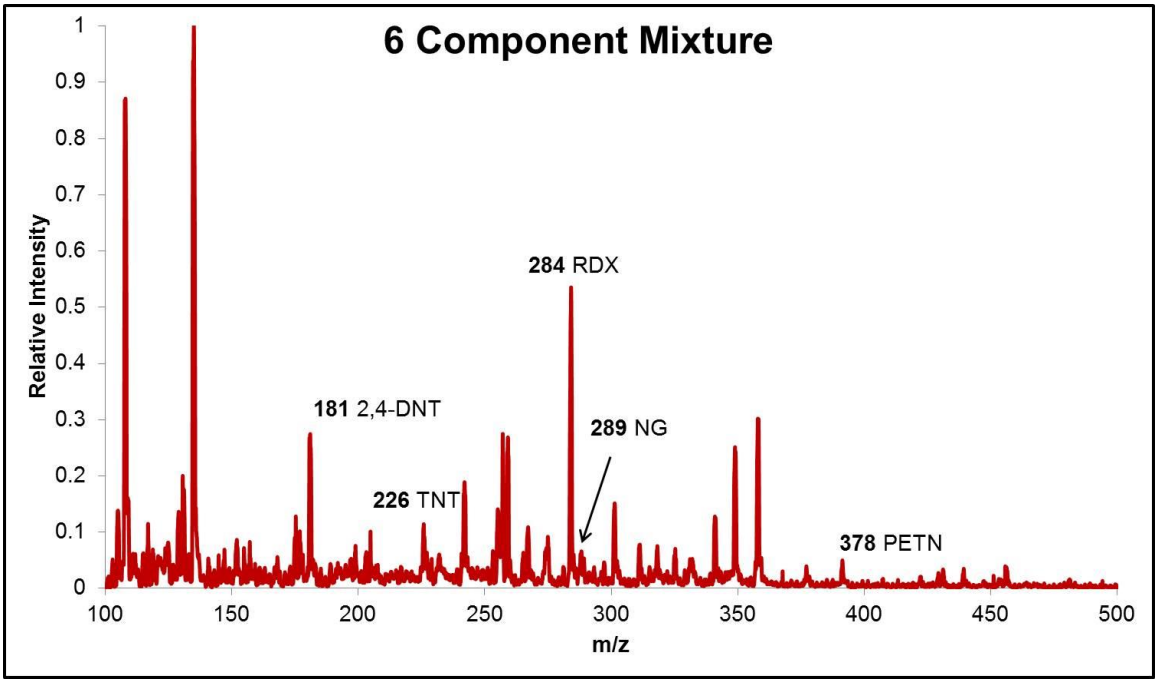

Figure A4.19 A representative mass spectrum of 6 component mixture analyzed by DESI-MS under the optimized parameters for negative mode.

Section A4.2 LTP-MS Search Lists and Representative Mass Spectra

Table A4.2 A copy of the negative ionization mode LTP-MS search list developed for the explosives cross-comparison study.

Mass	Formula	Assignment
181	C7H5N2O4	TNT [M-NO2] / Tetryl [M*-NO2-CH3] / 2,4-DNT [M-H] / 2,6-DNT [M-H]
183	C6H3N2O5	1,3-DNB [M+O-H]
197	C7H5N2O5	TNT [M-NO] / 2,4-DNT [M-H+O] / 2,6-DNT [M-H+O]
199	C6H3N2O6	AP [M-NO2NH4+OH]
210	C7H4N3O5	TNT [M-OH]
213	C6H3N3O6	1,3,5-TNB [M]
214	C2H4N3O9	EGDN [M+NO3]
226	C7H4N3O6	TNT [M-H]
227	C3H5N3O9	NG [M]
228	C6H2N3O7	AP [M-NH4] / Tetryl [M*-NH2CH3+O]
241	C7H5N4O6	Tetryl [M*-H]
244	C3H6N3O10	NG [M+OH]
257	C7H5N4O7	Tetryl [M*-H+O]
258	C4H8N3O10	DEGDN [M+NO3]
259	C7H7N4O7	2-A-4,6-DNT [M+NO3] / 4-A-2,6-DNT [M+NO3]
268	C3H6N7O8	RDX [M+NO2]
284	C3H6N7O9	RDX [M+NO3]
289	C3H5N4O12	NG [M+NO3]
302	C4H6N4O12	ETN [M]
319	C4H7N4O13	ETN [M+OH]
333	C5H9N4O13	PETN [M+OH]
342	C4H8N9O10	HMX [M+NO2]
349	C7H5N6O11	Tetryl [M*+NO2+NO3]
358	C4H8N9O11	HMX [M+NO3]
362	C5H8N5O14	PETN [M+NO2]
364	C4H6N5O15	ETN [M+NO3]
378	C5H8N5O15	PETN [M+NO3]
422	C13H8N7O10	Tetryl [2M-NO2CH4]
490	C6H12N13O14	RDX [2M+NO2]

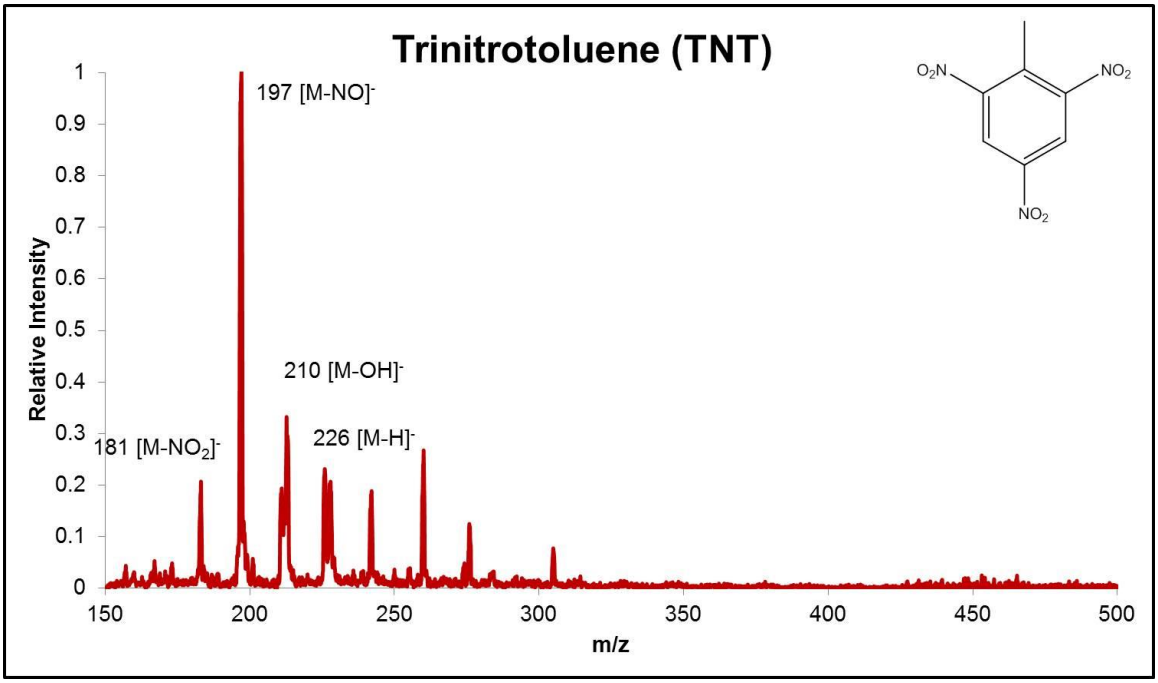

Figure A4.20 A representative mass spectrum of TNT analyzed by LTP-MS under the optimized parameters for negative mode.

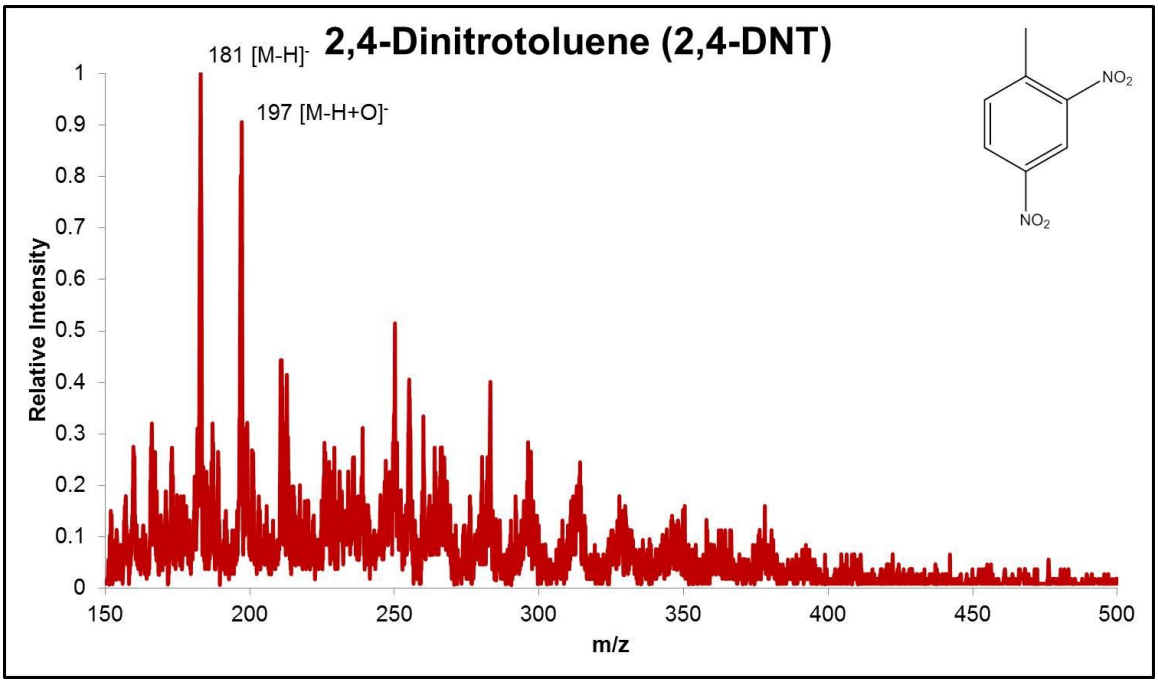

Figure A4.21 A representative mass spectrum of 2,4-DNT analyzed by LTP-MS under the optimized parameters for negative mode.

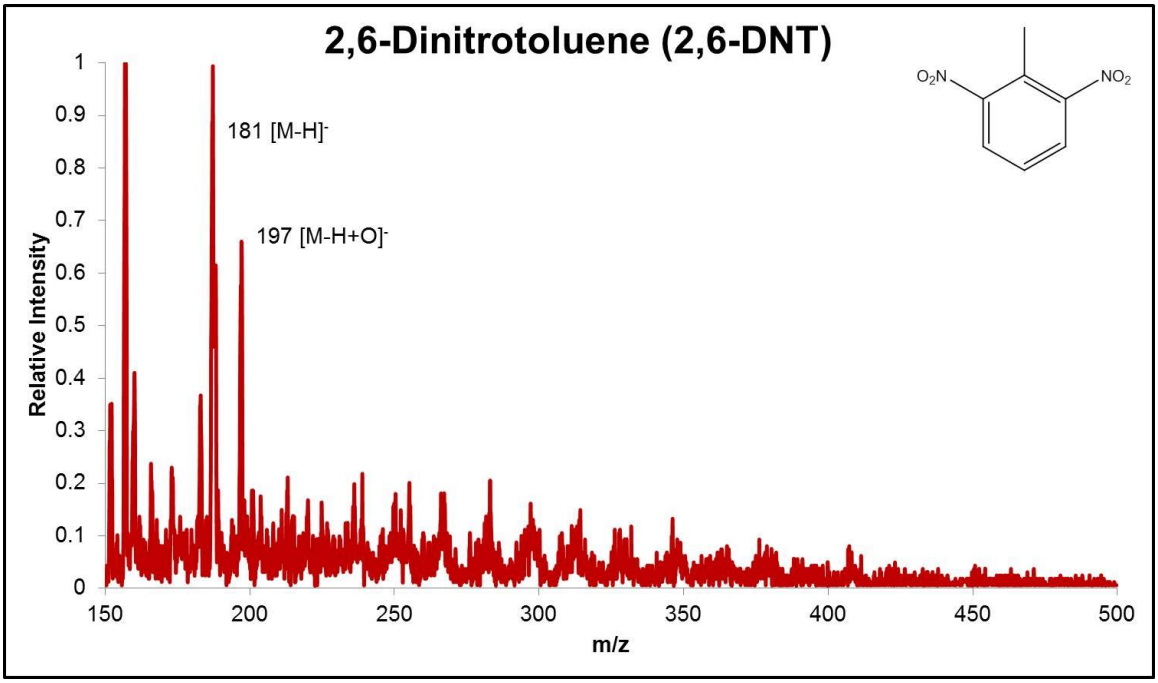

Figure A4.22 A representative mass spectrum of 2,6-DNT analyzed by LTP-MS under the optimized parameters for negative mode.

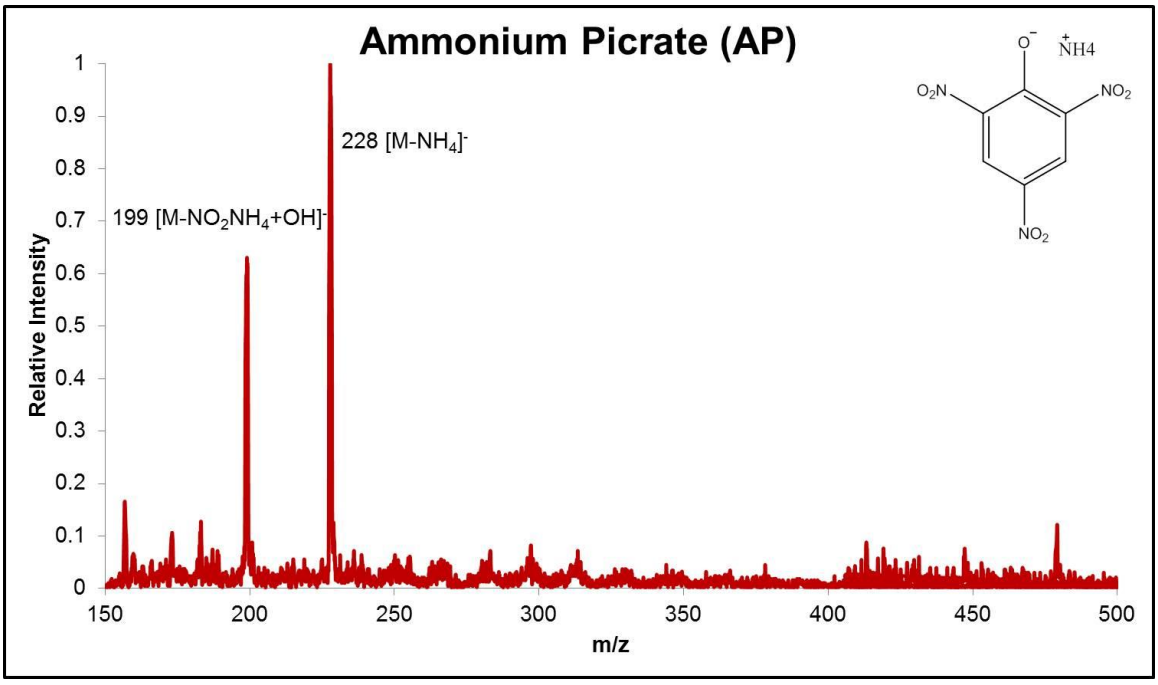

Figure A4.23 A representative mass spectrum of AP analyzed by LTP-MS under the optimized parameters for negative mode.

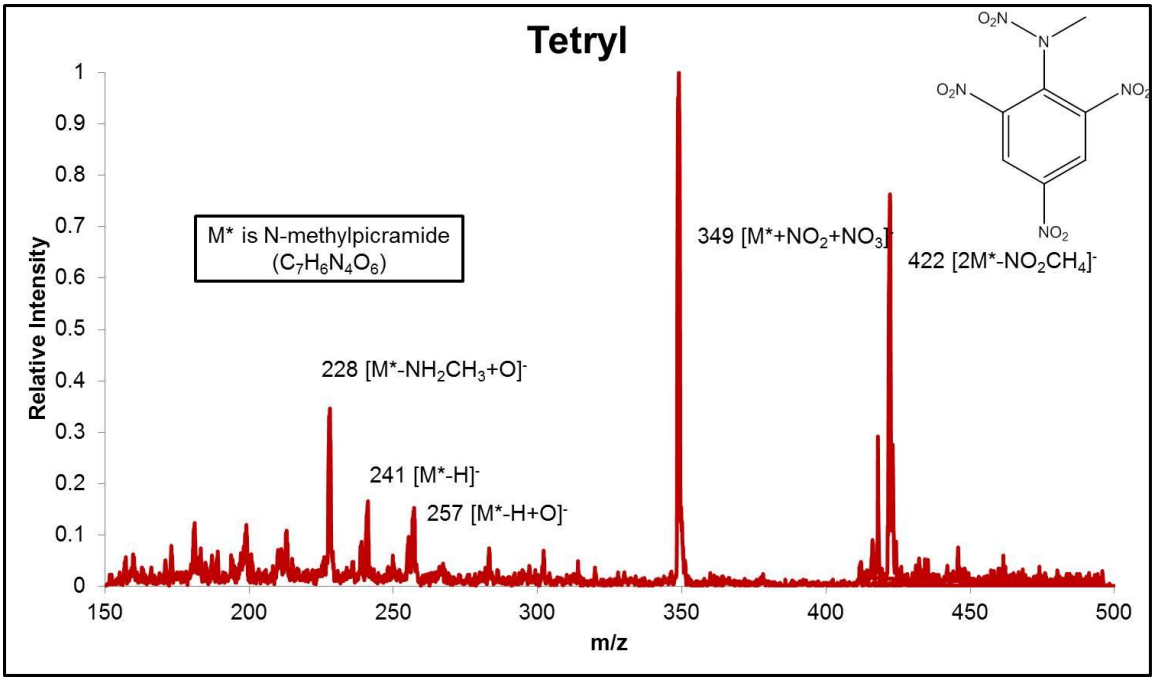

Figure A4.24 A representative mass spectrum of Tetryl analyzed by LTP-MS under the optimized parameters for negative mode.

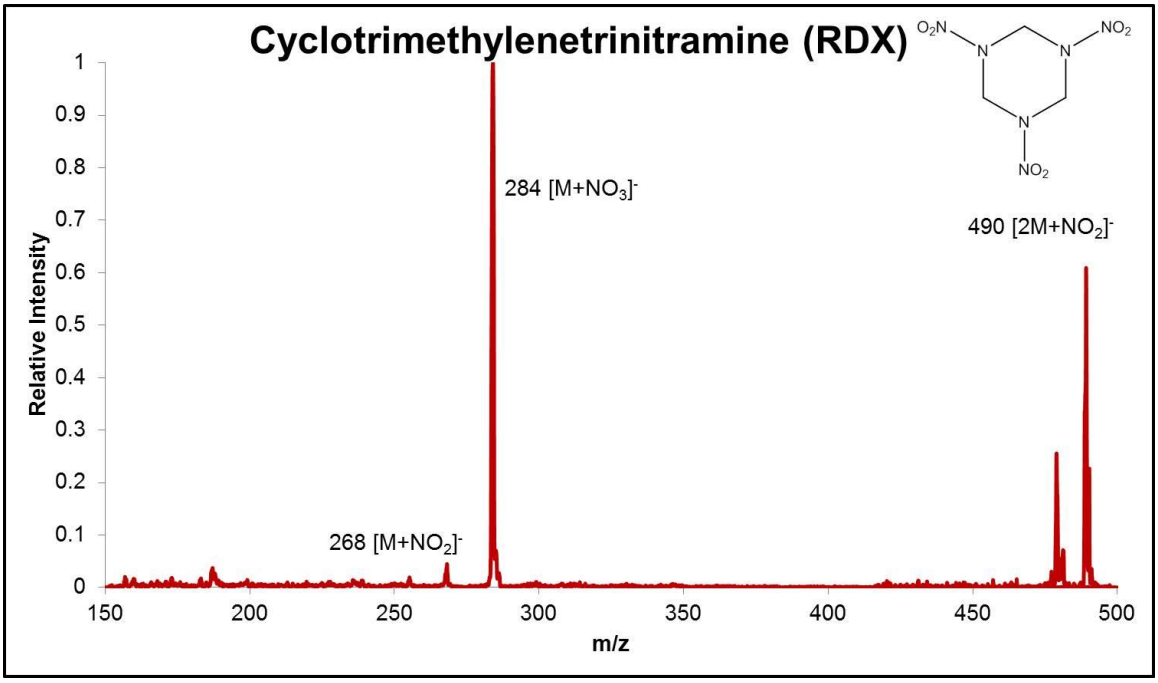

Figure A4.25 A representative mass spectrum of RDX analyzed by LTP-MS under the optimized parameters for negative mode.

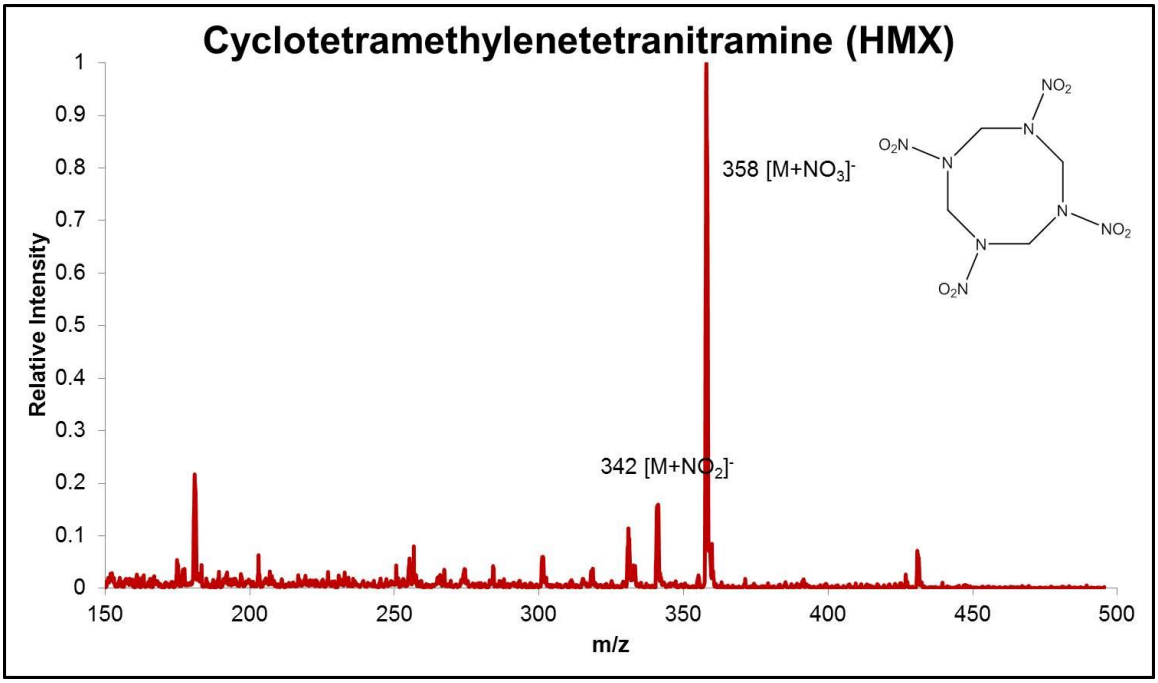

Figure A4.26 A representative mass spectrum of HMX analyzed by LTP-MS under the optimized parameters for negative mode.

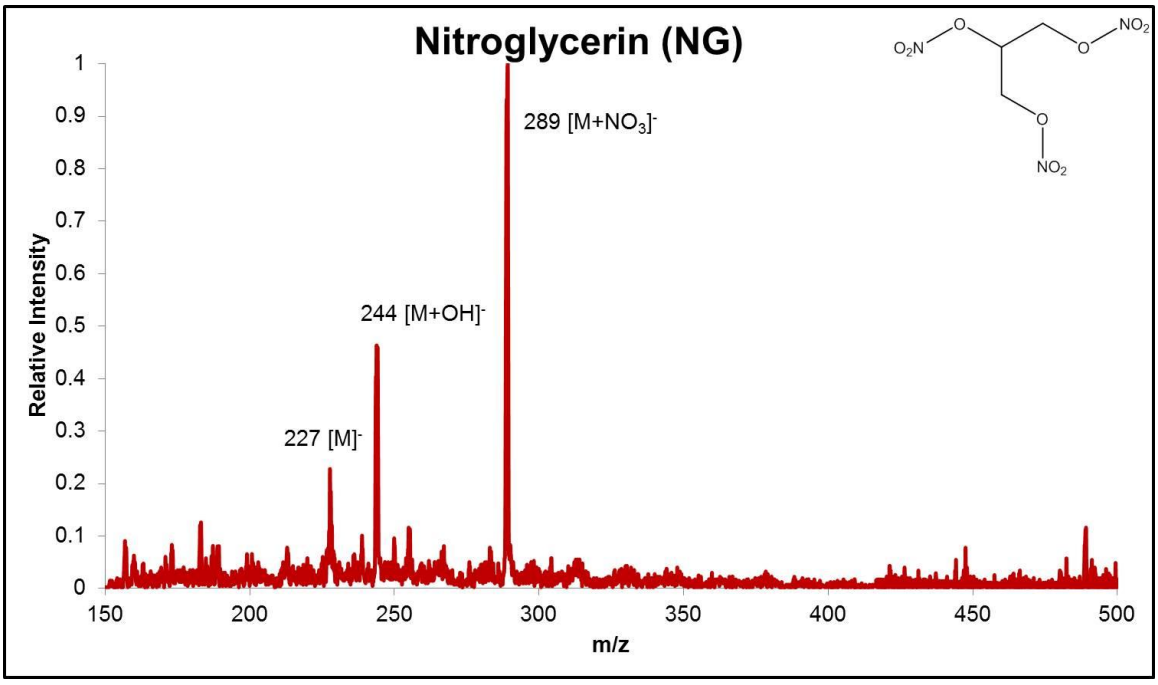

Figure A4.27 A representative mass spectrum of NG analyzed by LTP-MS under the optimized parameters for negative mode.

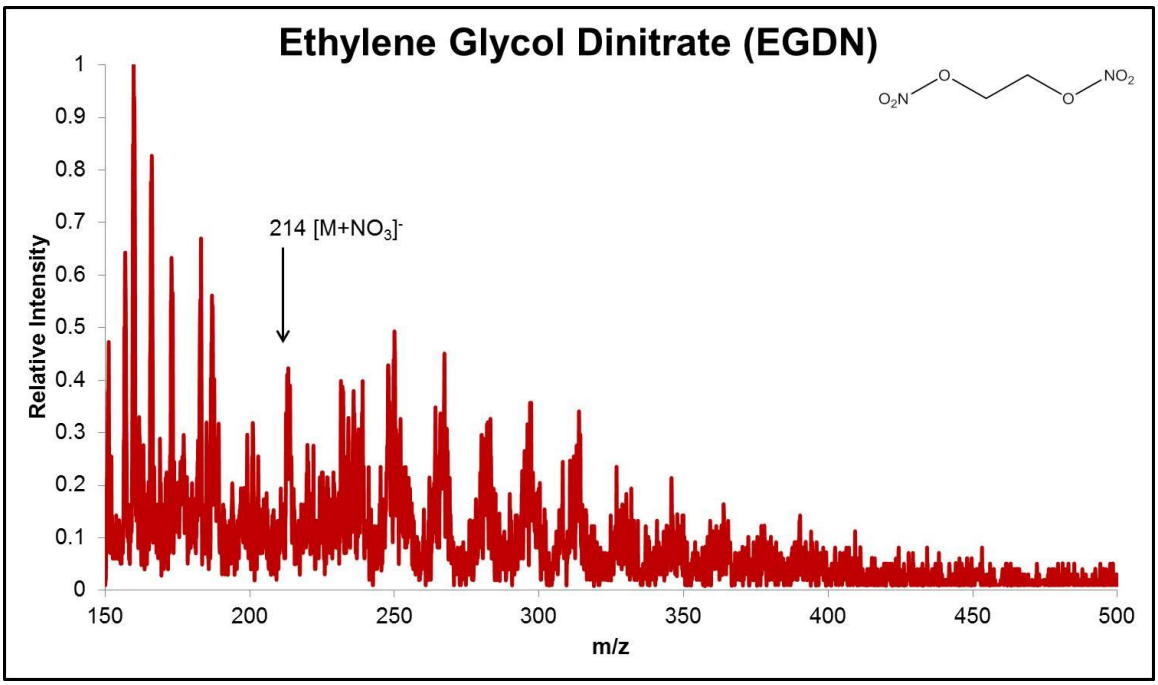

Figure A4.28 A representative mass spectrum of EGDN analyzed by LTP-MS under the optimized parameters for negative mode.

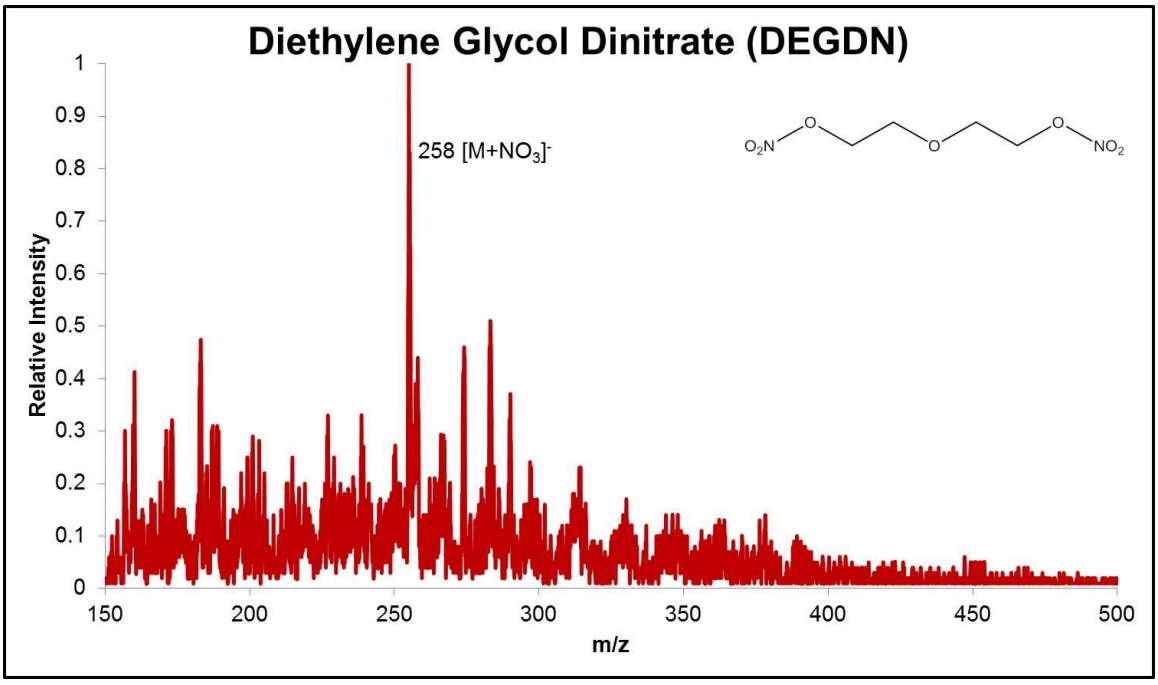

Figure A4.29 A representative mass spectrum of DEGDN analyzed by LTP-MS under the optimized parameters for negative mode.

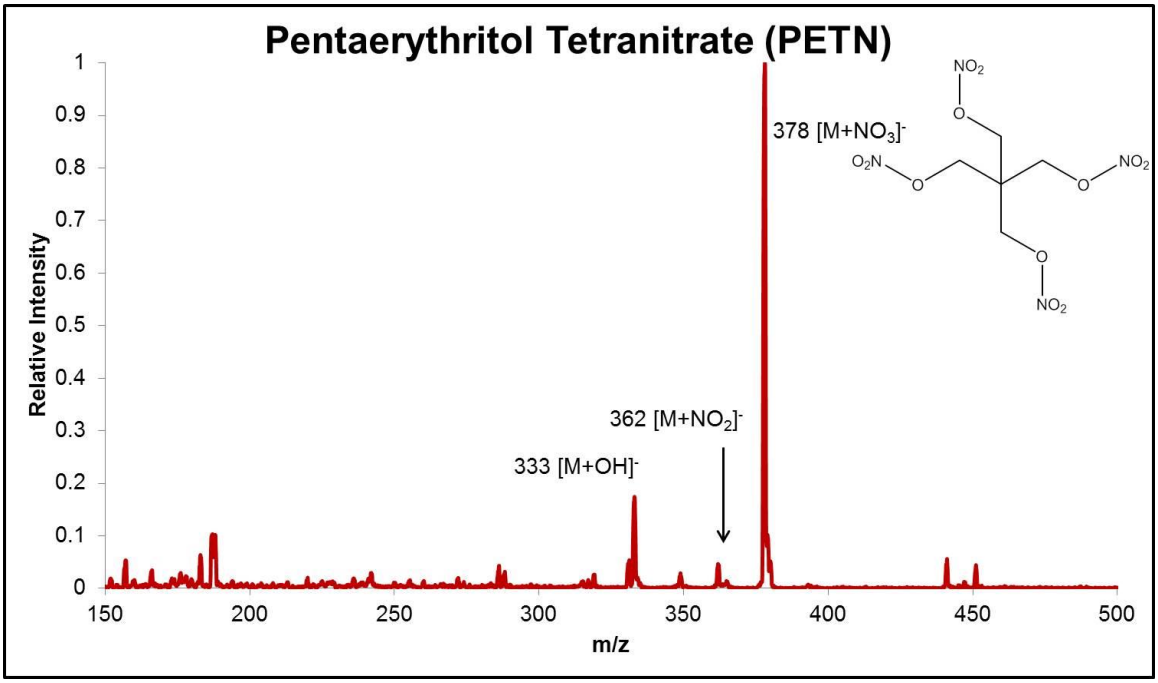

Figure A4.30 A representative mass spectrum of PETN analyzed by LTP-MS under the optimized parameters for negative mode.

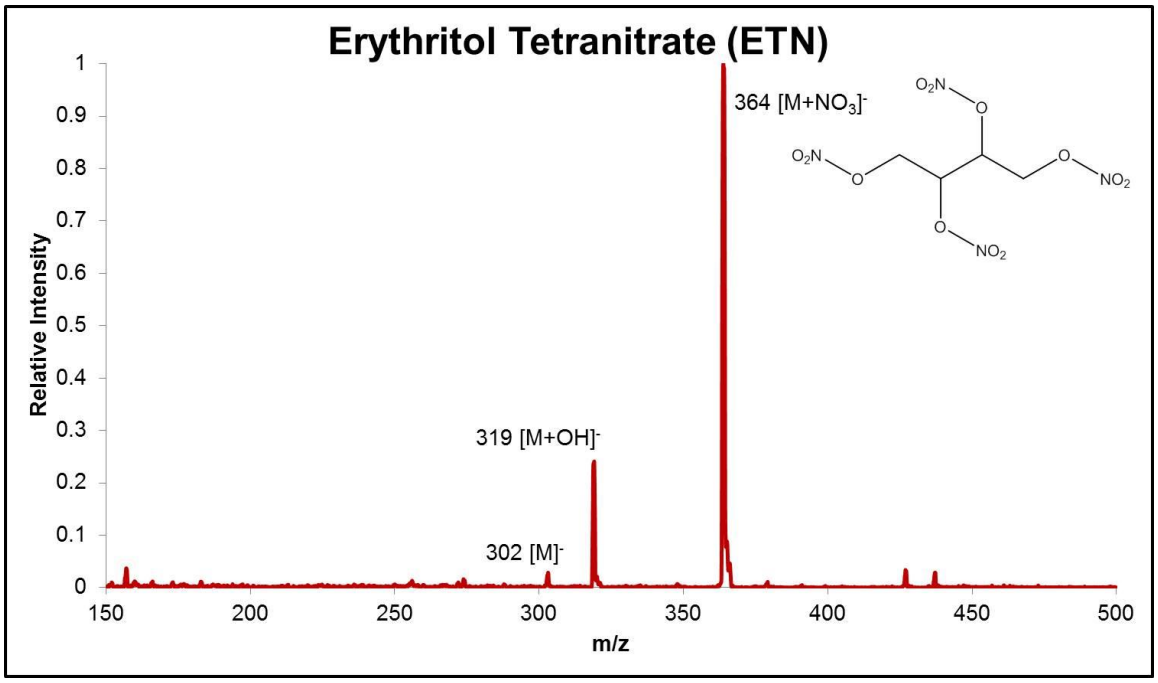

Figure A4.31 A representative mass spectrum of ETN analyzed by LTP-MS under the optimized parameters for negative mode.

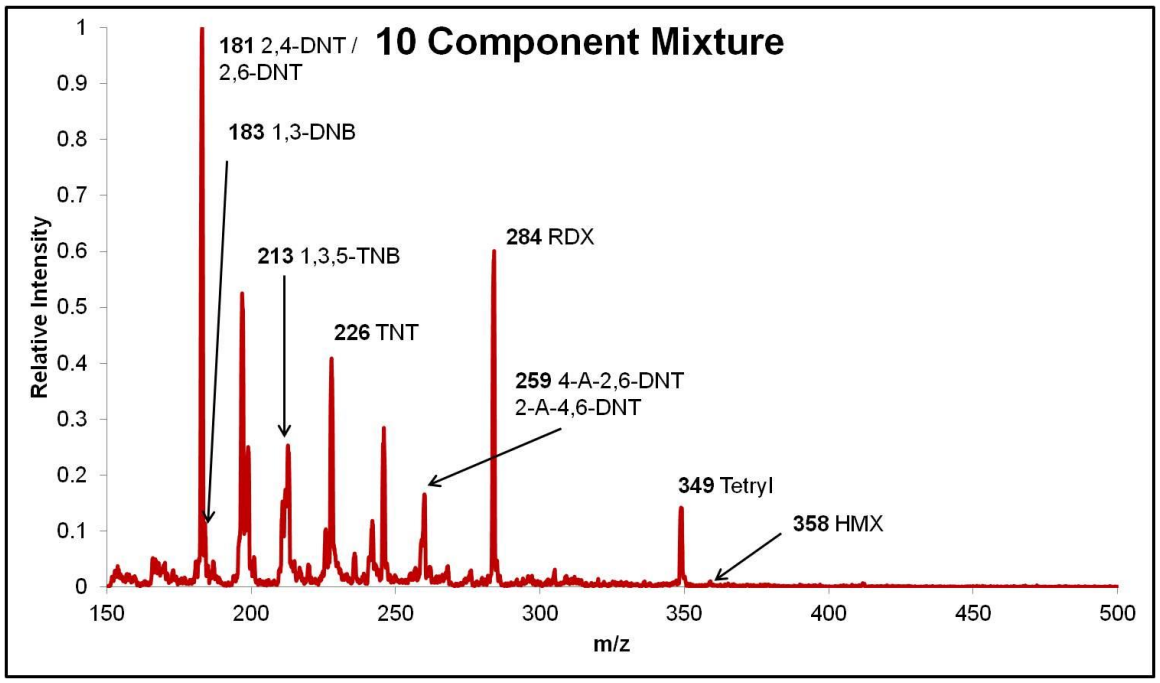

Figure A4.32 A representative mass spectrum of 10 component mixture analyzed by LTP-MS under the optimized parameters for negative mode.

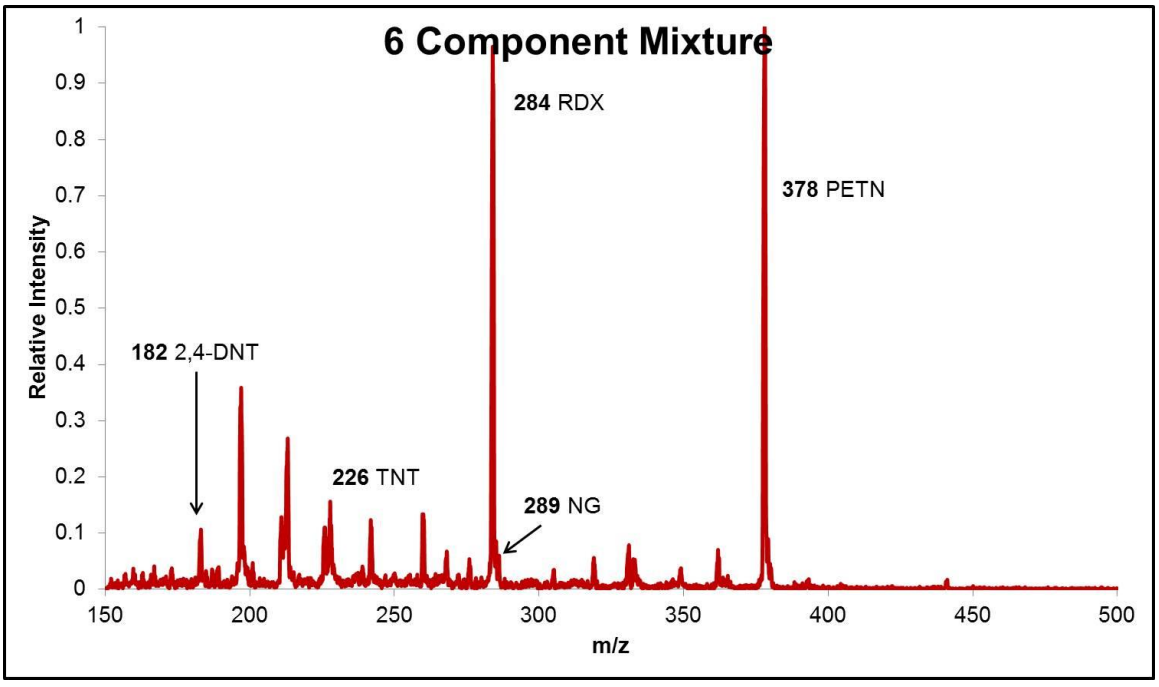

Figure A4.33 A representative mass spectrum of 6 component mixture analyzed by LTP-MS under the optimized parameters for negative mode.

Section A4.3 DEFFI-MS Search Lists and Representative Mass Spectra

Table A4.3 A copy of the negative ionization mode DEFFI-MS search list developed for the explosives cross comparison study

Mass	Formula	Assignment
138	C6H4N1O3	1,3-DNB [M-NO]
181	C7H5N2O4	Tetryl [M*-NO2-CH3] / 2,4-DNT [M-H] / 2,6-DNT [M-H]
196	C7H6N3O4	2-A-4,6-DNT [M-H] / 4-A-2,6-DNT [M-H]
197	C7H5N2O5	2,4-DNT [M-H+O] / 2,6-DNT [M-H+O]
210	C7H4N3O5	TNT [M-OH]
212	C6H2N3O6	1,3,5-TNB [M-H]
213	C6H3N3O6	1,3,5-TNB [M]
214	C2H4N3O9	EGDN [M+NO3]
226	C7H4N3O6	TNT [M-H]
228	C6H2N3O7	AP [M-NH4] Tetryl [M*-NHCH3+O]
230	C6H4N3O7	1,3-DNB [M+NO3]
231	C4H11N2O9	DEGDN [M+2H2O-H]
231	C6H5N3O8	1,3,5-TNB [M+H2O]
232	C7H7N3O4Cl1	2-A-4,6-DNT [M+Cl] / 4-A-2,6-DNT [M+Cl]
243	C7H7N4O6	2-A-4,6-DNT [M+NO2] / 4-A-2,6-DNT [M+NO2]
248	C6H3N3O6Cl1	1,3,5-TNB [M+Cl]
257	C3H6N6O6Cl1	RDX [M+Cl]
258	C4H8N3O10	DEGDN [M+NO3]
259	C7H7N4O7	2-A-4,6-DNT [M+NO3] / 4-A-2,6-DNT [M+NO3]
268	C3H6N7O8	RDX [M+NO2]
275	C6H3N4O9	1,3,5-TNB [M+NO3]
276	C2H4N4O12	EDGN [M+2NO3]
284	C3H6N7O9	RDX [M+NO3]
286	C7H4N5O8	Tetryl [M-H]
289	C3H5N4O12	NG [M+NO3]
306	C12H8N3O7	1,3-DNB [2M-NO]
315	C5H7N4O12	PETN [M-H]
339	C4H8N4O12	EGDN [2M+Cl]
342	C4H8N9O10	HMX [M+NO2]
349	C7H5N6O11	Tetryl [M*+NO2+NO3]
351	C5H8N4O12Cl1	PETN [M+Cl]
358	C4H8N9O11	HMX [M+NO3]
363	C14H11N4O8	2,4-DNT [2M-H] / 2,6-DNT [2M-H]
364	C4H6N5O15	ETN [M+NO3]
366	C4H8N5O15	EGDN [2M+NO3]
378	C5H8N5O15	PETN [M+NO3]

393	C14H13N6O8	2-A-4,6-DNT [2M-H] / 4-A-2,6-DNT [2M-H]
429	C14H14N6O8Cl1	2-A-4,6-DNT [2M+Cl] / 4-A-2,6-DNT [2M+Cl]
437	C12H8N7O14	TNT [2M-OH]
440	C14H14N7O10	2-A-4,6-DNT [2M+NO2] / 4-A-2,6-DNT [2M+NO2]
456	C14H14N7O11	2-A-4,6-DNT [2M+NO3] / 4-A-2,6-DNT [2M+NO3]
474	C12H8N7O14	AP [2M-NH4]
479	C6H12N12O12Cl1	RDX [2M+Cl]
490	C6H12N13O14	RDX [2M+NO2]
500	C14H10N7O14	TNT [2M+NO2]
506	C6H12N13O15	RDX [2M+NO3]
620	C17H6N11O16	PYX [M-H]
636	C14H10N11O19	Tetryl [M+M*+NO2+NO3]

.

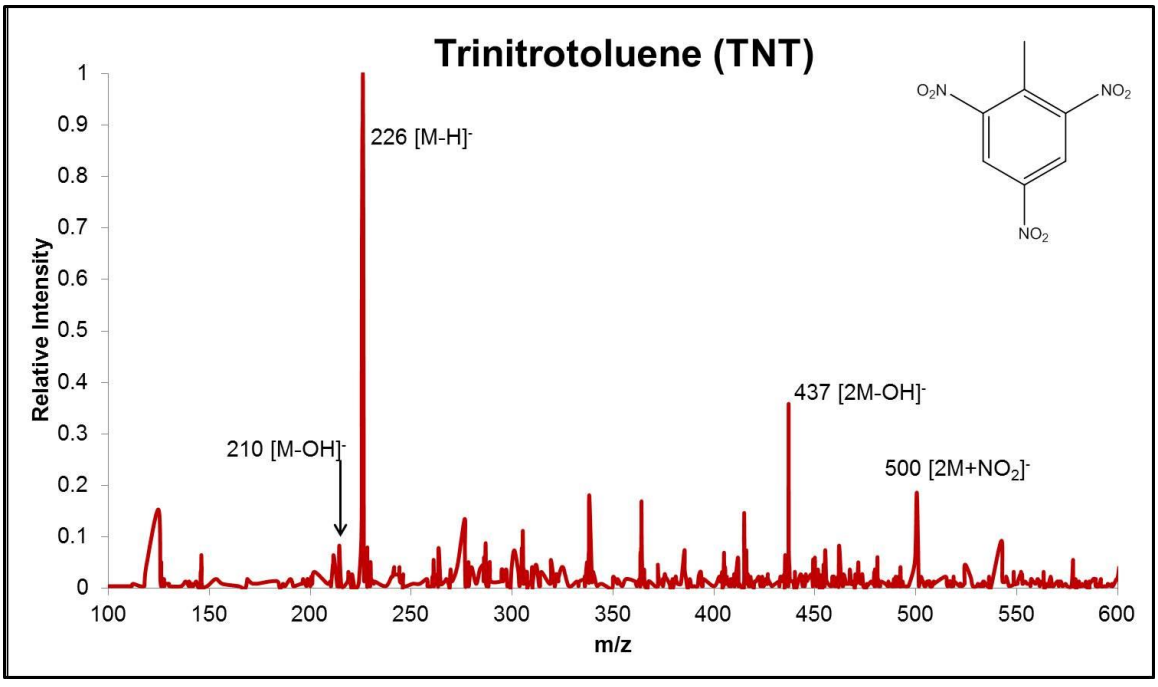

Figure A4.34 A representative mass spectrum of TNT analyzed by DEFFI-MS under the optimized parameters for negative mode.

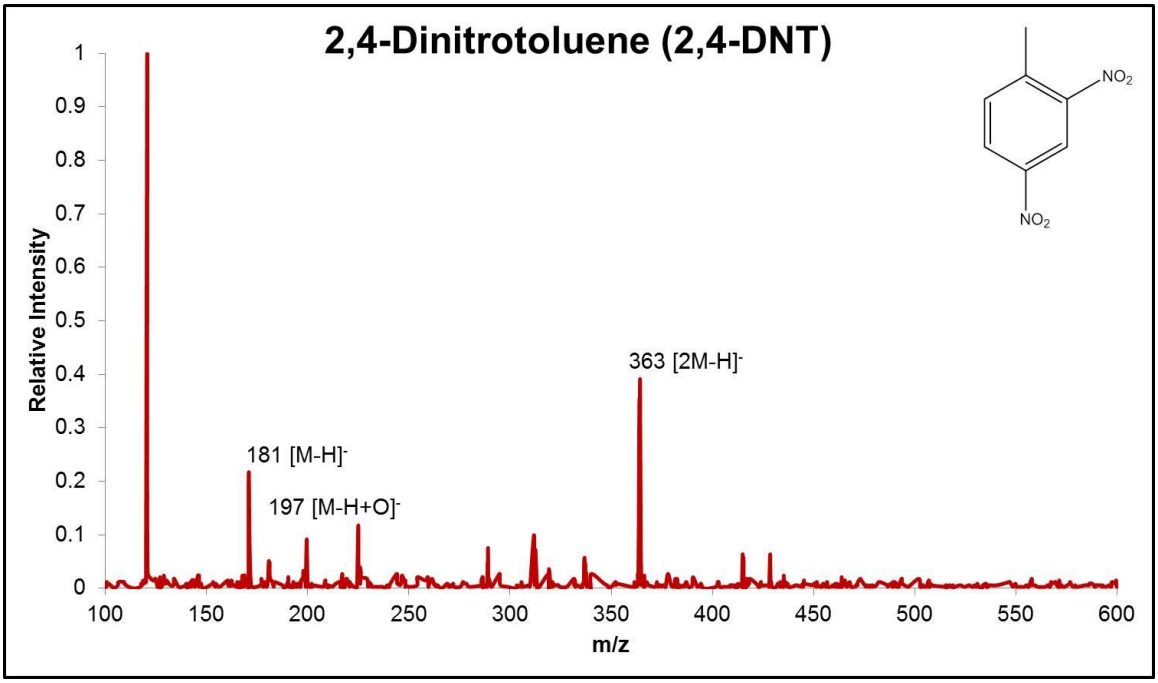

Figure A4.35 A representative mass spectrum of 2,4-DNT analyzed by DEFFI-MS under the optimized parameters for negative mode.

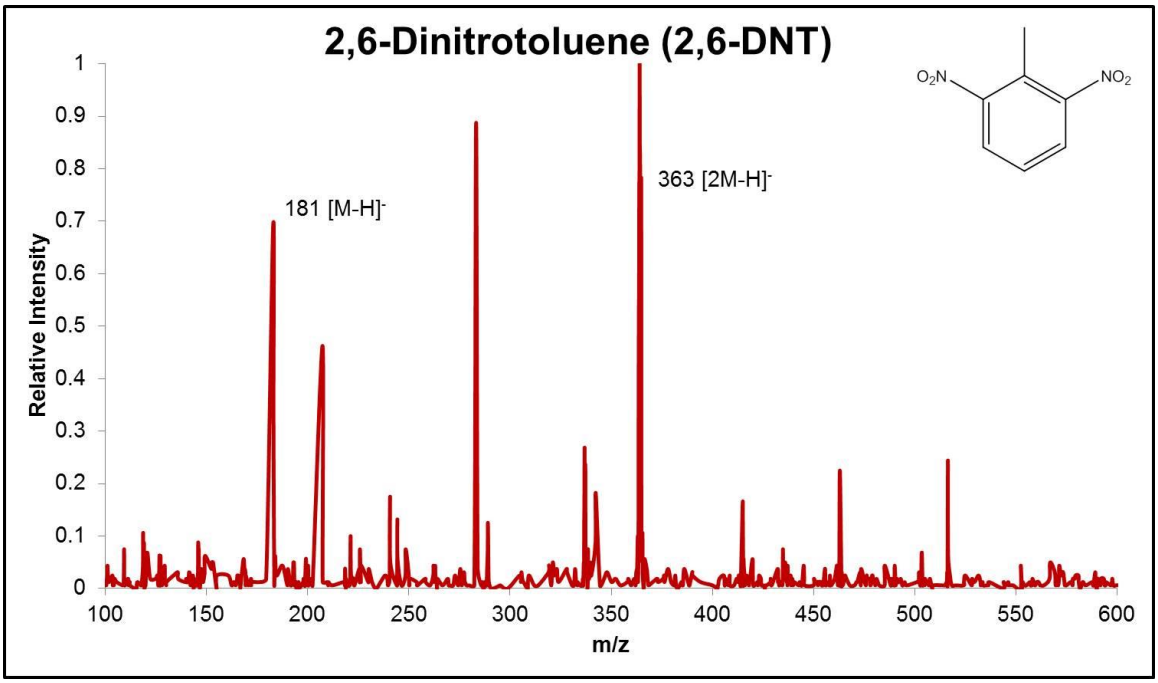

Figure A4.36 A representative mass spectrum of 2,6-DNT analyzed by DEFFI-MS under the optimized parameters for negative mode.

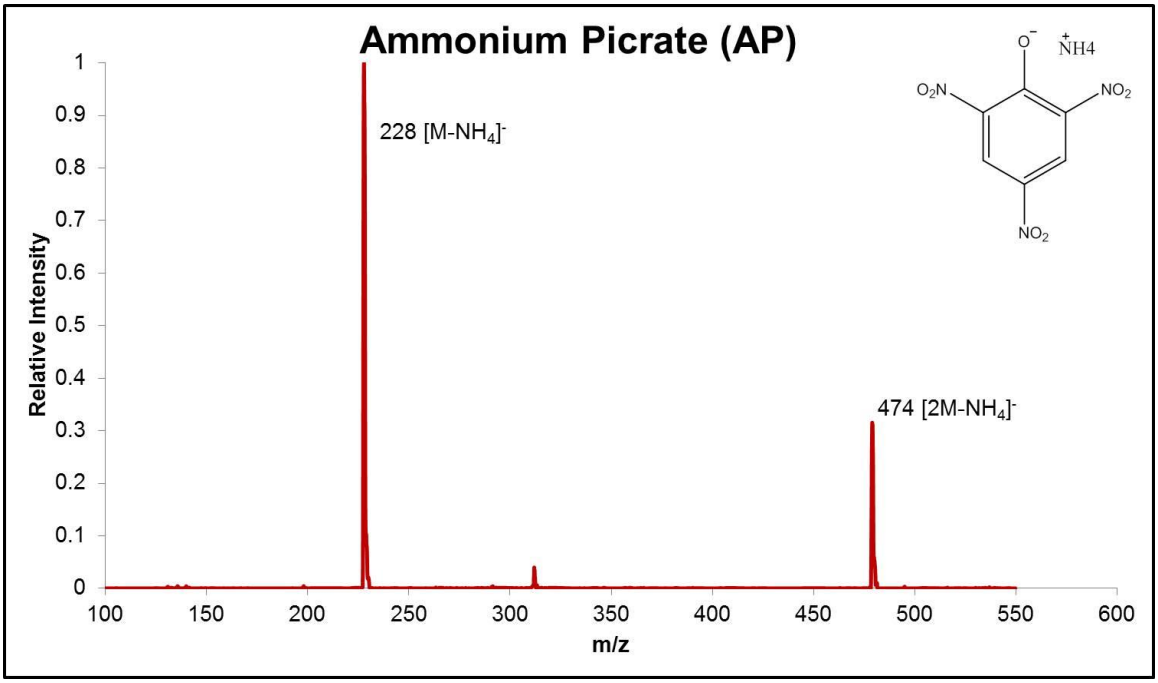

Figure A4.37 A representative mass spectrum of TNT analyzed by AP under the optimized parameters for negative mode.

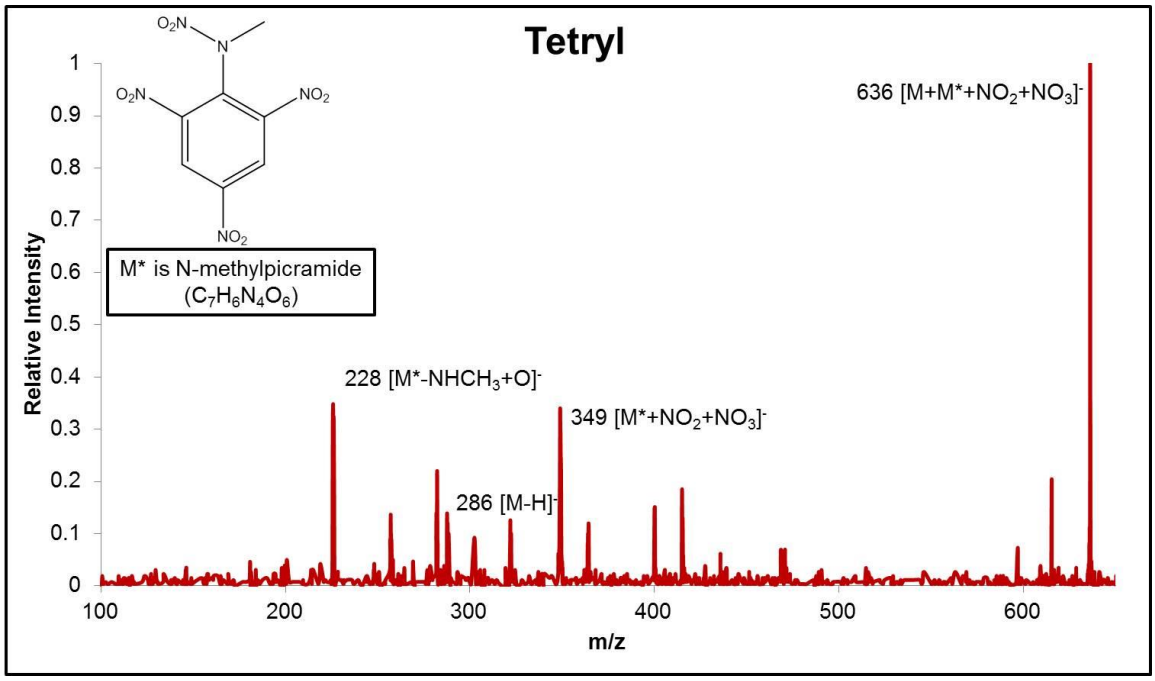

Figure A4.38 A representative mass spectrum of Tetryl analyzed by DEFFI-MS under the optimized parameters for negative mode.

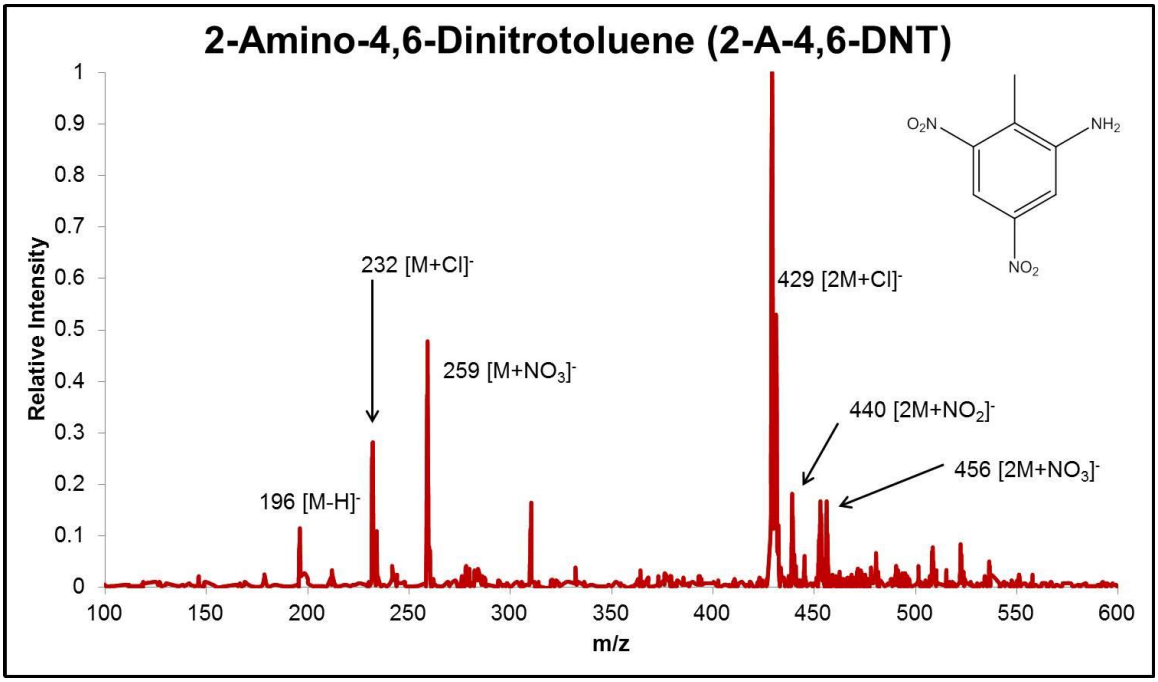

Figure A4.39 A representative mass spectrum of 2-A-4,6-DNT analyzed by DEFFI-MS under the optimized parameters for negative mode.

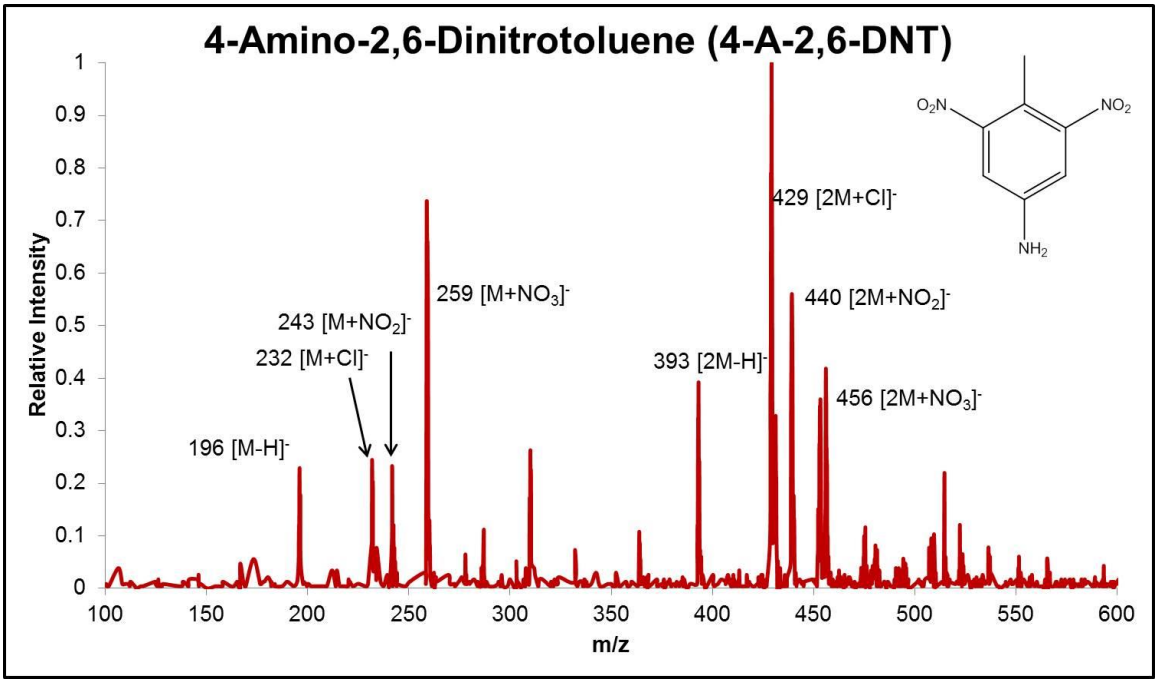

Figure A4.40 A representative mass spectrum of 4-A-2,6-DNT analyzed by DEFFI-MS under the optimized parameters for negative mode.

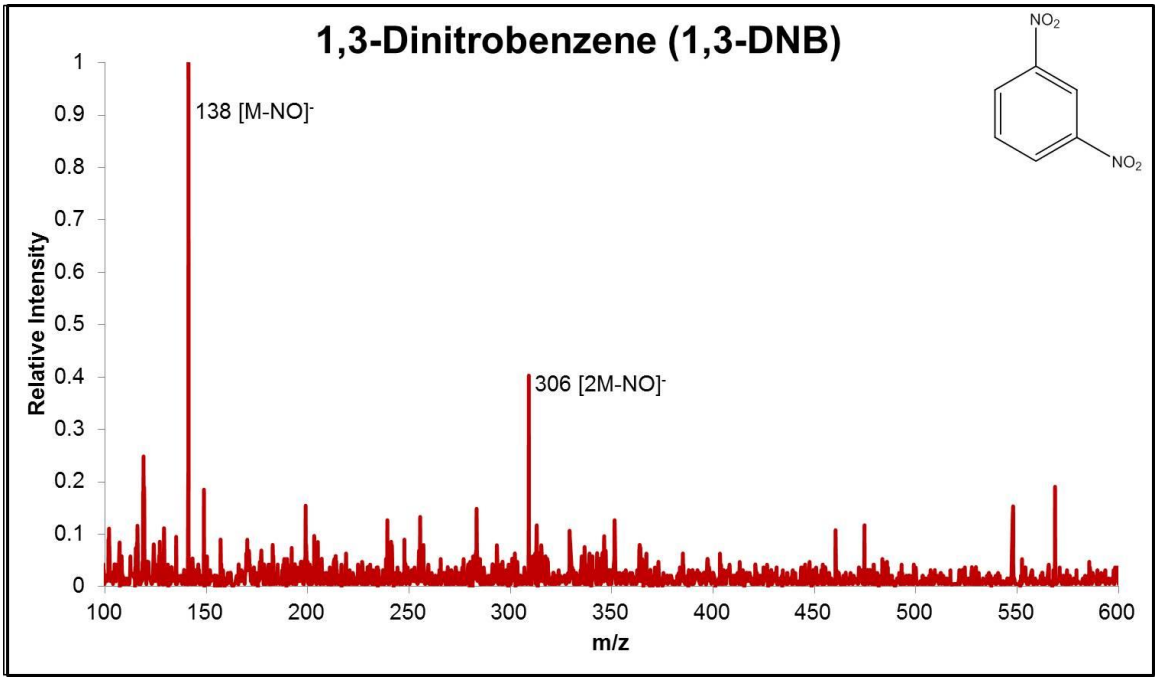

Figure A4.41 A representative mass spectrum of 1,3-DNB analyzed by DEFFI-MS under the optimized parameters for negative mode.

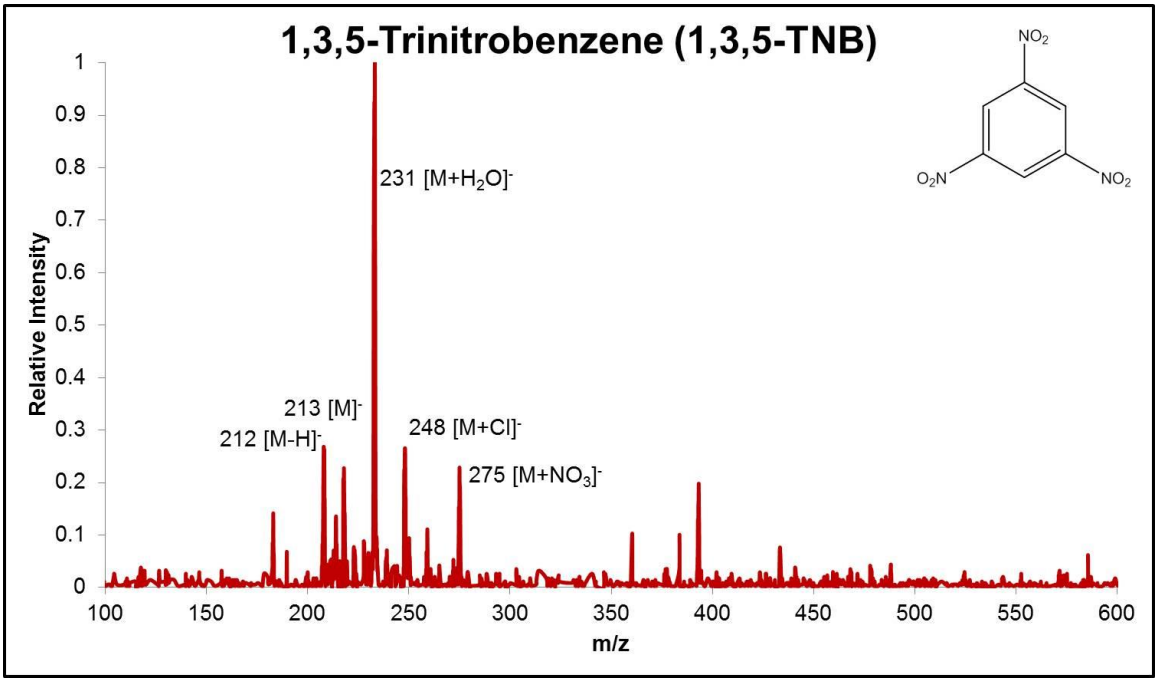

Figure A4.42 A representative mass spectrum of 1,3,5-TNB analyzed by DEFFI-MS under the optimized parameters for negative mode.

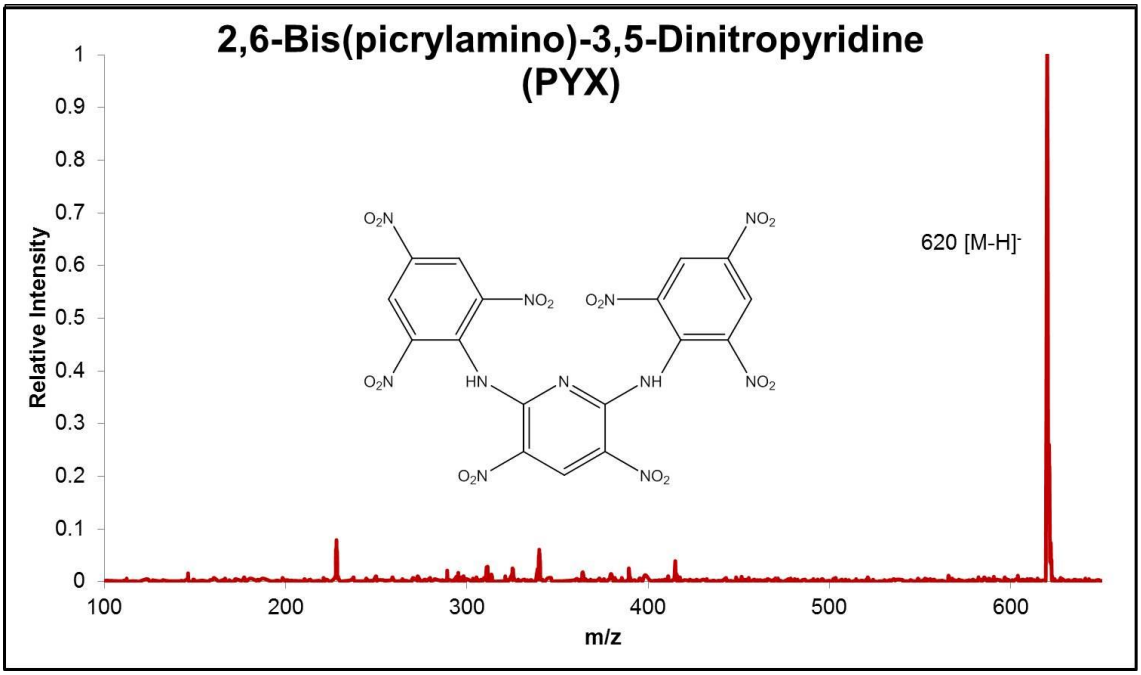

Figure A4.43 A representative mass spectrum of PYX analyzed by DEFFI-MS under the optimized parameters for negative mode.

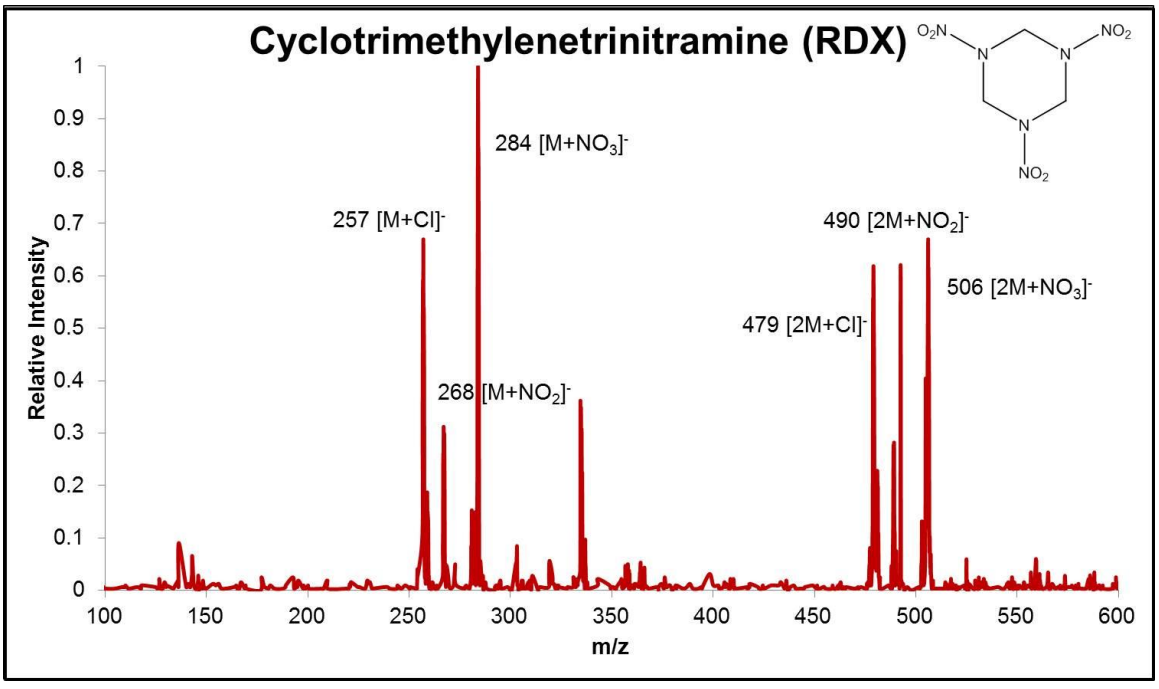

Figure A4.44 A representative mass spectrum of RDX analyzed by DEFFI-MS under the optimized parameters for negative mode.

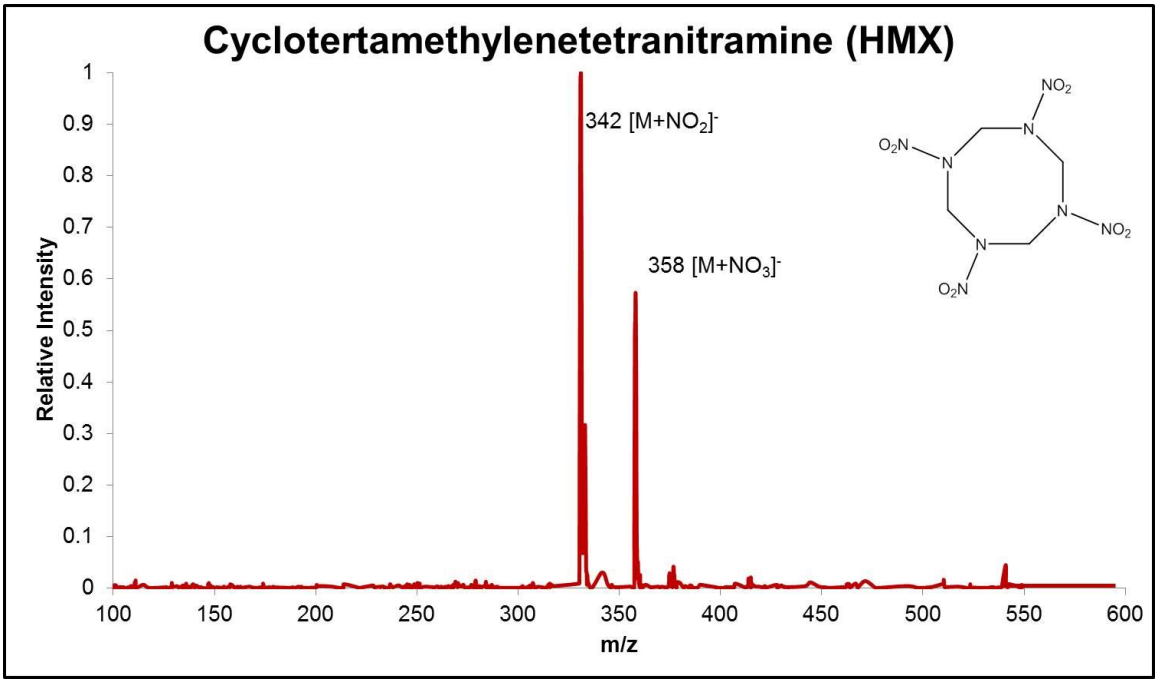

Figure A4.45 A representative mass spectrum of HMX analyzed by DEFFI-MS under the optimized parameters for negative mode.

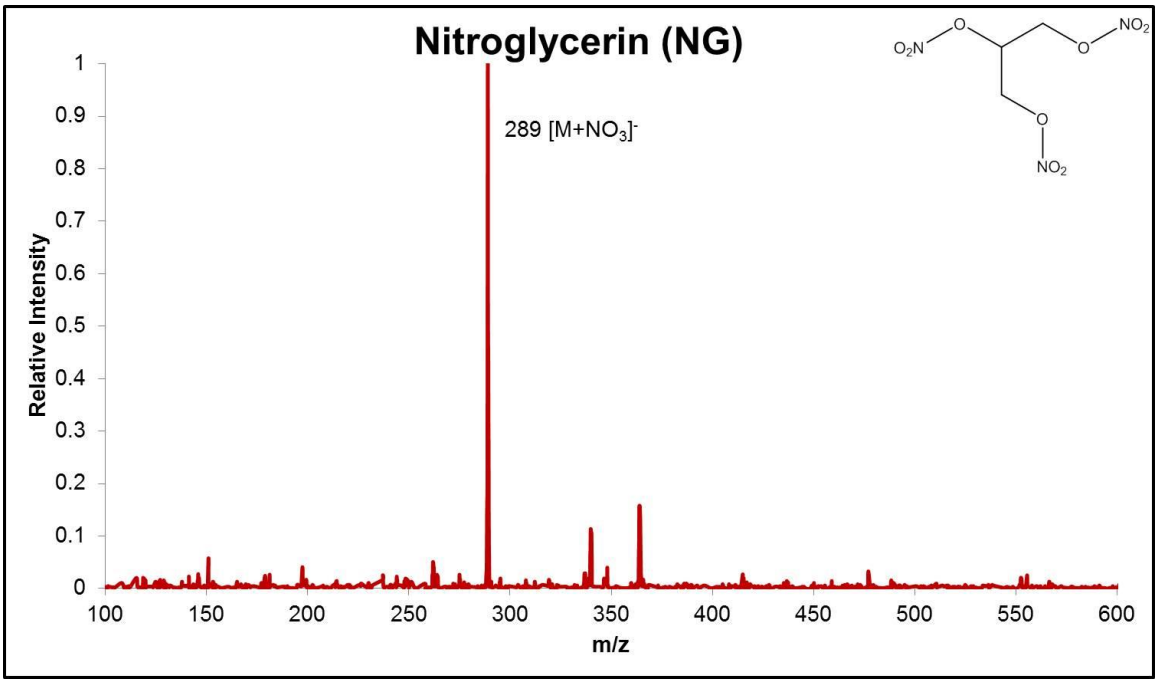

Figure A4.46 A representative mass spectrum of NG analyzed by DEFFI-MS under the optimized parameters for negative mode.

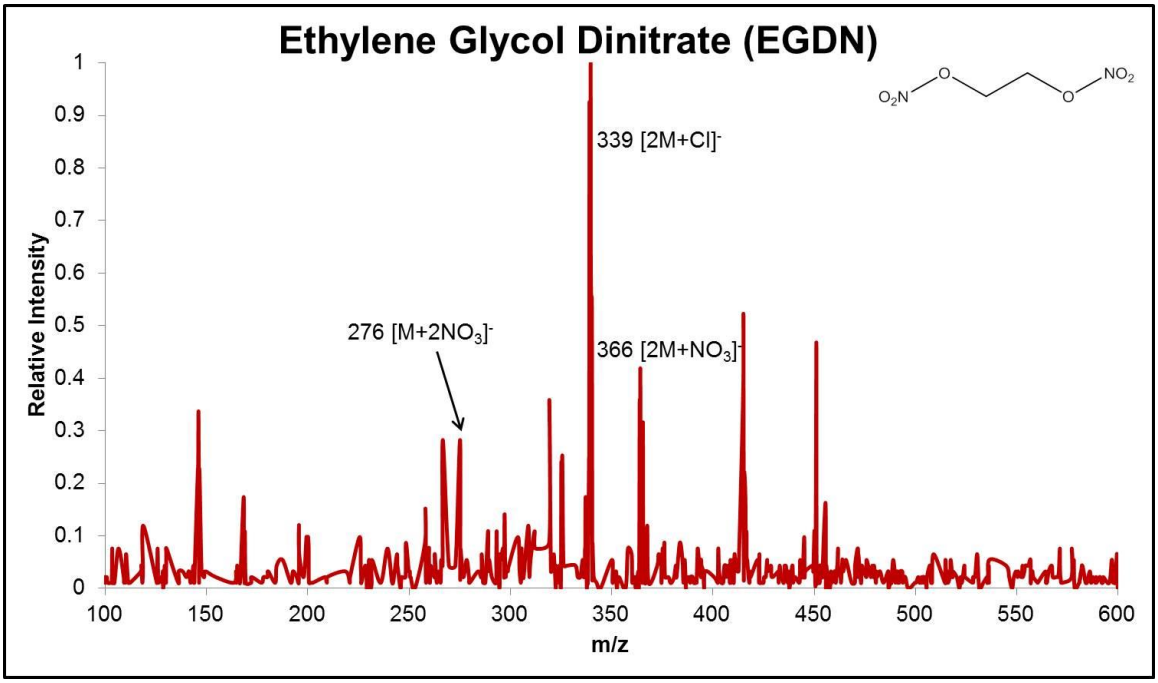

Figure A4.47 A representative mass spectrum of EGDN analyzed by DEFFI-MS under the optimized parameters for negative mode.

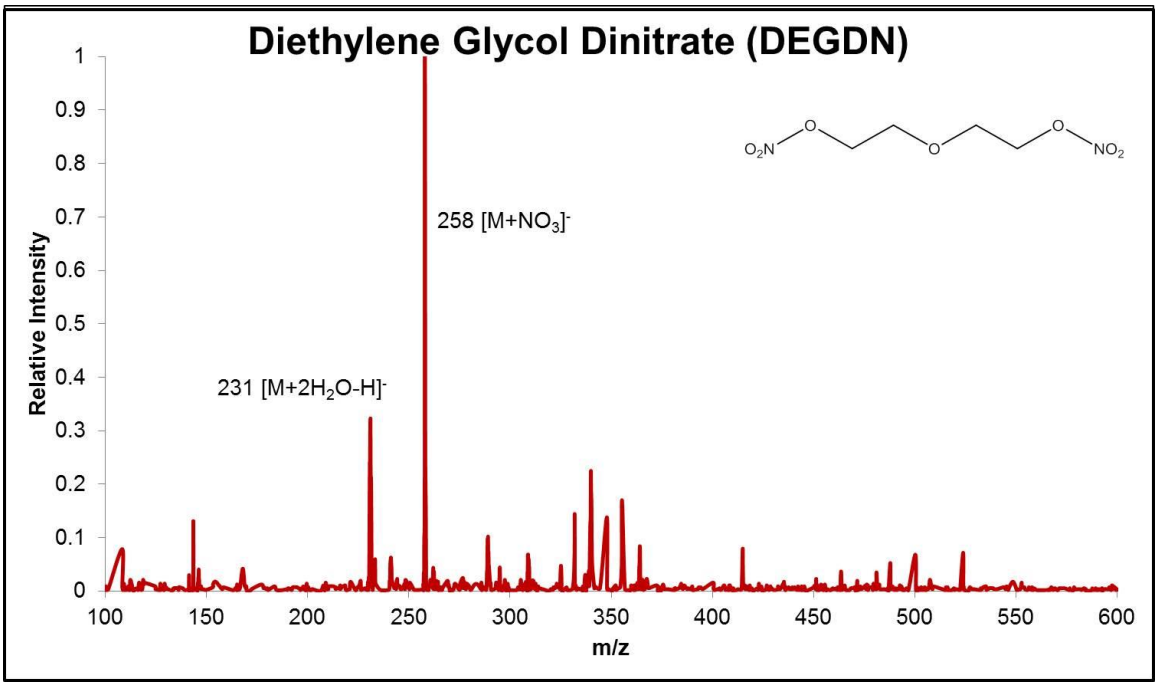

Figure A4.48 A representative mass spectrum of DEGDN analyzed by DEFFI-MS under the optimized parameters for negative mode.

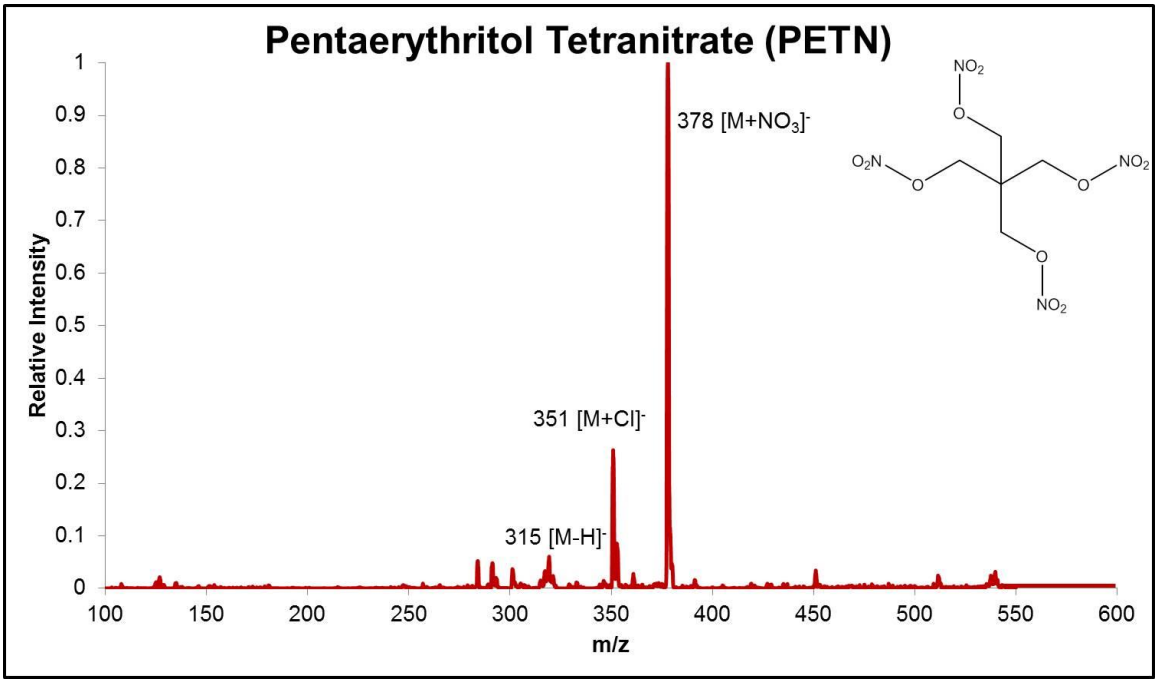

Figure A4.49 A representative mass spectrum of PETN analyzed by DEFFI-MS under the optimized parameters for negative mode.

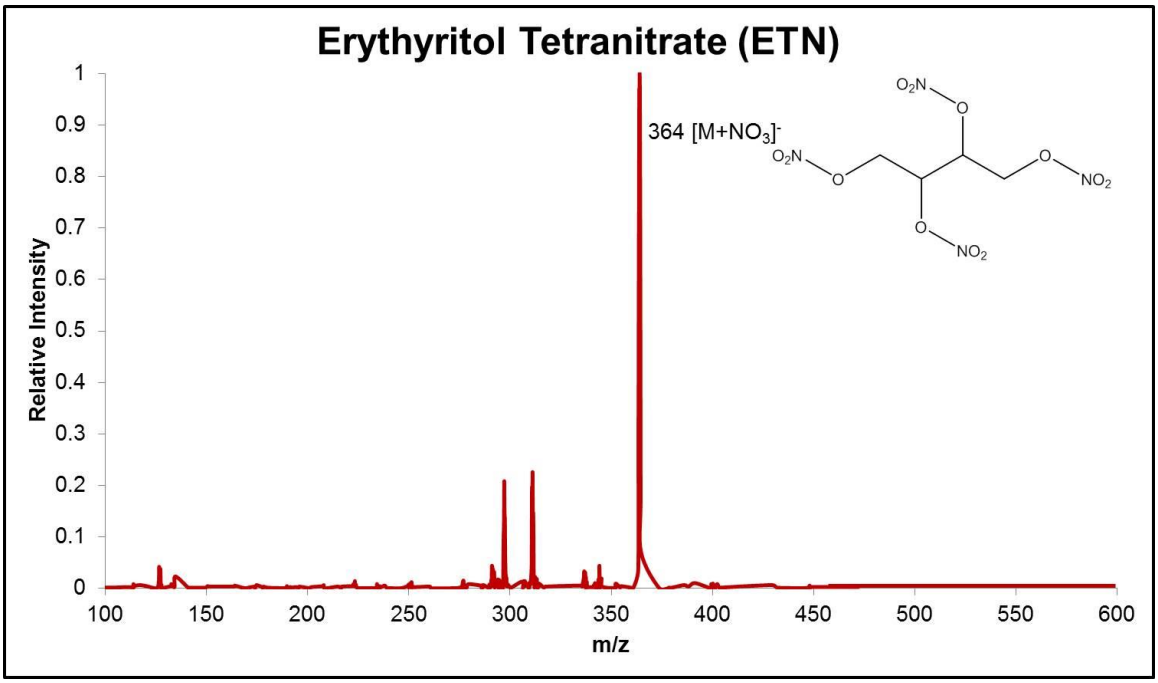

Figure A4.50 A representative mass spectrum of ETN analyzed by DEFFI-MS under the optimized parameters for negative mode.

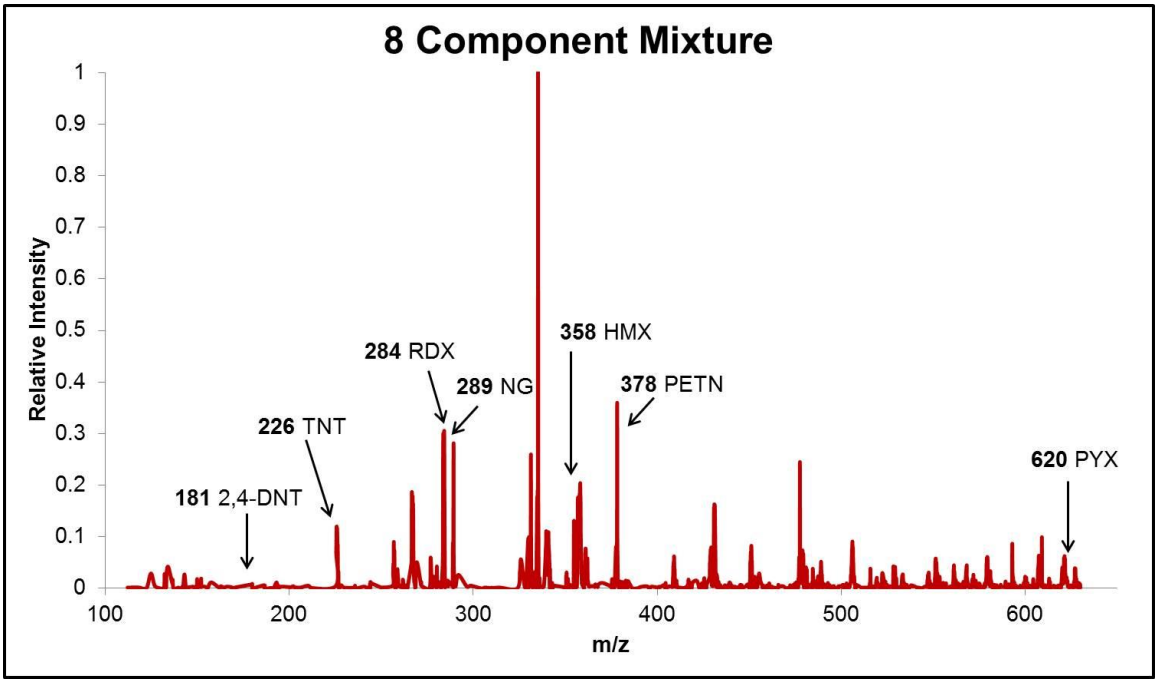

Figure A4.51 A representative mass spectrum of the 8 component mixture used for determining normalized yield analyzed by DEFFI-MS under the optimized parameters.

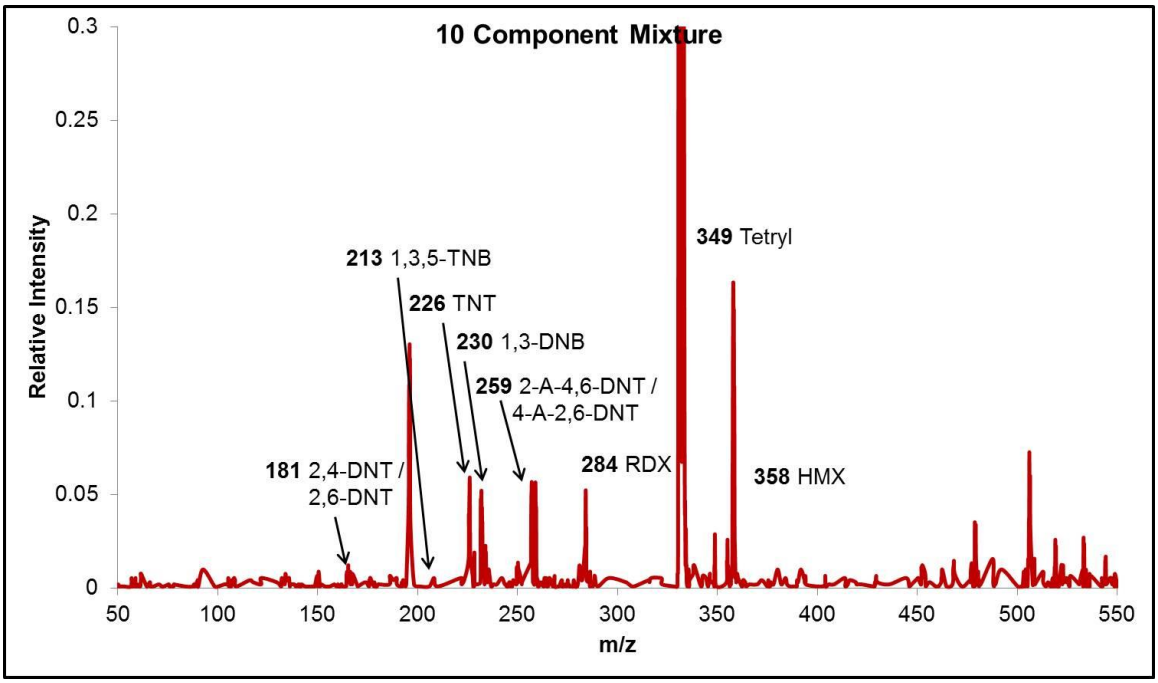

Figure A4.52 A representative mass spectrum of the 10 component mixture analyzed by DEFFI-MS under the optimized parameters for negative mode.

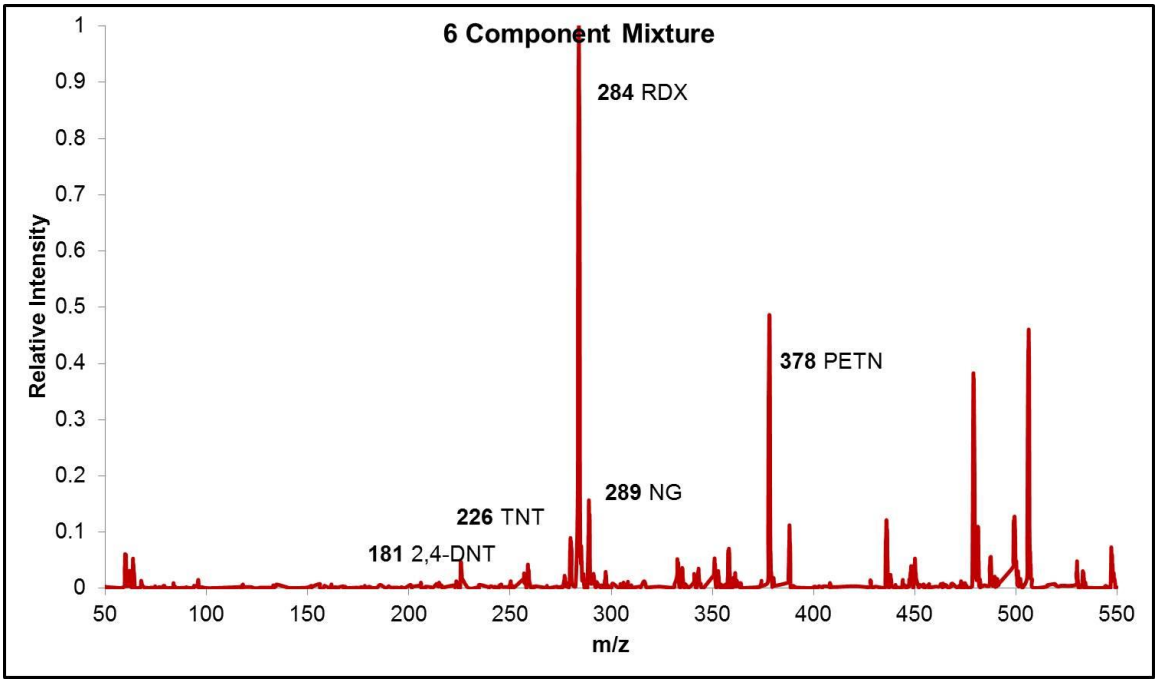

Figure A4.53 A representative mass spectrum of the 6 component mixture analyzed by DEFFI-MS under the optimized parameters for negative mode.

Appendix 5: Representative Mass Spectra and Additional Figures for Imaging using Desorption Electro-Flow Focusing Ionization Mass Spectrometry

This appendix contains information intended to support Chapter 5, imaging mass spectrometry of fingerprints using desorption electro-flow focusing ionization mass spectrometry (DEFFI-MS). Contained in this appendix are representative mass spectra for the target analytes monitored in the study and an example of how high spray solvent flow rates effect the quality of the chemical image.

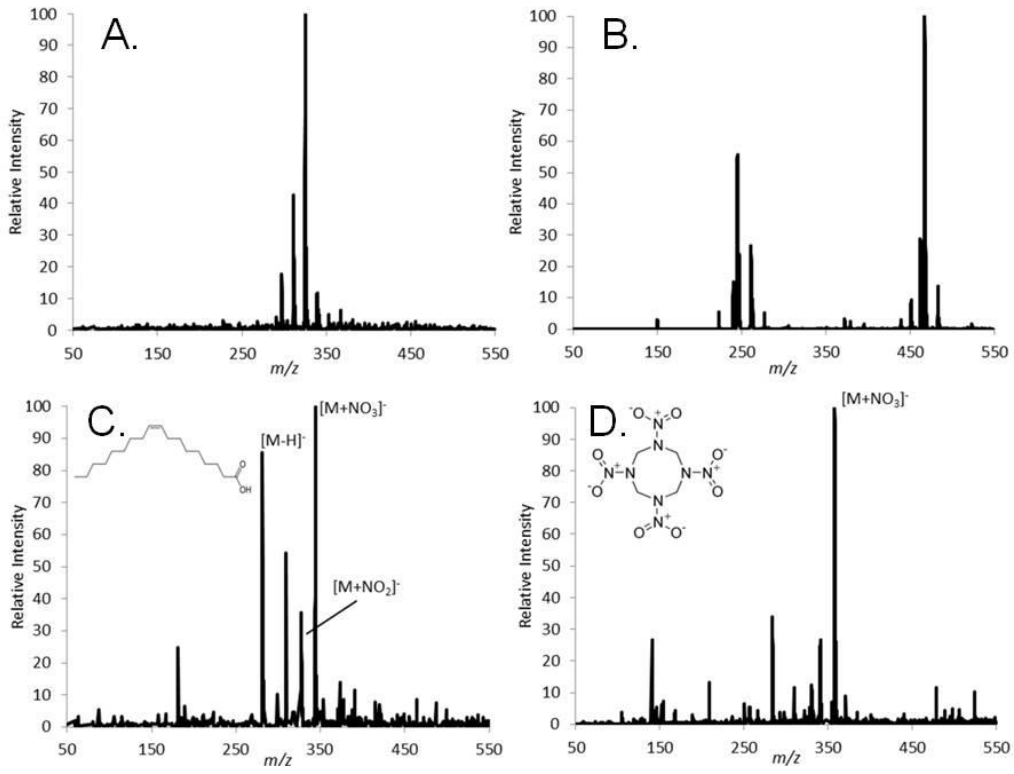

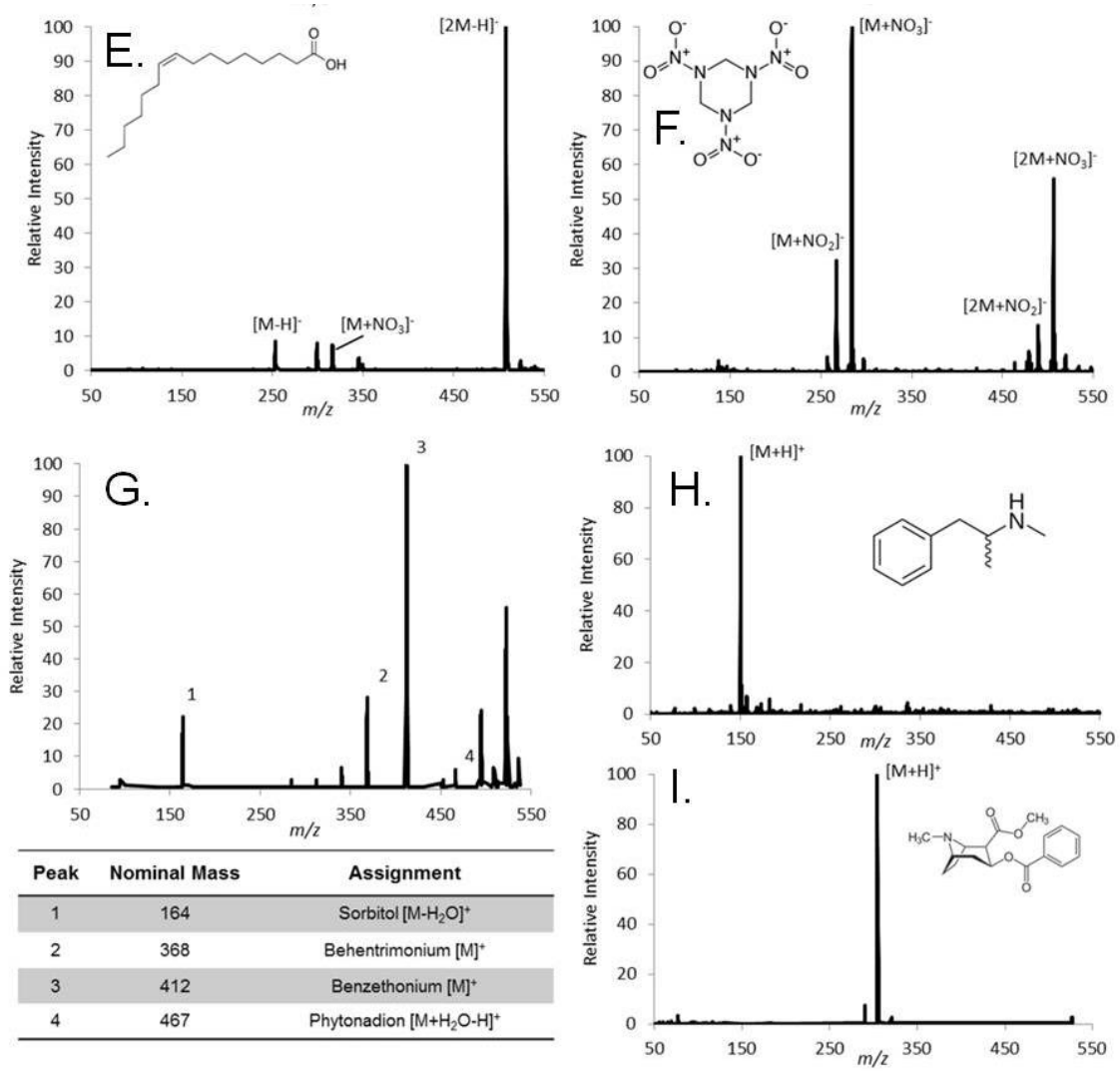

Peak	Nominal Mass	Assignment
1	164	Sorbitol $[M-H_2O]^+$
2	368	Behentrimonium $[M]^+$
3	412	Benzethonium $[M]^+$
4	467	Phytonadion $[M+H_2O-H]^+$

Figure A5.1 Representative mass spectra of the target analytes that were used in the DEFFI-MS imaging study. Mass spectra include negative and positive ion mass spectra of Sirchie fingerprint lift tape, (A.) and (B.) respectively. Negative ion mass spectra of 9-octadecenoic acid (C.), HMX (D.), 9-hexadecenoic acid (E.), and RDX (F.) are also shown. Positive ion mass spectra of gold bold lotion (G.), methamphetamine (H.), and cocaine (I.) are presented as well.

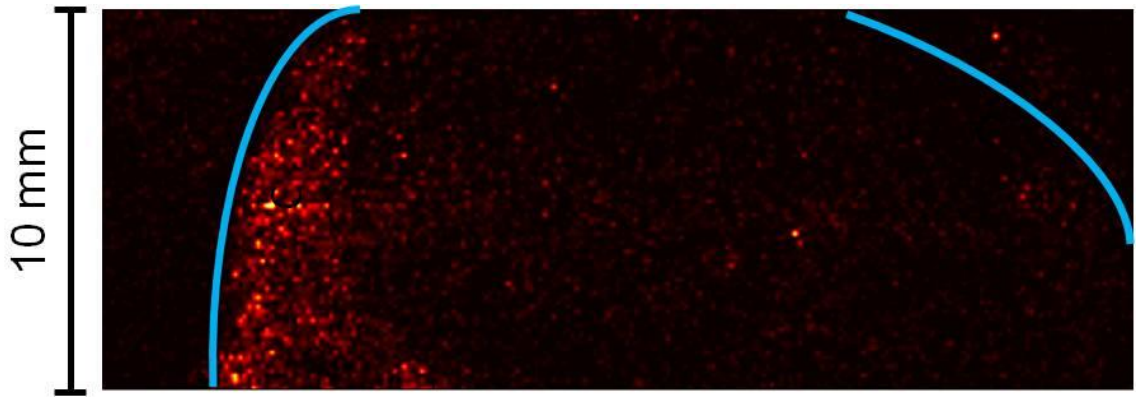

Figure A5.2 Partial chemical image of a latent fingerprint deposited onto tape that was imaged using a high solvent flow rate. Outline of the fingerprint is shown in blue.

References

(1) CINFSC; CSTL; CATS; PGA; DEPS. *Strengthening Forensic Science in the United States: A Path Forward*; National Academy of Sciences, 2009.

(2) Cooks, R. G.; Goodpaster, J.; van Asten, A. *Science on Location: Forensic Science on the Move*; CHE-1262145; National Science Foundation, 2013.

(3) Houck, M.; Siegel, J. *Fundamentals of Forensic Science*; Elsevier, 2006.

(4) Schafer, E. *Forensic Science*; Embar-Seddon, A.; Pass, A., Eds.; 2008.

(5) Department of Justice Office of Public Affairs. *U.S. Departments of Justice and Commerce Name Experts to First-ever National Commission on Forensic Science*; 2014.

(6) Holmgren, E.; Carlsson, H.; Goede, P.; Crescenzi, C. *J. Chromatogr. A* **2005**, *1099*, 127–135.

(7) Moore, D. S. *Rev. Sci. Instrum.* **2004**, *75*, 2499 –2512.

(8) Ewing, R. G.; Waltman, M. J.; Atkinson, D. A. *Anal. Chem.* **2011**, *83*, 4838–4844.

(9) Karpas, G. A. E., Z.; Karpas, Z. *Ion Mobility Spectrometry, Second Edition*; CRC Press, 2005.

(10) Furton, K. G.; Myers, L. J. *Talanta* **2001**, *54*, 487–500.

(11) Moore, D. S. *Sens. Imaging Int. J.* **2007**, *8*, 9–38.

(12) Moore, D.; Scharff, R. *Anal. Bioanal. Chem.* **2009**, *393*, 1571–1578.

(13) Ali, E. M. A.; Edwards, H. G. M.; Scowen, I. J. *J. Raman Spectrosc.* **2009**, *40*, 2009–2014.

(14) Eliasson, C.; Macleod, N. A.; Matousek, P. *Anal. Chem.* **2007**, *79*, 8185–8189.

(15) Almog, J.; Kraus, S.; Glattstein, B. *J. Energ. Mater.* **1986**, *4*, 159–167.

(16) Sisco, E.; Dake, J.; Bridge, C. *Forensic Sci. Int.* **2013**, *232*, 160–168.

(17) Cotte-Rodríguez, I.; Takáts, Z.; Talaty, N.; Chen, H.; Cooks, R. G. *Anal. Chem.* **2005**, *77*, 6755–6764.

(18) Garcia-Reyes, J. F.; Harper, J. D.; Salazar, G. A.; Charipar, N. A.; Ouyang, Z.; Cooks, R. G. *Anal Chem* **2010**, *83*, 1084–1092.

(19) Talaty, N.; Mulligan, C. C.; Justes, D. R.; Jackson, A. U.; Noll, R. J.; Cooks, R. G. *Analyst* **2008**, *133*, 1532–1540.

(20) Cotte-Rodríguez, I.; Chen, H.; Cooks, R. G. *Chem. Commun.* **2006**, 953.

(21) Na, N.; Zhang, C.; Zhao, M.; Zhang, S.; Yang, C.; Fang, X.; Zhang, X. *J. Mass Spectrom.* **2007**, *42*, 1079–1085.

(22) Popov, I. A.; Chen, H.; Kharybin, O. N.; Nikolaev, E. N.; Cooks, R. G. *Chem. Commun.* **2005**, 1953–1955.

(23) Song, Y.; Cooks, R. G. *Rapid Commun. Mass Spectrom.* **2006**, *20*, 3130–3138.

(24) Takáts, Z.; Wiseman, J. M.; Cooks, R. G. *J. Mass Spectrom.* **2005**, *40*, 1261–1275.

(25) Zhang, M.; Shi, Z.; Bai, Y.; Gao, Y.; Hu, R.; Zhao, F. *J. Am. Soc. Mass Spectrom.* **2006**, *17*, 189–193.

(26) Li, L.; Chen, T.-C.; Ren, Y.; Hendricks, P. I.; Cooks, R. G.; Ouyang, Z. *Anal. Chem.* **2014**.

(27) Ouyang, Z.; Cooks, R. G. *Annu. Rev. Anal. Chem.* **2009**, *2*, 187–214.

(28) Lee, H. *Advances in Fingerprint Technology*; 2nd ed.; CRC Press: Boca Raton, FL, 2001.

(29) Justice, N. I. of. The Fingerprint Sourcebook http://www.nij.gov/pubs-sum/225320.htm (accessed Mar 23, 2014).

(30) Faulds, H.; Hospital, T. *Nature* **1880**, *22*, 605.

(31) Edward Richard Henry. *Classification and Uses of Finger Prints*; George Routledge and Sons, 1900.

(32) Szynkowska, M. I.; Czerski, K.; Rogowski, J.; Paryjczak, T.; Parczewski, A. *Forensic Sci. Int.* **2009**, *184*, e24–26.

(33) Eberlin, L. S.; Liu, X.; Ferreira, C. R.; Santagata, S.; Agar, N. Y. R.; Cooks, R. G. *Anal Chem* **2011**, *83*, 8366–8371.

(34) Ifa, D. R.; Manicke, N. E.; Dill, A. L.; Cooks, R. G. *Science* **2008**, *321*, 805.

(35) Worley, C. G.; Wiltshire, S. S.; Miller, T. C.; Havrilla, G. J.; Majidi, V. *J. Forensic Sci.* **2006**, *51*, 57–63.

(36) Cooks, R. G. *Science* **2006**, *311*, 1566–1570.

(37) Harris, G. A.; Galhena, A. S.; Fernandez, F. M. *Anal. Chem.* **2011**, *83*, 4508 – 4538.

(38) Wu, C.; Dill, A. L.; Eberlin, L. S.; Cooks, R. G.; Ifa, D. R. *Mass Spectrom. Rev.* **2013**, *32*, 218–243.

(39) Hager, J. W. *Rapid Commun. Mass Spectrom.* **2002**, *16*, 512–526.

(40) Guilhaus, M.; Selby, D.; Mlynski, V. *Mass Spectrom. Rev.* **2000**, *19*, 65–107.

(41) Dass, C. *Fundamentals of Contemporary Mass Spectrometry*; John Wiley & Sons, Inc.: Hoboken, New Jersey, 2007.

(42) Skoog, D.; Holler, F. J.; Crouch, S. *Principles of Instrumental Analysis*; Sixth.; Thomson Brooks/Cole: Belmont, CA, 2007.

(43) Cody, R. B.; Laeamee, J. A.; Durst, D. H. *Anal. Chem.* **2005**, *77*, 2297 – 2302.

(44) Chernetsova, E. S.; Morlock, G. E.; Revelsky, I. A. *Russ. Chem. Rev.* **2011**, *80*, 235–255.

(45) Gross, J. H. *Anal. Bioanal. Chem.* **2014**, *406*, 63–80.

(46) Harris, G. Fundamentals of Ambient Metastable-Induced Chemical Ionization Mass Spectrometry and Atmospheric Pressure Ion Mobility Spectometry, Georgia Institute of Technology, 2011.

(47) McEwen, C. N.; Larsen, B. S. *J. Am. Soc. Mass Spectrom.* **2009**, *20*, 1518–1521.

(48) Takáts, Z.; Wiseman, J. M.; Gologan, B.; Cooks, R. G. *Science* **2004**, *306*, 471–473.

(49) Venter, A.; Sojka, P. E.; Cooks, R. G. *Anal. Chem.* **2006**, *78*, 8549–8555.

(50) Costa, A. B.; Graham Cooks, R. *Chem. Phys. Lett.* **2008**, *464*, 1–8.

(51) Takats, Z. *Science* **2004**, *306*, 471–473.

(52) Campbell, D. I.; Ferreira, C. R.; Eberlin, L. S.; Cooks, R. G. *Anal. Bioanal. Chem.* **2012**, *404*, 389–398.

(53) Mirabelli, M. F.; Chramow, A.; Cabral, E. C.; Ifa, D. R. *J. Mass Spectrom.* **2013**, *48*, 774–778.

(54) Forbes, T. P.; Brewer, T. M.; Gillen, G. *Analyst* **2013**, *138*, 5665–5673.

(55) Forbes, T. P.; Brewer, T. M.; Gillen, G. *Appl. Phys. Lett.* **2013**, *102*, 214102.

(56) Gañán-Calvo, A. M.; Montanero, J. M. *Phys. Rev. E* **2009**, *79*, 066305.

(57) Martín-Banderas, L.; Flores-Mosquera, M.; Riesco-Chueca, P.; Rodríguez-Gil, A.; Cebolla, Á.; Chávez, S.; Gañán-Calvo, A. M. *Small* **2005**, *1*, 688–692.

(58) Chan, G. C.-Y.; Shelley, J. T.; Wiley, J. S.; Engelhard, C.; Jackson, A. U.; Cooks, R. G.; Hieftje, G. M. *Anal. Chem.* **2011**, *83*, 3675–3686.

(59) Fridman, A.; Kennedy, L. J. *Plasma Physics and Engineering*; 2nd ed.; CRC Press: Boca Raton, FL, 2011.

(60) Albert, A.; Engelhard, C. *Anal. Chem.* **2012**, *84*, 10657–10664.

(61) Fahey, A. J.; Gillen, G.; Chi, P.; Mahoney, C. M. *Appl. Surf. Sci.* **2006**, *252*, 7312–7314.

(62) Zheng, L.; Wucher, A.; Winograd, N. *Anal. Chem.* **2008**, *80*, 7363 – 7371.

(63) Heeren, R. M. A.; Sweedler, J. V. *Int. J. Mass Spectrom.* **2007**, *260*, 89.

(64) Steiner, R. R.; Larson, R. L. *J. Forensic Sci.* **2009**, *54*, 617–622.

(65) Pfaff, A. M.; Steiner, R. R. *Forensic Sci. Int.* **2011**, *206*, 62–70.

(66) Howlett, S. E.; Steiner, R. R. *J. Forensic Sci.* **2011**, *56*, 1261–1267.

(67) Nilles, J. M.; Connell, T. R.; Stokes, S. T.; Dupont Durst, H. *Propellants Explos. Pyrotech.* **2010**, *35*, 446–451.

(68) ISO/CASCO. General Requirements for the Competence of Testing and Calibration Laboratories, 2005.

(69) Jones, R. W.; Cody, R. B.; McClelland, J. F. *J. Forensic Sci.* **2006**, *51*, 915–918.

(70) Chernetsova, E.; Bochkov, P.; Zatonskii, G.; Abramovich, R. *Pharm. Chem. J.* **2011**, *45*, 306–308.

(71) Nilles, J. M.; Connell, T. R.; Durst, H. D. *Anal. Chem.* **2009**, *81*, 6744–6749.

(72) Hajslova, J.; Cajka, T.; Vaclavik, L. *Trends Anal. Chem.* **2011**, *30*, 204–218.

(73) Swider, J. R. *J. Forensic Sci.* **2013**, *58*, 1601–1606.

(74) Rowell, F.; Seviour, J.; Lim, A. Y.; Elumbaring-Salazar, C. G.; Loke, J.; Ma, J. *Forensic Sci. Int.* **2012**, *221*, 84–91.

(75) Song, L.; Dykstra, A. B.; Yao, H.; Bartmess, J. E. *J. Am. Soc. Mass Spectrom.* **2009**, *20*, 42–50.

(76) Ledbetter, N. L.; Walton, B. L.; Davila, P.; Hoffmann, W. D.; Ernest, R. N.; Verbeck, G. F., 4th. *J. Forensic Sci.* **2010**, *55*, 1218–1221.

(77) Clemons, K.; Wiley, R.; Waverka, K.; Fox, J.; Dziekonski, E.; Verbeck, G. F. *J. Forensic Sci.* **2013**, *58*, 875–880.

(78) Wallace, N.; Hueske, E.; Verbeck, G. F. *Sci. Justice J. Forensic Sci. Soc.* **2011**, *51*, 196–203.

(79) Harper, J. D.; Charipar, N. A.; Mulligan, C. C.; Zhang, X.; Cooks, R. G.; Ouyang, Z. *Anal Chem* **2008**, *80*, 9097–9104.

(80) Green, F. M.; Salter, T. L.; Gilmore, I. S.; Stokes, P.; O'Connor, G. *Analyzer* **2010**, *135*, 731 – 737.

(81) Costa, A. B.; Cooks, R. G. *Chem. Commun.* **2007**, 3915–3917.

(82) Zadnik, S.; van Bronswijk, W.; Frick, A. A.; Fritz, P.; Lewis, S. W. *J. Forensic Identif.* **2012**, *63*, 593–608.

(83) Asbaugh, D. R. *Quantitative and Qualitative Friction Ridge Analysis: An Introduction to Basic and Advanced Ridgeology*; CRC Press: Boca Raton, FL, 1999.

(84) Ng, P.; Walker, S.; Tahtouh, M.; Reedy, B. *Anal. Bioanal. Chem.* **2009**, *394*, 2039–2048.

(85) Croxton, R. S.; Baron, M. G.; Butler, D.; Kent, T.; Sears, V. G. *Forensic Sci. Int.* **2010**, *199*, 93–102.

(86) Girod, A.; Ramotowski, R.; Weyermann, C. *Forensic Sci. Int.* **2012**, *223*, 10–24.

(87) Parnas, J.; Flachs, H.; Gram, L.; Wuurtz-JØrgensen, A. *Acta Neurol. Scand.* **2009**, *58*, 197–204.

(88) Barnes, A. J.; Smith, M. L.; Kacinko, S. L.; Schwilke, E. W.; Cone, E. J.; Moolchan, E. T.; Huestis, M. A. *Clin. Chem.* **2008**, *54*, 172–180.

(89) De La Torre, R.; Pichini, S. *Clin. Chem.* **2004**, *50*, 1961–1962.

(90) Antoine, K. M.; Mortazavi, S.; Miller, A. D.; Miller, L. M. *J. Forensic Sci.* **2010**, *55*, 513–518.

(91) James, W. D. *Andrew's Diseases of the Skin: Clinical Dermatology*; 10th ed.; Elseveir: New York, NY, 2006.

(92) Mong, G. M.; Petersen, C. E.; Clauss, T. R. W. *Advanced Fingerprint Analysis Project Fingerprint Constituents*; 1999.

(93) Yamada, Y.; Motoi, H.; Kinoshita, S.; Takada, N.; Okada, H. *Appl. Microbiol.* **1975**, *29*, 400–404.

(94) Johnson, H. L.; Maibach, H. I. *J. Invest. Dermatol.* **1971**, *56*, 182–188.

(95) Ricci, C.; Kazarian, S. G. *Surf. Interface Anal.* **2010**, *42*, 386–392.

(96) Stefaniak, A. B.; Harvey, C. J.; Wertz, P. W. *Int. J. Cosmet. Sci.* **2010**, *32*, 347–355.

(97) Wertz, P. W. *Int. J. Cosmet. Sci.* **2009**, *31*, 21–25.

(98) *Standard Guide for Evaluating Cleaning Performance of Ceramic Tile Cleaners*; D 5343 - 97; ASTM.

(99) D01 Committee. *Guide for Testing High-Performance Interior Architectural Wall Coatings*; ASTM International, 2010.

(100) Flanigan, J. The characterization of explosive residue within forensically processed fingerprints using Fourier transform infrared spectroscopy. Master's Thesis, George Washington University, 2011.

(101) Salter, T. L.; Green, F. M.; Gilmore, I. S.; Seah, M. P.; Stokes, P. *Surf. Interface Anal.* **2011**, *43*, 294–297.

(102) Szynkowska, M. I.; Czerski, K.; Grams, J.; Paryjczak, T.; Parczewski, A. *Imaging Sci. J.* **2007**, *55*, 180–187.

(103) Bright, N. J.; Webb, R. P.; Bleay, S.; Hinder, S.; Ward, N. I.; Watts, J. F.; Kirkby, K. J.; Bailey, M. J. *Anal Chem* **2012**.

(104) Bailey, M. J.; Ismail, M.; Bleay, S.; Bright, N.; Elad, M. L.; Cohen, Y.; Geller, B.; Everson, D.; Costa, C.; Webb, R. P.; Watts, J. F.; de Puit, M. *Analyst* **2013**, *138*, 6246.

(105) Bailey, M. J.; Jones, B. N.; Hinder, S.; Watts, J.; Bleay, S.; Webb, R. P. *Nucl. Instrum. Methods Phys. Res. Sect. B Beam Interact. Mater. At.* **2010**, *268*, 1929–1932.

(106) Mahoney, C. M.; Gillen, G.; Fahey, A. J. *Forensic Sci. Int.* **2006**, *158*, 39–51.

(107) Coumbaros, J.; Kirkbride, K. P.; Klass, G.; Skinner, W. *Forensic Sci. Int.* **2001**, *119*, 72–81.

(108) Denman, J. A.; Kempson, I. M.; Skinner, W. M.; Kirkbride, K. P. *Forensic Sci. Int.* **2008**, *175*, 123–129.

(109) Tamborini, G.; Wallenius, M.; Bildstein, O.; Pajo, L.; Betti, M. *Microchim. Acta* **2002**, *139*, 185–188.

(110) Betti, M.; Tamborini, G.; Koch, L. *Anal. Chem.* **1999**, *71*, 2616–2622.

(111) Bailey, M. J.; Bright, N. J.; Croxton, R. S.; Francese, S.; Ferguson, L. S.; Hinder, S.; Jickells, S.; Jones, B. J.; Jones, B. N.; Kazarian, S. G.; Ojeda, J. J.; Webb, R. P.; Wolstenholme, R.; Bleay, S. *Anal. Chem.* **2012**, *84*, 8514–8523.

(112) Ferguson, L.; Bradshaw, R.; Wolstenholme, R.; Clench, M.; Francese, S. *Anal. Chem.* **2011**, *83*, 5585–5591.

(113) Wolstenholme, R.; Bradshaw, R.; Clench, M. R.; Francese, S. *Rapid Commun. Mass Spectrom.* **2009**, *23*, 3031–3039.

(114) Wiseman, J. M.; Ifa, D. R.; Zhu, Y.; Kissinger, C. B.; Manicke, N. E.; Kissinger, P. T.; Cooks, R. G. *Proc. Natl. Acad. Sci.* **2008**, *105*, 18120–18125.

(115) Zhao, M.; Zhang, S.; Yang, C.; Xu, Y.; Wen, Y.; Sun, L.; Zhang, X. *J. Forensic Sci.* **2008**, *53*, 807–811.

(116) Ifa, D. R.; Gumaelius, L. M.; Eberlin, L. S.; Manicke, N. E.; Cooks, R. G. *Analyst* **2007**, *132*, 461–467.

(117) Miki, A.; Katagi, M.; Kamata, T.; Zaitsu, K.; Tatsuno, M.; Nakanishi, T.; Tsuchihashi, H.; Takubo, T.; Suzuki, K. *J. Mass Spectrom.* **2011**, *46*, 411–416.

(118) Robichaud, G.; Garrard, K. P.; Barry, J. A.; Muddiman, D. C. *J. Am. Soc. Mass Spectrom.* **2013**, *24*, 718–721.

(119) Bright, N. J.; Willson, T. R.; Driscoll, D. J.; Reddy, S. M.; Webb, R. P.; Bleay, S.; Ward, N. I.; Kirkby, K. J.; Bailey, M. J. *Forensic Sci. Int.* **2013**, *230*, 81–86.

(120) Archer, N. E.; Charles, Y.; Elliott, J. A.; Jickells, S. *Forensic Sci. Int.* **2005**, *154*, 224–239.

(121) Mountfort, K. A.; Bronstein, H.; Archer, N.; Jickells, S. M. *Anal Chem* **2007**, *79*, 2650–2657.

(122) Manier, M. L.; Cornett, D. S.; Hachey, D. L.; Caprioli, R. M. *J. Am. Soc. Mass Spectrom.* **2008**, *19*, 666–670.

(123) Emerson, B.; Gidden, J.; Lay Jr, J. O.; Durham, B. *J. Forensic Sci.* **2011**, *56*, 381–389.

(124) Uemi, M.; Ronsein, G. E.; Miyamoto, S.; Medeiros, M. H. G.; Di Mascio, P. D. *Chem. Res. Toxicol.* **2009**, *22*, 875 – 884.

(125) Dreyfus, M. A.; Tolocka, M. P.; Dodds, S. M.; Dykins, J.; Johnston, M. V. *J. Phys. Chem.* **2005**, *109*, 6242 – 6248.

(126) Downing, D. T.; Strauss, J. S.; Pochi, P. E. *J. Invest. Dermatol.* **1969**, *53*, 322–327.

(127) Buchanan, M. V.; Asano, K.; Bohanon, A. *Proc. SPIE* **1997**, *2941*, 89–95.

(128) National Ambient Air Quality Standards (NAAQS) | Air and Radiation | US EPA http://www.epa.gov/air/criteria.html (accessed Mar 23, 2014).

(129) Williams, J. P.; Scrivens, J. H. *Rapid Commun. Mass Spectrom.* **2008**, *22*, 187–196.

(130) Harris, G. A.; Kwasnik, M.; Fernández, F. M. *Anal. Chem.* **2011**, *83*, 1908–1915.

(131) Armenta, S.; Alcala, M.; Blanco, M. *Anal. Chim. Acta* **2011**, *703*, 114–123.

(132) D'Agostino, P. A.; Chenier, C. L. *Rapid Commun. Mass Spectrom.* **2010**, *24*, 1617–1624.

(133) Lapthorn, C.; Pullen, F.; Chowdhry, B. Z. *Mass Spectrom. Rev.* **2013**, *32*, 43–71.

(134) De Paoli, G.; Lewis Sr., S. A.; Schuette, E. L.; Lewis, L. A.; Connatser, R. M.; Farkas, T. *J. Forensic Sci.* **2010**, *55*, 962–969.

(135) Croxton, R. S.; Baron, M. G.; Butler, D.; Kent, T.; Sears, V. G. *J. Forensic Sci.* **2006**, *51*, 1329–1333.

(136) Pirman, D. A.; Yost, R. A. *Anal. Chem.* **2011**, *83*, 8575–8581.

(137) Pirman, D. A.; Reich, R. F.; Kiss, A.; Heeren, R. M. A.; Yost, R. A. *Anal. Chem.* **2013**, *85*, 1081–1089.

(138) Magnúsdóttir, K.; Kristinsson, J.; Jóhannesson, B. *Læknablaðið* **2010**, *96*, 626–628.

(139) Crawford, E.; Musselman, B. *Anal. Bioanal. Chem.* **2012**, *403*, 2807–2812.

(140) Rothenbacher, T.; Schwack, W. *Rapid Commun. Mass Spectrom. RCM* **2009**, *23*, 2829–2835.

(141) Pontes, H.; Guedes de Pinho, P.; Casal, S.; Carmo, H.; Santos, A.; Magalhães, T.; Remião, F.; Carvalho, F.; Lourdes Bastos, M. *J. Chromatogr. Sci.* **2009**, *47*, 272–278.

(142) Porter, W. H.; Auansakul, A. *Clin. Chem.* **1982**, *28*, 75–78.

(143) Yarita, T.; Nakajima, R.; Otsuka, S.; Ihara, T.; Takatsu, A.; Shibukawa, M. *J. Chromatogr. A* **2002**, *976*, 387–391.

(144) Jackson, D. S.; Crockett, D. F.; Wolnik, K. A. *J. Forensic Sci.* **2006**, *51*, 827–831.

(145) Laramée, J. A.; Durst, D. H.; Connell, T. R. *Am. Lab.* **2009**.

(146) Da Costa, R. S.; Santos, S. R. .; Almeida, L. F.; Nascimento, E. C. .; Pontes, M. J.; Lima, R. A. .; Simões, S. S.; Araújo, M. C. U. *Microchem. J.* **2004**, *78*, 27–33.

(147) Pontes, M. J. C.; Santos, S. R. B.; Araújo, M. C. U.; Almeida, L. F.; Lima, R. A. C.; Gaião, E. N.; Souto, U. T. C. P. *Food Res. Int.* **2006**, *39*, 182–189.

(148) Yildirim, A.; Ozturk, F. E.; Bayindir, M. *Anal. Chem.* **2013**, *85*, 6384–6391.